AFGL-TR-85-0043

ENVIRONMENTAL INTERACTIONS TECHNOLOGY STATUS

N.J. STEVENS
M.E. KIRKPATRICK
R.C. CHAKY
J.E. HOWARD
G.T. INOUYE
E.W. BERAN

TRW, INCORPORATED
ELECTRONICS AND DEFENSE SECTOR
ONE SPACE PARK
REDONDO BEACH, CA 90278

Edited by:

CAPT C.J. FRUSHON
1LT M.J. GIGER
W.N. HALL

AIR FORCE GEOPHYSICS LABORATORY
SPACE PHYSICS DIVISION
SPACE SYSTEMS TECHNOLOGY BRANCH

SCIENTIFIC REPORT No. 1
OCTOBER 1986

APPROVED FOR PUBLIC RELEASE: DISTRIBUTION UNLIMITED

AIR FORCE GEOPHYSICS LABORATORY
AIR FORCE SYSTEMS COMMAND
UNITED STATES AIR FORCE
HANSCOM AIR FORCE BASE, MASSACHUSETTS 01731

"This technical report has been reviewed and is approved for publication"

William N. Hall

WILLIAM N. HALL
Contract Manager

Edward C. Jonson

EDWARD C. JONSON, Lt. Col., USAF
Space Systems Technology Branch Chief

FOR THE COMMANDER

Rita C. Sagalyn

RITA C. SAGALYN
Space Physics Division Director

This report has been reviewed by the ESD Public Affairs Office (PA) and is releasable to the National Technical Information Service (NTIS).

Qualified requestors may obtain additional copies from the Defense Technical Information Center. All others should apply to the National Technical Information Service.

If your address has changed, or if you wish to be removed from the mailing list, or if the addressee is no longer employed by your organization, please notify AFGL/DAA, Hanscom AFB, MA 01731. This will assist us in maintaining a current mailing list.

Do not return copies of this report unless contractual obligations or notices on a specific document requires that it be returned.

UNCLASSIFIED
SECURITY CLASSIFICATION OF THIS PAGE

REPORT DOCUMENTATION PAGE

1a REPORT SECURITY CLASSIFICATION Unclassified	1b RESTRICTIVE MARKINGS
2a SECURITY CLASSIFICATION AUTHORITY	3 DISTRIBUTION / AVAILABILITY OF REPORT Approved For Public Release: Distribution Unlimited
2b DECLASSIFICATION / DOWNGRADING SCHEDULE	
4 PERFORMING ORGANIZATION REPORT NUMBER(S)	5 MONITORING ORGANIZATION REPORT NUMBER(S) AFGL-TR-85-0043
6a NAME OF PERFORMING ORGANIZATION TRW, Inc. 6b OFFICE SYMBOL (If applicable)	7a NAME OF MONITORING ORGANIZATION Air Force Geophysics Laboratory
6c ADDRESS (City, State, and ZIP Code) Electronics and Defense Sector One Space Park Redondo Beach, CA 90278	7b ADDRESS (City, State, and ZIP Code) AFGL/PHE Hanscom AFB, MA 01731-5000
8a NAME OF FUNDING / SPONSORING ORGANIZATION Air Force Geophysics Laboratory 8b OFFICE SYMBOL (if applicable) PHE	9 PROCUREMENT INSTRUMENT IDENTIFICATION NUMBER F19628-84-C-0038
8c ADDRESS (City, State, and ZIP Code) AFGL/PHE Hanscom AFB, MA 01731-5000	10 SOURCE OF FUNDING NUMBERS PROGRAM ELEMENT NO. 63410F; PROJECT NO. 2821; TASK NO 01; WORK UNIT ACCESSION NO AA
11 TITLE (Include Security Classification) (U) Environmental Interactions Technology Status	
12 PERSONAL AUTHOR(S) N.J. Stevens, M.E. Kirkpatrick, R.C. Chaky, J.E. Howard, G.T. Inouye, E.W. Beran	
13a TYPE OF REPORT Scientific Rpt. No. 1 13b TIME COVERED FROM _____ TO _____	14 DATE OF REPORT (Year, Month, Day) 1986 October 15 PAGE COUNT 198
16 SUPPLEMENTARY NOTATION Edited By: Capt C.J. Frushon, 1Lt M.J. Giger, W.N. Hall	

17 COSATI CODES		
FIELD	GROUP	SUB-GROUP

18 SUBJECT TERMS (Continue on reverse if necessary and identify by block number)
Spacecraft Environmental Interactions; Spacecraft Charging; Radiation Analysis; Meteoroid/Debris Impacts; Solar Radiation; Single Event Upsets; Electromagnetic Fields; Large Systems; High-Powered Spacecraft.

19 ABSTRACT (Continue on reverse if necessary and identify by block number)

Spacecraft environmental interactions technology is reviewed in this report. The potential interactions in seven environment categories are identified, assessed, and rated for research maturity and system impact. The seven environment categories are: Plasma, High-Energy Radiation, Neutral Particles, Meteoroid and Debris, Solar Radiation, Self-Generated, and Electromagnetic. The review was conducted by literature and contract searches as well as contact with key experts in the various fields. The goal of this review was to identify those interactions that could have a serious impact on future spacecraft system performance. The maturity of the interaction technology was then rated to assess whether or not current technology could be used to support future missions.

20 DISTRIBUTION / AVAILABILITY OF ABSTRACT ☐ UNCLASSIFIED/UNLIMITED ☒ SAME AS RPT ☐ DTIC USERS	21 ABSTRACT SECURITY CLASSIFICATION Unclassified
22a NAME OF RESPONSIBLE INDIVIDUAL Carl J. Frushon, Capt, USAF	22b TELEPHONE (Include Area Code) 22c OFFICE SYMBOL AFGL/PHE

DD FORM 1473, 84 MAR 83 APR edition may be used until exhausted.
All other editions are obsolete

SECURITY CLASSIFICATION OF THIS PAGE
UNCLASSIFIED

TABLE OF CONTENTS

PAGE

LIST OF TABLES xi

LIST OF FIGURES xii

1.0 EXECUTIVE SUMMARY 1

2.0 INTRODUCTION 4

2.1 ORGANIZATION 4

2.2 SEI RATING SCHEME 5

3.0 PLASMA ENVIRONMENT INTERACTIONS 7

3.1 GENERAL ENVIRONMENT DESCRIPTION 7

3.2 HIGH ALTITUDE SPACECRAFT CHARGING 7

3.2.1 Interaction Environment 7

3.2.2 Discussion of Interaction 10

3.2.2.1 Surface Charging 13

3.2.2.1.1 Background 13
3.2.2.1.2 Modeling 16
3.2.2.1.3 Factors Influencing Charging 22
3.2.2.1.4 Discharges 26
3.2.2.1.5 Coupling to Systems 32

3.2.2.2 Dielectric Bulk Charging 35

3.2.2.2.1 Background 35
3.2.2.2.2 Modeling 38

3.2.3 Research Maturity Rating 38

3.2.4 System Impact Rating 41

TABLE OF CONTENTS (Continued)

PAGE

3.2.5 Mitigation Techniques 41

3.3 POLAR-AURORAL SPACECRAFT CHARGING 42

3.3.1 Interaction Environment 42

3.3.2 Discussion of Interaction 47

3.3.2.1 Background 47
3.3.2.2 Modeling 52
3.3.2.3 Discharges 52

3.3.3 Research Maturity Rating 52

3.3.4 System Impact Rating 55

3.3.5 Mitigation Techniques 55

3.4 HIGH-VOLTAGE SYSTEM INTERACTIONS 55

3.4.1 Interaction Environment 55

3.4.2 Discussion of Interaction 55

3.4.2.1 Background 55
3.4.2.2 Modeling 62
3.4.2.3 Concentrator Solar Array 62
3.4.2.4 Discharges 69
3.4.2.5 Power Transmission Alternatives 69

3.4.3 Research Maturity Rating 75

3.4.4 System Impact Rating 75

3.4.5 Mitigation Techniques 75

4.0 HIGH ENERGY RADIATION ENVIRONMENT INTERACTIONS 76

4.1 GENERAL ENVIRONMENT DESCRIPTION 76

4.1.1 Trapped Radiation Environment 76

TABLE OF CONTENTS (Continued)

PAGE

4.1.2 Solar Flares 74

4.1.3 Cosmic Ray Environment 82

4.2 RADIATION DAMAGE 88

4.2.1 Interaction Environment 88

4.2.2 Discussion of Interaction 88

4.2.2.1 Electronics 88
4.2.2.2 Solar Arrays 91
4.2.2.3 Materials 91

4.2.3 Research Maturity Rating 91

4.2.4 System Impact Rating 92

4.2.5 Mitigation Techniques 92

4.3 SINGLE EVENT UPSETS (SEUs) 92

4.3.1 Interaction Environment 92

4.3.2 Discussion of Interaction 93

4.3.3 Research Maturity Rating 96

4.3.4 System Impact Rating 96

4.3.5 Mitigation Techniques 96

4.4 RADIATION HAZARDS TO MAN-IN-SPACE 100

4.4.1 Interaction Environment 100

4.4.2 Discussion of Interaction 100

4.4.3 Research Maturity Rating 100

4.4.4 System Impact Rating 100

TABLE OF CONTENTS (Continued)

PAGE

4.4.5 Mitigation Techniques 100

5.0 NEUTRAL ENVIRONMENT INTERACTIONS 103

5.1 GENERAL ENVIRONMENT DESCRIPTION 103

5.2 ATMOSPHERIC DRAG 103

5.2.1 Discussion of Interaction 103

5.2.2 Research Maturity Rating 107

5.2.3 System Impact Rating 107

5.2.4 Mitigation Techniques 107

5.3 ATOMIC OXYGEN SURFACE EROSION 107

5.3.1 Discussion of Interaction 107

5.3.2 Research Maturity Rating 112

5.3.3 System Impact Rating 112

5.3.4 Mitigation Techniques 112

5.4 SURFACE GLOW 112

5.4.1 Discussion of Interaction 112

5.4.2 Research Maturity Rating 114

5.4.3 System Impact Rating 114

5.4.4 Mitigation Techniques 114

5.5 CHEMICAL REACTIONS 115

5.5.1 Discussion of Interaction 115

5.5.2 Research Maturity Rating 115

TABLE OF CONTENTS (Continued)

PAGE

5.5.3 System Impact Rating 115

5.5.4 Mitigation Techniques 115

5.6 SPUTTERING 115

5.6.1 Discussion of Interaction 115

5.6.2 Research Maturity Rating 116

5.6.3 System Impact Rating 116

5.6.4 Mitigation Techniques 116

6.0 PARTICLE ENVIRONMENT INTERACTIONS 117

6.1 MICROMETEOROID IMPACTS 117

6.1.1 Interaction Environment 117

6.1.2 Discussion of Interaction 117

6.1.3 Research Maturity Rating 121

6.1.4 System Impact Rating 123

6.1.5 Mitigation Techniques 123

6.2 MAN-MADE DEBRIS IMPACTS 123

6.2.1 Interaction Environment 123

6.2.2 Discussion of Interaction 126

6.2.3 Research Maturity Rating 126

6.2.4 System Impact Rating 130

6.2.5 Mitigation Techniques 130

TABLE OF CONTENTS (Continued)

PAGE

7.0 SOLAR OPTICAL RADIATION ENVIRONMENT INTERACTIONS 131

7.1 GENERAL ENVIRONMENT DESCRIPTION 131

7.2 SURFACE DEGRADATION 131

7.2.1 Discussion of Interaction 131

7.2.2 Research Maturity Rating 134

7.2.3 System Impact Rating 134

7.2.4 Mitigation Techniques 134

7.3 THERMAL FORCES 134

7.3.1 Discussion of Interaction 134

7.3.1.1 Momentum Transfer 134
7.3.1.2 Thermal Expansion Stress 135

7.3.2 Research Maturity Rating 136

7.3.3 System Impact Rating 136

7.3.4 Mitigation Techniques 136

7.4 BIOLOGICAL HAZARD 136

7.4.1 Discussion of Interaction 136

7.4.2 Research Maturity Rating 139

7.4.3 System Impact Rating 139

7.4.4 Mitigation Techniques 139

8.0 SELF-GENERATED ENVIRONMENT INTERACTIONS 140

8.1 CONTAMINATION DUE TO OUTGASSING MATERIALS 140

TABLE OF CONTENTS (Continued)

PAGE

8.1.1 Interaction Environment 140

8.1.2 Discussion of Interaction 140

8.1.3 Research Maturity Rating 143

8.1.4 System Impact Rating 143

8.1.4.1 Surface Contamination 143
8.1.4.2 Sensor Degradation 143

8.1.5 Mitigation Techniques 143

8.2 THRUSTER EFFLUENT CONTAMINATION 144

8.2.1 Interaction Environment 144

8.2.2 Discussion of Interaction 144

8.2.2.1 Chemical Rockets 144
8.2.2.2 Attitude Control Jets 145
8.2.2.3 Ion Thrusters 145

8.2.3 Research Maturity Rating 145

8.2.4 System Impact Rating 145

8.2.5 Mitigation Techniques 145

8.3 NUCLEAR POWER SYSTEM INTERACTIONS 146

8.3.1 Interaction Environment 146

8.3.2 Discussion of Interaction 146

8.3.2.1 Effect of the Environment on Reactor Operations 146
8.3.2.2 Effect of Reactor Operations on the Environment 146
8.3.2.3 Effects of the Reactor Induced Environment 146

8.3.3 Research Maturity Rating 147

8.3.4 System Impact Rating 147

TABLE OF CONTENTS (Continued)

PAGE

8.3.5 Mitigation Techniques 147

9.0 ELECTROMAGNETIC ENVIRONMENT INTERACTIONS 148

9.1 GENERAL ENVIRONMENT DESCRIPTION 148

9.2 DISCUSSION OF INTERACTIONS 148

9.2.1 Motion Generated Electric Fields 148

9.2.2 Current Generated Forces 151

9.2.3 Configuration Generated Torques 153

9.3 RESEARCH MATURITY RATING 153

9.4 SYSTEM IMPACT RATING 153

9.5 MITIGATION TECHNIQUES 155

10.0 CONCLUDING REMARKS 156

11.0 REFERENCES 157

11.1 INTRODUCTION (Section 2.0) 157

11.2 PLASMA ENVIRONMENT INTERACTIONS (Section 3.0) 157

11.3 HIGH ENERGY RADIATION ENVIRONMENT (Section 4.0) 168

11.4 NEUTRAL ENVIRONMENT (Section 5.0) 171

11.5 PARTICLE ENVIRONMENT (Section 6.0) 174

11.6 SOLAR OPTICAL RADIATION ENVIRONMENT (Section 7.0) 174

11.7 SELF-GENERATED ENVIRONMENT (Section 8.0) 175

11.8 ELECTROMAGNETIC ENVIRONMENT (Section 9.0) 179

LIST OF TABLES

PAGE

Table 1.1 Spacecraft Environmental Interactions Rating Summary 3

Table 2.1 Rating Scheme for Environment Interactions 5

Table 3.1 Recommended Geomagnetic Substorm Design Environment 10

Table 3.2 Precipitation Electron Energy Variations (Mid Latitudes) 47
A. Post-Midnight Maxima
B. Pre-Noon Maxima

Table 3.3 Precipitation Electron Energy Variations (High Latitudes) 49
A. Pre-Noon Integral Number Flux Maximum
B. Average Energy Minimum

Table 4.1 Operational Satellites that Experienced Single Event Upsets 93

Table 4.2 Devices Tested for Heavy Ion Induced SEU 97

Table 4.3 Summary of Latchup Test Results 99

Table 5.1 Atomic Oxygen Surface Erosion:
Highly Reactive and Non-Reactive Materials 111

Table 5.2 Atomic Oxygen Mass Loss Rates 111

Table 6.1 Micrometeoroid Impacts Expected at 1 A.U. from the Sun 121

Table 6.2 Debris Impacts Expected in a 400 km Orbit 126

Table 7.1 UV Degradation of Thermal Control Surfaces at LEO 133

Table 7.2 UV Degradation of Thermal Control Surfaces at GEO 133

LIST OF FIGURES

PAGE

Figure 3.1 Magnetosphere Geometry 8

Figure 3.2 Magnetosphere Plasmas 9

Figure 3.3 Schematic View on the Geomagnetic Equatorial Plane of Electron and Proton Injection Event During Growth Phase of a Substorm . . . 11

Figure 3.4 Average Substorm Characteristic 12

Figure 3.5 Occurrence of Satellite Anomalies in Local Time 14

Figure 3.6 Spacecraft Charging 15

Figure 3.7 NASCAP Generated Satellite Model
A. Spin Stabilized Spacecraft 17
B. Three-Axis Stabilized Spacecraft 18

Figure 3.8 Charging History of Spacecraft Ground 19
A. Spin Stabilized Spacecraft
B. Three-Axis Stabilized Spacecraft

Figure 3.9 Predicted Charging Levels
A. Spin Stabilized Spacecraft 20
B. Three-Axis Stabilized Spacecraft 21

Figure 3.10 Differential Charging of 2 mil Kapton: Comparison of NASCAP and One-Dimensional Model Results 23

Figure 3.11 NASCAP Model of a Typical GEO Communications Satellite 24

Figure 3.12 Typical NASCAP Results of GEO Satellite Charging 25

Figure 3.13 Effect of Dielectric Thickness on Charging (Severe Substorm) 27

Figure 3.14 Effect of Resistivity on Voltage: 2 mil Kapton (Severe Substorm) . . . 28

Figure 3.15 ATS-5 Spacecraft 29

Figure 3.16 ATS-6 Spacecraft 30

Figure 3.17 ATS-5 and ATS-6 Eclipse Charging Levels 31

LIST OF FIGURES (Continued)

PAGE

Figure 3.18 Discharge on DSCS II Antenna 33

Figure 3.19 Discharge Process 34

Figure 3.20 Discharge Coupling Processes 36

Figure 3.21 Predicted Structural Potentials After 2 μC Discharge (Antenna) . . . 37

Figure 3.22 Monoenergetic Beam Dielectric Charging (Typical Results) 39

Figure 3.23 Electric Field vs Time (Teflon) 40

Figure 3.24 Aurora 43

Figure 3.25 Ionospheric Electron Density in an Aurora 45

Figure 3.26 Auroral Electron Beam Environment 46
A. Number Flux Distribution as Function of K_p
B. Energy Flux Distribution as Function of K_p

Figure 3.27 DMSP Charging Event:
Environment and Induced Vehicle Potential 48

Figure 3.28 DMSP Polar-Auroral Charging Incidents 50

Figure 3.29 Impact of Vehicle Size on Auroral Charging
(Simple Model Predictions) 51

Figure 3.30 Differential Charging in Response
to a 10 keV Injection (1-D Model) 53

Figure 3.31 POLAR Code Shuttle Application 54
A. POLAR Code Shuttle Model
B. Quiet Environment Ion Density Profiles Showing Wake Region

Figure 3.32 Plasma Number Density vs Altitude in Equatorial Orbit 56

Figure 3.33 Space Station Plasma Environments (Units 10^6 cm^{-3}) 57

Figure 3.34 Solar Array Segment Ground Test Results (Area = 1058 cm^2) 59

LIST OF FIGURES (Continued)

PAGE

Figure 3.35 Effect of Voltage and Defect Size on Leakage Current (Positive Voltage applied to 5 mil Kapton Electrode) 60

Figure 3.36 Spacecraft High-Voltage System Environment Interactions 61

Figure 3.37 NASCAP/LEO Solar Array Model 63

Figure 3.38 NASCAP/LEO Solar Array Voltage Predictions 64

Figure 3.39 Cassegrainian Concentrator Solar Array 65
A. Solar Cell Array
B. Concentrator Solar Cell Schematic

Figure 3.40 Concentrator Cell Current Collection Test Data 66
A. Electron Collection
B. Ion Collection

Figure 3.41 Concentrator Solar Cell Electron Collection Model 67

Figure 3.42 Concentrator Solar Cell Ion Collection Model 68

Figure 3.43 Shutdown Thresholds 70

Figure 3.44 Arc Discharge Rate for Solar Cells 71

Figure 3.45 Enhance Electron Emission Test Schematic 72

Figure 3.46 Enhanced Electron Emission Surface Voltage Test Results 73

Figure 3.47 A.C. Power Distribution Concept 74

Figure 4.1 Natural Environment Isoflux Contours: Electrons (E > 0.5 MeV) 77

Figure 4.2 Natural Environment Isoflux Contours: Protons (E > 0.5 MeV) 78

Figure 4.3 Omnidirectional Flux at the Geomagnetic Equator 79
A. Electron Map
B. Proton Map

Figure 4.4 Proton Flux Densities at 296 km Altitude 80

LIST OF FIGURES (Continued)

PAGE

Figure 4.5 Electron Constant Flux Contours at 400 km Altitude (E > 0.5 MeV) 81

Figure 4.6 Solar Particle Access to Earth Orbits 83

Figure 4.7 Solar Flare Environments for Solar Particle Events 84

Figure 4.8 Solar Minimum Cosmic Ray Environment: Free Field during the Quiet Period 85

Figure 4.9 Solar Maximum Cosmic Ray Environment: Free Field during the Disturbed Period 86

Figure 4.10 Solar Maximum Cosmic Ray Environment: 426 km Orbit during the Disturbed Period 87

Figure 4.11 Shielding Effectiveness Against Natural Radiation Environment 89

Figure 4.12 *Radiation Analysis of Semiconductor Technology* 90

Figure 4.13 Ionizing Path through Semiconductors 94
A. Cosmic Ray Induced Upset
B. Proton Induced Upset

Figure 4.14 Cosmic Ray Effect in Electronic Devices 95

Figure 4.15 Astronaut EVA Equipment 102

Figure 5.1 Atmospheric Density Profile 104

Figure 5.2 Kinetic Temperature vs Altitude 105

Figure 5.3 Neutral Environment 106

Figure 5.4 Effective Drag vs Altitude 108

Figure 5.5 Mass Loss on 0.5 mil Mylar Disk 110
A. Ram Exposed Mylar Disk
B. Mylar Disk UV Control Sample

Figure 5.6 Shuttle Glow on STS-3 113

LIST OF FIGURES (Continued)

PAGE

Figure 6.1 Micrometeoroid Environment 118

Figure 6.2 Average Cumulative Micrometeoroid Flux vs Spacecraft Area 119

Figure 6.3 Micrometeoroid Impact Damage in a Solar Max Thermal Blanket 120
A. Initial Impact Hole
B. Secondary Layer Spalling Damage

Figure 6.4 Penetration Capability of Micrometeoroid Particles 122

Figure 6.5 Comparison of Orbital Debris Data with Micrometeoroid Model . . 124

Figure 6.6 Man-Made Debris Environment 125

Figure 6.7 Paint Flake Impact Damage in a Solar Max Thermal Louver 127
A. Initial Impact Hole in Aluminum
B. Secondary Layer Spalling Damage

Figure 6.8 Average Cumulative Debris Flux vs Spacecraft Area (400 km Orbit) 128

Figure 6.9 Penetration Capability of Debris Particles 129

Figure 7.1 The Solar Spectrum 132

Figure 7.2 Solar Array Flight Experiment (Artist's Conception) 137

Figure 7.3 Thermal Effects on Flexible Structures (SAFE) 138
A. Nominal Structure
B. Deformed Structure

Figure 8.1 Outgassing and Thruster Flow Patterns in a Spacecraft 141

Figure 8.2 Enhanced Contamination Measured on the SCATHA Spacecraft 142

Figure 9.1 Total Magnetic Field Intensity (in Gauss) on the Earth's Surface (Epoch 1965) [7] 149

Figure 9.2 The B-L Coordinate System 150

LIST OF FIGURES (Continued)

PAGE

Figure 9.3 Induced Stress vs Applied Voltage 152
A. Stresses Acting on a 0.005 cm Insulator
B. Experimental Results

Figure 9.4 Motion and Current Induced Effects in a Solar Array Power Source 154

1.0 EXECUTIVE SUMMARY

This Environmental Interaction Technology Status report fills the need for a comprehensive survey of the many natural environment hazards that may affect large, high-powered spacecraft proposed for future United States Air Force (USAF) missions. Such a document is required so that potential environmentally induced hazards can be recognized and mitigation techniques incorporated early in the design phases of these programs.

Experience with operational satellites has shown that severe interactions between spacecraft systems and the natural space environment can occur. These interactions, ranging from nuisance electronic switching to mission failure, were not anticipated in previous system designs and were only identified during recent spacecraft operations. Since future spacecraft will be larger and operate at higher power levels, environmentally induced effects could be more serious at all orbital altitudes. It is with the desire to prevent operational surprises from environment interactions, and their subsequent costly retrofits, that this study was undertaken.

This report presents an overview of the interactions, their current research status, and their system impact. The interactions were grouped into seven environmental categories: Plasma Environments (Section 3), High Energy Radiation Environments (Section 4), Neutral Environments (Section 5), Particle Environments (Section 6), Solar Radiation Environments (Section 7), Self-Generated Environments (Section 8), and Electromagnetic Environments (Section 9).

The plasma environment category considers interactions with space plasmas having particle energies less than 100 keV. The high energy radiation environments category discusses effects resulting from interactions with electrons and ions having particle energies greater than 100 keV. The neutral environment category is concerned with low altitude, non-charged particle interactions (e.g. atomic oxygen erosion). The particle environment category covers micrometeoroid and man-made debris impacts. The solar radiation environment category considers ultraviolet, visible, and near infrared solar interactions. The self-generated interactions category is concerned with contamination from various sources. Finally, the electromagnetic environment category discusses interactions with magnetic fields. Extensive references are provided on each interaction and are located at the end of this report (Section 11).

An initial list of seventy-five possible interactions was condensed to twenty-four for this summary. Each interaction was rated for research maturity in both experimental and analytical areas for Low Earth (LEO), Polar Earth (PEO), and Geosynchronous Earth (GEO) Orbits. The impact of each of these interactions on system performance was also rated. The ratings were based upon a scale of 1 to 5 where 5 represented COMPLETE knowledge for the maturity rating and CATASTROPHIC for the rating for impact on the system. The rating scheme is discussed in Section 2.2.

The summary of the ratings for the 24 interactions is given in Table 1.1. In general, the ratings show some expected results and some surprises. Charged particle

interactions (both plasma and high energy radiation environments) have serious system impacts. Yet, the state-of-knowledge of these interactions is not complete, even after years of study. There are still significant technology gaps that must be filled.

The neutral environment interactions of drag and atomic oxygen surface erosion have received considerable attention recently. While these effects can be catastrophic, the technology for mitigating these effects is rapidly growing. Other neutral environment interactions, however, still have technology gaps even though the system impact can be serious.

The return of hardware to earth after years in space is proving that meteoroid and debris impacts on spacecraft surfaces can be serious. There are gaps in the man-made debris population models and on the effect of these impacts on materials to be used in future, large space systems.

The ratings would indicate that solar radiation effects would have small system impacts. This is generally true, however, under specific applications the impact could be serious. For example, a large solar panel experiment bowed during eclipse due to differential expansion of the various materials used. Once back in sunlight the panel flattened. Such fluctuations were not anticipated. If similar materials or design procedures were incorporated into a future system, the impact could be serious.

The electromagnetic environment interactions all have a COMPLETE research maturity rating. Yet, the effect of these interactions on large system performance is not well understood. From the brief overview conducted within this report, it is felt that these interactions could be serious and should be evaluated.

This study has shown that there are interactions that could cause serious system impacts. The technology for these interactions is in varying states of development. Thus, developing a complete set of design guidelines and Military Standards is not possible at this time. In the case of immature technologies, information should be catalogued and made available to designers to insure that the potential hazard of the interaction is recognized.

Table 1.1
Spacecraft Environmental Interactions Rating Summary

INTERACTION	RATING								
	System Impact			Research Maturity					
				Theory			Experiment		
	LEO	PEO	GEO	LEO	PEO	GEO	LEO	PEO	GEO
PLASMA ENVIRONMENT:									
- High Altitude Charging	-	-	4	-	-	4	-	-	4
- Polar-Auroral Charging	1	4	1	-	3	-	-	3	-
- High-Voltage Interactions	4	4	1	3	3	1	3	3	1
HIGH ENERGY RADIATION:									
- Radiation Damage to:									
- Electronics	-	4	4	-	4	4	-	4	4
- Solar Arrays	-	4	4	-	4	4	-	4	4
- Materials	-	3	3	-	3	3	-	3	3
- Single Event Upsets	-	4	4	-	4	4	-	4	4
- Radiation Hazards to Man	-	4	4	-	4	4	-	4	4
NEUTRAL ENVIRONMENT:									
- Atmospheric Drag	5	5	1	3	3	-	3	3	-
- Atomic Oxygen Surface Erosion	5	5	1	3	3	-	4	4	-
- Surface Glow	3	3	1	3	3	-	3	3	-
- Chemical Reactions	3	3	1	4	4	-	3	3	-
- Sputtering	4	4	1	2	2	-	2	2	-
PARTICLE ENVIRONMENT:									
- Micrometeoroid Impact	4	4	4	4	4	4	3	3	3
- Man-Made Debris Impact	4	4	4	3	2	2	3	2	2
SOLAR RADIATION ENVIRONMENT:									
- Surface Coating Degradation	2	2	2	5	5	5	4	4	4
- Thermal Forces	3	3	3	4	4	4	4	4	4
- Biological Hazard	1	1	1	4	4	4	4	4	4
SELF-GENERATED ENVIRONMENT:									
- System Outgassing	4/5	4/5	4/5	3	3	3	4	4	4
- Thruster Effluent	4/5	4/5	4/5	3	3	3	3	3	3
- Nuclear Systems	5	5	5	4	4	4	4	4	4
ELECTROMAGNETIC ENVIRONMENT:									
- Motion-Induced Electric Fields	4	4	4	5	5	5	5	5	5
- Current-Generated Forces	4	4	4	5	5	5	5	5	5
- Magnetic Torques	4	4	1	5	5	5	5	5	5

Note: (-) Indicates Interaction is Not Applicable to the Designated Orbit

2.0 INTRODUCTION

The Spacecraft Environmental Interaction Study was undertaken to fill a pressing need for a comprehensive survey of the natural environment hazards facing the large, high-powered spacecraft proposed for future USAF missions. Such a survey was required so that all potential hazards could be recognized and mitigation techniques incorporated early in the spacecraft design phase. This will save costly retrofits and delays later in the program.

Experience has shown that the natural environment can interact with spacecraft surfaces and systems, disrupting operations. For example, the degradation of electronic components in the space radiation environment has long been recognized. This degradation can lead to eventual failure when the cumulative dose exceeds thresholds for specific parts [1]. Interactions have been noted in geosynchronous orbiting spacecraft when systems were upset due to encounters with geomagnetic substorm environments [2]. Anomalous events were also correlated with galactic cosmic ray impacts [3]. The disruptions arising from these interactions range from correctable nuisance anomalies to component failures which caused loss of mission. After many years of study and evaluation the interactions are now better understood, however, anomalies continue to occur [4].

At the present time, the USAF is contemplating future space missions that use large, high powered spacecraft. Missions are in the planning stages, such as Space Based Radar, that use large platforms exposed to the space environment while requiring multi-kilowatts of power for operation. This new generation of spacecraft must operate in a variety of orbits ranging from low altitude equatorial and polar to beyond geosynchronous. Prior experience can not guarantee that all possible interactions with the natural space environment will be considered in these designs. Costly retrofits will be required if these interactions are uncovered late in the vehicle planning stages.

The Air Force Geophysics Laboratory (AFGL) funded this study to: (1) rank the possible impact of natural environment interactions for future military systems; (2) aid designers and program managers in recognizing the importance of these interactions; and (3) foster the incorporation of mitigation techniques early in the vehicle design process. These goals are aimed at minimizing the need for costly spacecraft modifications late in the systems acquisition process.

2.1 ORGANIZATION OF REPORT

The natural environmental interactions identified are presented within seven categories: Plasma Environments (Section 3), High Energy Radiation Environments (Section 4), Neutral Environments (Section 5), Particle Environments (Section 6), Solar Radiation Environments (Section 7), Self-Generated Environments (Section 8), and Electromagnetic Environments (Section 9).

This division of environments is for convenience of discussion and is not a prioritization of their importance. The plasma environment category considers

interactions with electrons and ions having energies less than 100 keV. The high energy radiation environments category discusses effects resulting from interactions with electrons and ions having energies greater than 100 keV. The neutral environment category is concerned with the low altitude, non-charged environment (e.g. atomic oxygen erosion). The particle environment category considers interactions with the meteoroid and man-made debris environments. The solar radiation environment category considers the ultraviolet, visible, and near infrared spectrum from the Sun. The well established technology associated with these interactions is only summarized here. The self-generated environment category deals with contamination and nuclear power system operations. Finally, the electromagnetic environment category discusses interactions with the Earth's magnetic field.

The discussion of each Spacecraft Environment Interaction (SEI) within each environment category is summarized by discussing the following topics: Specific Environment Description, Discussion of SEI, Research Maturity Rating, System Impact Rating, and Mitigation Techniques. The information presented in the following discussions is derived from literature searches and key expert inputs. Extensive references for each category are located in Section 11 for convenient access.

2.2 SEI RATING SCHEME

The scheme used to rate these interactions addresses both research maturity and potential impact on the performance of a spacecraft system. Both rating factors use a scale of 1 to 5 (Table 2.1).

Table 2.1
Rating Scheme for Environment Interactions

System Impact	Maturity
1. Negligible	1. Negligible
2. Small	2. Slight
3. Moderate	3. Moderate
4. Large	4. Considerable
5. Catastrophic	5. Complete

Research maturity ratings are judgments, based upon available information, of what is known about the interaction technology. These ratings are divided into a theoretical and experimental maturity. A rating of (1) implies negligible understanding - little if anything has been started towards understanding this interaction. A rating of (2) implies slight understanding - at least preliminary models have been formulated. A rating of (3) implies moderate understanding - models have been tested or discussed in detail. A rating of (4) implies considerable understanding - some open questions remain. Finally, a rating of (5) implies essentially complete understanding of the interaction.

The system impact rating is a judgment on the degree to which an interaction would affect the performance of any system. This has to be a broad judgment since an

interaction could be catastrophic to some systems but have a negligible effect on others. For example, contamination would be catastrophic to cryogenically cooled infrared (IR) sensors, but would be negligible for external surfaces used for cavity closeouts. System impact ratings in this report refer to the most seriously impacted system. The system impact scale runs from 1 (NEGLIGIBLE) to 5 (CATASTROPHIC).

The purpose of rating these interactions in this manner is twofold. First, serious interactions can be immediately identified. Second, if the maturity rating of the serious interaction is low, this would indicate that additional work should be done in this area to develop the technology so that it can be incorporated into spacecraft design.

3.0 PLASMA ENVIRONMENT INTERACTIONS

This section discusses interactions with space plasmas having particle energies less than 100 keV. High Altitude Spacecraft Charging, Polar-Auroral Spacecraft Charging, and High-Voltage System Interactions will be discussed in detail.

3.1 GENERAL ENVIRONMENT DISCUSSION

The space plasma environment surrounding the Earth, as illustrated in Figure 3.1, is very complex. This environment is dynamic and changes continually. The plasma environment discussion here can be simplified since the goal is directed towards engineering level interactions rather than a scientific treatise on the environment.

The magnetospheric plasma resides mainly in three more or less distinct regions: (i) the plasmasphere of cool (< 1 eV) plasma consisting of electrons, protons, and oxygen ions; (ii) the plasma sheet, a region of warm (6 keV) plasma, mostly electrons, protons with oxygen, and helium ions; and (iii) the radiation belts, consisting mainly of electrons, protons with energies of 1 to 10 MeV, and a minority of heavier ions in the 100 MeV range. The principal plasma environment of concern is that in which particle energies have been arbitrarily limited to 100 keV. This environment resides in the plasmasphere and plasma sheet regimes (Figure 3.2).

The plasmasphere is an asymmetric, roughly toroidal body of plasma extending from the lower altitudes of the atmosphere to an equatorial radius of about four Earth radii (4 R_e). During prolonged quiet times the outer boundary, called the plasmapause, can reach 10 R_e. The plasmasphere co-rotates with the rotating ionospheric electric field. This traps ionospheric ions and electrons, resulting in particle densities that can reach 10^6 cm^{-3} on the equator at low altitudes while falling off to about 1 cm^{-3} at geosynchronous altitudes (6.6 R_e). The high thermal plasma density in low altitude (> 100 km), low inclination (< 50°) orbits minimizes charging interactions with spacecraft systems. The plasma sheet, an extended region of warm plasma outside the plasmasphere, extends away from the Sun for at least several tens of Earth radii, as shown in Figure 3.2. The region between the plasmapause, the outer limit of the plasmasphere, and the inner edge of the plasma sheet is called the plasma trough. The trapped radiation belts are discussed in Section 4.0.

3.2 HIGH ALTITUDE SPACECRAFT CHARGING

This interaction results in the charging of geosynchronous spacecraft surfaces by geomagnetic substorm environments. This charging results in enhanced electrostatic contamination and can initiate discharges. It has been called "spacecraft charging".

3.2.1 Interaction Environment

The environment of concern here is the geomagnetic substorms encountered in the regions around geosynchronous altitudes [6,9,11-17]. These substorms arise when the solar wind particles interact with the Earth's magnetic field so that the particles are swept

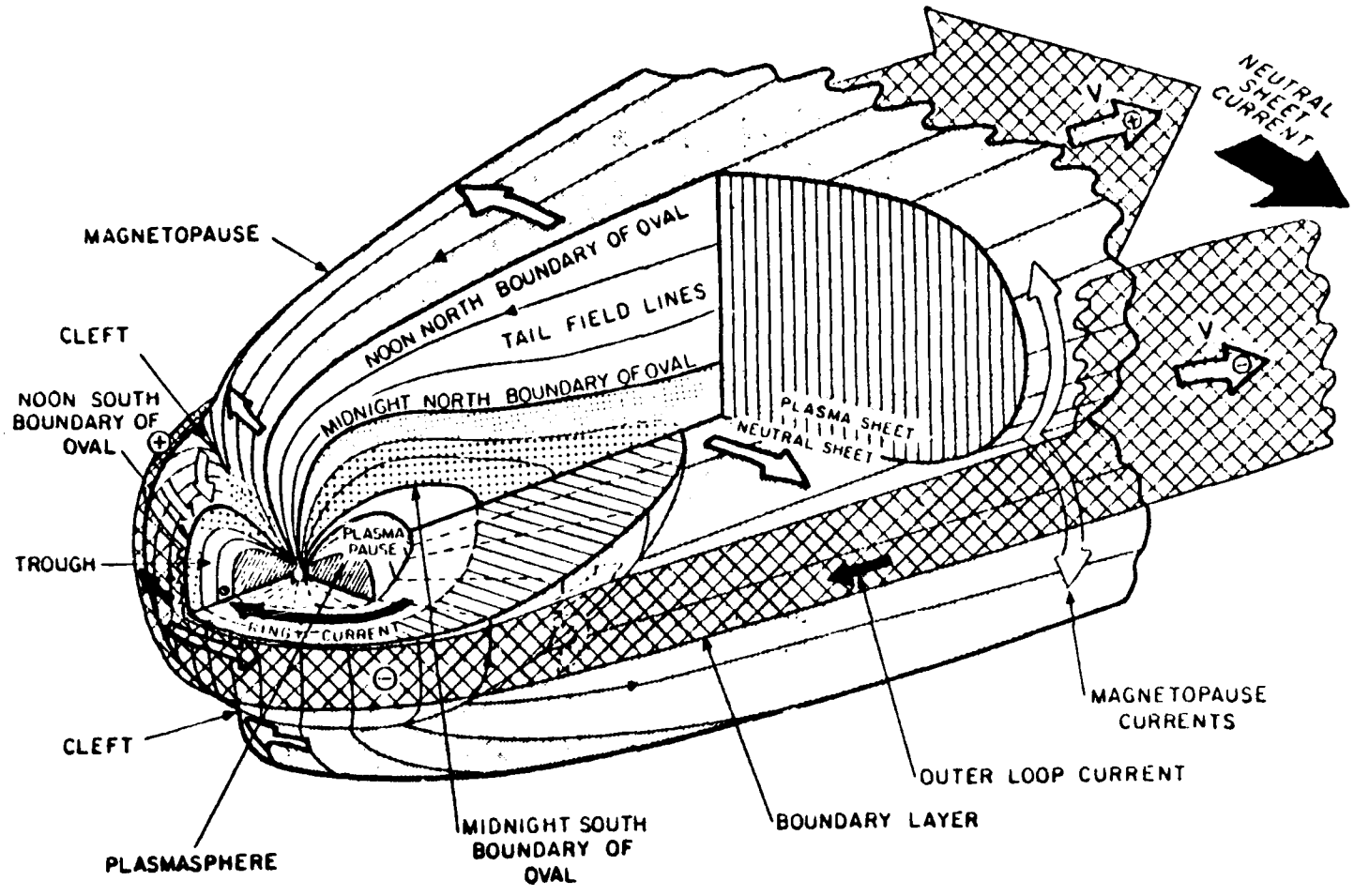

Figure 3.1 Magnetosphere Geometry

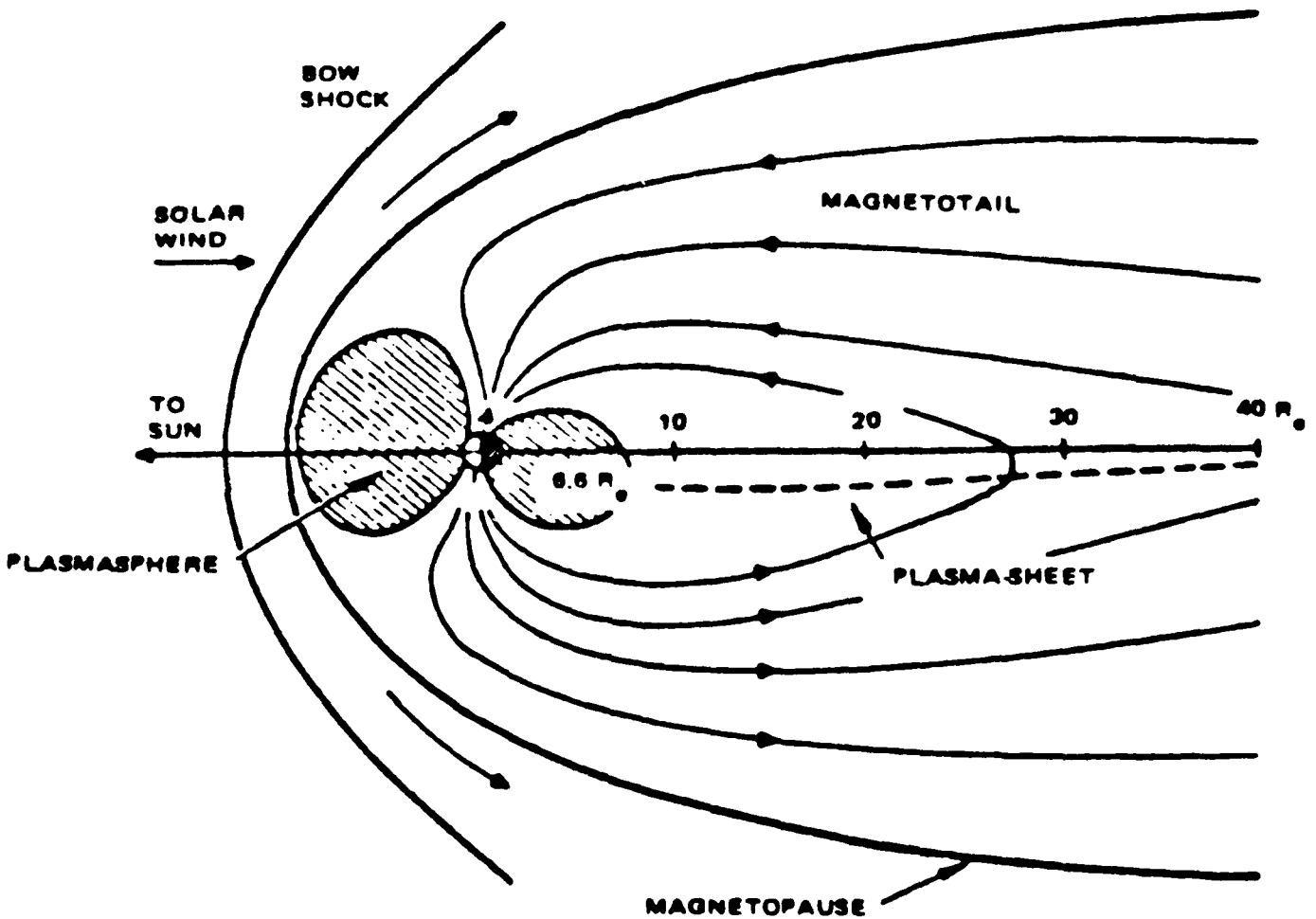

Figure 3.2 Magnetosphere Plasmas

out along the field lines and are then accelerated back toward Earth through the plasma trough. These particles are accelerated to kiloelectron volt (keV) levels. When they intercept the closed magnetic field lines around the Earth, they are dispersed according to their energies and species (Figure 3.3) [17]. This injection of more energetic particles always occurs at local midnight. The dispersion cloud then moves around the Earth interacting with the atmosphere along the magnetic field lines. This interplay in the environment eventually results in the auroras which are observed in both hemispheres.

The substorm environment can be represented as a cloud of energetic particles with irregular boundaries. Within this cloud, the intensity can vary. There is also evidence that the electron flux can be preferentially aligned along magnetic field lines [9]. Spacecraft tend to move into and through this cloud. Therefore, the charging levels encountered by any spacecraft can vary depending upon the conditions encountered.

For design purposes, the environment can be described in terms of current densities and characteristic energies or temperatures. Only a single Maxwellian distribution is given, since this specification typically results in the largest predicted differential charging of spacecraft surfaces. The recommended design environment is given in Table 3.1 [18]. The likelihood of observing current densities and temperatures of a given magnitude or larger are shown in Figure 3.4 [18].

Table 3.1
Recommended Geomagnetic Substorm Design Environment

Electron Density	1.12 cm^{-3}
Proton Density	Ø.236 cm^{-3}
Electron Temperature	12.Ø keV
Proton Temperature	29.5 keV
Electron Current Density	Ø.33 nA/cm^2
Proton Current Density	2.5 pA/cm^2

3.2.2 Discussion of Interaction

Spacecraft charging is a very active field of both analytical and experimental study. A large body of literature exists which includes several books [19-20], monographs [18,21] and conference proceedings [22-25]. Several review papers are also available describing laboratory and in-orbit experiments, analytical and numerical models, "worst case" environments [12], and practical mitigation techniques. The interaction considered here is applicable to spacecraft placed in or near geosynchronous orbit (4 to 8 R_e). The energetic electrons do not reach the low altitude equatorial orbits. The dense, low energy, plasma would also prevent any surface charging effects.

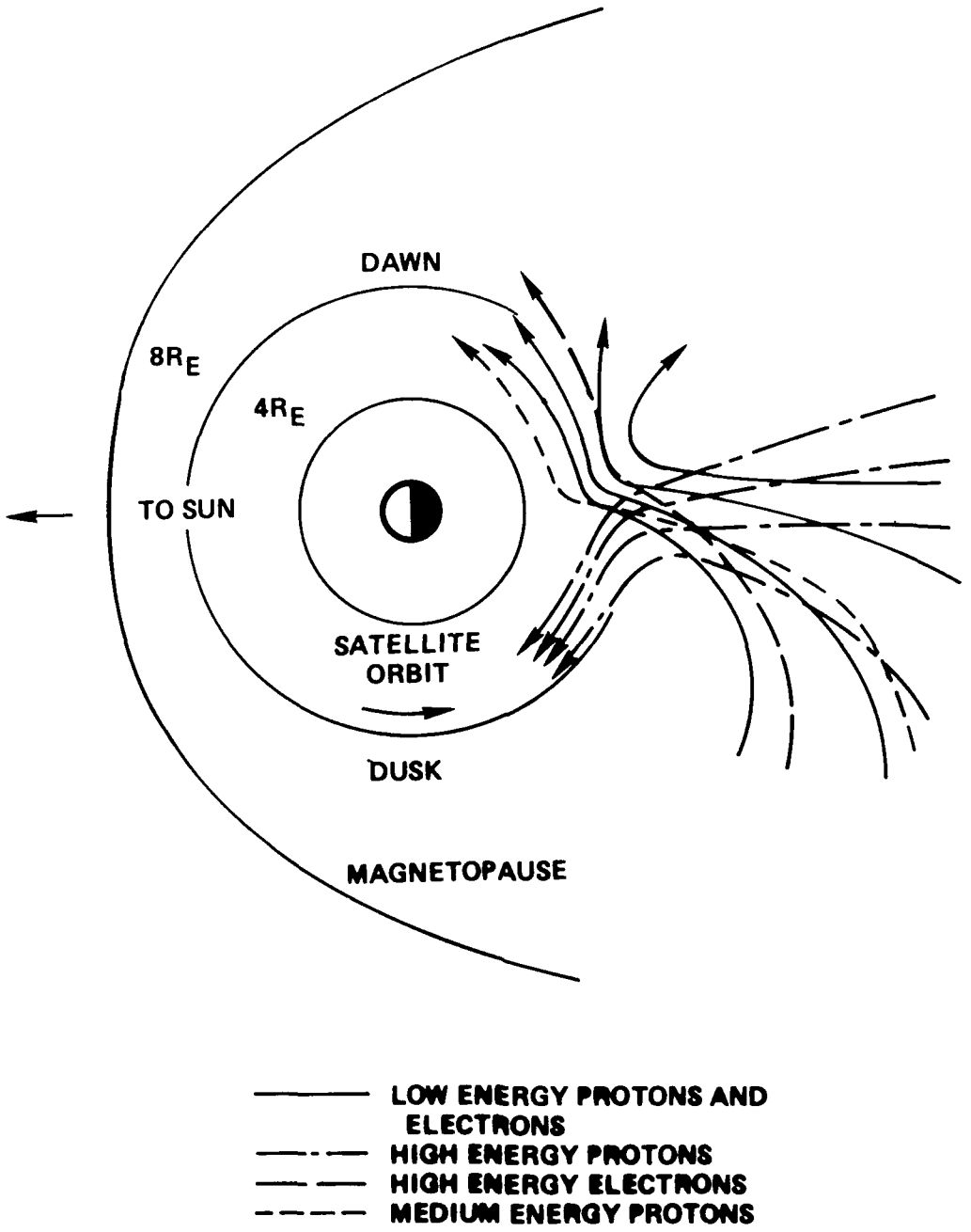

Figure 3.3 Schematic View on the Geomagnetic Equatorial Plane of Electron and Proton Injection Event During Growth Phase of a Substorm.

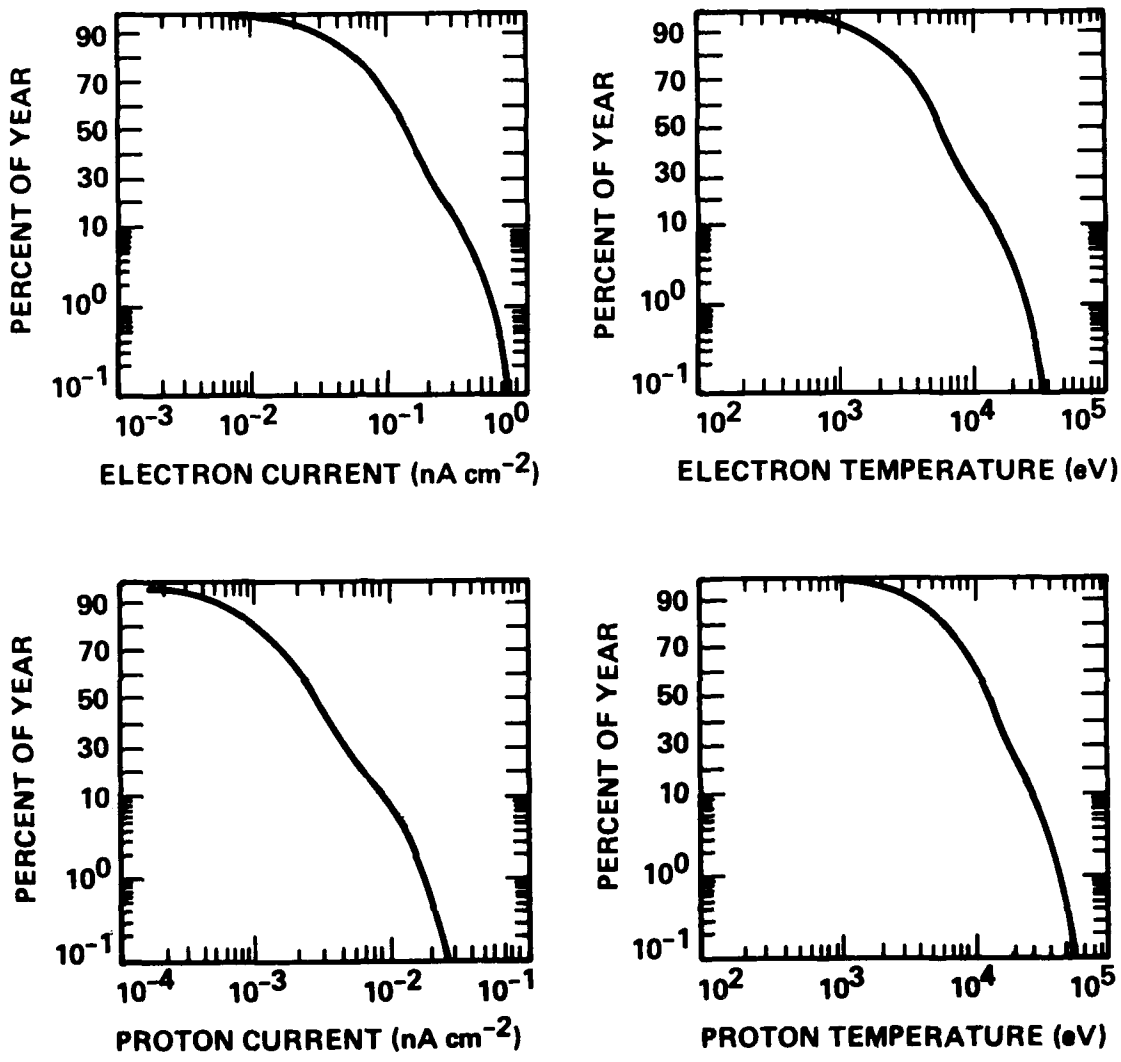

Figure 3.4 Average Substorm Characteristics

Historically, this interaction was found when spacecraft electronic system anomalies were correlated with geomagnetic substorm fluxes in geosynchronous orbits [2]. These anomalies were initially found to occur at specific times in the orbit as shown in Figure 3.5. This figure shows a polar plot of the time of occurrence of anomalies on five geosynchronous satellites during the early 1970s. The occurrence of anomalies corresponded to the region where the substorms were expected. Laboratory testing seemed to indicate that electron flows at the substorm level could charge the spacecraft surfaces to the point where discharges would occur. The need to understand these interactions intensified when an USAF communications satellite failed.

Surface charging interactions result from the deposition of charge on or just within the exterior surfaces of the spacecraft. Bulk charging results from the deposition of charge within exterior or interior dielectrics. Both types of charging phenomena are possible in geomagnetic substorms.

Spacecraft charging effects have been studied in a number of laboratory [26-30] and space flight experiments. Flight experiments were conducted on the Applications Technology Satellites (ATS) 5 and 6 [31-33] and the Spacecraft Charging at High Altitudes (SCATHA) satellite [34]. Charging experiments on ATS 5 and 6 demonstrated the ability of electron emitters and plasma sources to control spacecraft potentials in geosynchronous orbits and evaluated spacecraft size effects. The SCATHA satellite was dedicated solely to experiments to evaluate charging effects. This satellite contained 13 experiments to measure the environment particle fluxes as a function of energy and to conduct engineering measurements on surface charging, discharge characterization, and satellite potential control techniques. Launched in January 1979, SCATHA has provided useful data on all phases of geomagnetic substorm charging.

3.2.2.1 *Surface Charging*

3.2.2.1.1 Background

The charging of spacecraft surfaces results from the requirement that the net current to a surface (or spacecraft) be zero [35-39]. As shown in Figure 3.6, a spacecraft encounters several possible current fluxes in space. Surface potentials, relative to space, change in order to control the incoming currents and maintain the required current balance. In normal, quiescent conditions, the spacecraft is subjected to low energy plasma currents ($\approx 10^{-10}$ Amps/cm^2) which can generate secondary currents from the surface ($\approx 10^{-11}$ Amps/cm^2) [40]. Photoemission currents from sunlit surfaces are on the order of 10^{-9} Amps/cm^2. Since the sunlit current could be larger than the others, the surface potential would become slightly positive to maintain the required net zero current to the spacecraft. In a substorm, high energy electron currents ($\approx 10^{-10}$ to 10^{-9} Amps/cm^2) strike the spacecraft and drive the surfaces to large negative potentials.

In general, one may distinguish two types of spacecraft charging effects: absolute charging, where a potential is established between the spacecraft surface and the ambient plasma; and differential charging, involving a potential difference between adjacent surfaces of the spacecraft [40]. Absolute charging generally occurs in eclipse charging

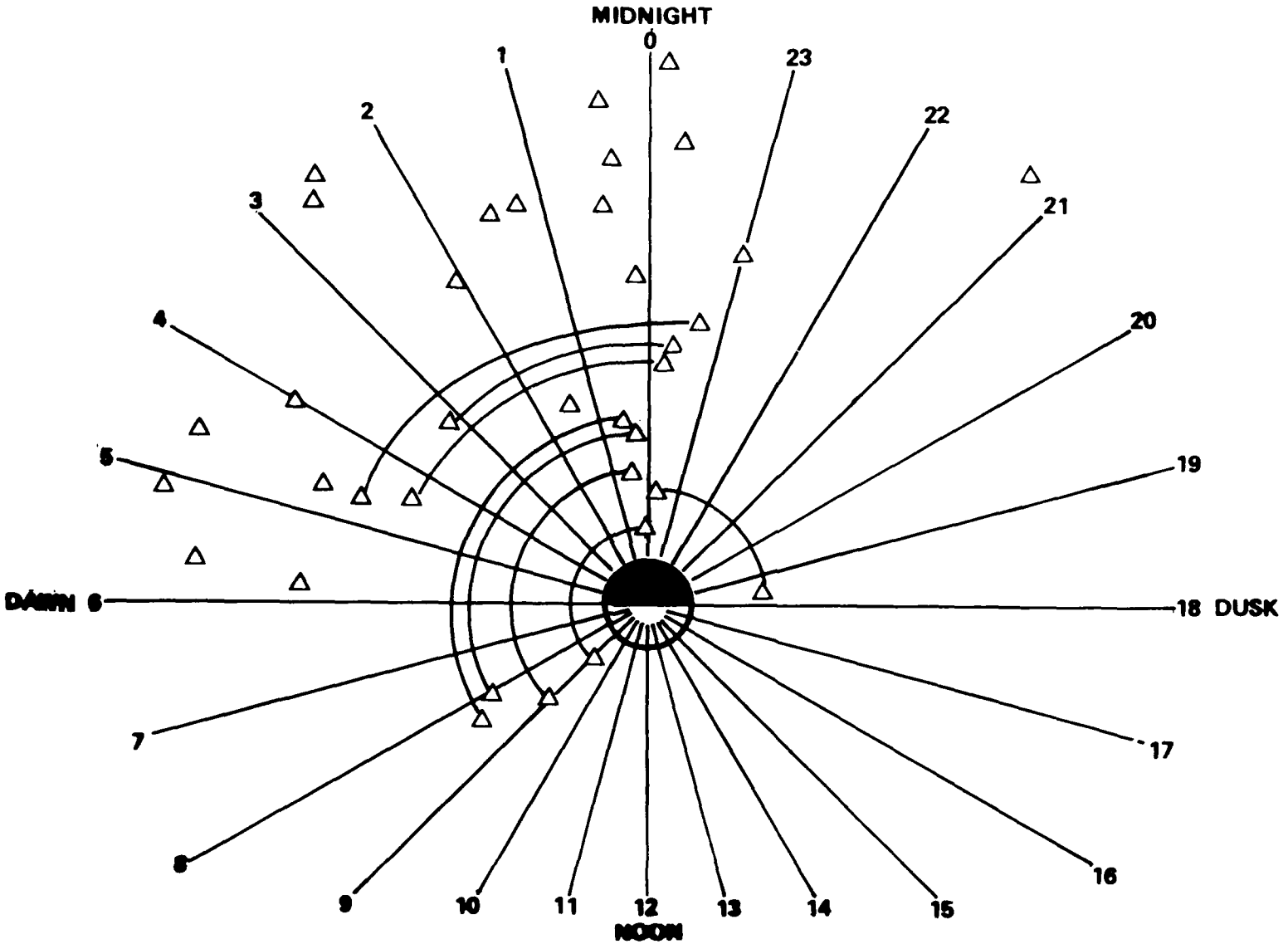

Figure 3.5 Occurrence of Satellite Anomalies in Local Time

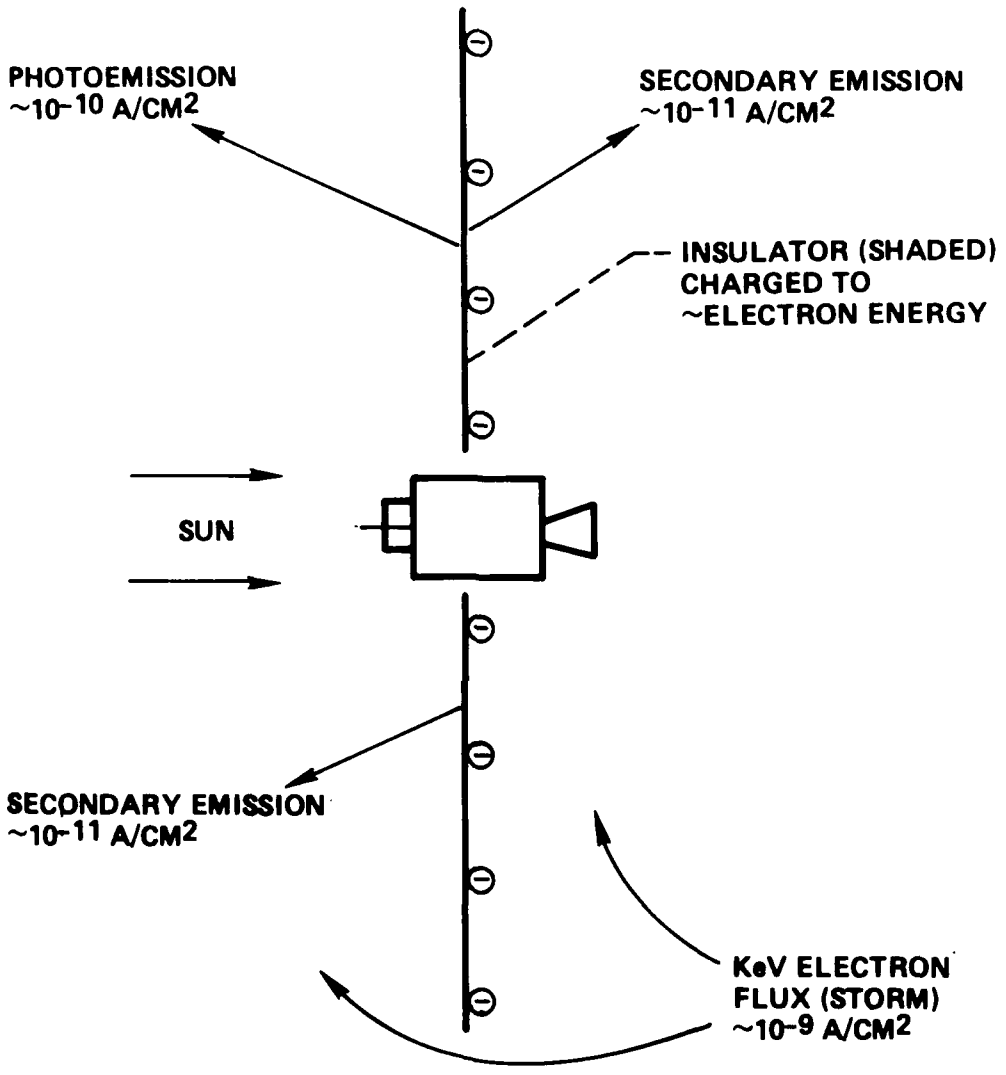

Figure 3.6 Spacecraft Charging

conditions and the potential follows the substorm intensity.

Differential charging arises because of different electrical properties between contiguous spacecraft parts (e.g. metal versus dielectric) or because of different ambient conditions (e.g. sunlit versus shaded surfaces) [41]. If this differential voltage exceeds breakdown thresholds, then arcing occurs (Section 3.2.2.1.4). This can produce transients which can couple into electrical circuits, resulting in on-orbit anomalies and failures. Differential charging also leads to potential barrier formation, in which the large electric fields from shaded dielectrics surround the spacecraft and deflect incoming charged particles, thus controlling the charging level of the spacecraft.

3.2.2.1.2 Modeling

Several analytical and numerical models have been devised to calculate surface potentials as a function of time and substorm conditions. These models range from one-dimensional representations for simple geometries and single materials to elaborate computer codes to predict the potentials in three dimensions (i.e. NASA Charging Analyzer Program or NASCAP).

In all cases the surface potential depends on the balance achieved by the sum of all currents striking the surface:

$$J_e + J_i + J_{se} + J_{bs} + J_{ph} + J_L + C_s \, dV/dt = 0$$

where:

J_e	= incident electron current density	J_{bs}	= backscattered current density
J_i	= incident ion current density	J_{ph}	= photoemission current density
J_{se}	= secondary emission current density	J_L	= leakage current density
dV/dt	= time rate of change of voltage	C_s	= dielectric capacitance

The currents collected by a surface change its voltage and this influences the collection of its neighbors. The NASCAP computer program compensates for these effects when making charging predictions of three dimensional objects [42-48]. Examples of models for both spinning and three-axis stabilized spacecraft are shown in Figures 3.7, 3.8, and 3.9 for charging under sunlight conditions [49].

The spin stabilized spacecraft (Figure 3.7A) must rotate to maintain its attitude. However, since the antennas must face Earth, this area is decoupled from the rotating cylindrical portion of the spacecraft. The antennas turn one full revolution per day. The three-axis stabilized spacecraft (Figure 3.7B) always has its solar arrays facing the Sun, while the body rotates one revolution per day to keep its antennas facing the Earth. The structure potential for spin stabilized spacecraft charging is less negative than the three-axis stabilized spacecraft, however, the differential charging appears to be about the same on both. The regions where equipotential contours are close together in the predicting charging level plots (Figures 3.9A & 3.9B) can be used to indicate possible breakdown sites.

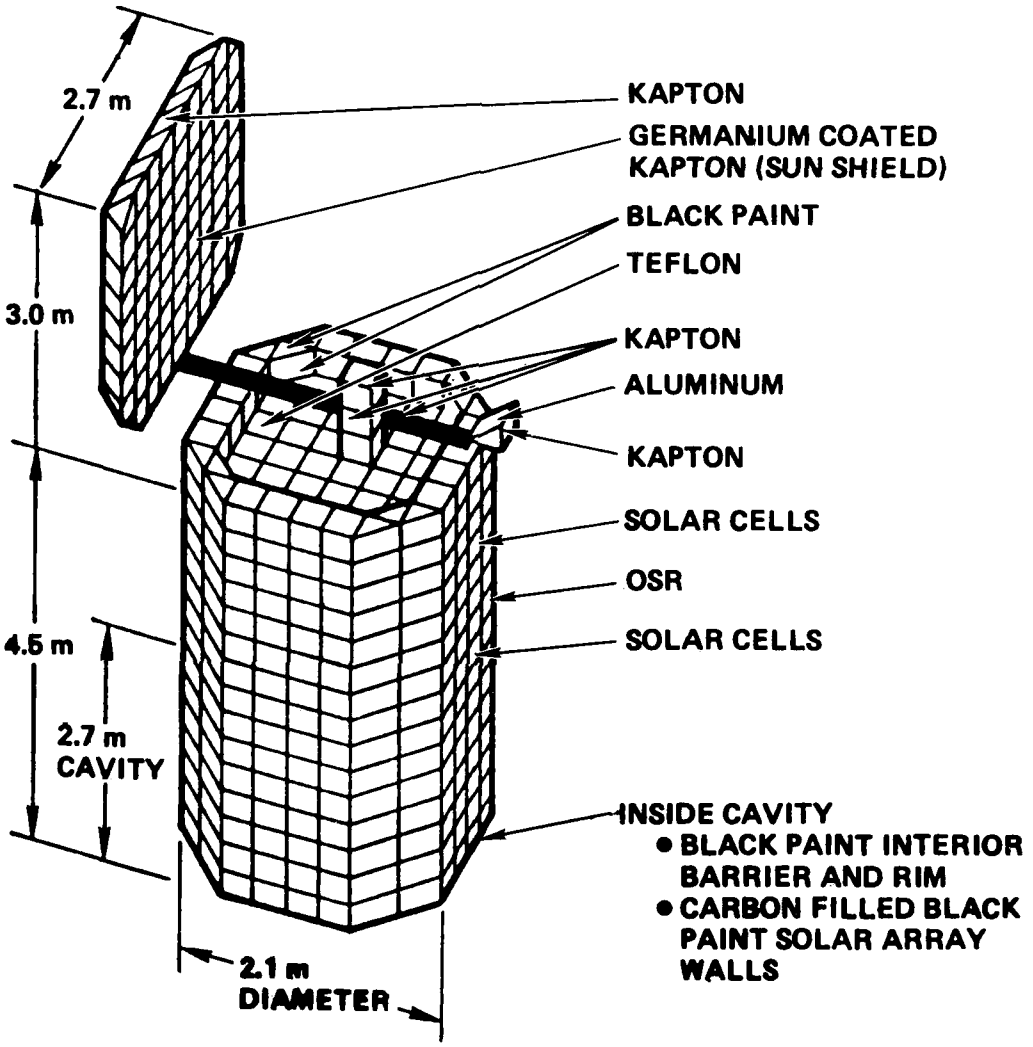

(A) Spin Stabilized Spacecraft

Figure 3.7 NASCAP Generated Satellite Model

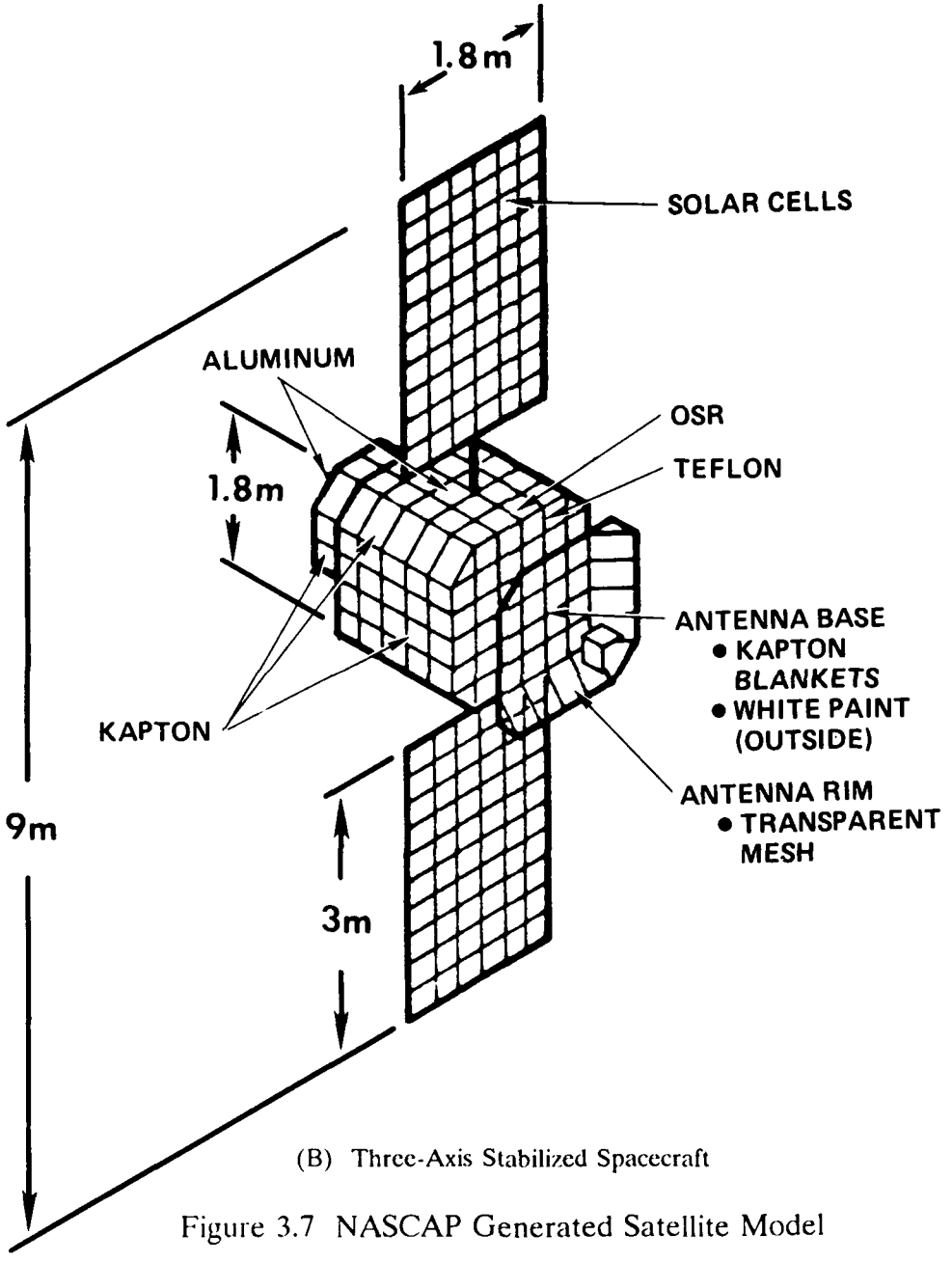

(B) Three-Axis Stabilized Spacecraft

Figure 3.7 NASCAP Generated Satellite Model

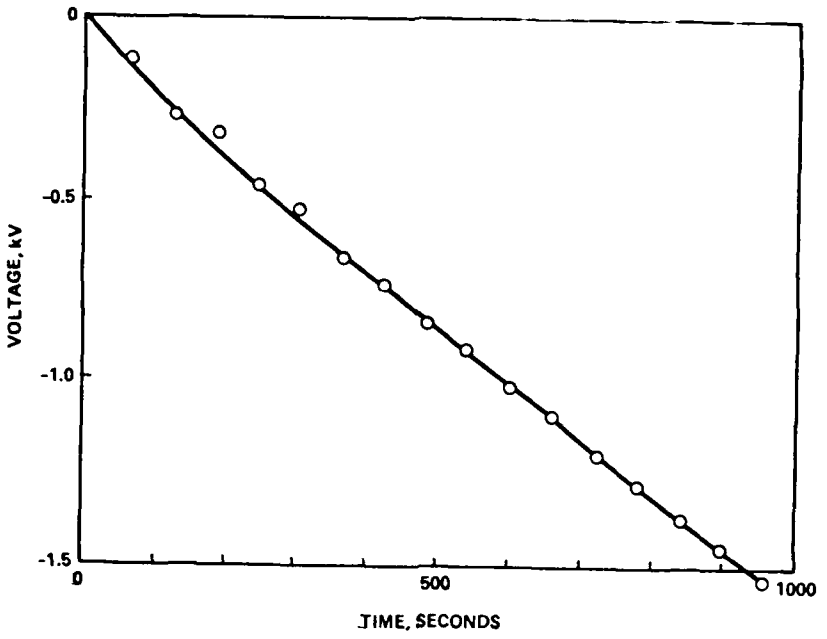

(A) Spin Stabilized Spacecraft

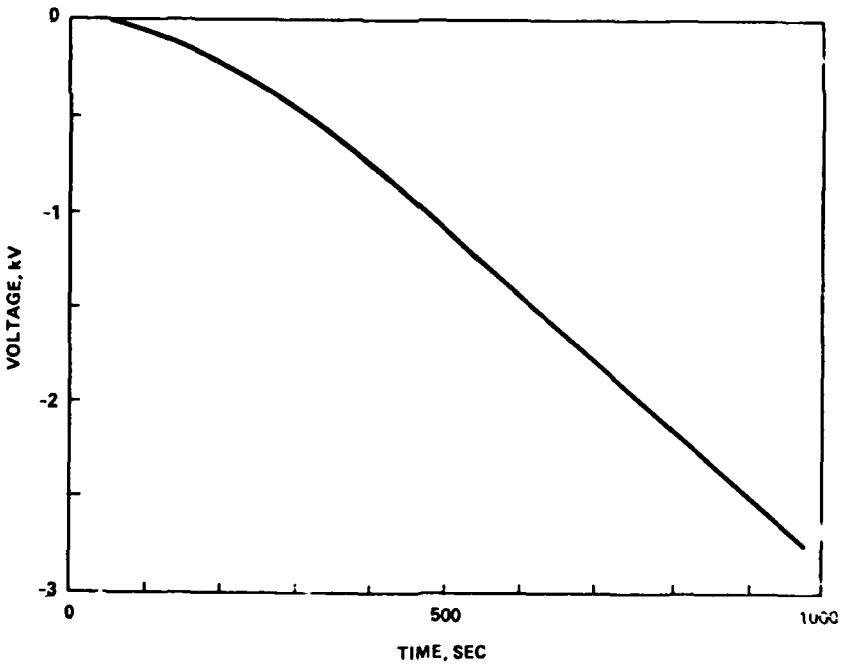

(B) Three-Axis Stabilized Spacecraft

Figure 3.8 Charging History of Spacecraft Ground

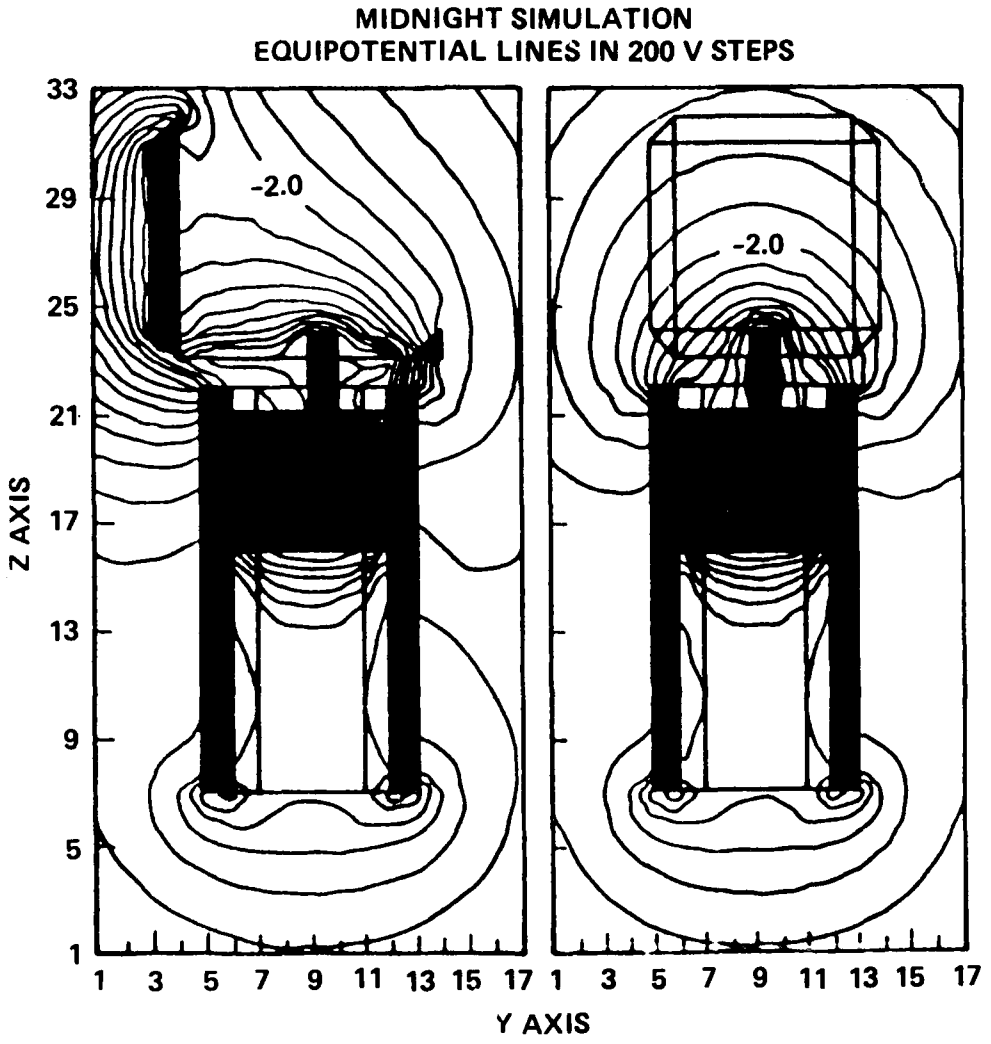

(A) Spin Stabilized Spacecraft

Figure 3.9 Predicted Charging Levels

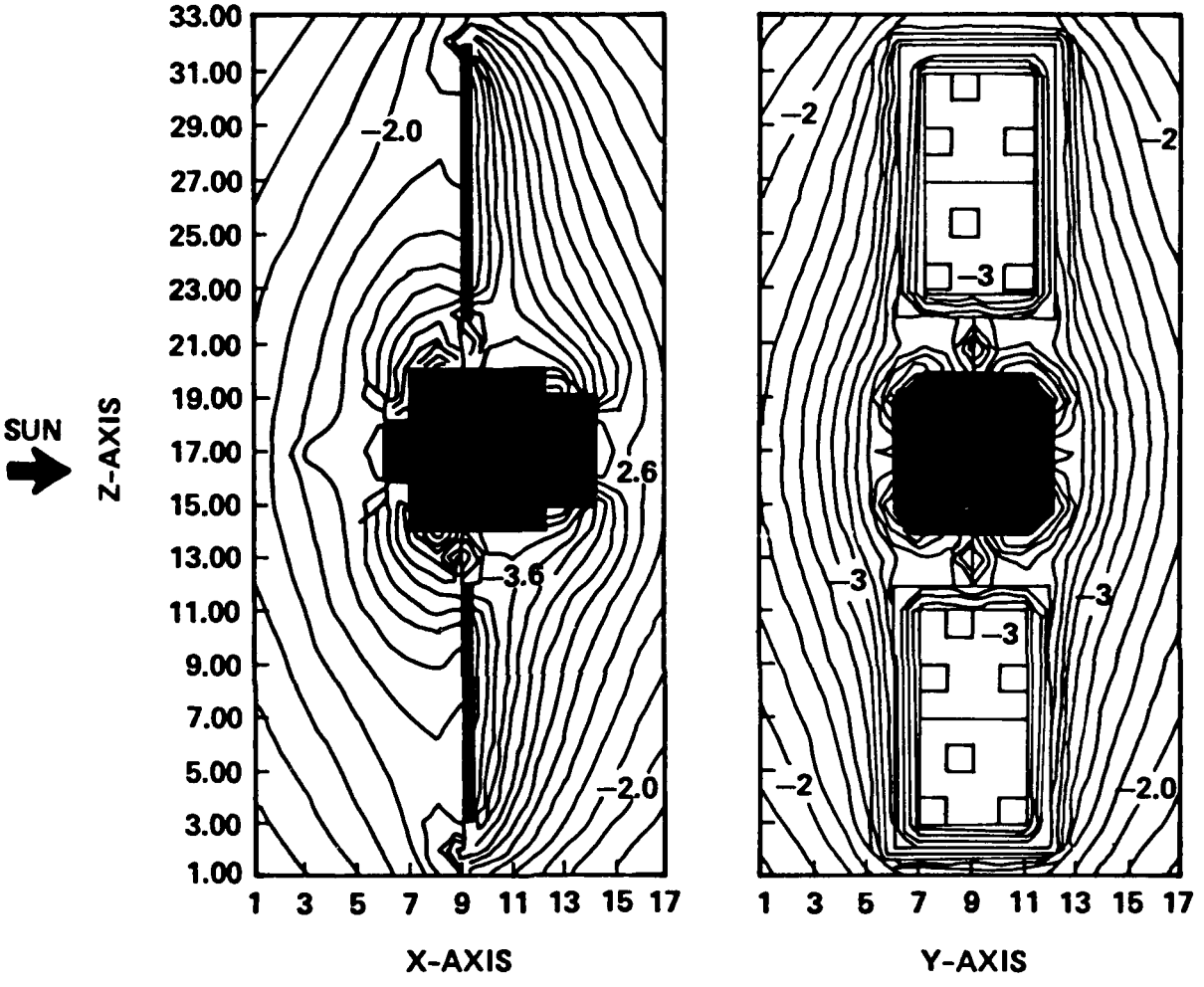

(B) Three-Axis Stabilized Spacecraft

Figure 3.9 Predicted Charging Levels

The NASCAP runs usually consume considerable computer time. Depending on the computer, this time requirement varies from one to several hours per run. There is a tendency to use one-dimensional models for "quick response" engineering answers [36]. These 1-D models yield answers quickly on microcomputer systems. Care must be taken, however, in interpreting the results of these fast, simplified modeling computations. There is usually no coupling allowed between the various surfaces and configuration and barrier effects are excluded. In addition, the simplified codes predict different time histories for charging materials.

Figure 3.10 illustrates the difference in predicted differential charging time histories using the NASCAP and 1-D Model codes. In this example, a shaded 2 mil thick piece of Kapton, from the previous three-axis stabilized spacecraft model, is subjected to a severe substorm and compared to the results of a 1-D code using the same environment. Note that surface resistance is not included in the 1-D model while it is included in the 3-D NASCAP model. The results show that the 1-D model would predict slower charging rates for Kapton than the NASCAP model. Thus, the simplified analysis could lead one to assume that there would not be a problem, when in fact one may exist. This illustrates the strong configuration effects that must be considered in these analyses and that quick-response codes do not necessarily predict worse case conditions.

3.2.2.1.3 Factors Influencing Charging

In addition to the spacecraft configuration effect illustrated above, several other factors can influence the charging levels achieved by geosynchronous spacecraft. Substorm intensity plays a strong role in the charging levels attained by spacecraft. This intensity can vary due to the solar cycle, the accelerating mechanism (still unknown at this time), or the variation within the dissipating substorm cloud. A minimum threshold level in substorm average intensity (as determined by the characteristic energy) has been reported to be necessary in order for spacecraft surfaces to be charged. For spacecraft designed and built in the 1970s, the substorm had to have a characteristic energy greater than 3 keV to cause significant surface charging [50]. Recently, a relationship between particle flux and charging has also been established [11].

Another factor influencing charging is photoemission from sunlit surfaces and shadowing. The predicted potentials for a three-axis stabilized spacecraft (Figure 3.11) encountering a severe substorm are shown in Figure 3.12 for both sunlight and eclipse charging events [51]. In an eclipse charging event, the potential profiles are initially uniform, indicating that the whole spacecraft charges as a unit. After a period of time, differential charging develops due to the different secondary emission properties of the various materials. At the end of the eclipse, when the spacecraft enters sunlight, photoemission current discharges the spacecraft as a unit.

The sunlit charging case, however, can create a more severe differential charging condition. If the dark side of the array is non-conductive (in this case, Kapton), it will charge to large negative values. The Kapton voltages then control the charging of the rest of the spacecraft by generating strong electric fields that eventually surround the spacecraft, limiting the fluxes incident upon the surfaces and thereby reducing the photo

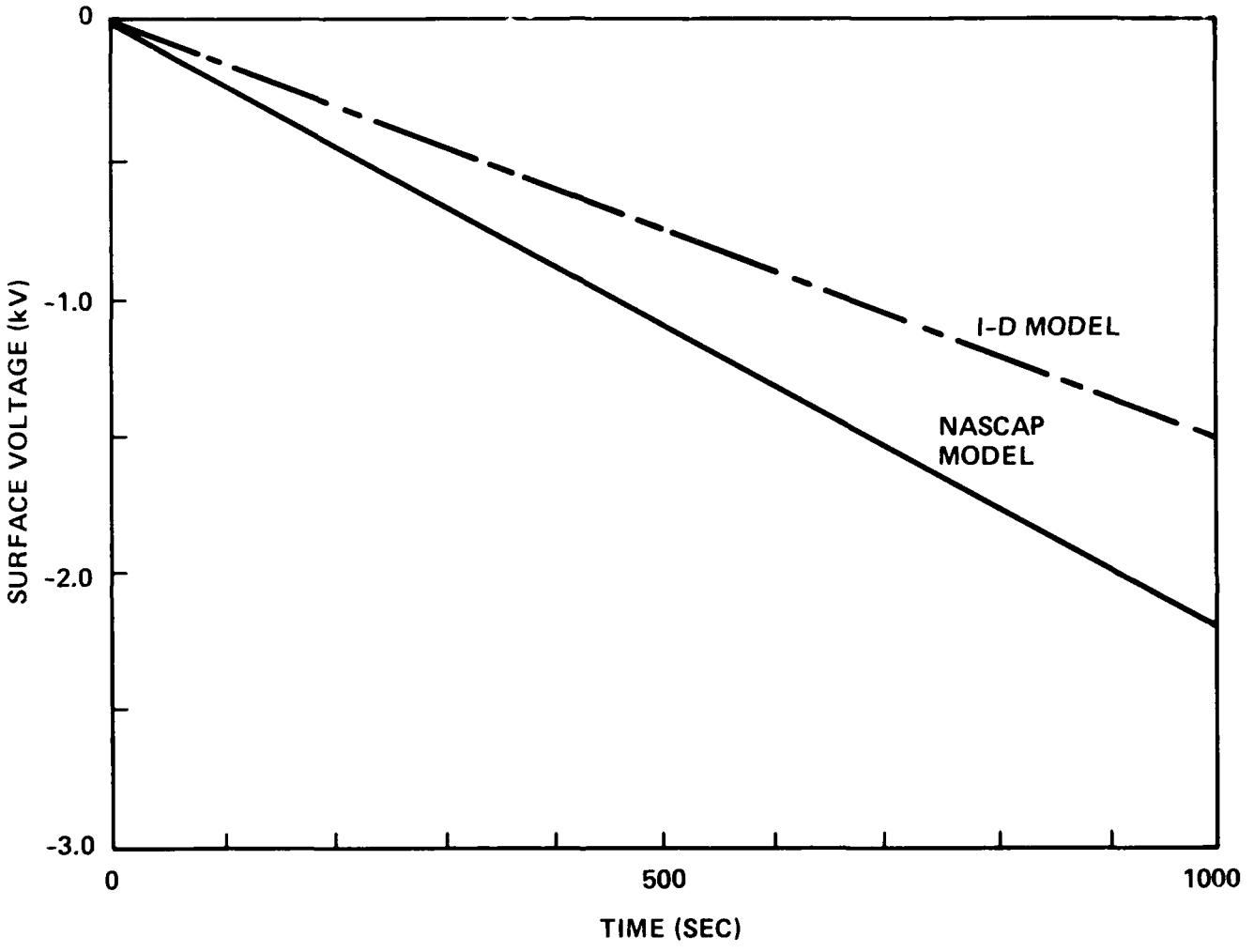

Figure 3.10 Differential Charging of 2 mil Kapton: Comparison of NASCAP and One-Dimensional Model Results

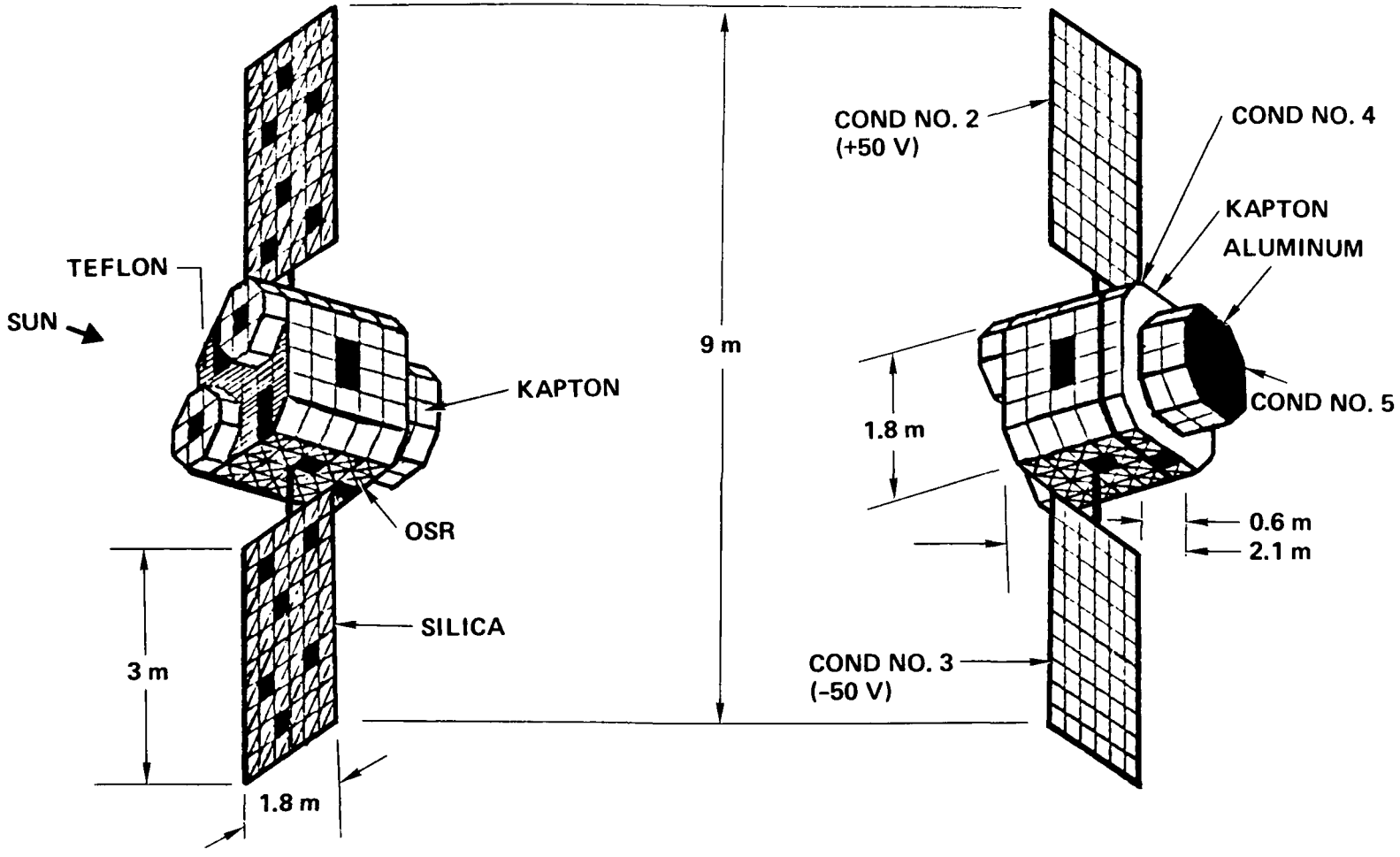

Figure 3.11 NASCAP Model of a Typical GEO Communications Satellite

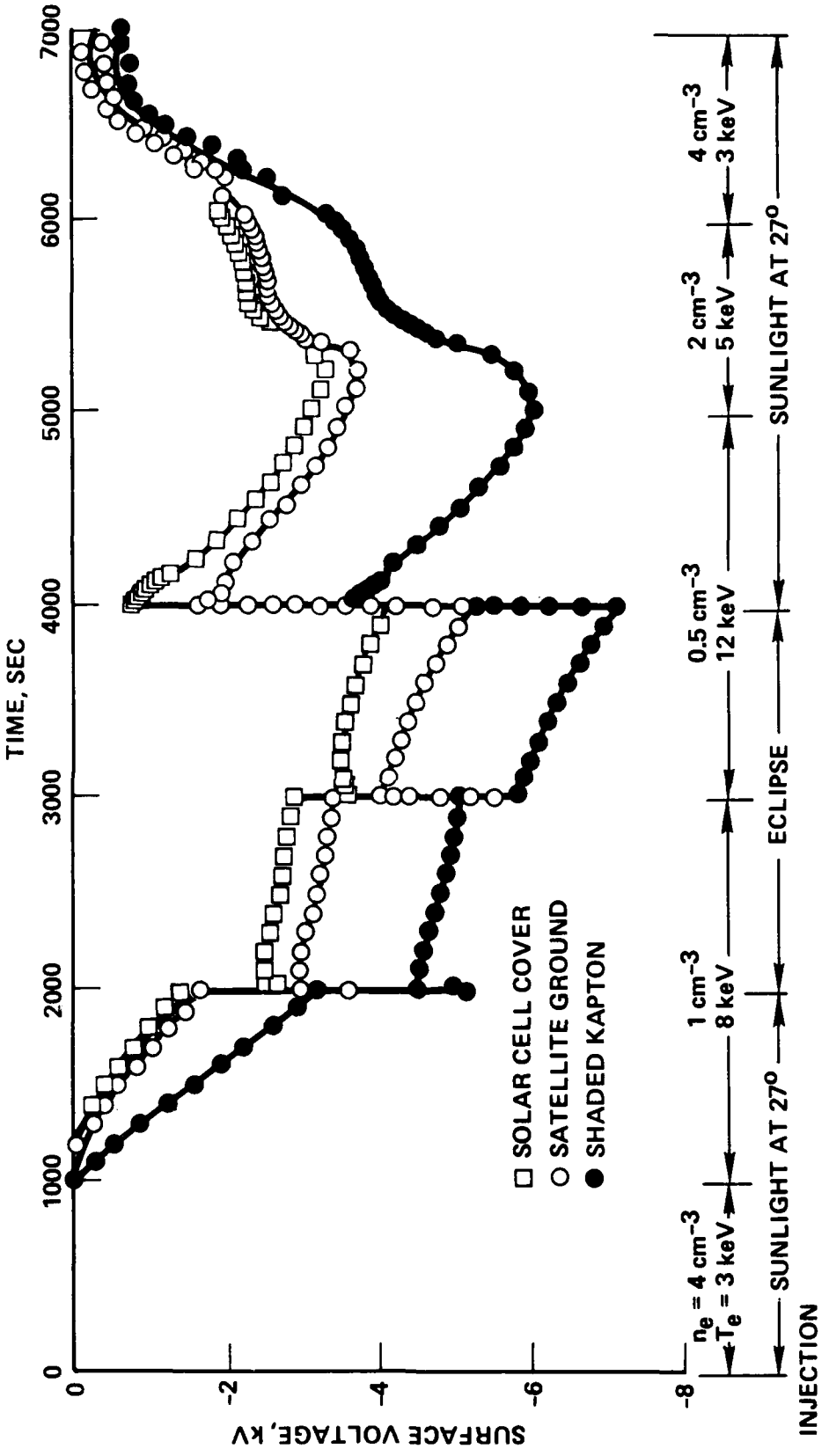

Figure 3.12 Typical NASCAP Results of GEO Satellite Charging

and secondary emitted currents from the surfaces. These shadowed portions of spacecraft surfaces can develop significant voltage differences, giving rise to discharges. The photoemission characteristics of sunlit surfaces are not well known [52-56].

As indicated previously, spacecraft stabilization can have an effect on the charging behavior in sunlight charging conditions. A spin stabilized spacecraft will rotate in sunlight such that the cylindrical sides will be sunlit and only the ends will be shadowed [40]. This will result in negative structure potentials of a few hundred volts. Dielectrics not in sunlight, however, can charge to their characteristic levels, resulting in strong gradients through the dielectrics. The three-axis stabilized spacecraft, on the other hand, could have structure potentials that reach -2000 volts. The dielectrics will still charge to their characteristic levels, possibly resulting in a less severe voltage gradient through the dielectric. In eclipse, both types of spacecraft will charge as units in the initial phases of the substorm encounter.

The properties of spacecraft surface materials also have an effect on spacecraft charging potentials. The conductivity and the secondary yields of the dielectric surfaces all affect the current balance and, hence, the surface potential. The change from 5 mil to 1 and 2 mil thick dielectrics in the present day spacecraft increases the leakage through the dielectric and reduces the differential voltage attained in a given substorm (Figure 3.13).

Another means of limiting the surface potentials is by controlling surface resistance to provide an additional leakage path. This must be done by bringing a ground plane to the surface to prevent charge build-up at the edges of dielectrics. Dielectric coatings, like paint (surface resistivity $\approx 10^{10}$ to 10^{11} ohms/m^2), can be used to increase the current leakage from the surface to the structure, thereby lowering the differentials. Figure 3.14 illustrates the effect of surface resistance on surface potentials.

The effect of spacecraft size on the levels of charging was first evaluated by comparing the charging levels observed on ATS-5 with those observed on ATS-6 during simultaneous substorms and eclipse charging events [32]. ATS-5 (Figure 3.15) was a spinning satellite about 1.3 m in diameter and 2 m in length. ATS-6 (Figure 3.16) was a stabilized satellite in which the end-to-end solar array dimension was 16.5 m. The near-cubical spacecraft housing module, which supported the 9.1 m parabolic reflector, was about 1.6 m on a side. Both satellites had similar particle detection instrumentation to determine their structure potential in substorms. Since this was eclipse charging, it was anticipated that the different stabilization of the two spacecraft would not influence the charging levels. It was found that both vehicles charged to the same value in eclipse charging events, although ATS-6 was $\approx$ 5 times larger (Figure 3.17). Presently, there has been no attempt to determine if the charging levels of future, large, high-powered satellites would be different from present-day satellite levels.

3.2.2.1.4 Discharges

As stated previously, when the surface voltage exceeds a threshold, discharges can occur [56-64]. These discharges may occur because of a gradient between the dielectric

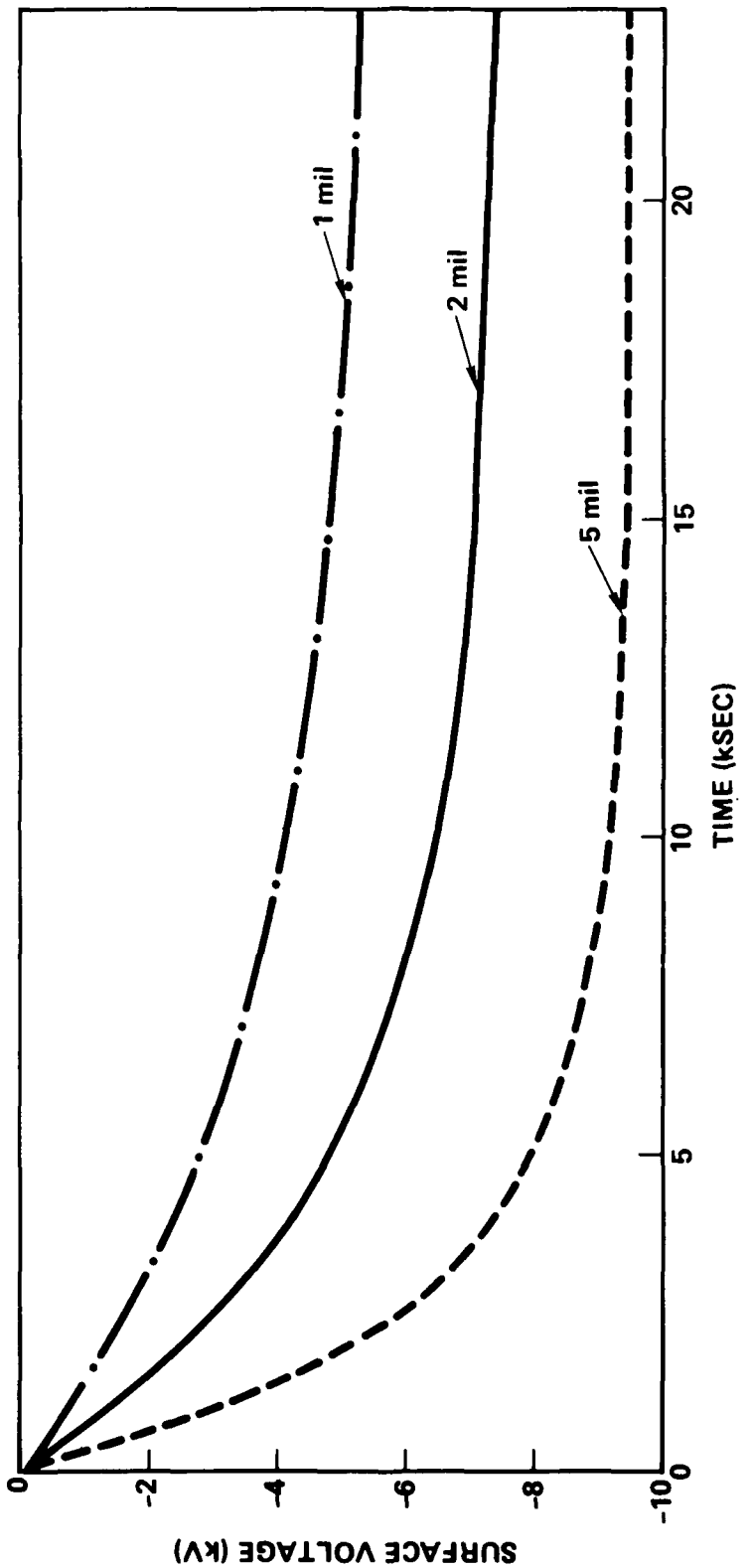

Figure 3.13 Effect of Dielectric Thickness on Charging (Severe Substorm)

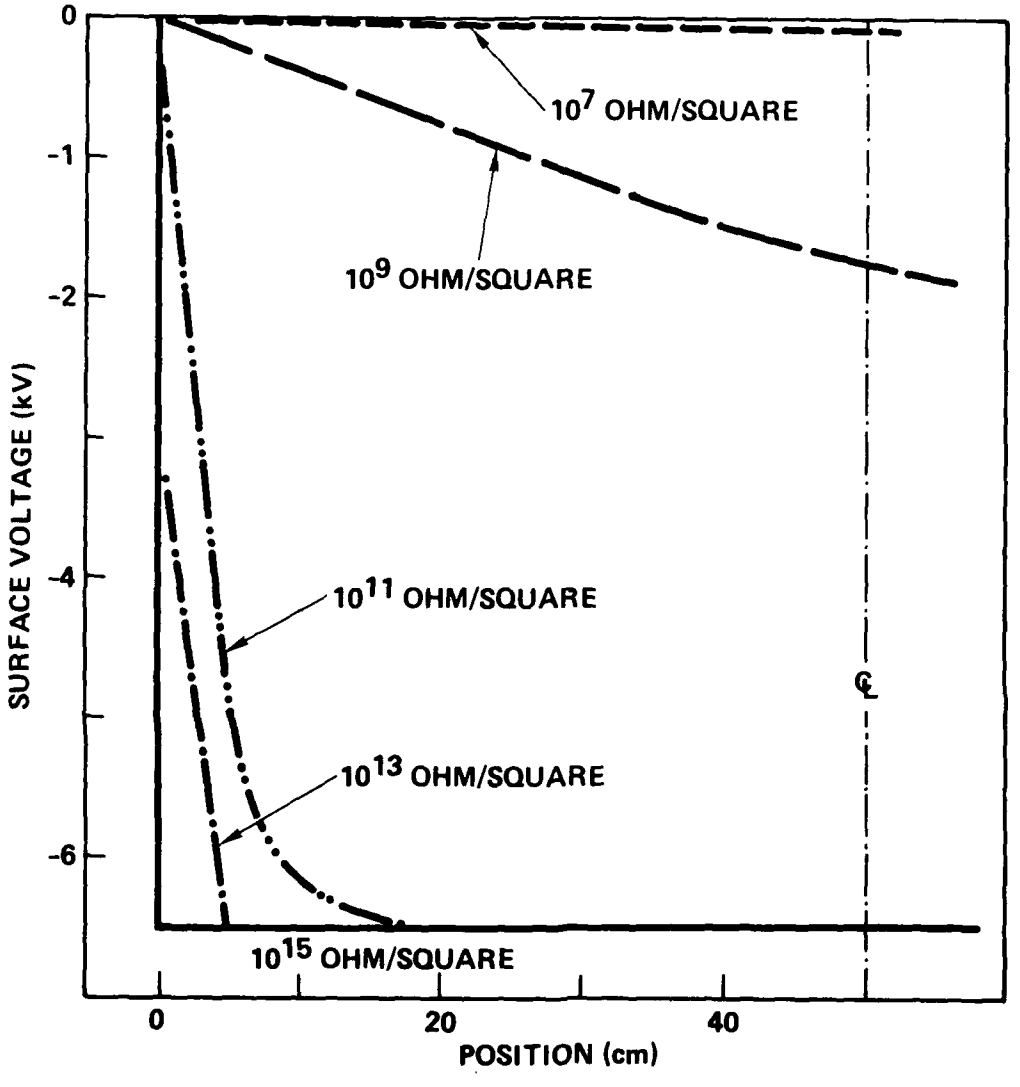

Figure 3.14 Effect of Resistivity on Voltage: 2 mil Kapton (Severe Substorm)

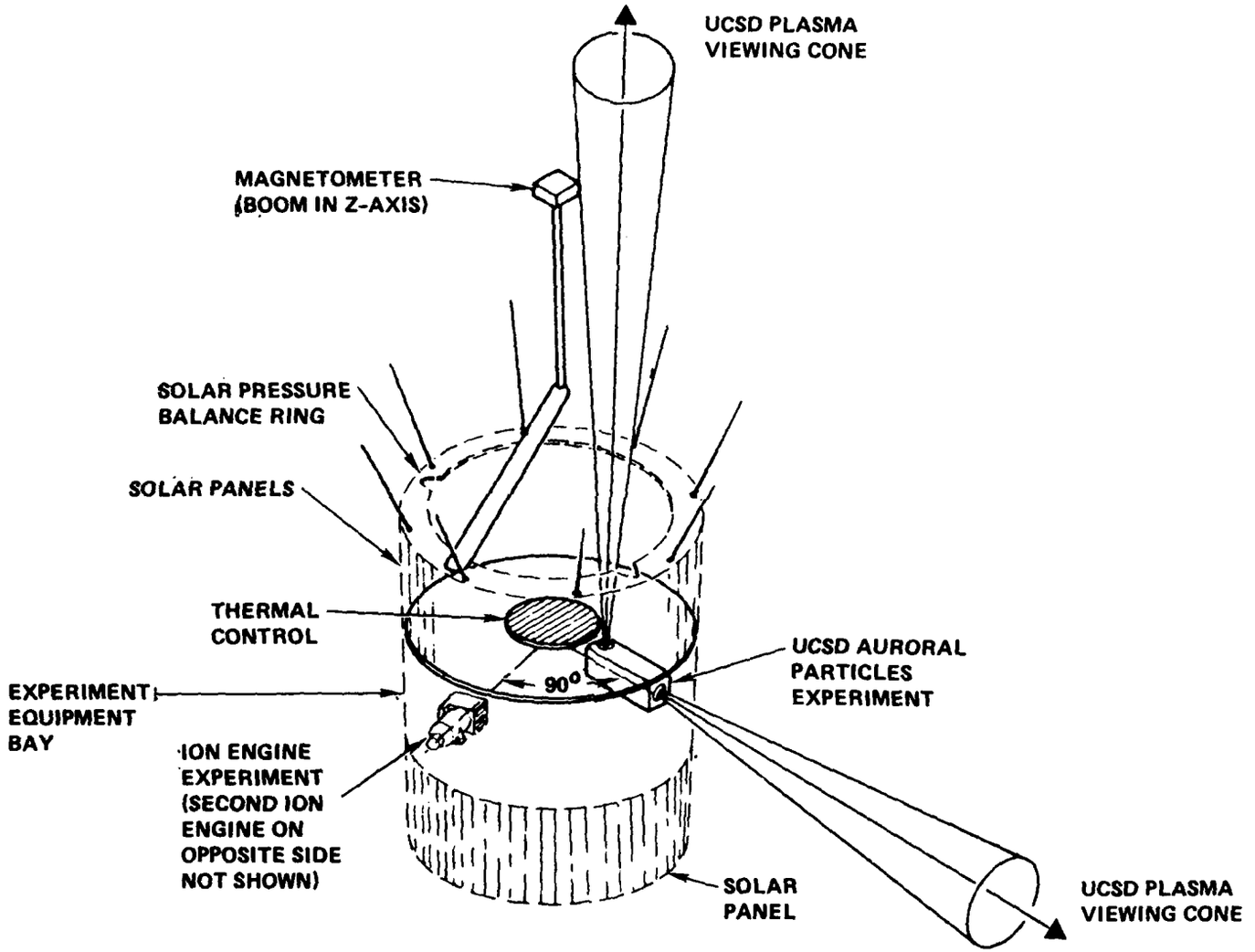

Figure 3.15 ATS-5 Spacecraft

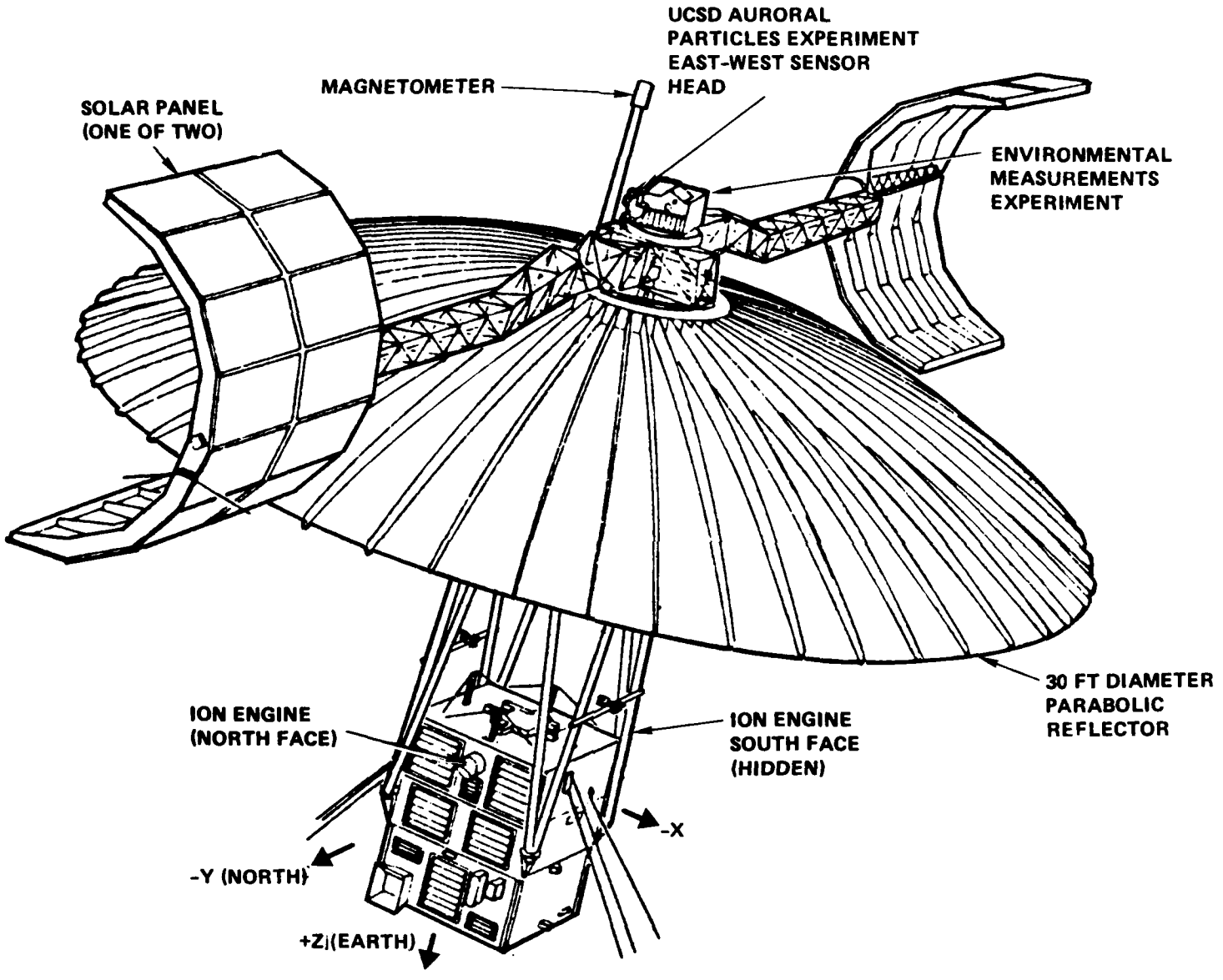

Figure 3.16 ATS-6 Spacecraft

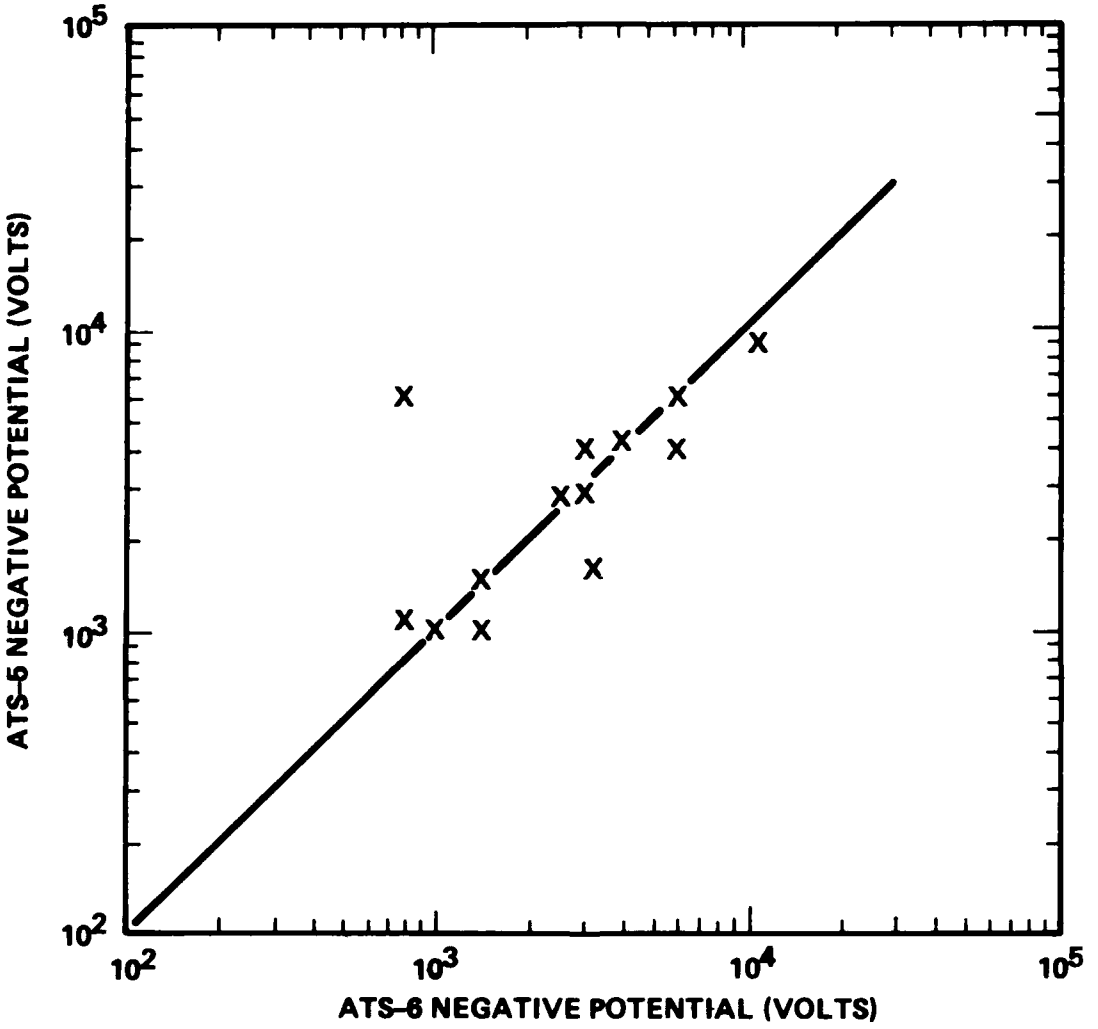

Figure 3.17 ATS-5 and ATS-6 Eclipse Charging Levels

surface and the substrate below (primarily in gaps, edges, or through imperfections in the dielectric) or from gradients between surfaces. This discharge process was first illustrated in a laboratory test using a Defense Systems Communication Satellite (DSCS II) communications antenna (Figure 3.18). A metalized mylar sheet was charged with a power supply until a discharge occurred. While the charging process in this test was not the same as occurs in space, the test was valuable because it demonstrated that discharges seek out openings and imperfections to complete a circuit. Note the discharge attachment points in the folds of the thermal blanket and at the antenna edge openings.

A discharge in space causes a change in charge distribution [18]. It is currently believed that electrons are ejected into space rather than being injected into the structure. This belief is based upon the fact that the voltage gradients between the various elements on the spacecraft surfaces are at relatively low differential values (< 5 kV) if the surfaces are strongly coupled to the structure (i.e. all metal and metalized surfaces are well grounded). There is no evidence that such small gradients can result in breakdowns to the structure. Electron loss to space triggered by relatively low voltage gradients, however, has been shown to occur.

The discharge process involves the following steps [18]: (1) A discharge is triggered and electrons are ejected to space; (2) Locally, the surface voltage changes since there is charge lost and the capacitance to space is fixed; and (3) Currents flow in the structure to neutralize dielectric polarization charges at the discharge site. Discharges initiated by surface charging are assumed to occur under the following conditions (Figure 3.19): (1) If a voltage gradient greater than 2×10^5 V/cm exists between the dielectric surface and the metallic substrate (It is assumed that the breakdown will occur at a dielectric edge); (2) If a metal surface is at least 1000 volts more negative than the surrounding dielectric surfaces; or (3) If an isolated metalized dielectric is at least 1000 volts more negative than the adjacent spacecraft structure (This type of breakdown transfers charge directly to the spacecraft).

3.2.2.1.5 Coupling To Systems

It is known that the substorm environment can charge spacecraft surfaces until discharges are possible. The problem, though, is how does the discharge transient couple into the spacecraft system? Coupling has been addressed but has not been adequately treated in charging studies to date [65-68]. An attempt at modeling the coupling phenomenon for a flight program was conducted for the Voyager program using an EMC code called Specification and Electromagnetic Compatibility Analysis Program (SEMCAP) [69,70]. The program predicted which systems would upset and led to numerous design changes that significantly hardened the spacecraft to discharge transients. SEMCAP was also used to predict voltages induced by test arcs. On average, the predictions underestimated the induced voltages by 6 dB, and the standard deviation between the measured and predicted voltages was about 20 dB. This discrepancy indicates that coupling analysis results can only be used for qualitative design guidance.

There are two possible mechanisms that will allow coupling into the system [1,71-72]. The first is that the transient couples via a direct radiative path from the

Figure 3.18 Discharge on DSCS II Antenna

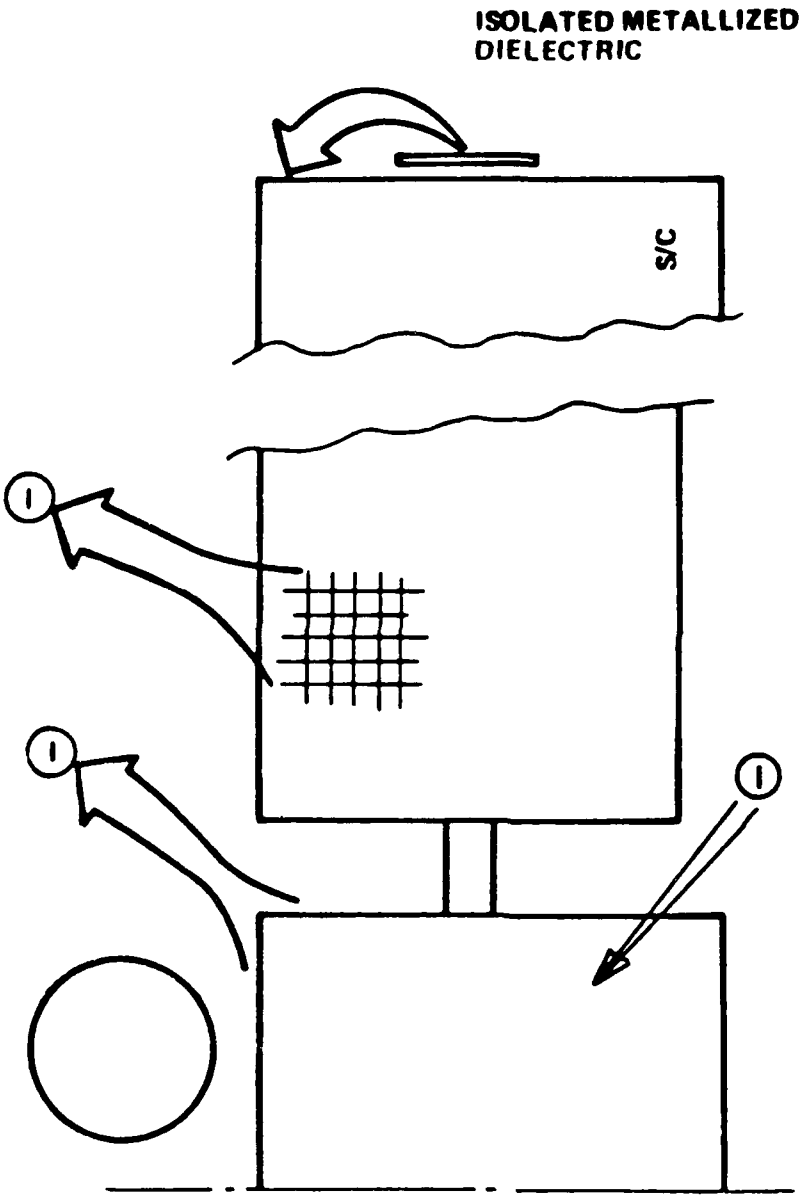

Figure 3.19 Discharge Process

discharge site to a device that transports the energy into the system (Figure 3.20). This requires either a coupling antenna or an opening into the vehicle.

The second mechanism requires a current to flow in the structure. The current generation concept can be explained as follows. Charge loss or transfer means that the voltage of the structure relative to space must change. Present-day spacecraft are capacitively coupled to space with a value of about 10^{-10} Farads. Since this capacitance value is fixed, a charge loss will cause a change in voltage potential transient. The voltage transient then induces skin currents to flow within the structure. The magnetic field generated by the currents could then couple to the spacecraft wiring harness, inducing transients in the electrical circuits. In addition to the conducted transients, there is the possibility that the radiated component from the discharge may couple into antennas on the spacecraft and enter their circuits. In either case, the transient traveling in the electrical system could produce a signal causing the anomaly in the electronics logic. Since substorms can occur frequently in geosynchronous orbits, pulsing in circuits may happen often and eventually overstress a component, possibly leading to failure.

Circuit analysis, using a lumped element modeling technique, has been applied to spacecraft [49]. Such computations indicate that AC impedance in the structure is significant. This can result in different parts of the structure being at different potentials. Figure 3.21 illustrates the structure transient response to a 2 μC discharge occurring on the communications antenna of a three-axis stabilized spacecraft.

3.2.2.2 *Dielectric Bulk Charging*

3.2.2.2.1 Background

As a result of the SCATHA experiments, it became apparent that not all charging/ discharging events were due to surface charging phenomena. Discharges were occurring when the surface charge monitors indicated no charge. It is now believed that these transient events on SCATHA are the result of charge deposition within dielectric materials [21]. Substorm measurements indicated that there was a sufficient flux of high energy particles to cause this deposition. It is believed that satellites are still experiencing upsets from this type of charging [4,73].

Bulk charging, resulting from charge particles being deposited within dielectrics, can pose a significant hazard if the leakage rate within the dielectric is low compared to the incoming flux. The charge decay time constant may be as much as several days for materials with resistivities as high as 10^{15} to 10^{18} ohm-cm. It is thus possible that charge buildup can occur over many days, even though the incoming flux varies over the orbit period. It should be emphasized here that internal charging of dielectrics is a flux dependent effect, because of the leakage, and is not simply a function of the integrated flux, effluence, or dose. Buried charge discharges, either to space or the structure, would produce a similar response in the spacecraft as do surface discharges. These discharges could also result in damage to dielectrics.

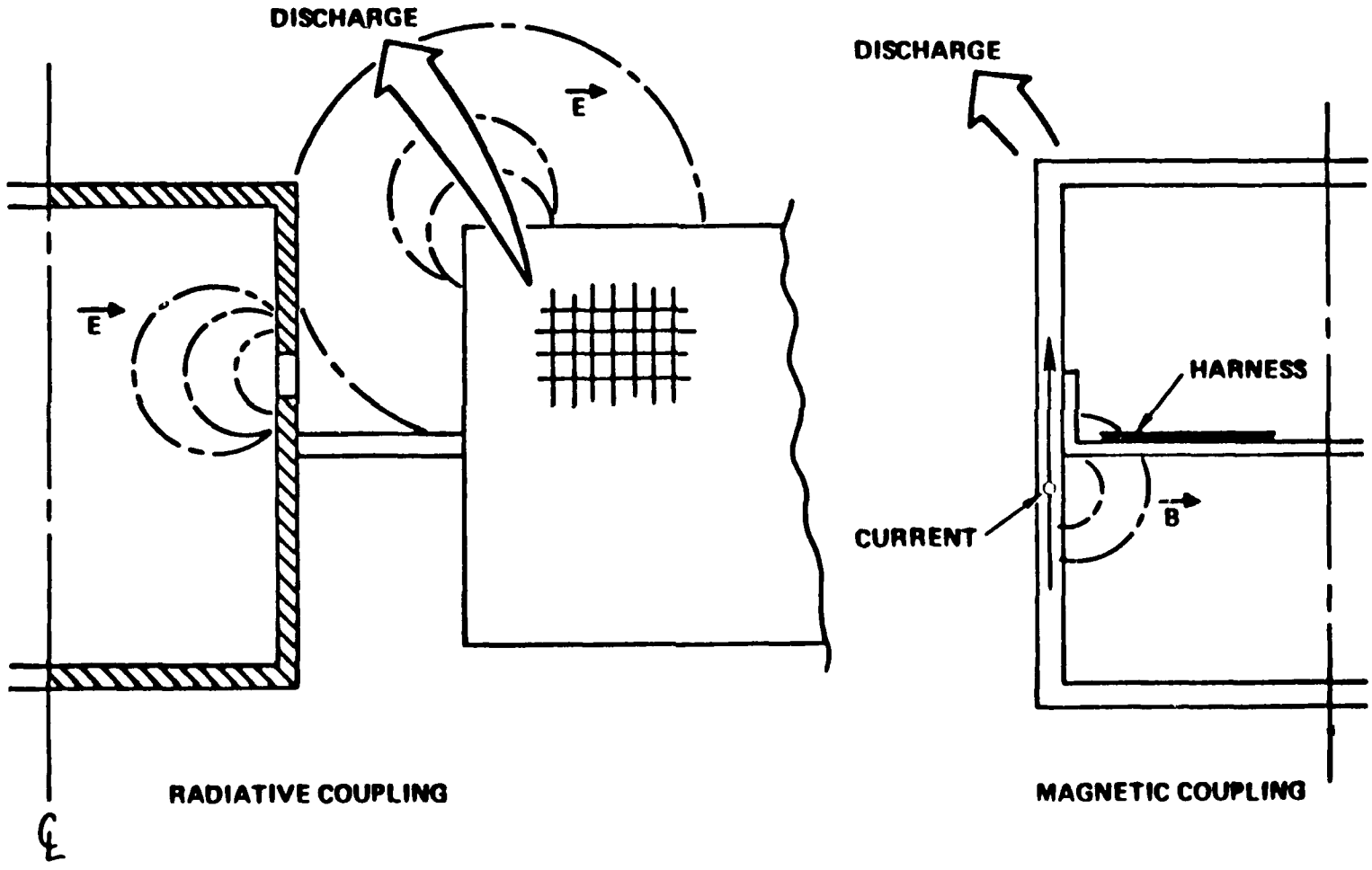

Figure 3.20 Discharge Coupling Processes

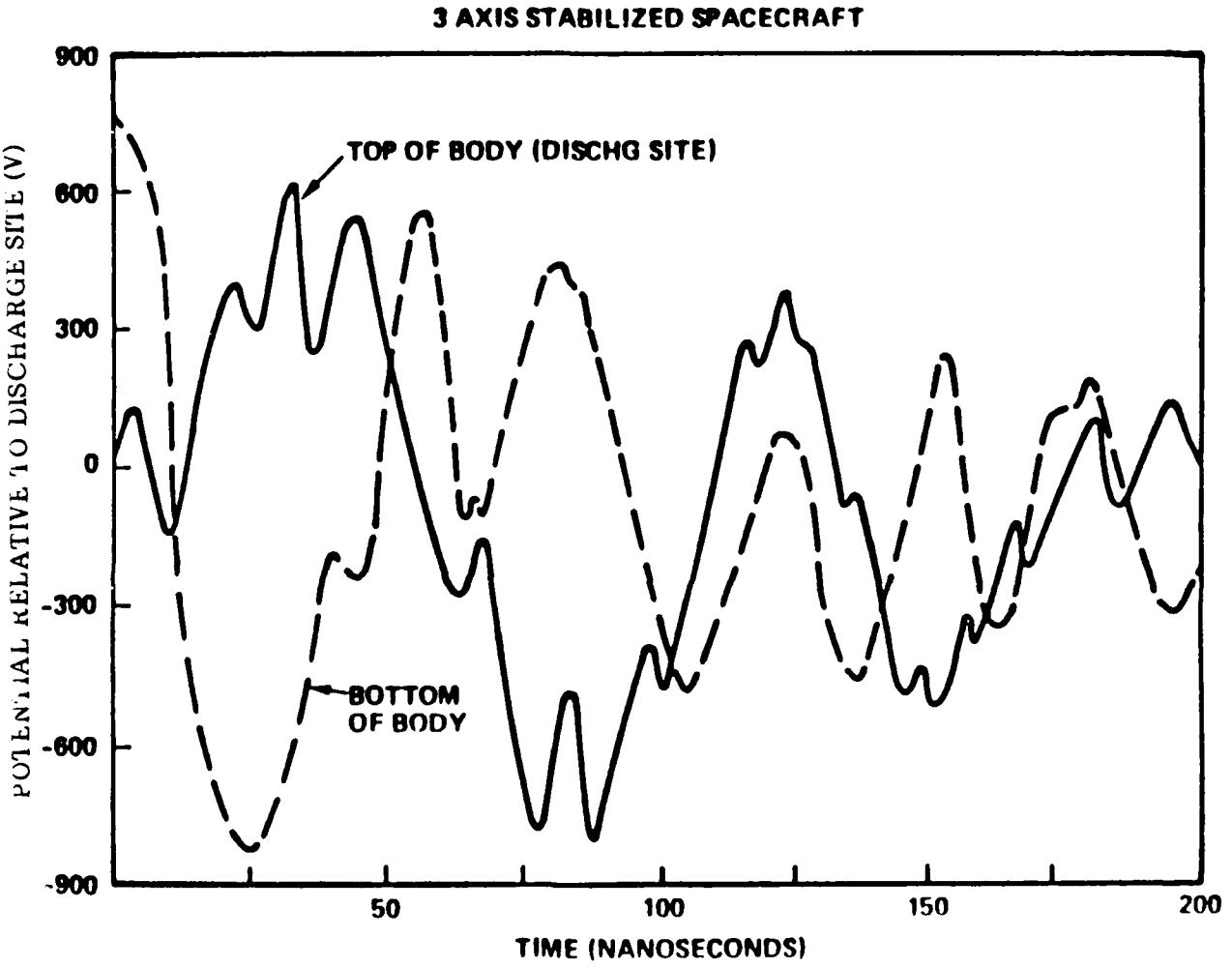

Figure 3.21 Predicted Structural Potentials After 2 μC Discharge (Antenna)

3.2.2.2.2 Modeling

The bulk charging phenomenon has been studied for years in laboratory simulations using monoenergetic electron beams [74-83]. The classic experiment, conducted in a vacuum, uses a dielectric sandwiched between two thin metal electrodes (Figure 3.22). Both electrodes are usually grounded. One electrode is then irradiated with high energy electrons, and the current to ground is measured from the other electrode. From this information, the electric field (E) and the charge distribution (ρ) within the dielectric is deduced. These quantities are determined from Maxwell's equation and the continuity equation:

$$\frac{\partial E}{\partial x} = \frac{\rho}{\epsilon} \quad ; \quad \frac{\partial \rho}{\partial t} + \frac{\partial J(x)}{\partial x} = 0$$

where: $J(x) = J_D + \sigma E$ $\qquad \sigma = \sigma_o + K\,[dD(x)/dt]^n$

$J(x)$ = total current $\qquad J_D$ = electron deposition current

ρ = charge density $\qquad \epsilon$ = dielectric constant

σ = conductivity $\qquad \sigma_o$ = dark conductivity

$[dD(x)/dt]$ = radiation dose rate $\qquad K, n$ = constants

The source terms for the calculation of the field and charge distributions are the electron deposition current and the dose rate. This set of equations is usually solved by elaborate transport computer codes. Typical results are shown in Figure 3.23. Such numerical calculations have been shown to be in agreement with measured values for these experiments. The results indicate that, depending upon the incident particle flux and energy, electric fields and charge distributions can build up either towards the front or back of the sample.

The modeling of this phenomenon is still underway. Tests have been conducted with exterior surfaces not electrically connected to the spacecraft conducting frame. The results are being compared to the model predictions. The correlation between mono-energetic beams and substorm energetic electrons has not been completed. To quantify the effect of a discharge from electron deposition, the charge lost must be specified. This value is not known at this time.

3.2.3 Research Maturity Rating

The research maturity for high altitude, geosynchronous charging, for both theory and experiment, was rated CONSIDERABLE (4). The rationale for this judgment is that spacecraft charging effects have been investigated for the past 10 years by the US Air Force and NASA and considerable information has been amassed. The substorm energetic particle environment has been catalogued, "worst-case" substorm plasma and particle values defined, and statistical models of the occurrence of substorms developed. A spacecraft charging analytical computer modeling tool called NASCAP has been developed by NASA and the Air Force to predict geosynchronous surface charging. Models are being developed to compute bulk charging effects. Extensive ground simulation procedures have been developed to characterize new spacecraft materials.

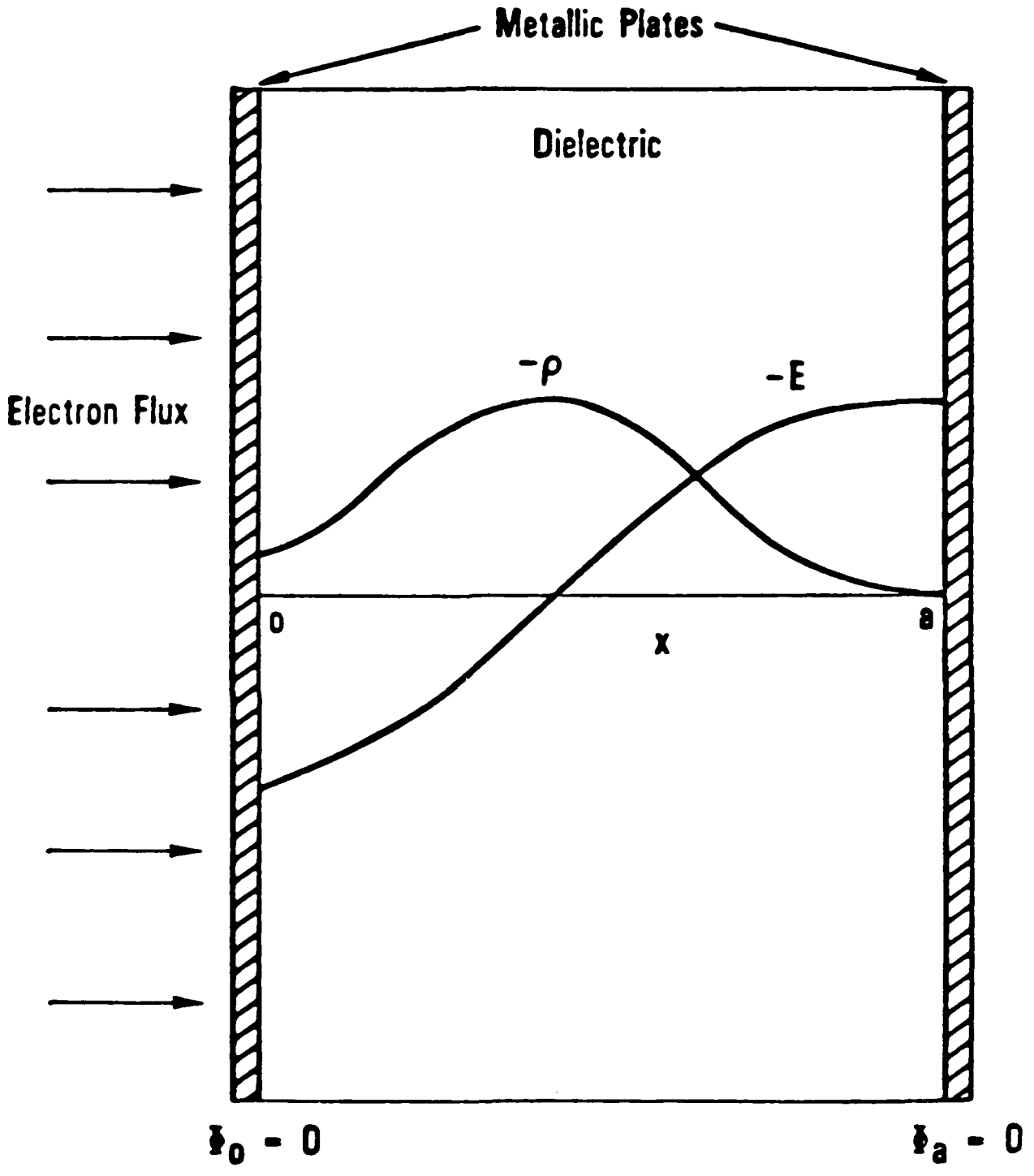

Figure 3.22 Monoenergetic Beam Dielectric Charging (Typical Results)

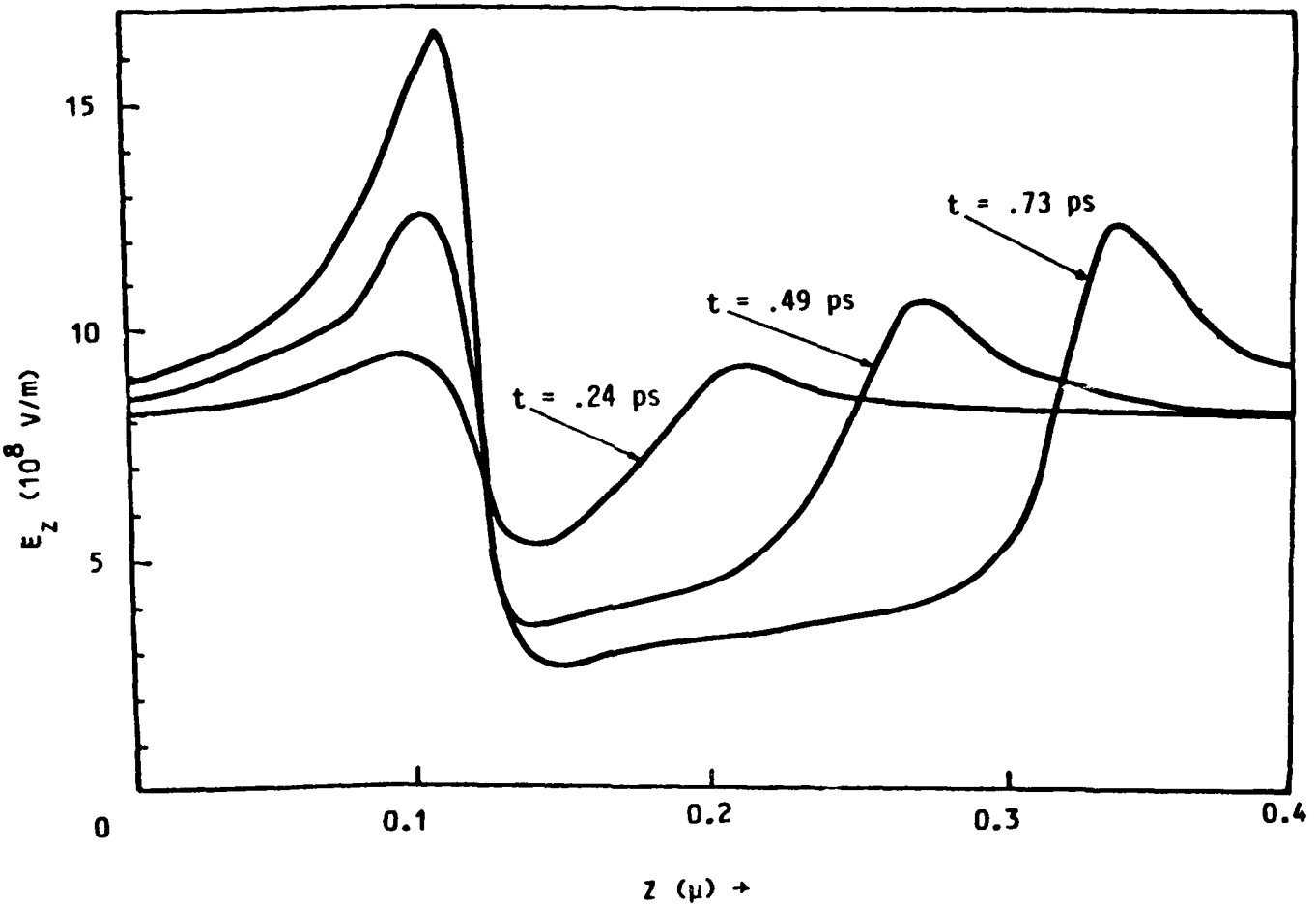

Figure 3.23 Electric Field vs Time (Teflon)

Test procedures have been developed (but not as universally adopted) to test spacecraft for susceptibility to electrical transients from arc discharges. Finally, a Spacecraft Charging at High Altitude (SCATHA) flight experiment continues to provide data on the characteristics of this phenomenon. The rating would have been COMPLETE (5) if the details of the coupling mechanisms, for transferring the effects of arc discharges on the spacecraft surface into interior harnesses, were more firmly established.

3.2.4 System Impact Rating

There are three basic system impacts or hazards arising from high altitude charging interactions in geosynchronous orbit. First, the discharges resulting from both surface and bulk charging can couple into the electronic system as an electromagnetic noise source and produce anomalous switching. These switching events generally occur in the attitude control systems, communications systems, and occasionally in the telemetry system. There is evidence that the discharge transient can be severe enough to cause a component failure. What is uncertain at this time is whether or not a failure results from a single encounter or as the result of an accumulated response to a large number of discharge transients over a long period of time. The recorded failures generally occur only after a few years of operation. Regardless of the mechanism, the component failures noted to date have resulted in degraded satellite capability (even mission failure).

The second hazard is the degradation of surface properties due to discharges. The discharge process can cause loss of materials, especially metal films and adhesives, resulting in changes in the electro-optical properties of the coatings over a long period of time. This can result in the spacecraft operating at different, usually higher, temperatures than anticipated.

The third hazard results from the surfaces being charged. Surface charging can enhance contamination by attracting back any ionized or ionizable contaminants which can then adhere to the surface. One possible result is increasing solar absorptance, causing a rise in surface temperatures and eventual overheating of the spacecraft. There apparently is no way to cause a temperature decrease by contaminating a surface. Charging can also influence the behavior of instruments. Sensor optics can be coated by the contaminants, decreasing sensor operational capability. Finally, scientific instruments can provide erroneous data when their reference ground potential has an unknown bias.

The impact of all of these hazards was rated CONSIDERABLE (4). This rating was based upon the fact that a majority of spacecraft charging events are considered correctable nuisances rather than catastrophes. Agreement on the impact of charging is further complicated by the great difficulty in proving that charging was in fact the initial cause for any anomalies. Even in cases where the system or satellite failed, there have been other possible explanations besides spacecraft charging.

3.2.5 Mitigation Techniques

Several possible passive mitigation techniques to reduce the effects of spacecraft charging events on system performance have been proposed. These are: (1) Make the

exterior surfaces as conductive as possible. Bulk conductivities of $\approx 10^9$ mho-cm are usually satisfactory for controlling this interaction. (2) Ground all metal surfaces with a resistance of not more than 1 MΩ. (3) Shield all sensitive circuit harnesses and ground the shield. (4) Filter all sensitive circuits for transients in the range of 1 to 100 MHz. (5) Employ standard EMI noise suppression techniques in sensitive circuits. And (6) consider AC impedance as well as DC resistance in the spacecraft design.

Active techniques can also be used to control spacecraft surface potentials. Since charging is the result of a current balance, an additional ejected electron current could compensate for the incident substorm particle currents and result in reduction of the structure potential. Space flight experiments have demonstrated that plasma sources are effective for controlling charging [31,33,86]. These sources control both the structure potential and the dielectric surface potentials. AFGL is currently developing a Charge Control System (CCS) containing a plasma source for controlling charging on geosynchronous spacecraft [87]. By employing both passive and active mitigation techniques into present and future spacecraft, it is believed that the effects of high altitude charging can be reduced and even eliminated.

3.3 POLAR-AURORAL SPACECRAFT CHARGING

The significance of this interaction was identified based upon measurements of charging on polar-orbiting satellites.

3.3.1 Interaction Environment

Electrons and protons from the Sun enter the magnetosphere tail, are energized, and travel along magnetic field lines, eventually interacting with the Earth's atmosphere. One result is a dynamic phenomenon called aurora. The concept of currents flowing along the magnetic field lines was first proposed by Birkeland in 1908 and updated in 1964 by Bostrom [88-93].

The concept of the auroral oval, the region where the probability of occurrence of auroras exceed 0.7, was originally used to describe the location where optical auroras were observed [94]. Later, it has also been found useful in describing other phenomena, including the precipitation of energetic electrons which produce the auroras. The oval extends completely around the Earth although, in some orientations, observation of optical auroras is masked by sunlight. The auroras are found in a band, somewhat circular in form, with its center displaced towards the night side of the Earth. It has a greater latitudinal extent on the dark, or midnight, side. The oval forms a fixed pattern, relative to the sun, which changes in geographical location as the Earth rotates beneath. The distance across the oval increases as world wide geomagnetic activity increases. Auroras can appear at lower latitudes at magnetically active times.

The satellite auroral photos (Figure 3.24) demonstrate how the aurora can have spatial variations, particularly in north-south extent. Local midnight is at the center of each of the two aurora photos. On the right, where the aurora would be described as quiet, it has a narrow latitudinal extent. A spacecraft crossing this at right angles would

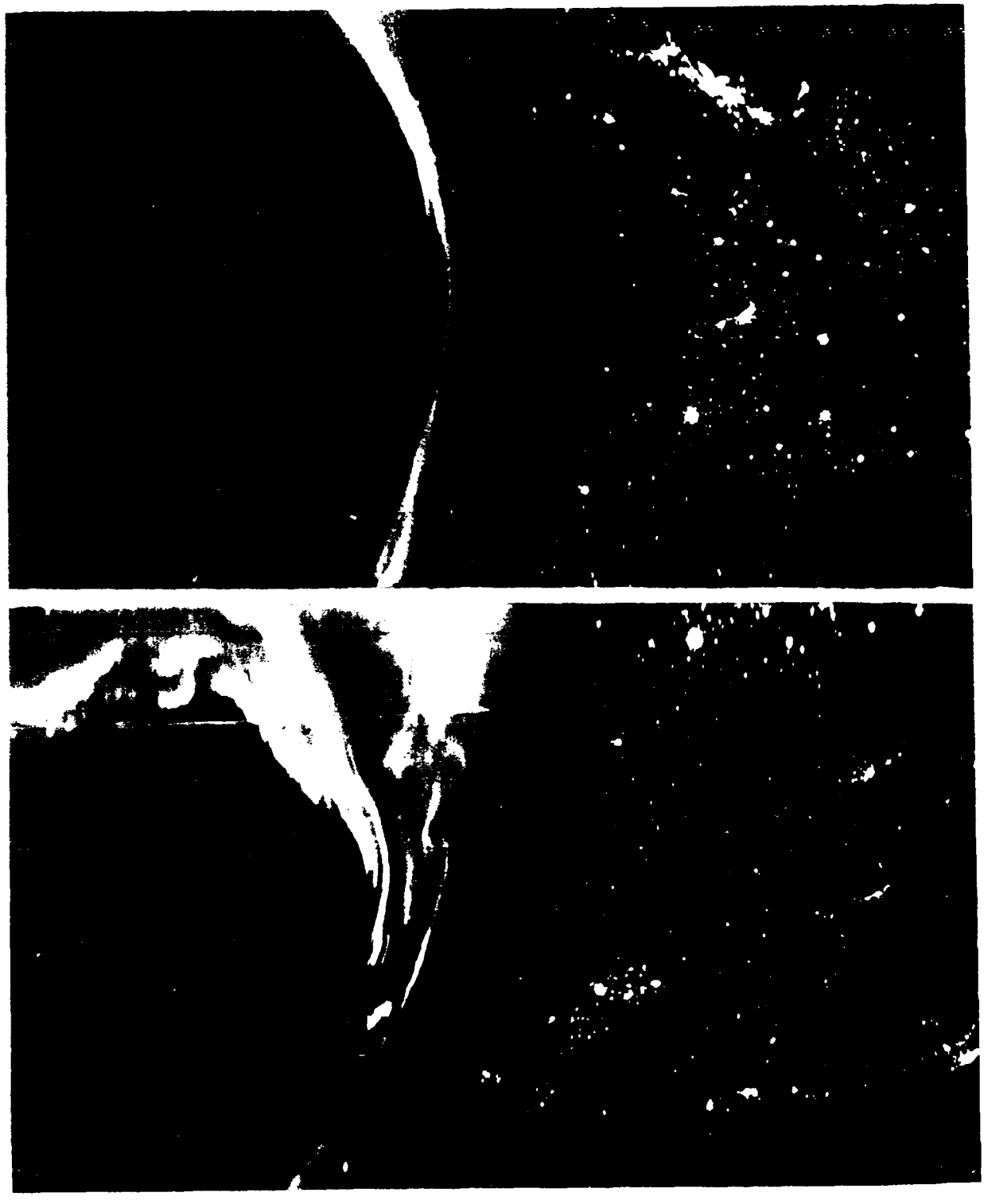

be exposed to energetic auroral particles for only a few seconds. As the angle between the orbit and the narrow auroral arc decreases, the time spent within the auroral band increases. An orbit tangent to a relatively narrow arc could result in exposure to energetic aurora electrons for tens of seconds, even if the aurora is not disturbed. The bottom photo, taken during a different orbit of the same satellite, shows that the aurora has a wider latitudinal extent during a geophysical disturbance, and, depending upon the exact orbit, a spacecraft would encounter the energetic electrons for tens to hundreds of seconds.

Auroras can last for one to two hours but there can be significant temporal variations within that period. All-sky photos taken of an aurora show that the aurora can change from a negligible glow to fill the field of view (900 km) in 2 to 3 minutes [94]. The altitude dependence of the electron density in an aurora is indicated in Figure 3.25 from a March 1978 event. This data only extends to 320 km.

The particle distributions of auroral currents have been measured by instruments on DMSP and STP P78-1 satellites [95-97]. This data was collected over a long period of time and represents a statistical model of the auroral environment correlated to the geomagnetic activity index, K_p. The satellites were in 800 to 900 km orbits. Figure 3.26 shows the integrated number of particles and total energy fluxes from these flights, summed over latitude in each half-hour magnetic local time (MLT) for each value of K_p.

Similar data show that the high latitude electron precipitation region separates into two parts based on the average energy. There is a region of relatively energetic electrons ($E > 600$ eV) and one of lower energies.

In the energetic electron region, the average energy of the precipitating electrons has significant magnetic local time (MLT) variation, but in general, is highest on the morning side of the auroral oval. Note that MLT is defined such that the Earth-Sun line on the magnetic equator is local noon. There are two local maxima in energy; the first between 0600 and 1200 MLT and the second within several hours of midnight. The characteristics of these two maxima are given in Table 3.2. Note that the average energy of the post midnight maximum is between 3 and 5 keV in the latitude range between 63° and 67°

The less energetic electron region extends from the edge of the energetic electron region to the pole. The majority of the precipitating electrons at high latitudes have low energies. The highest number fluxes are found on the day side. Within the day side region of less energetic electron precipitation, there is a clear pre-noon maximum for all values of $K_p < 6$ (Table 3.3).

In addition to the average statistical auroral models given above, there are "worst-case" environments that can be experienced. These severe charging environments appear on the night side of the aurora and can have electron current density values up to 10^2 nA/cm and characteristic energies of up to 15 keV. The ambient thermal plasma ($E < 2$ eV) also varies. At times, severe auroras can be accompanied by low ambient plasma density.

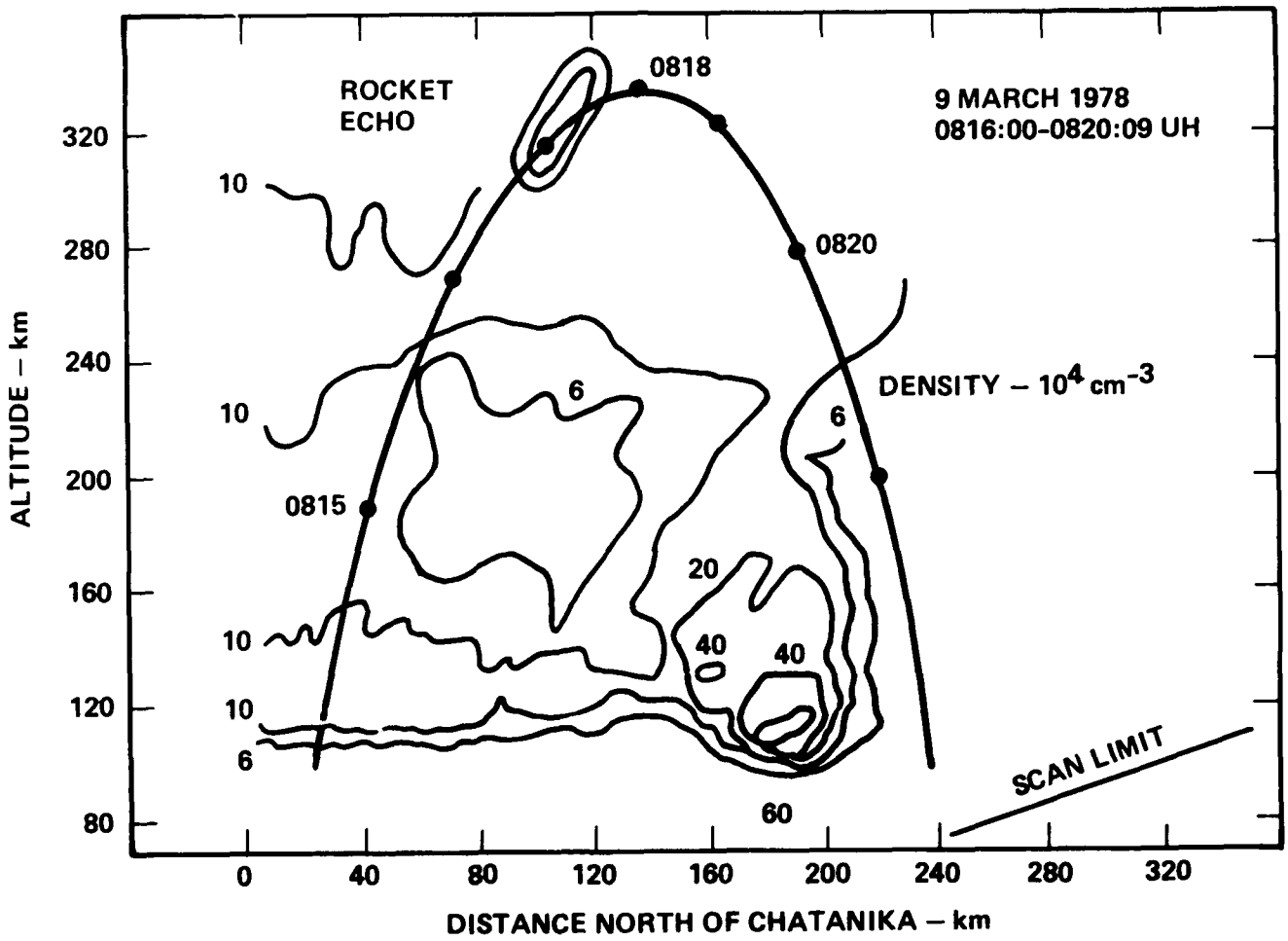

Figure 3.25 Ionospheric Electron Density in an Aurora

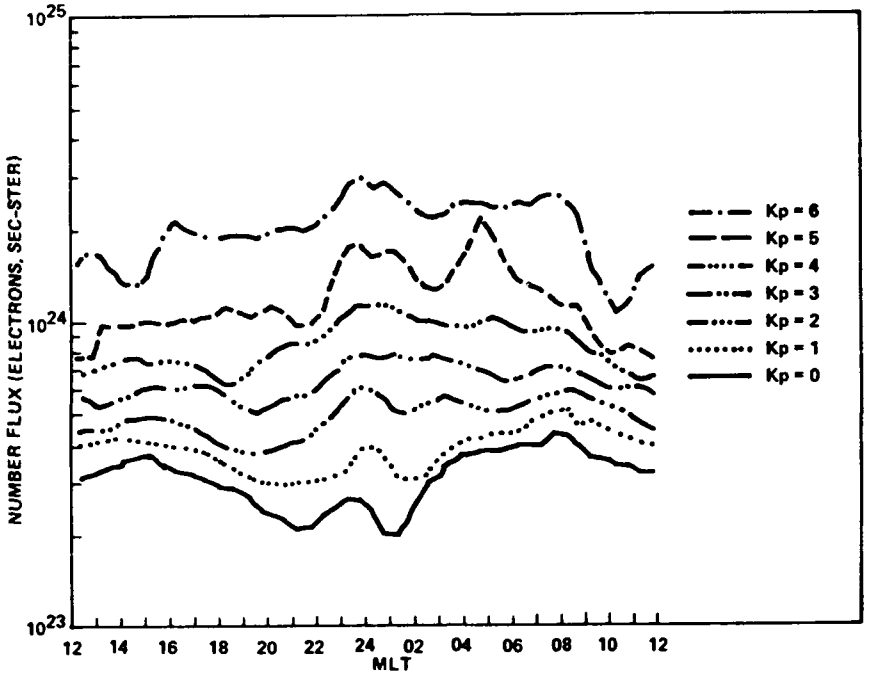

(A) Number Flux Distribution as a Function of K_p

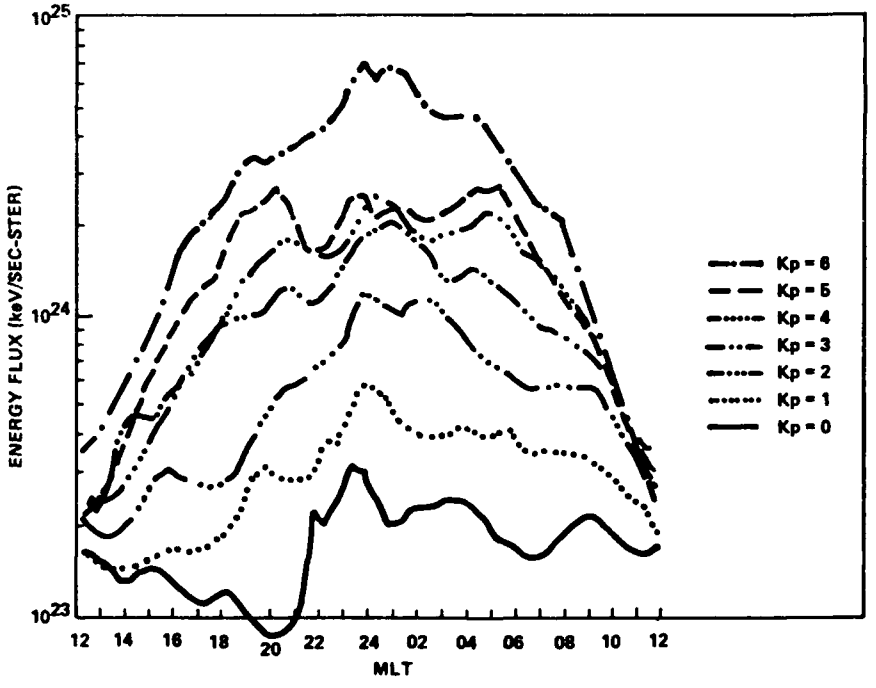

(B) Energy Flux Distribution as a Function of K_p

Figure 3.26 Auroral Electron Beam Environment

Table 3.2
Precipitating Electron Energy Variations (Mid Latitude)

(A) Post-Midnight Maxima

K_p	Average Energy (keV)	Energy Flux (keV/cm^2-sec-ster)	Magnetic Latitude (°)	MLT
Ø	3.9Ø	$1.57 \times 1Ø^{8}$	64	23ØØ-233Ø
1	3.2Ø	$1.48 \times 1Ø^{8}$	66	Ø23Ø-Ø3ØØ
2	3.78	$3.9Ø \times 1Ø^{8}$	65	Ø13Ø-Ø2ØØ
3	3.93	$6.98 \times 1Ø^{8}$	65	Ø13Ø-Ø2ØØ
4	3.46	$7.1Ø \times 1Ø^{8}$	66	ØØØØ-ØØ3Ø
5	—	—	—	—
6-	5.87	$1.67 \times 1Ø^{9}$	63	Ø23Ø-Ø3ØØ

(B) Pre-Noon Maxima

K_p	Average Energy (keV)	Energy Flux (keV/cm^2-sec-ster)	Magnetic Latitude (°)	MLT
Ø	2.97	$2.16 \times 1Ø^{7}$	71	14ØØ-143Ø
1	3.9Ø	$6.34 \times 1Ø^{7}$	7Ø	Ø93Ø-1ØØØ
2	5.68	$1.Ø7 \times 1Ø^{8}$	7Ø	1Ø3Ø-11ØØ
3	5.4Ø	$1.38 \times 1Ø^{8}$	69	1ØØØ-1Ø3Ø
4	5.Ø2	$9.42 \times 1Ø^{7}$	67	1ØØØ-1Ø3Ø
5	4.81	$1.33 \times 1Ø^{8}$	66	Ø93Ø-1ØØØ
6-	1.8Ø	$1.Ø6 \times 1Ø^{8}$	65	Ø93Ø-1ØØØ

3.3.2 Discussion of Interaction

3.3.2.1 *Background*

Data on this type of interaction has been obtained over the past few years from instruments on DMSP satellites [98,99]. These instruments have shown that, during a severe event, the structure potential can change rapidly over a period of seconds. For example, a charging event in which the DMSP structure potential reached -440 volts is shown in Figure 3.27. This event occurred when the satellite was in darkness. A factor significantly contributing to this level of charging was that the local thermal plasma density at that time was relatively low.

An important characteristic of this event was the rapid changes in potential. The whole event was over in about 20 seconds and the peak voltages lasted only seconds. The spacecraft potentials changed at the same time as the auroral particle intensities. Note that the spacecraft charged as a complete unit and with negligible time delay. This response is typical of a spacecraft experiencing "absolute charging" at geosynchronous altitudes (Section 3.2.2.1).

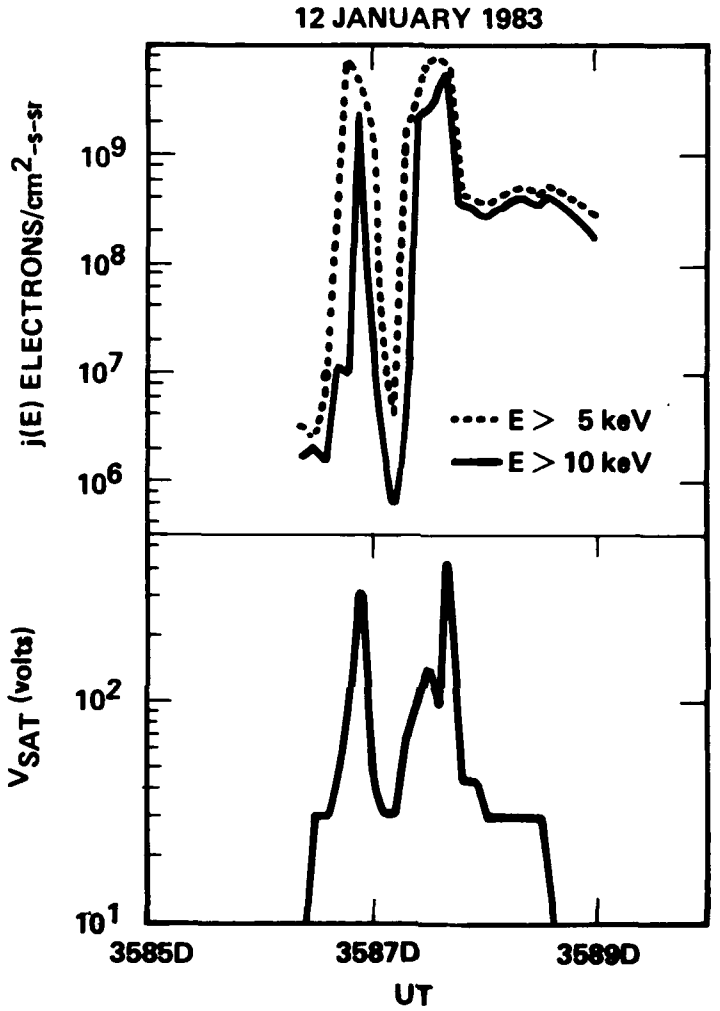

Figure 3.27 DMSP Charging Event: Environment and Induced Vehicle Potential

Table 3.3
Precipitating Electron Energy Variations (High Latitudes)

(A) Pre-Noon Integral Number Flux Maximum

K_p	Average Energy (eV)	Integral Number Flux (E/cm^2-sec ster)	Integral Energy Flux (E/cm^2-sec-ster)	Magnetic Latitude (°)	MLT
Ø	232	3.05×10^8	7.04×10^7	79	Ø8ØØ-Ø83Ø
1	272	3.22×10^8	8.45×10^7	78	Ø8ØØ-Ø83Ø
2	256	3.32×10^8	8.43×10^7	78	Ø93Ø-1ØØØ
3	187	3.80×10^8	7.03×10^7	77	11ØØ-113Ø
4	552	3.61×10^8	1.95×10^8	74	Ø83Ø-Ø9ØØ
5	465	4.10×10^8	1.66×10^8	73	Ø83Ø-Ø9ØØ

(B) Average Energy Minimum

K_p	Average Energy (eV)	Integral Energy Flux (keV/cm^2-sec-ster)	Magnetic Latitude (°)	MLT
Ø	199	4.57×10^7	81	11ØØ-113Ø
1	183	4.88×10^7	81	113Ø-12ØØ
2	168	3.83×10^7	81	113Ø-12ØØ
3	165	4.44×10^7	79	11ØØ-113Ø
4	162	3.96×10^7	78	113Ø-12ØØ
5	147	3.18×10^7	78	123Ø-13ØØ
6-	184	7.29×10^7	76	12ØØ-123Ø

The longevity of charging conditions is illustrated by measurements made by two different DMSP spacecraft passing through the same event at different times and trajectories (Figure 3.28) [96]. The spacecraft charged to similar levels even though separated in time by 36 minutes.

The -440 volt structure potentials measured by DMSP are not expected to seriously impact system performance. These satellites experienced this charging level on several occasions while apparently not experiencing any anomalous system behavior. The concern is directed more towards possible charging effects on very large spacecraft in polar orbits. An initial analysis of a large structure encountering a severe auroral current flux in darkness indicated that the structure could reach a significantly larger negative potential than a smaller spacecraft (Figure 3.29) [100].

The relatively large electron current densities in an auroral beam must be balanced by collection of ambient ions. The ion collection depends upon the ratio of the spacecraft characteristic radius to the plasma characteristics (i.e. Debye length). The ion collection becomes space charge limited for large spacecraft in DMSP orbits. As the vehicle size expands the potential must become more negative to inhibit the electron

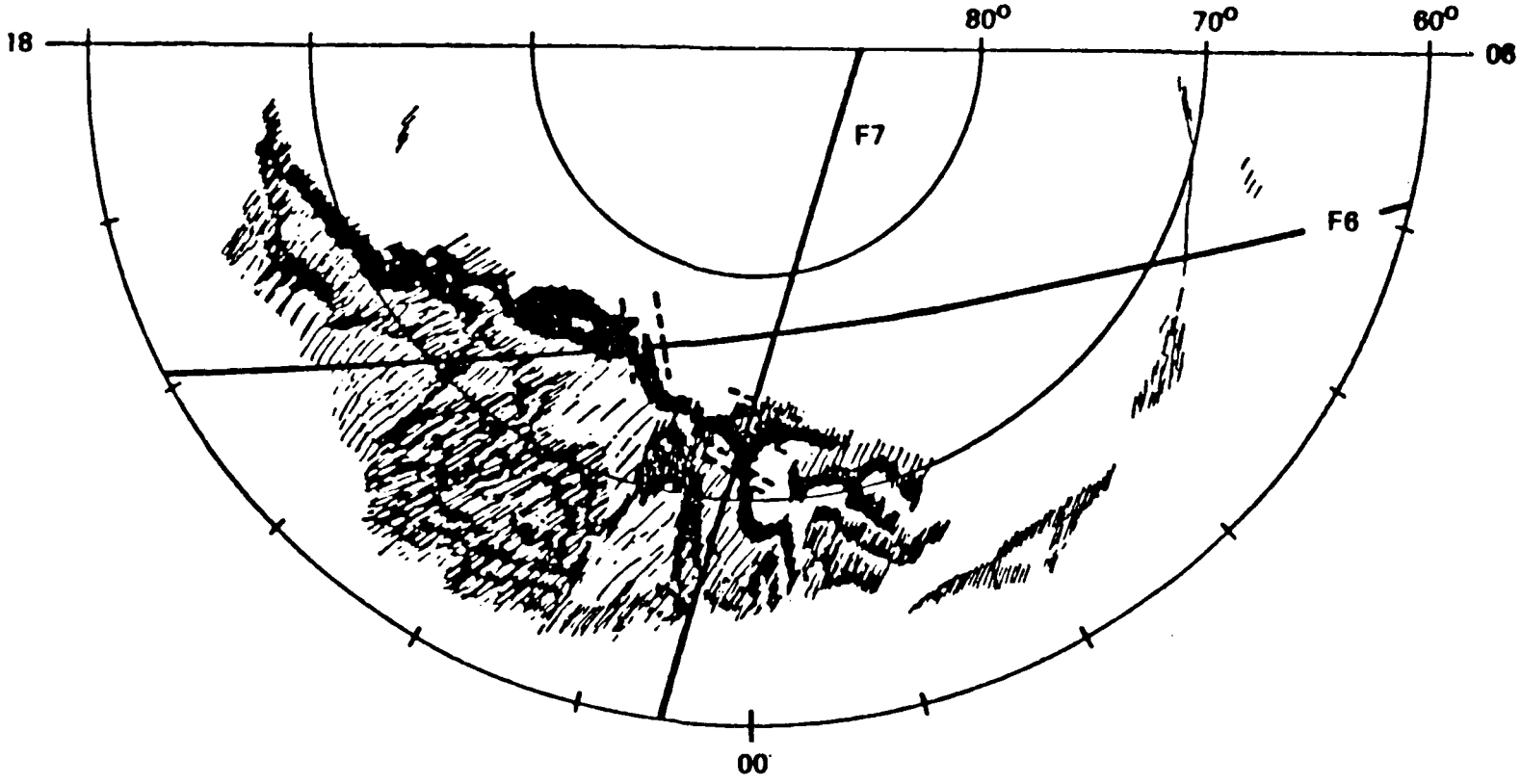

F6 SATELLITE CHARGING: 47709–47727 UT
F7 SATELLITE CHARGING: 49842–49915 UT

Figure 3.28 DMSP Polar-Auroral Charging Incidents

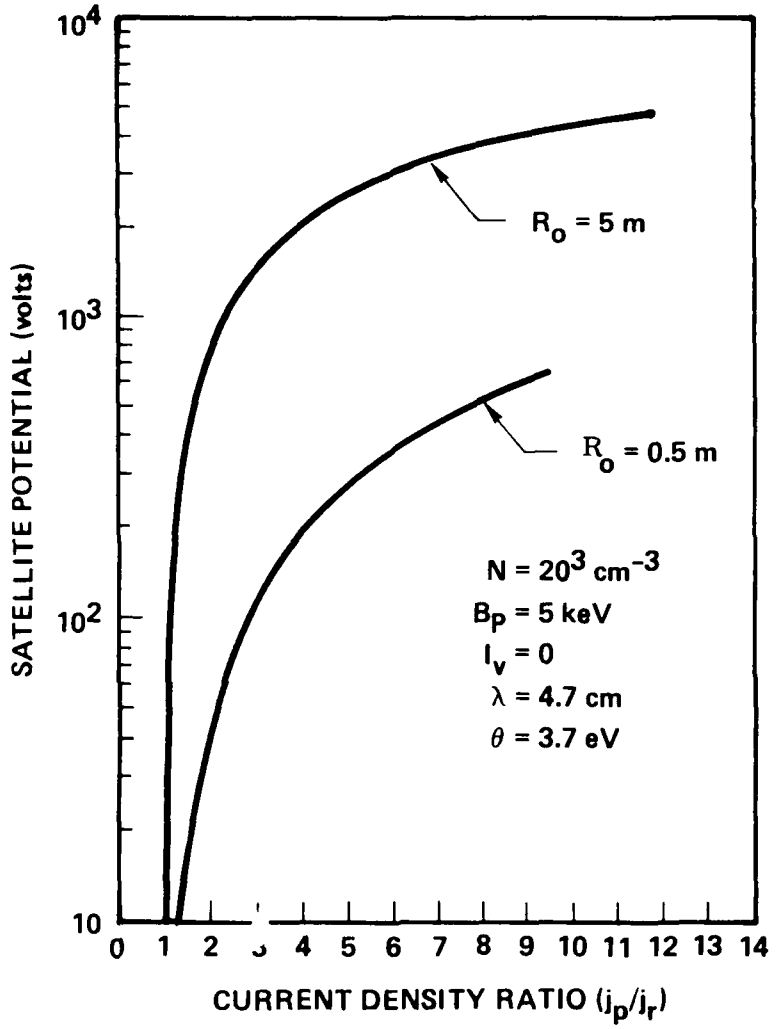

Figure 3.29 Impact of Vehicle Size on Auroral Charging (Simple Model Predictions)

collection and enhance ion collection. Recent studies of large spacecraft behavior in polar storms, using more sophisticated computer programs, are confirming that size is an important factor in charging magnitude. Under conditions where ion collection is orbit limited, charging is independent of spacecraft size [101-104].

Polar-auroral charging of large structures generates concern for possible interactions between the structure and an astronaut on Extra Vehicular Activity (EVA) [105-107]. The astronaut could be differentially charged, especially in the vehicle wake. If the charging levels are significant, then discharges could occur. This concept has been studied, but no definite conclusions have been reached.

Another concern in this interaction is the rate at which charging occurs. In geosynchronous charging conditions, differential charging requires minutes to build up to substantial levels. Polar-auroral charging events, on the other hand, are over in a matter of seconds, according to data available from DMSP. However, the auroral current densities are between one and two orders of magnitude larger than those experienced in geosynchronous substorms. This higher current density results in a far more rapid development of differential charging. A comparison of differential charging development under GEO and PEO charging conditions is shown in Figure 3.30. As can be seen, differential voltages can build up in milliseconds under polar charging conditions. With the more rapid development of differential charging comes the higher probability of sudden discharges and system upsets.

3.3.2.2 *Modeling*

A three-dimensional computer code called POLAR, Potential Of Large Objects in the Auroral Region, is being developed by S-Cubed for AFGL to evaluate polar-auroral charging interactions for large space vehicles [101]. A POLAR model of the shuttle is shown in Figure 3.31A and the prediction of ion density profiles is shown in Figure 3.31B. The Shuttle is moving in the +Z direction and creates a wake behind the vehicle (cargo bay region). The plasma environment is vastly different in the wake region, from that outside the wake, and must be considered when evaluating this interaction.

3.3.2.3 *Discharges*

There is no reason to believe that discharges following polar-auroral charging will differ from those following geosynchronous charging. The charging can exceed the discharge thresholds especially as the physical size of the vehicle increases. The resulting discharges may then interfere with spacecraft systems.

3.3.3 Research Maturity Rating

The research maturity for polar-auroral charging, both theoretical and experimental, was rated MODERATE (3). The rationale for this rating is that the implications of this phenomenon are just beginning to be studied. Auroral charging has been studied for many years, however the effects of vehicle size on possible charging levels is only a recent development (circa 1980). The environment characteristics are

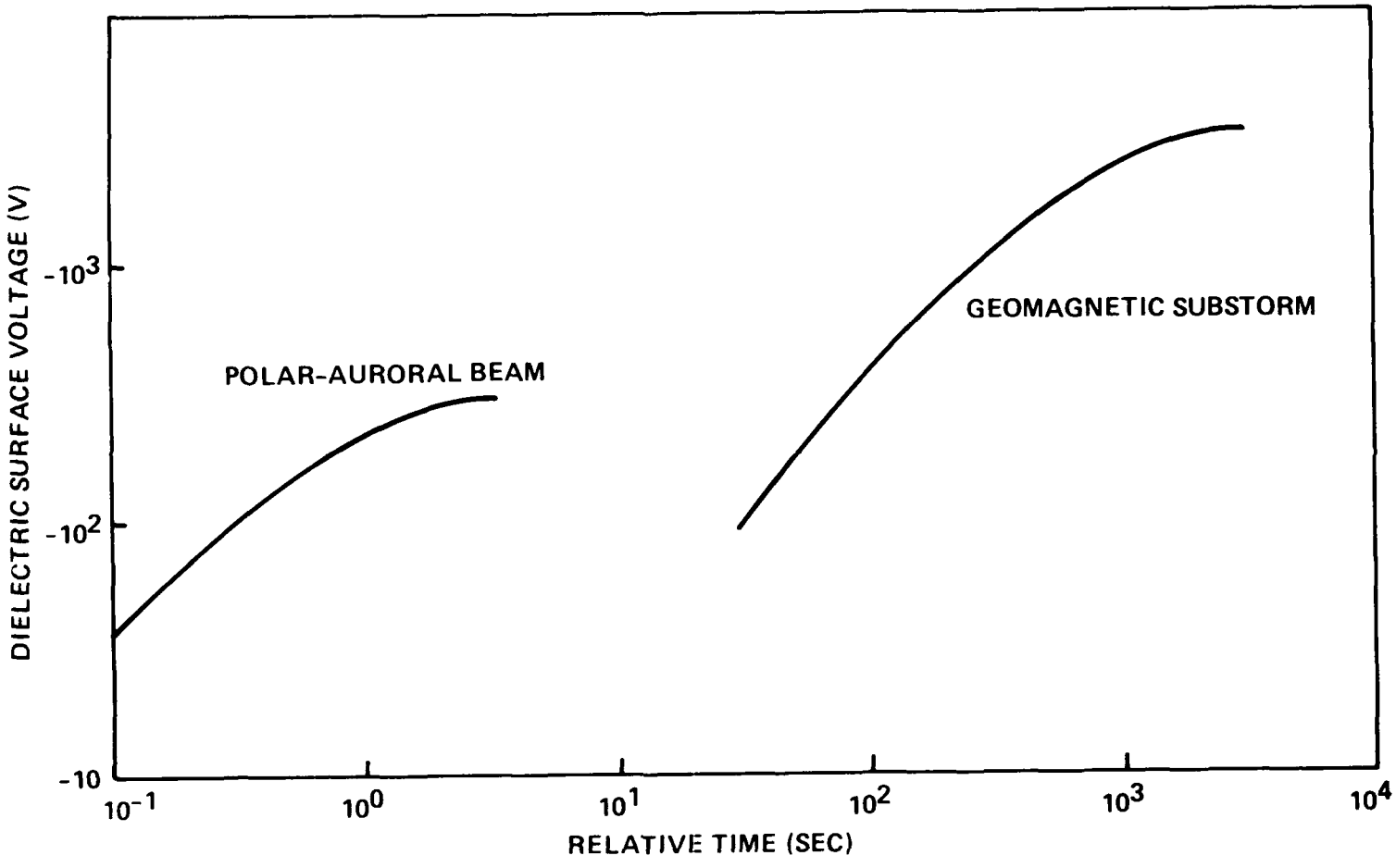

Figure 3.30 Differential Charging in Response to a 10 keV Injection (1-D Model)

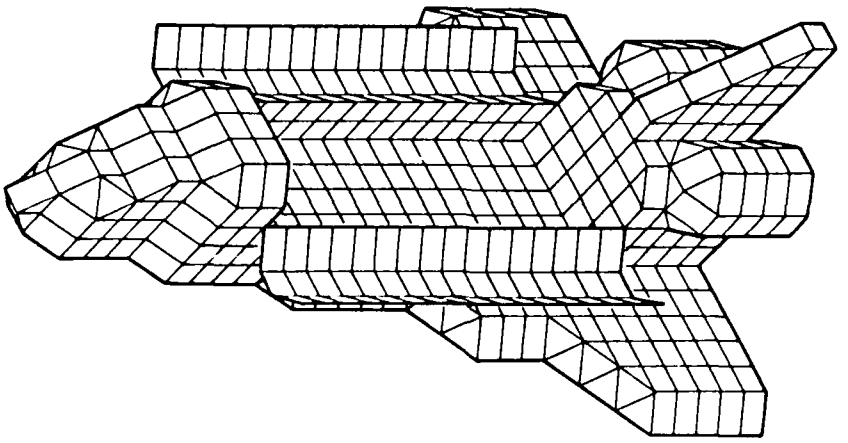

(A) POLAR Code Shuttle Model

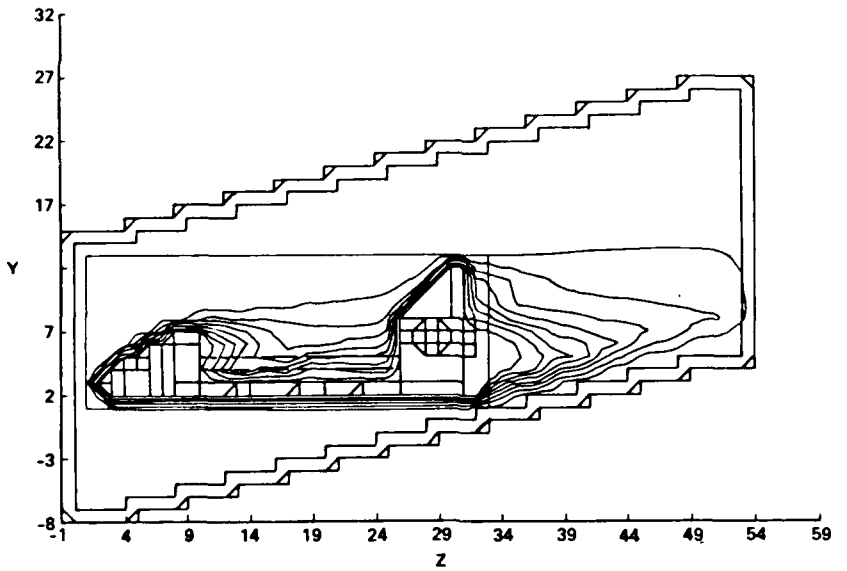

(B) Quiet Environment Ion Density Profiles Showing Wake Region

Figure 3.31 POLAR Code Shuttle Application

being assembled, and while a "worst-case" environment has been discussed, there is still no indication how often such storms would be expected in orbit. The modeling effort has produced the computer code POLAR, but the code is still being validated and is not yet available to the aerospace industry.

3.3.4 System Impact Rating

The system impact rating of polar-auroral charging is the same as that of high altitude charging discussed in Section 3.2.4, namely, it was rated CONSIDERABLE (4) for polar orbiting missions. It was rated NEGLIGIBLE (1) for equatorial, low Earth orbit and geosynchronous orbits due to the absence of auroral type energetic electrons.

3.3.5 Mitigation Techniques

The mitigation techniques for this interaction are the same as those for high altitude charging (Section 3.2.5).

3.4 HIGH-VOLTAGE SYSTEM INTERACTIONS

This class of interaction is applicable to any system in which conductors, biased to high voltages, are exposed to the space plasma environment. These conductors are usually surrounded by dielectrics with only a small portion, if any, of the conductor exposed. The interaction will be discussed in terms of a solar array operating at high voltages (> 100 volts), but the effects of this interaction are applicable to other high-voltage systems (e.g. exposed high-voltage wires in other types of power systems).

3.4.1 Interaction Environment

The environment of concern in this interaction is the thermal plasma environment with characteristic energies less than 2 eV (Figure 3.32) [6]. It is this low energy plasma that can interact with the electric fields generated by the voltage on the spacecraft. As shown in this figure, the plasma density varies with altitude, peaking at about 300 km with a density of about 3×10^6 particles per cubic centimeter. The variation of this plasma with latitude is shown in Figure 3.33. The thermal plasma density falls off to less than one particle per cubic centimeter at geosynchronous altitudes. Since this interaction is directly proportional to the plasma density, it is of more concern at lower altitudes where the density is greater than 10^3 cm^{-3}.

3.4.2 Discussion of Interaction

3.4.2.1 *Background*

The interactions of concern here result from the operation of high-voltage systems in the space plasma environment. This effect was first identified by a series of experiments run in a plasma simulation facility during the late 1960s [108]. In these experiments, a biased wire surrounded by a cylindrical dielectric coating was exposed to a plasma environment in a vacuum chamber. Only the tip of the wire was exposed. It was

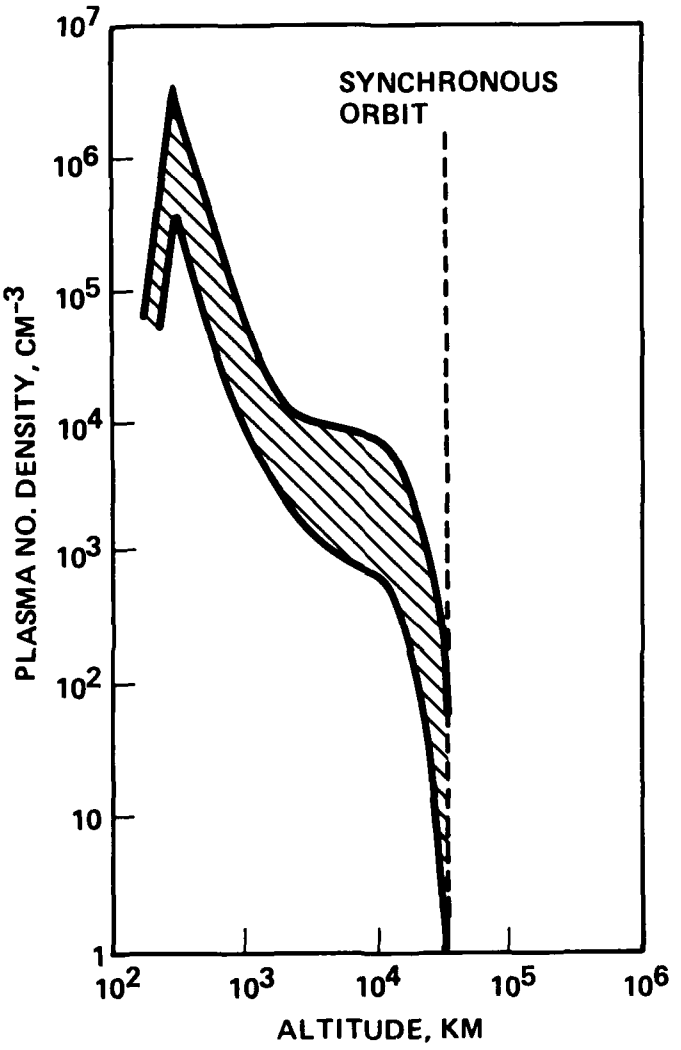

Figure 3.32 Plasma Number Density vs Altitude in Equatorial Orbit

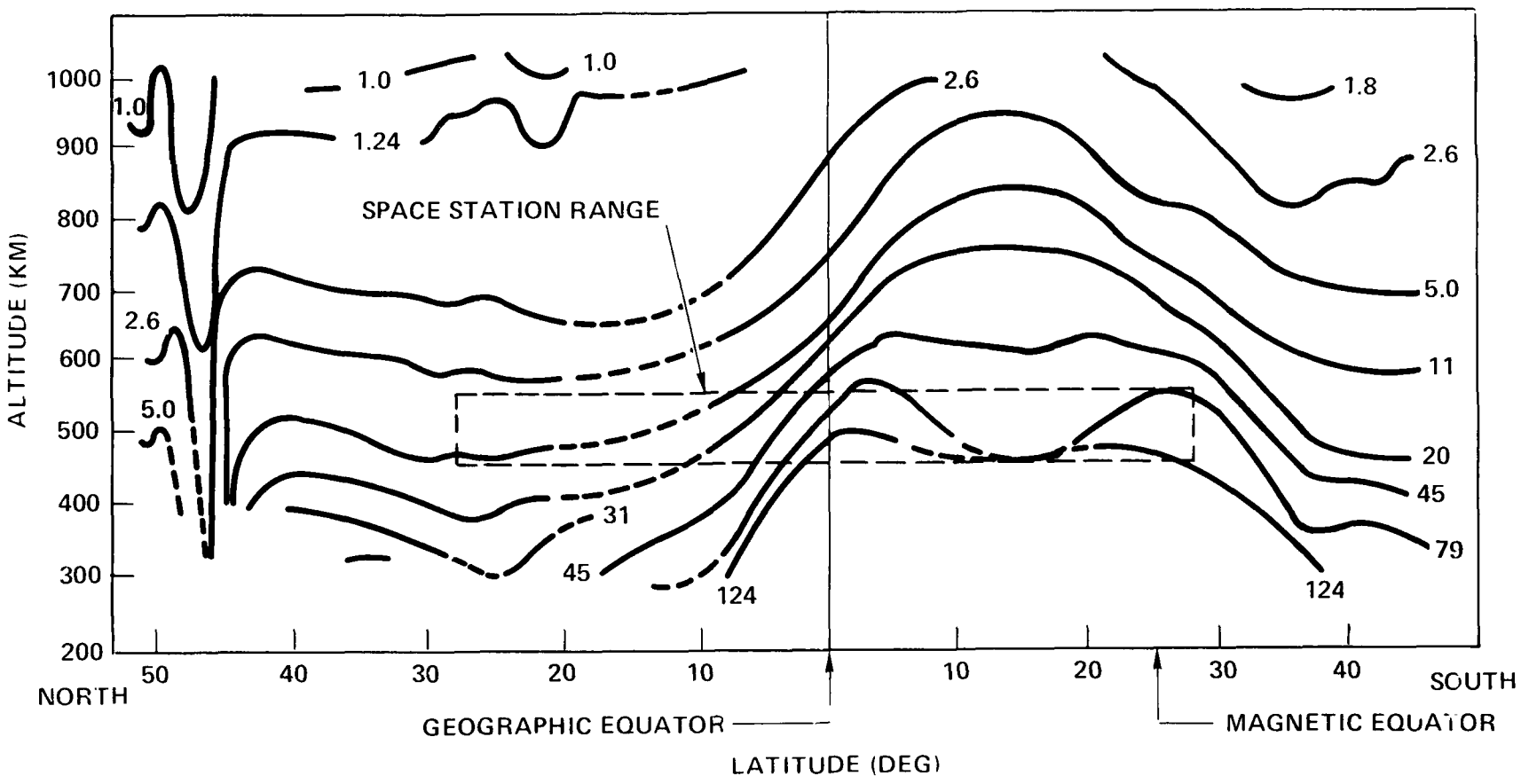

Figure 3.33 Space Station Plasma Environments (Units 10^4 cm^{-3})

anticipated that this tip would act as a plasma probe and collect current as the voltage increased until a saturation value was achieved. However, the current collected from the plasma increased dramatically once the bias exceeded +100 volts. It was eventually found that the dielectric surface contributed electrons to the collection process. Additional testing has shown that biased planar solar array segments behave in a similar fashion [109-121].

Laboratory tests have shown that there are two basic effects that occur when solar array segments are biased to positive and negative voltages. When the array is biased positive with respect to the plasma, electrons are collected. This collection is proportional to the potential, the plasma density, and the metallic interconnect area. When the potential exceeds 100 volts, the collected current becomes proportional to the whole panel area (Figure 3.34) [122,123]. It has also been found that small pinholes in dielectrics, which expose a biased conductor to the plasma, can also exhibit this enhanced current collection capability (Figure 3.35) [112,124-126].

When the array is biased negatively with respect to the plasma, breakdowns occur. Breakdowns have an apparent threshold voltage which is plasma density dependent [112,116,123] and apparently result when electric fields develop between solar cell interconnect cavities. High-voltage interactions, discovered during laboratory testing with plasma simulators, have been verified by the Plasma Interaction Experiment (PIX) flights [49,127,128-131].

Since the effects found in laboratory simulations are plasma density dependent, this interaction will be more important in LEO and PEO. In GEO, the thermal plasma density is so low that the voltage threshold, for which the effect becomes significant, is in the tens of kilovolts range [116]. The high-voltage system interaction of concern to prospective space systems is shown in Figure 3.36 [116]. This system consists of a central body or spacecraft surrounded by two large solar array wings. The solar array is assembled using standard construction techniques (i.e. the cover slides do not completely shield the metallic interconnects from the plasma environment). These cell interconnects are at various voltages depending on their location in the series-parallel array circuit. Thus, the interconnects can act as plasma probes attracting or repelling charged particles. At some location in the array, the generated voltage is equal to the space plasma potential. Cell interconnects at voltages positive with respect to this point collect electrons from the space plasma. Interconnects at negative voltages collect ions. The system floats such that the net current is zero. The array floats predominantly negative, since the electrons are more mobile than the ions. The electron and ion current collection from the plasma can be considered to be a parasitic current loop representing a power loss, since it is in parallel with the electrical load on the spacecraft.

The concentration of electric fields to cavities formed by the cover slides and interconnects causes breakdown in the negative voltage regions of the array. These breakdowns result in charge loss to the plasma and can momentarily interrupt power generation. In addition to field concentration type breakdowns, there exists the possibility of breakdowns between circuits. Imperfections in insulation and substrate dielectrics, caused by long term environment exposure (via meteoroid/debris impacts,

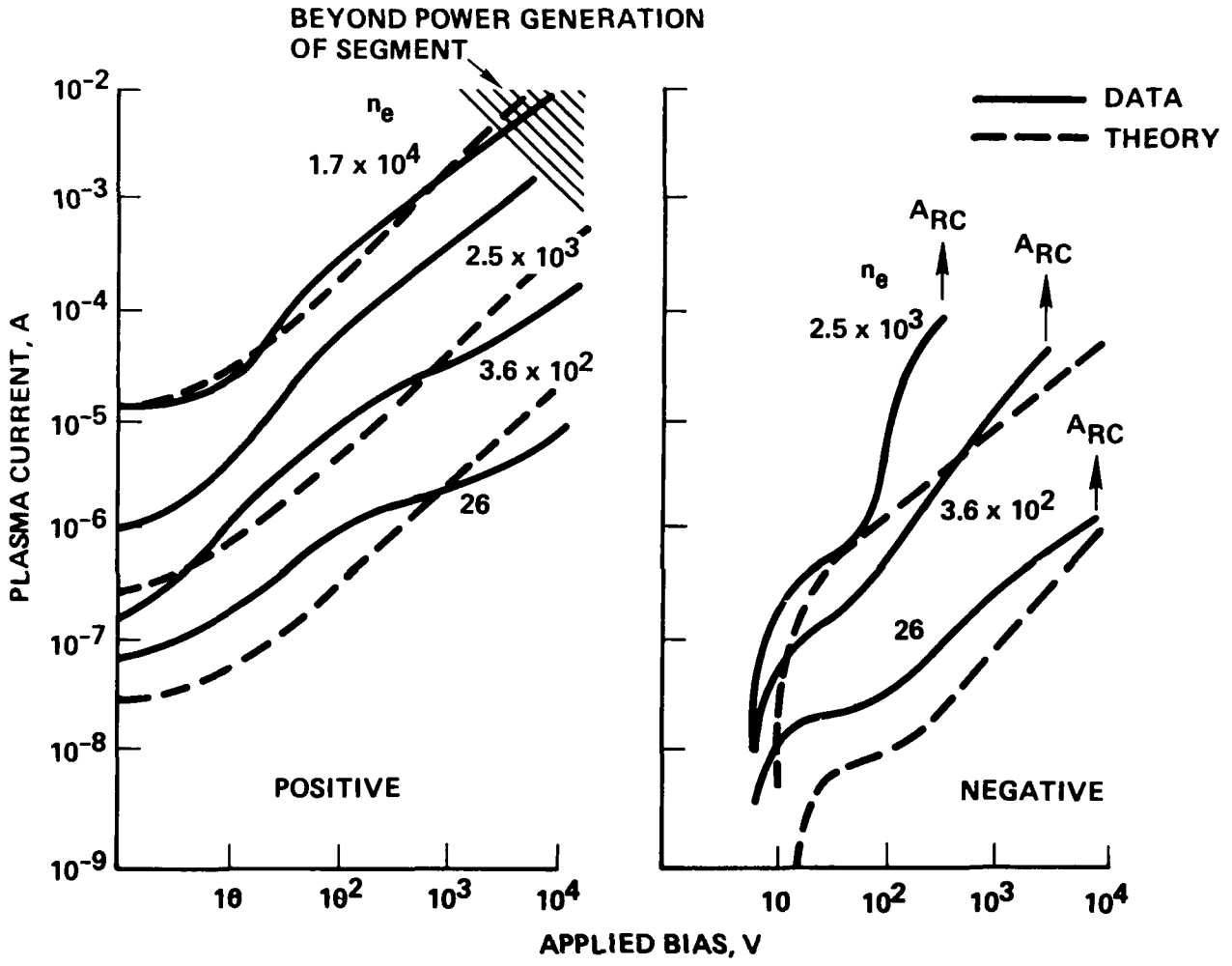

Figure 3.34 Solar Array Segment Ground Test Results (Area = 1058 cm^2)

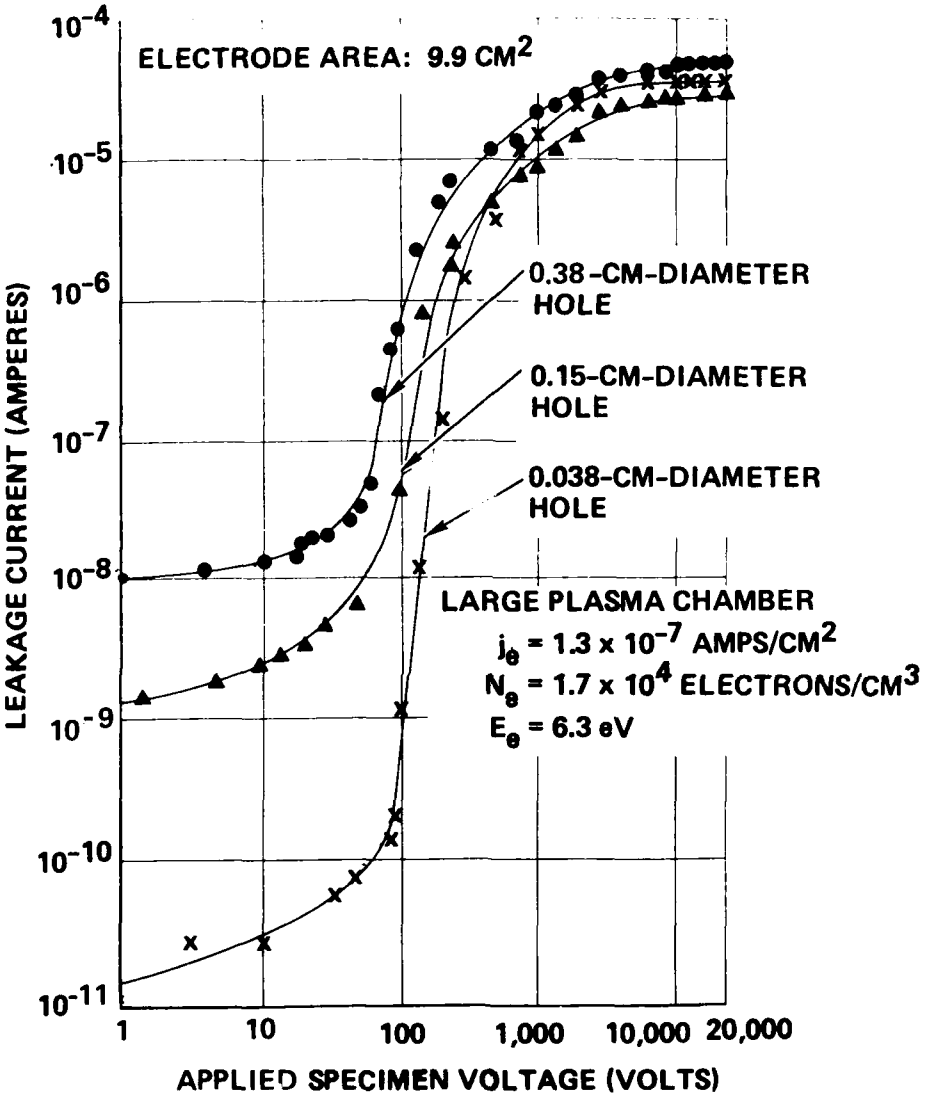

Figure 3.35 Effect of Voltage and Defect Size on Leakage Current
(Positive Voltage applied to 5 mil Kapton Electrode)

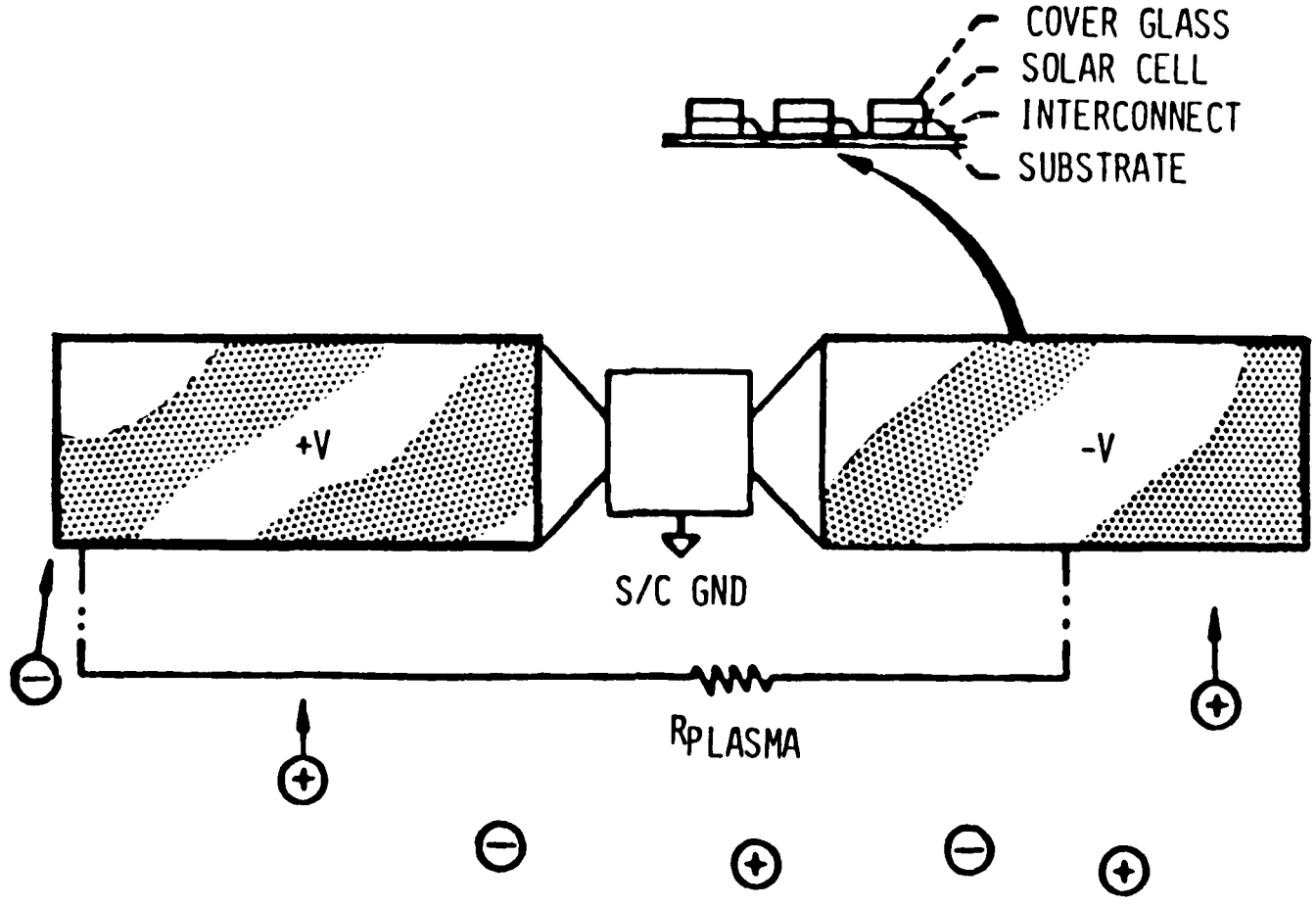

Figure 3.36 Spacecraft High-Voltage System Environment Interactions

high energy ion sputtering, or atomic oxygen erosion in low Earth orbits), can cause additional enhanced current collection and parasitic power loss. Carbonization of the insulation due to discharges can potentially result in unintentional shunts of portions of the array, and consequently, power losses.

3.4.2.2 *Modeling*

A three-dimensional computer tool to analyze low altitude solar arrays is being developed by S-Cubed for the NASA-Lewis Research Center. This code, an outgrowth of the NASCAP computer code, is designed to handle large planar solar arrays operating in dense plasma environments, typical orbits between 300 and 600 km. At present, the code, called NASCAP/LEO, will compute the floating potentials for a solar array operating in a low Earth space environment [132-134]. The NASCAP/LEO capability is demonstrated in Figures 3.37 and 3.38 by a small solar array model and the predicted potentials. These figures illustrate the snap-over phenomenon [122] exhibited in the high voltage solar array collection process. The ability to predict negative voltage breakdown has not been demonstrated. The code predictions have yet to be validated.

In addition to NASCAP/LEO, there are other three-dimensional [135] and simple current balance (based upon probe theory) models that have been used to predict array performance in space [121,136]. These models appear to reasonably predict floating potentials for arrays and their collected currents. The results of these computations have shown that the collected currents, for an isolated solar array in LEO (300 to 500 km), are considerably less than 1% of the line current, for operating voltages up to 1000 volts. Hence, plasma coupling power loss is probably not significant.

3.4.2.3 *Concentrator Solar Arrays*

Concentrator solar arrays have been proposed as an alternate to planar arrays. This type of array uses a mirror to focus the sunlight onto a small solar cell. This approach makes higher-efficiency, higher-cost gallium arsenide solar cells competitive to silicon solar cells. A Cassegrainian solar array segment and cell design is illustrated in Figure 3.39 [137]. This type of array contains a primary mirror, secondary mirror, and light collector surrounding the small solar cell. No cover glass is required.

Only recently has a study been undertaken to evaluate the response of this solar cell to a plasma environment [137]. A single cell was biased in a simulation chamber to obtain the data shown in Figure 3.40. Power loss to space should be minimal, since there was no positive bias snap-over condition exhibited. In fact, electron collection current under positive biases tends to saturate. There were, however, discharges under negative bias conditions at about the same threshold as with the planar cells.

A preliminary attempt at modeling high-voltage interactions with the concentrator array was based upon this data using plasma probe theory [137]. It appears that the voltages are all confined to the light catcher region of the cell and will not expand into the space plasma (Figure 3.41 and 3.42). This may indicate that this type of array would have less influence on the spacecraft potential relative to the space plasma.

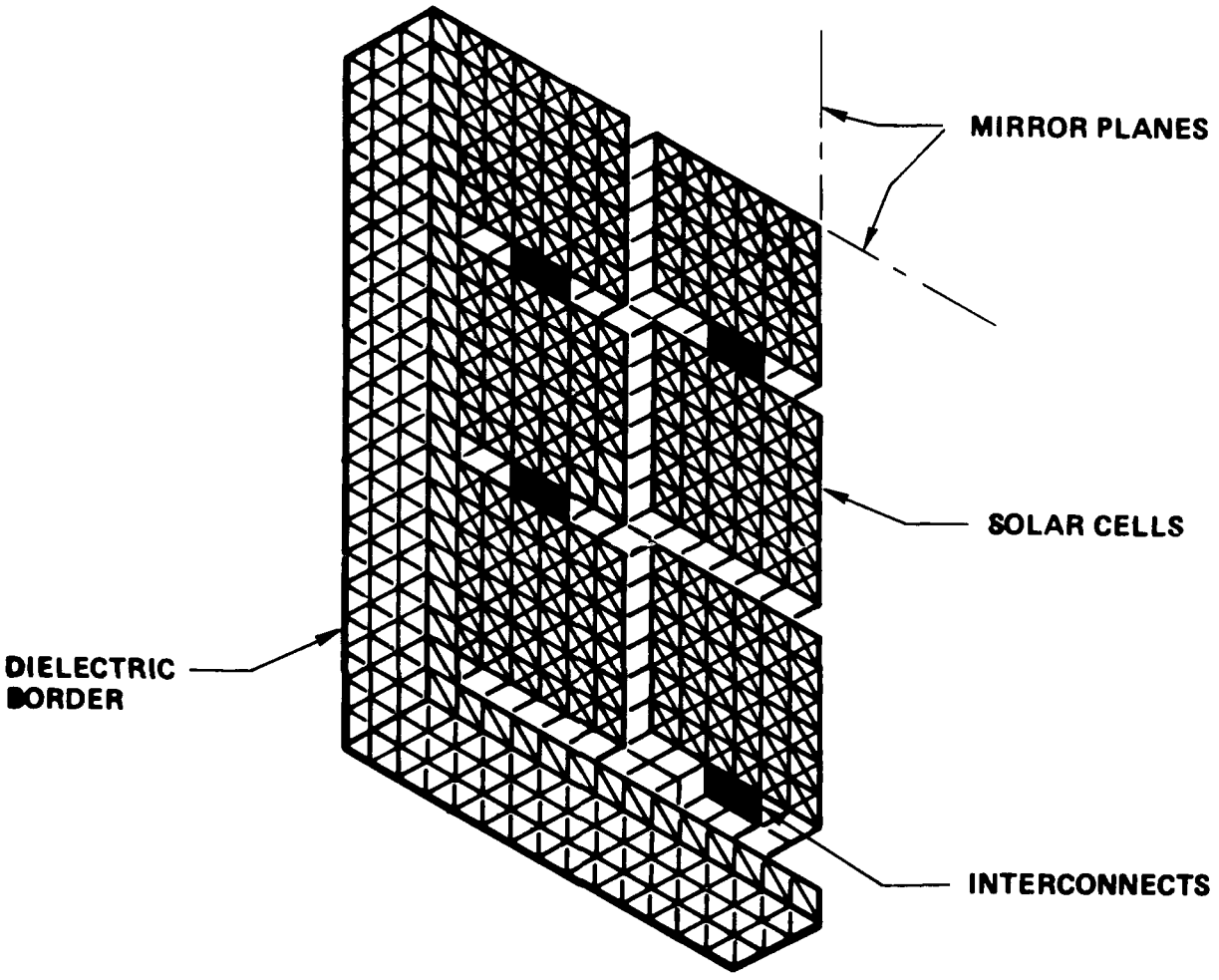

Figure 3.37 NASCAP/LEO Solar Array Model

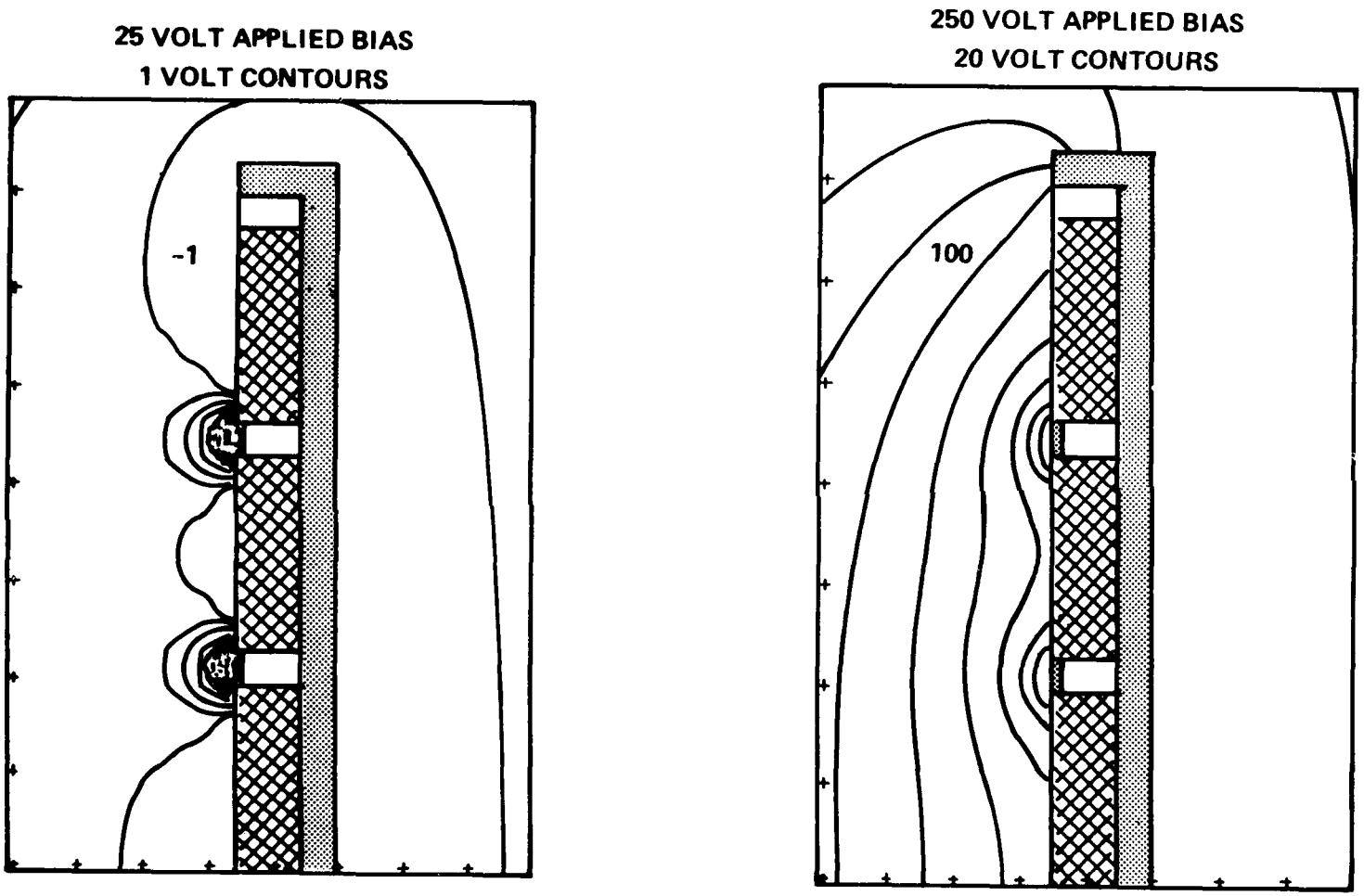

Figure 3.38 NASCAP/LEO Solar Array Voltage Predictions

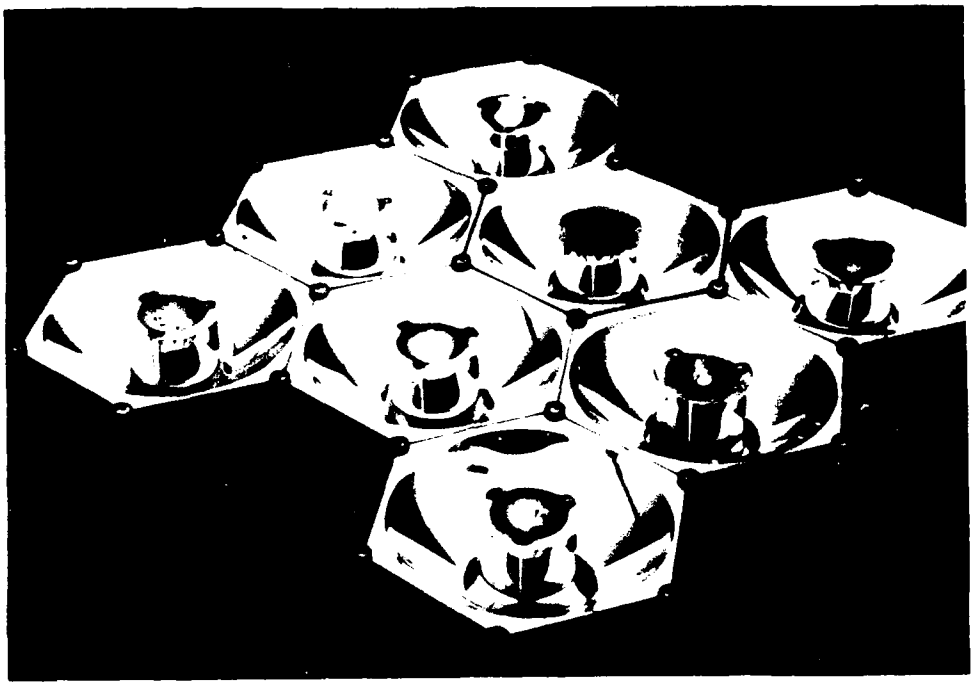

(A) Solar Cell Array

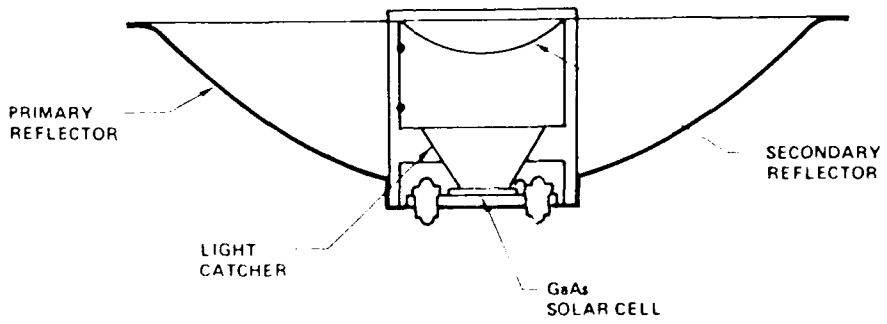

(B) Concentrator Solar Cell Schematic

Figure 3.39 Cassegrainian Concentrator Solar Array

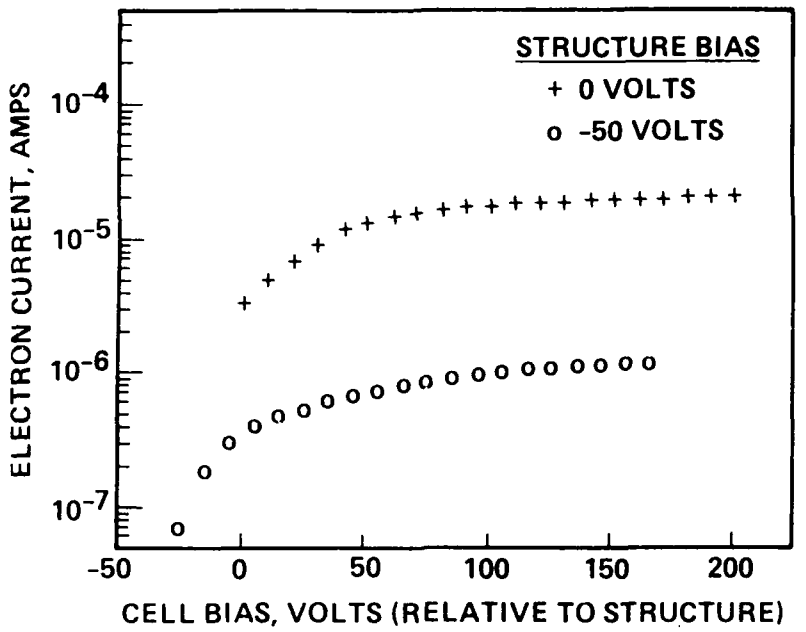

(A) Electron Collection

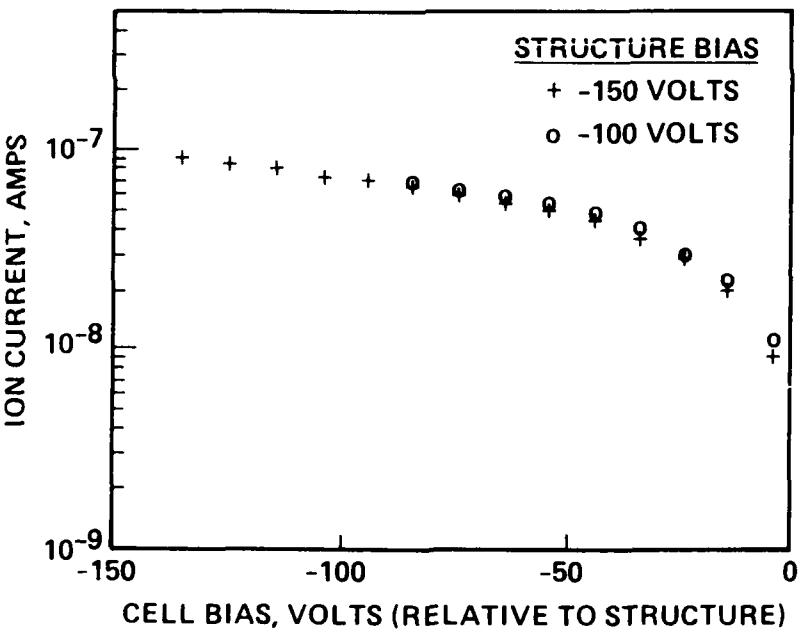

(B) Ion Collection

Figure 3.40 Concentrator Cell Current Collection Test Data

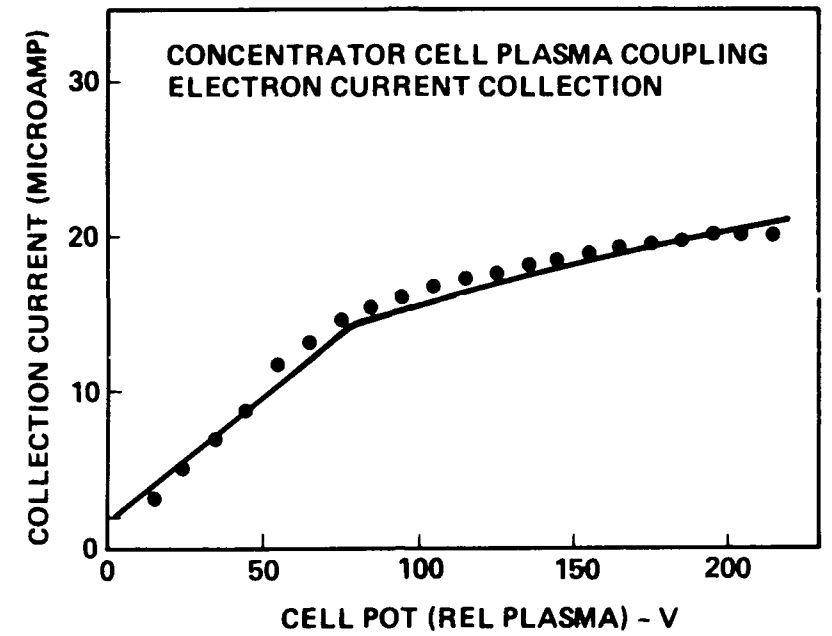

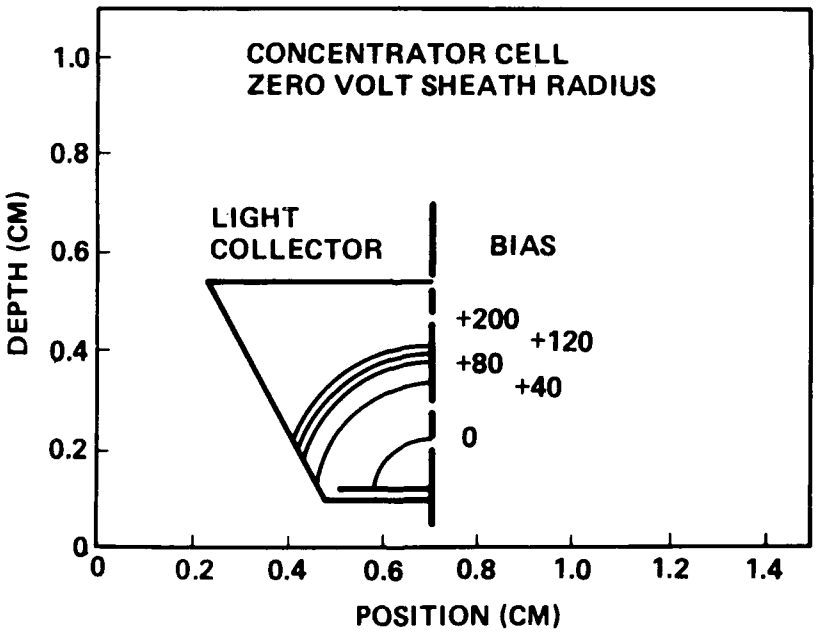

Figure 3.41 Concentrator Solar Cell Electron Collection Model

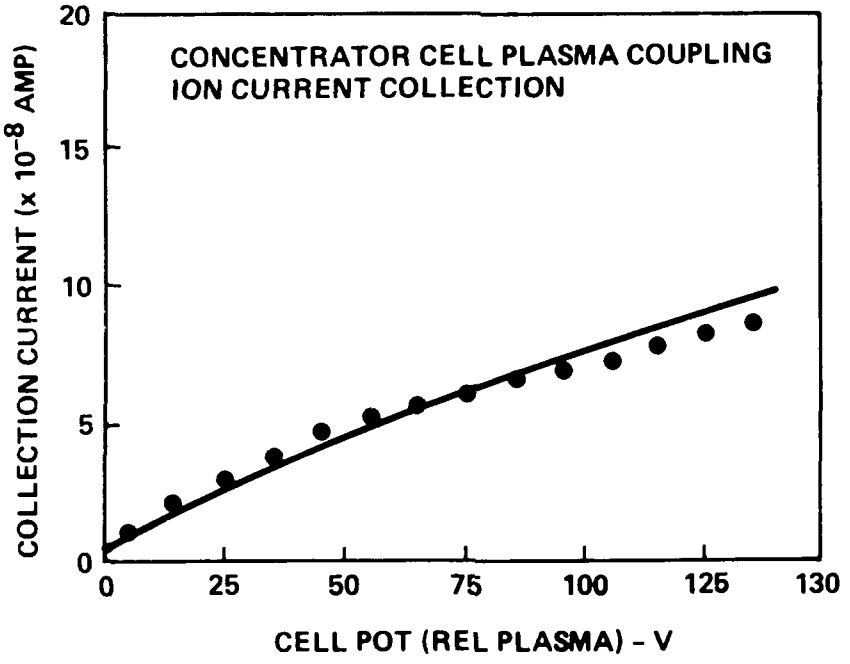

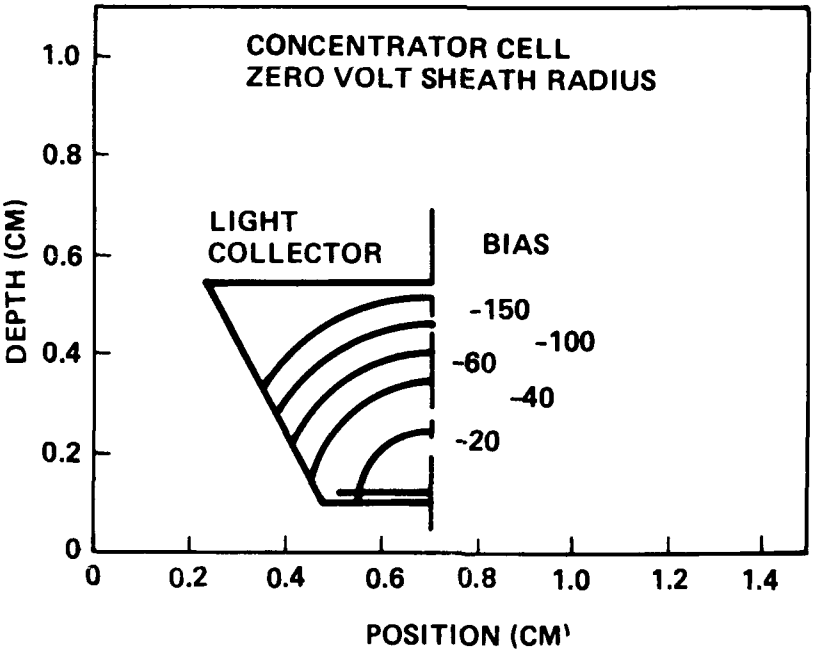

Figure 3.42 Concentrator Solar Cell Ion Collection Model

3.4.2.4 *Discharges*

A further concern about high-voltage system interactions is the effect of array discharges on power system performance. Negative-bias voltage breakdowns in solar arrays have been studied for the past several years in laboratory simulators [112,116-118,122,138-142]. The results initially were summarized as discharge threshold voltage versus plasma density (or altitude), as shown in Figure 3.43. Subsequent work has indicated that there is a time dependence as well. Thus, it is more appropriate to discuss breakdowns in terms of arcs per second [143]. Arc breakdown rate information has been assembled for the Space Station, based upon a combination of ground data and space flight results (Figure 3.44). This data base is still incomplete because a discrepancy exists between the space and ground data. A breakdown voltage threshold of about -200 to -250 volts seems to exist for LEO conditions.

An analysis of a specific power system configuration is required to determine the response to array discharges [136]. A discharge in a solar array could produce oscillations in the power supplied to the load. It may or may not shut down the array [144]. The question of long term degradation, resulting from the discharges, has also not yet been resolved.

A second form of discharge phenomenon could arise from the operation of solar arrays at high voltage. This phenomenon has been called "zenering" [59] or "enhanced electron emission" [64,145] and has been studied only in the laboratory. The phenomenon appears to be related to illumination of a biased array exposed to a plasma in a laboratory chamber (Figures 3.45). The characteristics of the discharge are that the floating potential changes for minutes at a time and the monitoring signal is exceptionally noisy (Figure 3.46). It appears that small discharges continually occur and may cause space system bypass diodes to fail [146]. However, the phenomenon has not been studied sufficiently to assess its true impact.

3.4.2.5 *Power Transmission Alternatives*

It has been proposed that some space power system plasma interactions could be minimized if power generated on the array, at a design voltage consistent with space environment interactions, was transmitted to the load via an AC transmission line [147,148]. This space power system would more closely resemble a ground commercial power plant (Figure 3.47).

The frequencies considered for operating this transmission line for the NASA Space Station are usually given as either 400 or 20,000 Hz. The high frequency level is near the ion resonance frequency for the ion densities expected in low orbits (Figure 3.47). Operation at a naturally resonant frequency could increase coupling, causing a power loss in the system. Such a loss has been discussed, but no calculations are available to quantify the severity of the interaction. The 20 kHz operating frequency is also in the range of the possible discharge durations (up to 50 μsec or longer). This could lead to a resonance effect in the circuit which may not have been adequately evaluated.

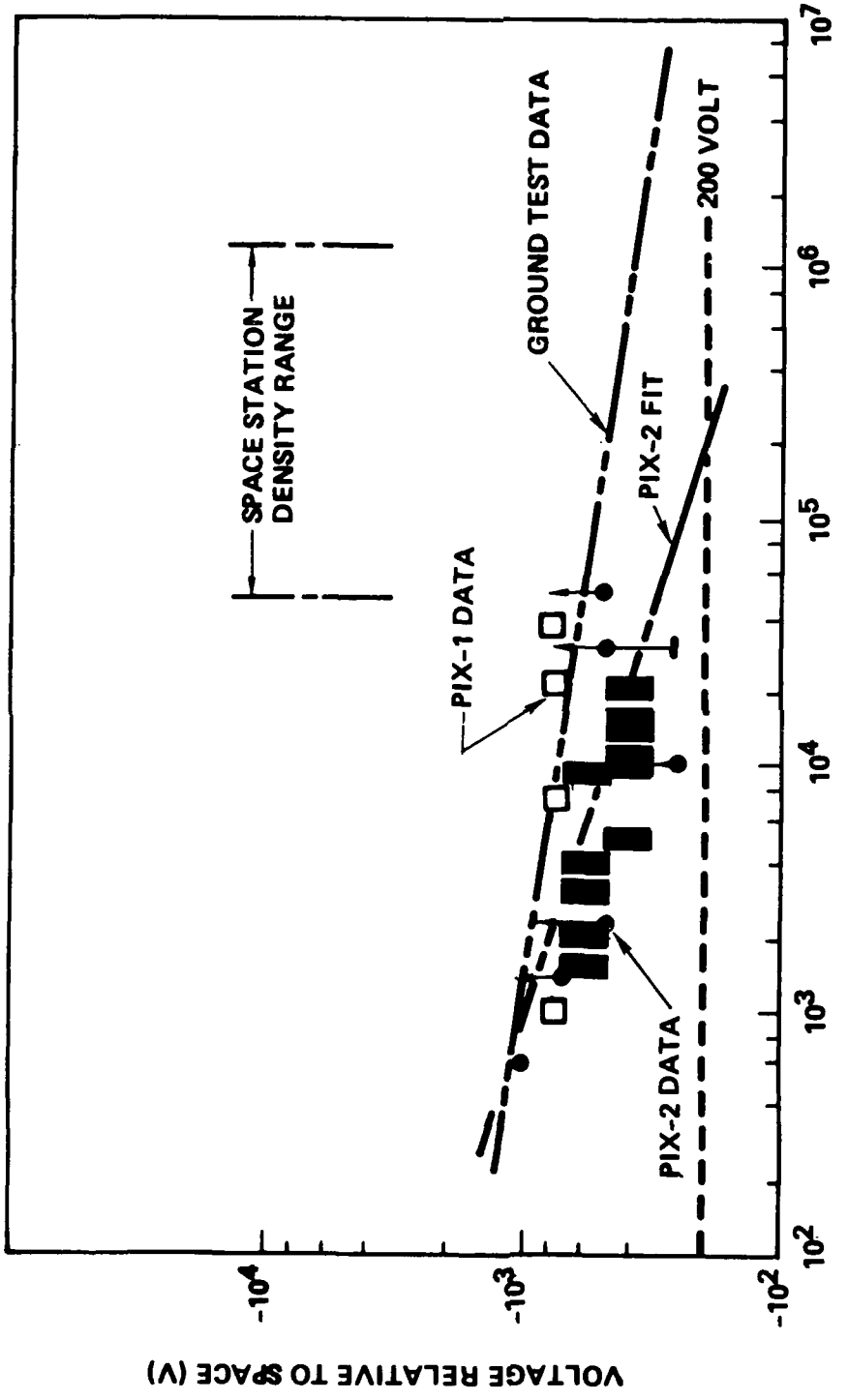

Figure 3.43 Shutdown Thresholds

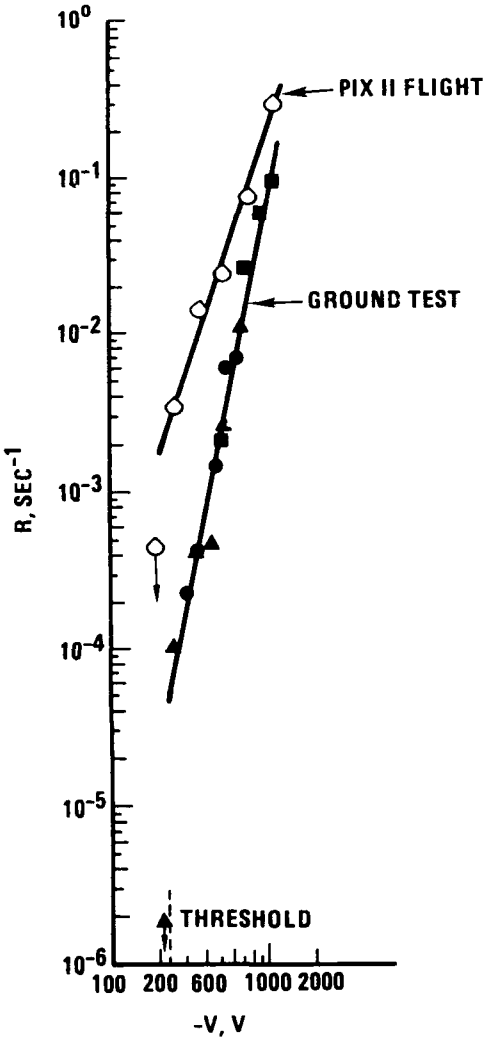

Figure 3.44 Arc Discharge Rate for Solar Cells

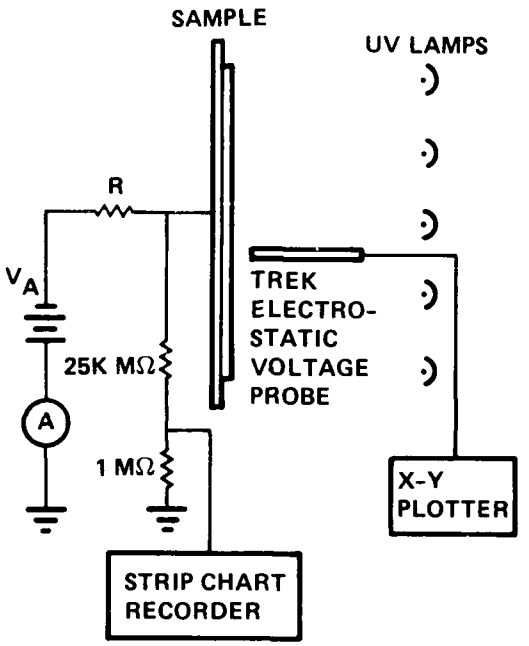

Figure 3.45 Enhanced Electron Emission Test Schematic

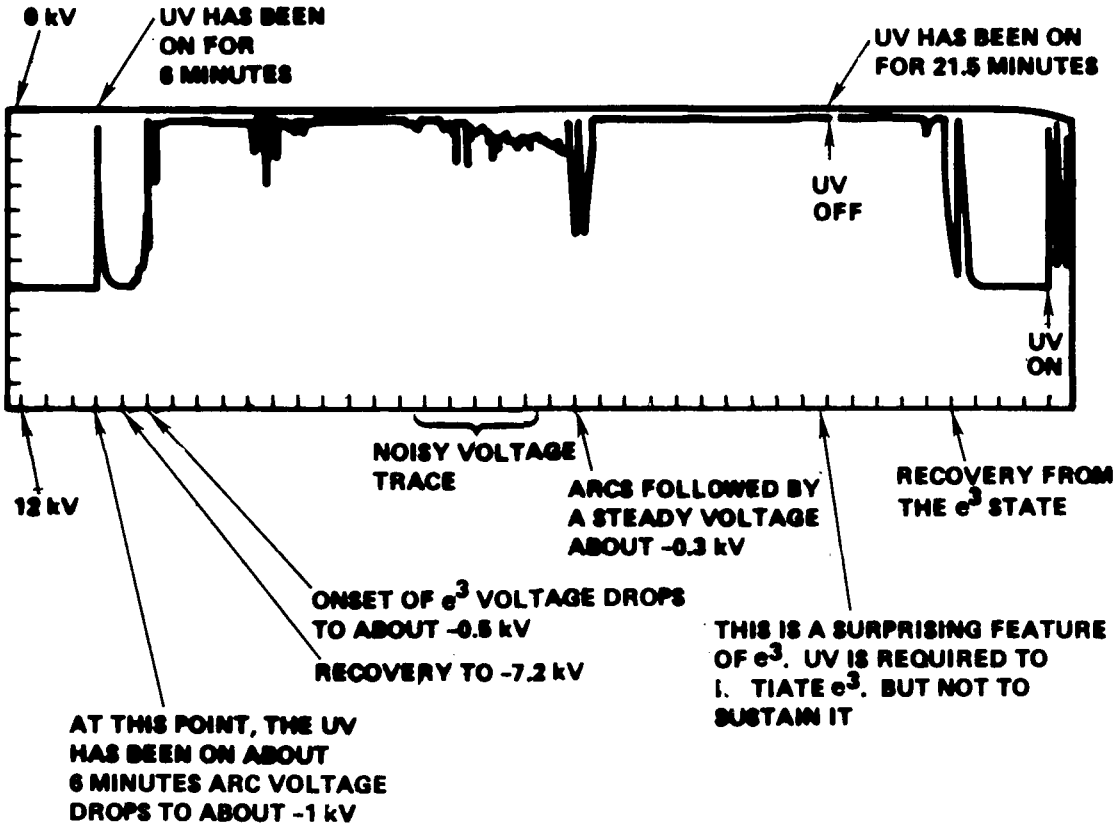

Figure 3.46 Enhanced Electron Emission Surface Voltage Test Results

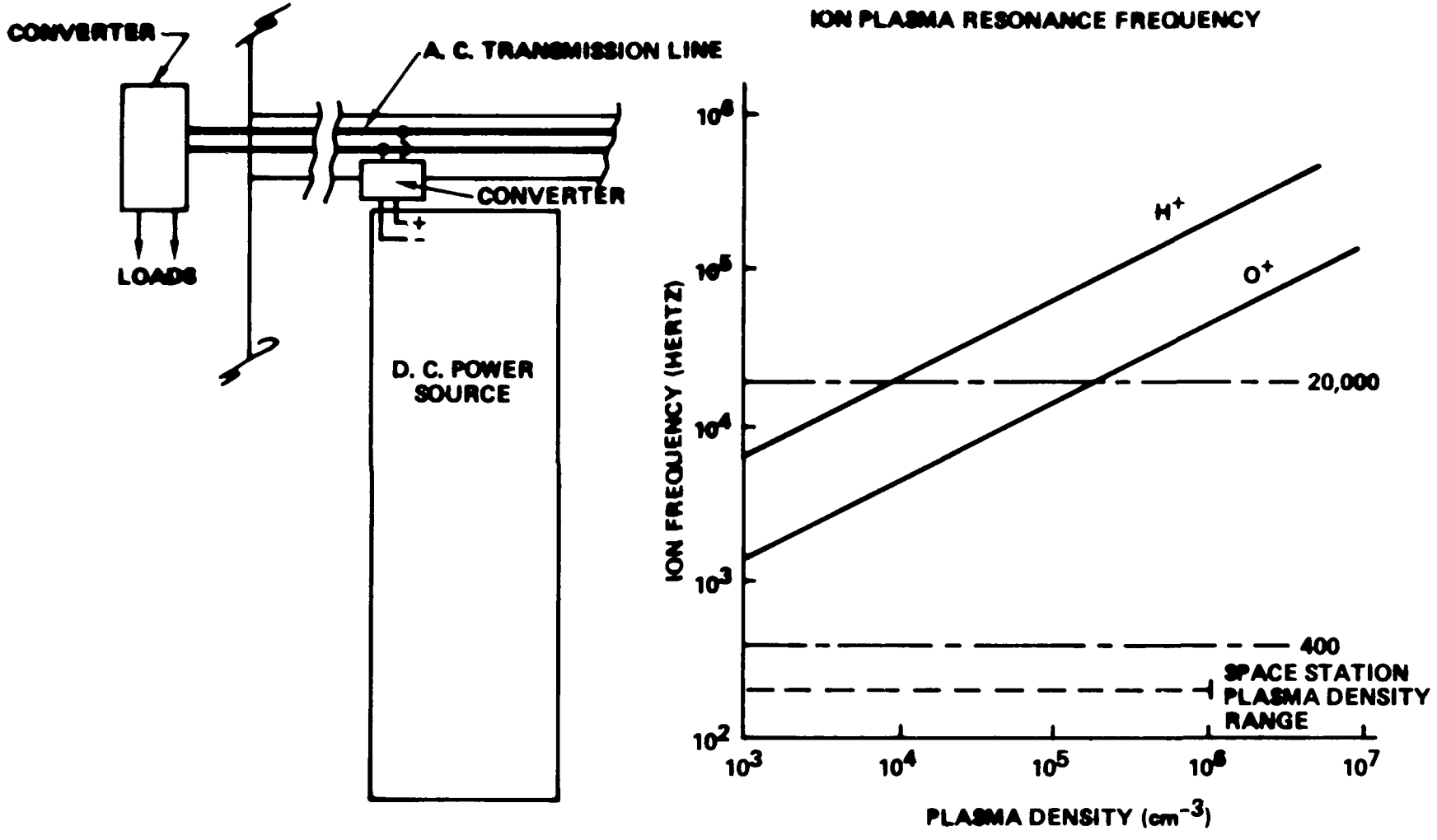

Figure 3.47 A.C. Power Distribution Concept

3.4.3 Research Maturity Rating

This interaction has been studied over the past 17 years in both laboratory and auxiliary payload space experiments. The state of knowledge of the interaction, however, is not complete. This is based upon incomplete NASCAP/LEO validation, lack of complete experimental data, inadequate scaling relationships, and the current state of development of discharge models. Therefore, the maturity was rated MODERATE (3).

3.4.4 System Impact Rating

High-voltage system interactions with the space plasma have been rated as having a SERIOUS (4) impact in LEO and PEO and a NEGLIGIBLE (1) effect in GEO.

3.4.5 Mitigation Techniques

Mitigation techniques for this interaction are limited until the phenomenon is better understood. One approach is to limit operational voltages to levels believed to be safe ($<$ 200 volts). Treatment of the interconnects might be effective. Use of a biased surrounding panel might cause the array to float at a more positive potential, decreasing the likelihood for discharges. Finally, a plasma thruster may also keep the potential at a more positive value, reducing the concern for discharges. None of these techniques have been evaluated, tested, or optimized.

4.0 HIGH ENERGY RADIATION ENVIRONMENT INTERACTIONS

This section considers interactions with the energetic particle environment. The topics which will be discussed are: Radiation Damage to Electronics, Solar Arrays, and Materials; Single Event Upsets; and Radiation Hazards to Man-In-Space.

4.1 GENERAL ENVIRONMENT DESCRIPTION

This environment consists of particles with energies in the range of 100 keV to hundreds of MeV and even higher for cosmic rays. These particles are a factor in the design of future large spacecraft, since they penetrate through the exterior skin of the vehicle into the interior. The three elements of this high energy environment to be discussed are: the trapped radiation belts, solar flares, and cosmic rays.

4.1.1 Trapped Radiation Environment

The National Space Sciences Data Center, located at NASA Goddard Space Flight Center, has developed and maintains models of the trapped electron and proton environments in the magnetosphere [149-152]. Other models are also available [6,153]. This information is available as maps of energetic particle fluxes, which are usually given in terms of isoflux contours (particles/cm^2-sec) for electrons and protons having energies greater than 0.5 MeV. Figure 4.1 and 4.2 are examples of such isoflux contour plots. Note that the inner and outer radiation belts are defined by these contours.

The inner radiation belt is a toroidal region, predominantly comprised of energetic electrons, at altitudes between 1 and 2 R_e (6.4 to 12.8 $\times$ 10^3 km). The outer belt is a somewhat larger region, predominantly protons, centered about a geocentric distance of approximately 5 R_e. The plasma sheet is the main source of most radiation belt particles. In addition, some high energy inner belt protons are decayed neutrons, trapped after being emitted as by-products of cosmic ray interactions with the atmosphere.

While the isoflux r[illegible]seem to indicate that the energetic particle environment only exists above 1000 km (Figure 4.3), this is not true for all orbits. There is a region between South America and Africa where the energetic environment extends to lower altitudes. This region is referred to as the South Atlantic Anomaly (Figure 4.4) [6]. Low inclination equatorial orbiting spacecraft can enter this region periodically (Figure 4.5). High inclination orbiting vehicles can also transit this region. In addition, the energetic electron regions extend to lower altitudes in the polar regions as illustrated in Figure 4.5 for a 400 km orbit. These environments are significant for spacecraft in LEO and PEO.

4.1.2 Solar Flares

Periodically, the Sun emits very energetic protons, alpha particles, and, at certain times, electrons. These events, part of the more generalized disturbance known as solar flares, are divided into two categories: ordinary and anomalously large.

The occurrence, intensity, duration, and distribution of energy in Solar Particle

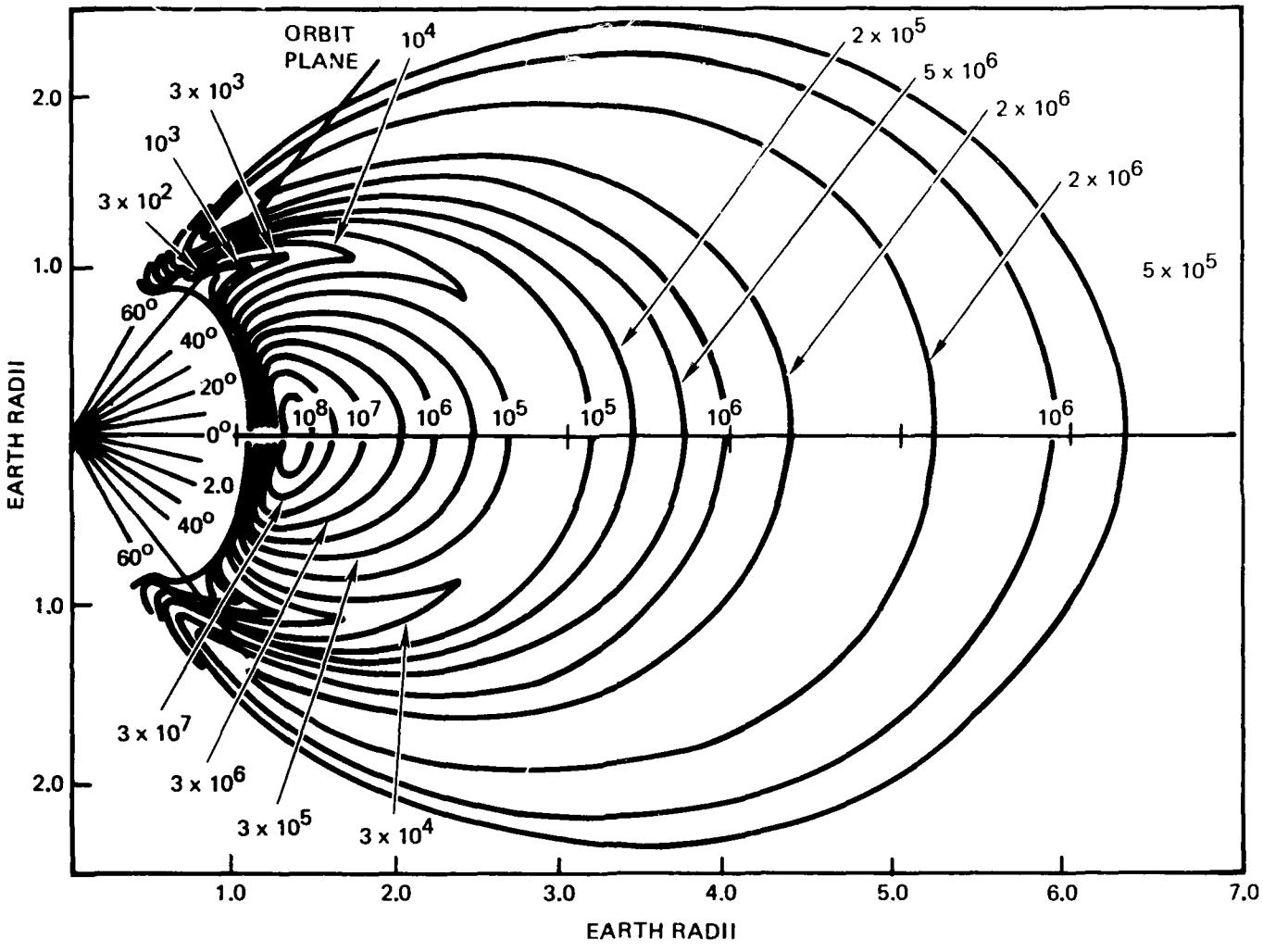

Figure 4.1 Natural Environment Isoflux Contours: Electrons (E > 0.5 MeV)

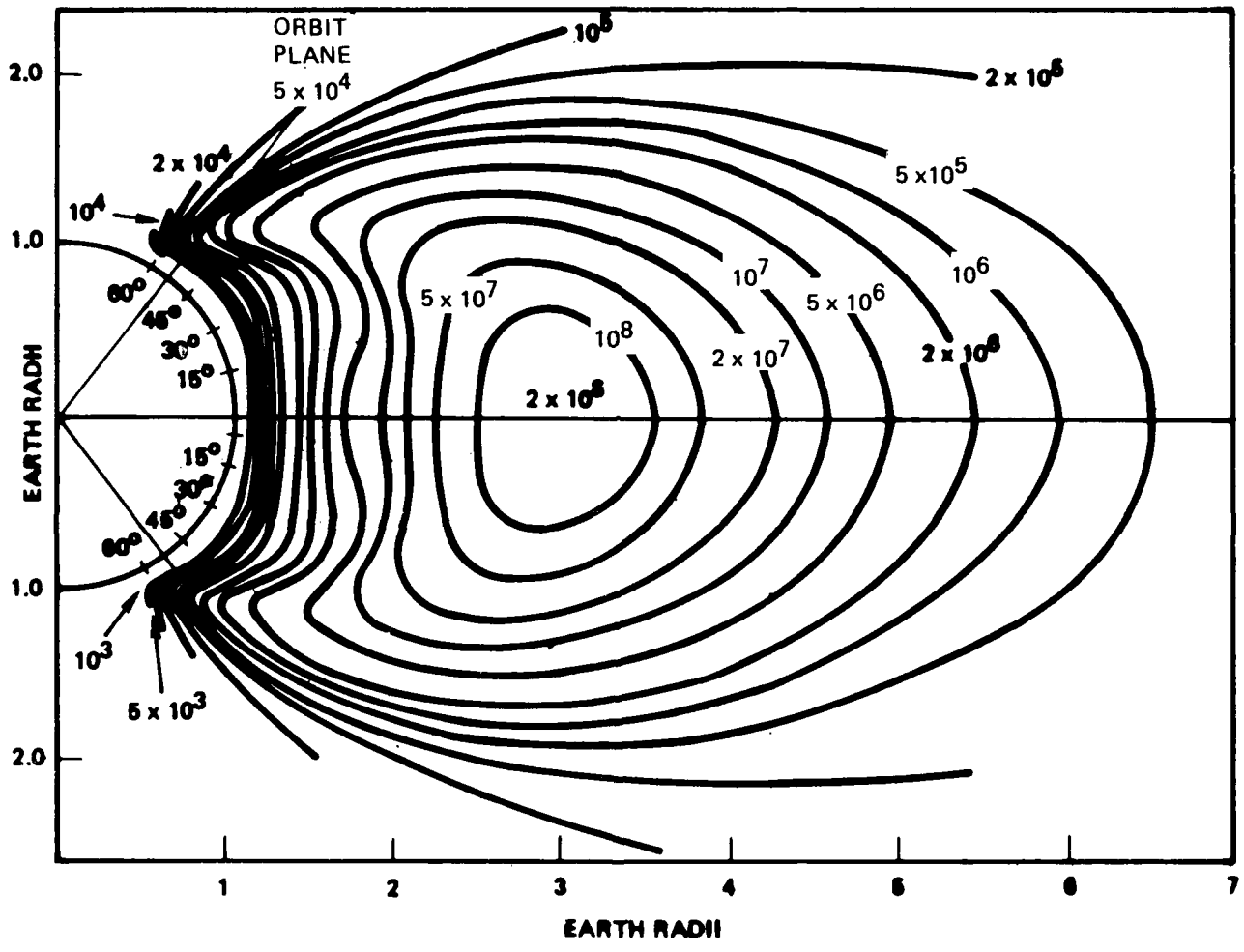

Figure 4.2 Natural Environment Isoflux Contours: Protons (E > 0.5 MeV)

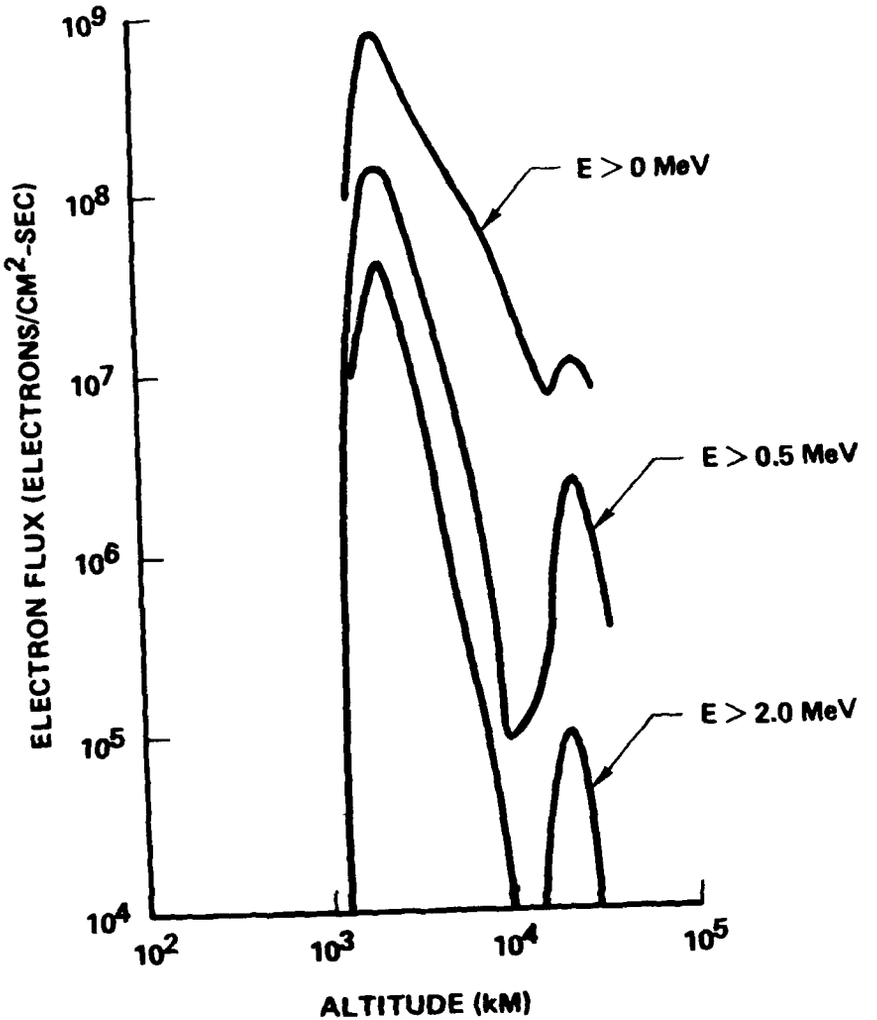

A. Electron Map

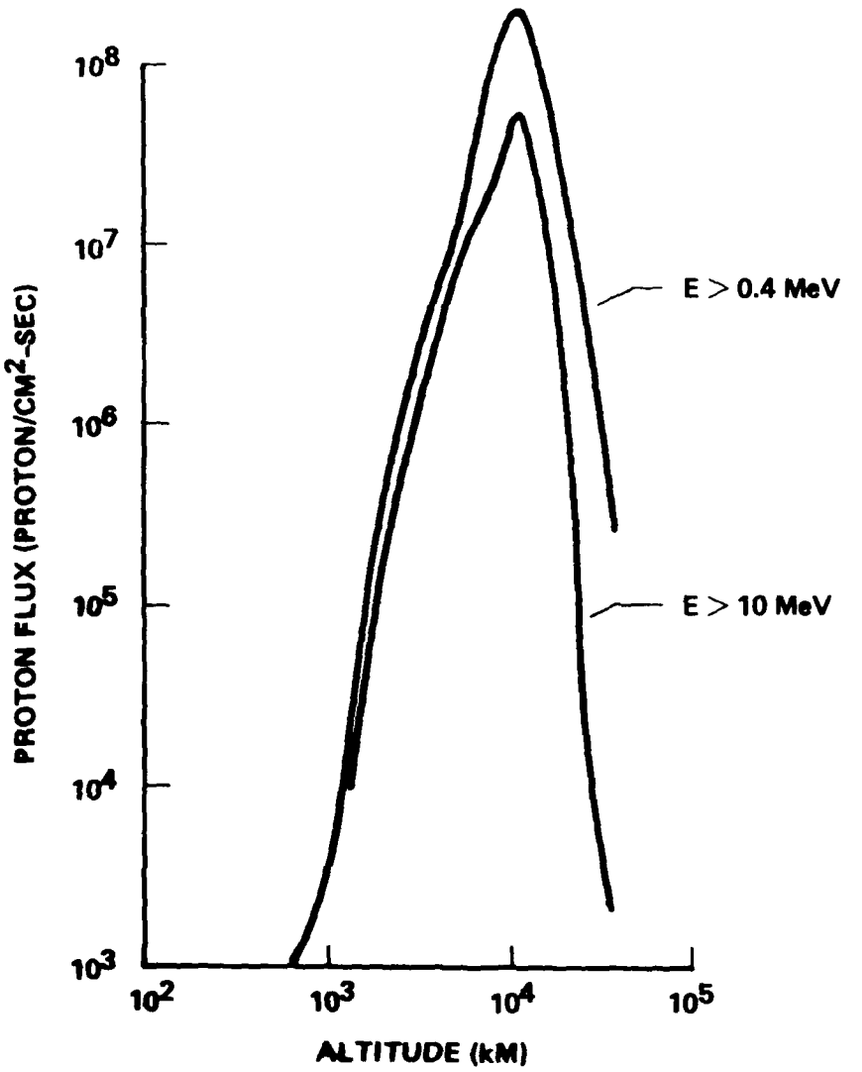

B. Proton Map

Figure 4.3 Omnidirectional Flux at the Geomagnetic Equator

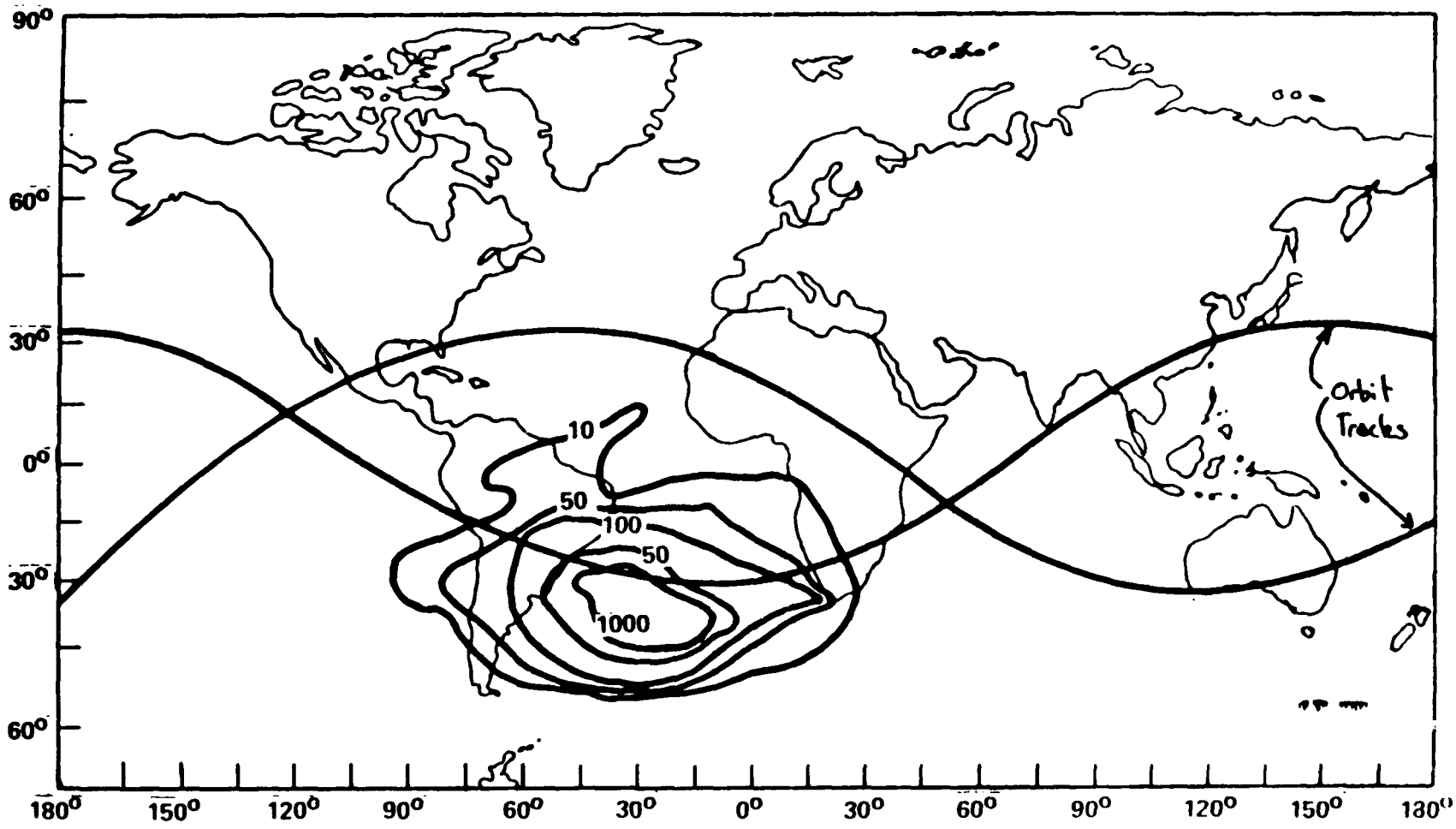

Figure 4.4 Proton Flux Densities at 296 km Altitude

Figure 4.5 Electron Constant Flux Contours at 400 km Altitude (E > 0.5 MeV)

Events (SPE) are highly unpredictable, although there is strong correlation with the eleven year solar cycle. Near sunspot maxima (1968, 1979, 1990) approximately 5 to 6 significant events can be expected per year. Near sunspot minima (1963, 1974, 1985, 1996) few significant events are expected. Based upon solar cycles 19 and 20 [154-155], the most intense events (November 12, 1960 and August 4, 1972) tend to occur 36 to 45 months after the peak in sunspot number. These events can dominate the radiation dose received by a long-lived satellite mission and are highly significant to astronaut safety and system effectiveness. For example, the SPE events of August 1972 contributed over 80% of the total radiation dose experienced during the entire solar cycle 20.

Although SPEs occur randomly, real-time observations of the solar disk in optical and radio wavelengths can reliably indicate whether major events have occurred. Depending upon the location of the flaring region on the Sun, solar observations can determine, within hours, when the effects will reach Earth. The duration of an SPE can be from a few hours to several days, as was the case of the intense SPE of August 4-9, 1972 [156]. During an SPE, near-Earth space, from the magnetic poles to about 60° geomagnetic latitude (magnetic L-shells > 4), experiences solar particle bombardment. Spacecraft located on magnetic field lines that have their origin within the SPE region (Figure 4.6) experience a nearly omnidirectional flux of solar particles.

The energy spectrum of solar flare particles incident on a spacecraft is highly dependent upon altitude and orbit inclination, due to geomagnetic shielding. For example, satellites in GEO experience the flux continuously for the duration of the event. Polar orbiting spacecraft, on the other hand, are affected for the duration of their orbit spent above the equatorward cut-off latitude. In the polar regions, the energetic solar proton flux in a large SPE exceeds the normal cosmic ray flux background by several orders of magnitude. The fluxes seen by a spacecraft in a 426 km polar orbit, for both ordinary and anomalously large events, are illustrated in Figure 4.7.

4.1.3 Cosmic Ray Environment

The cosmic ray environment is an interstellar, ionized gas that permeates the entire solar system [157]. Outside of the Earth's magnetic field, it provides an omnidirectional flux of ions ranging from hydrogen to nickel, with particle energies ranging from 10^6 to 10^{20} eV. The effluence of these particles for a quiet period during solar minimum is shown in Figure 4.8 while the flux for a disturbed period during solar maximum is shown in Figure 4.9. Note that particles with the same rigidity, or E/m ratio, behave similarly regardless of atomic species. Thus, it is traditional to plot the spectrum in units of MeV/atomic-mass-unit. Also note that the disturbed periods include small solar flares.

The Earth's magnetic field effectively shields regions of space from these cosmic ray particle fluxes. This is illustrated in Figure 4.10, which shows the expected cosmic ray environments for a solar minimum disturbed period in a 426 km orbits with a 30° or 90° inclination. This environment is of greatest concern for polar and geosynchronous orbits, but is less important for low inclination Earth orbits.

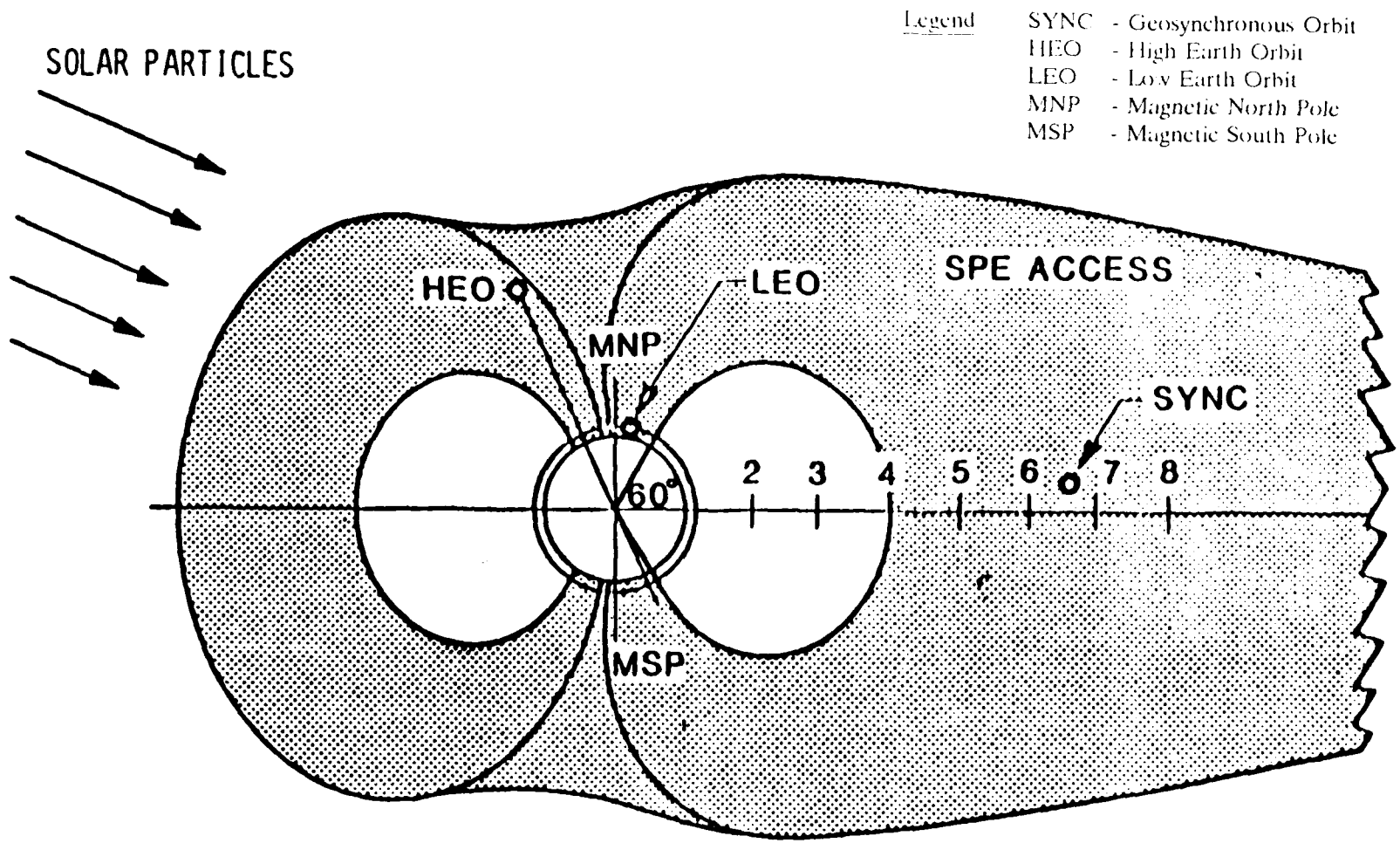

Figure 4.6 Solar Particle Access to Earth Orbits

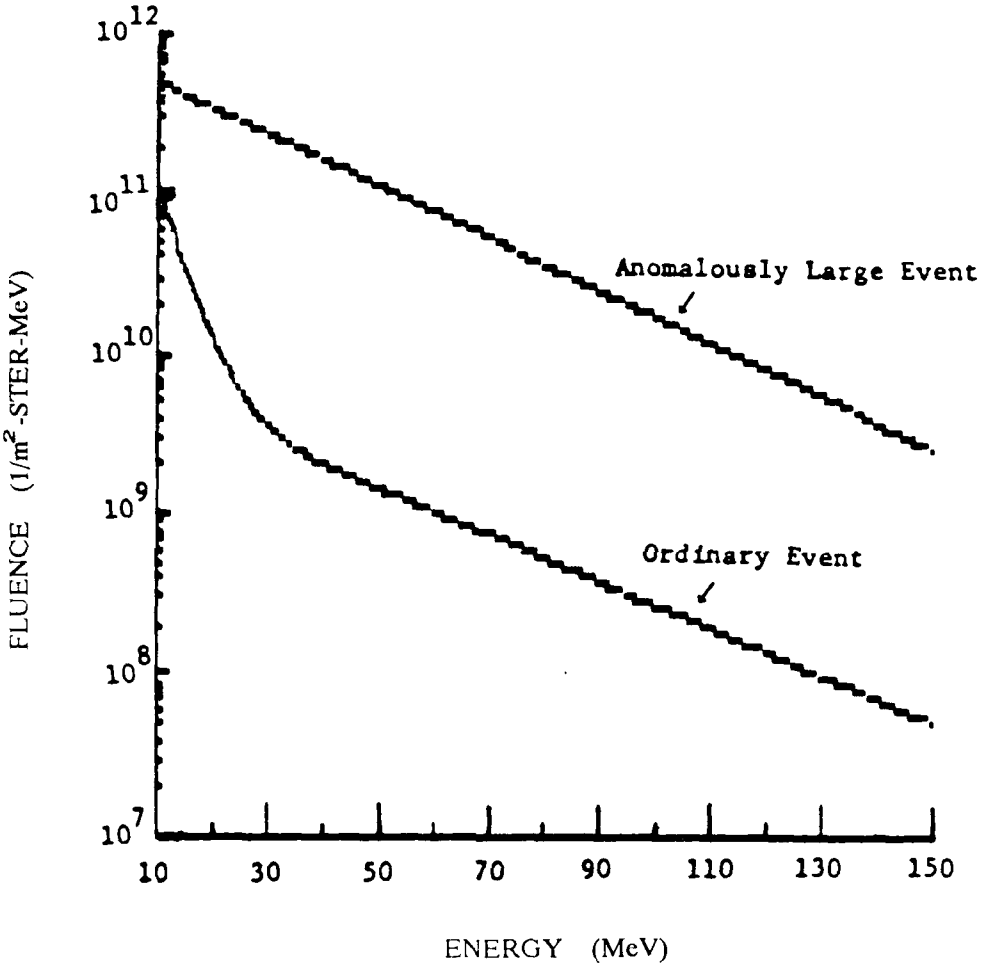

Figure 4.7 Solar Flare Environments for Solar Particle Events

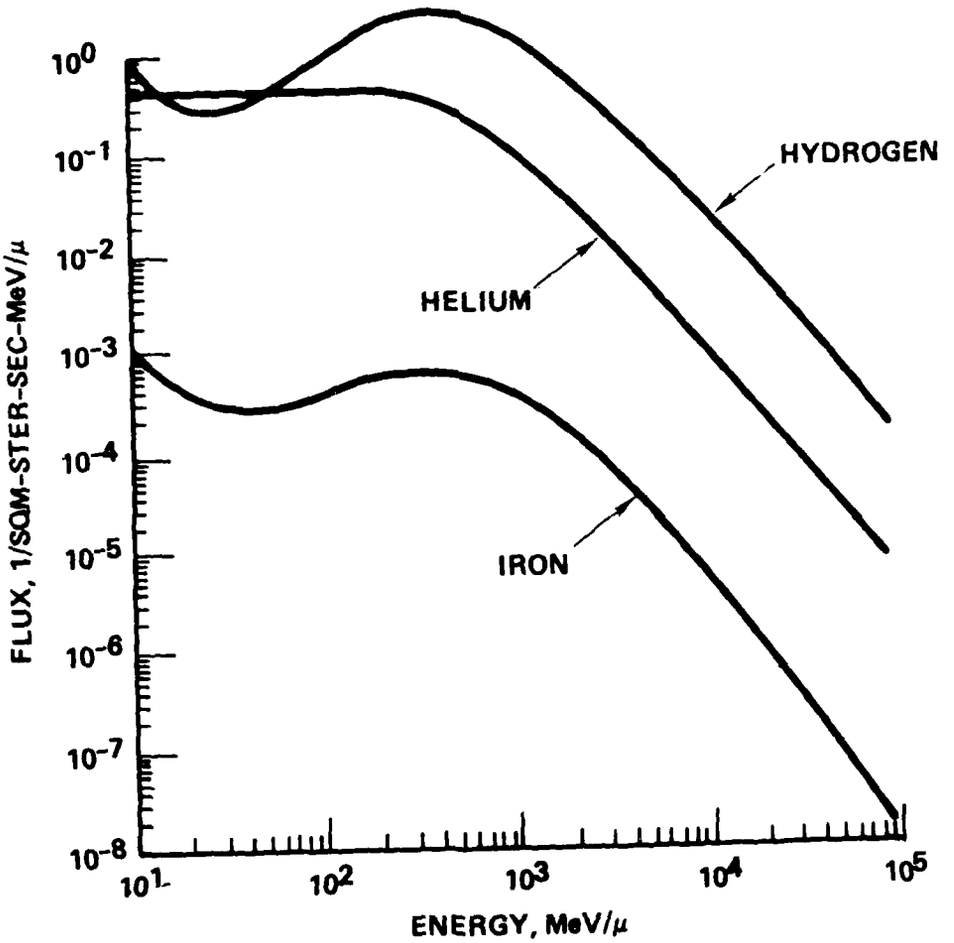

Figure 4.8 Solar Minimum Cosmic Ray Environment:
Free Field during the Quiet Period

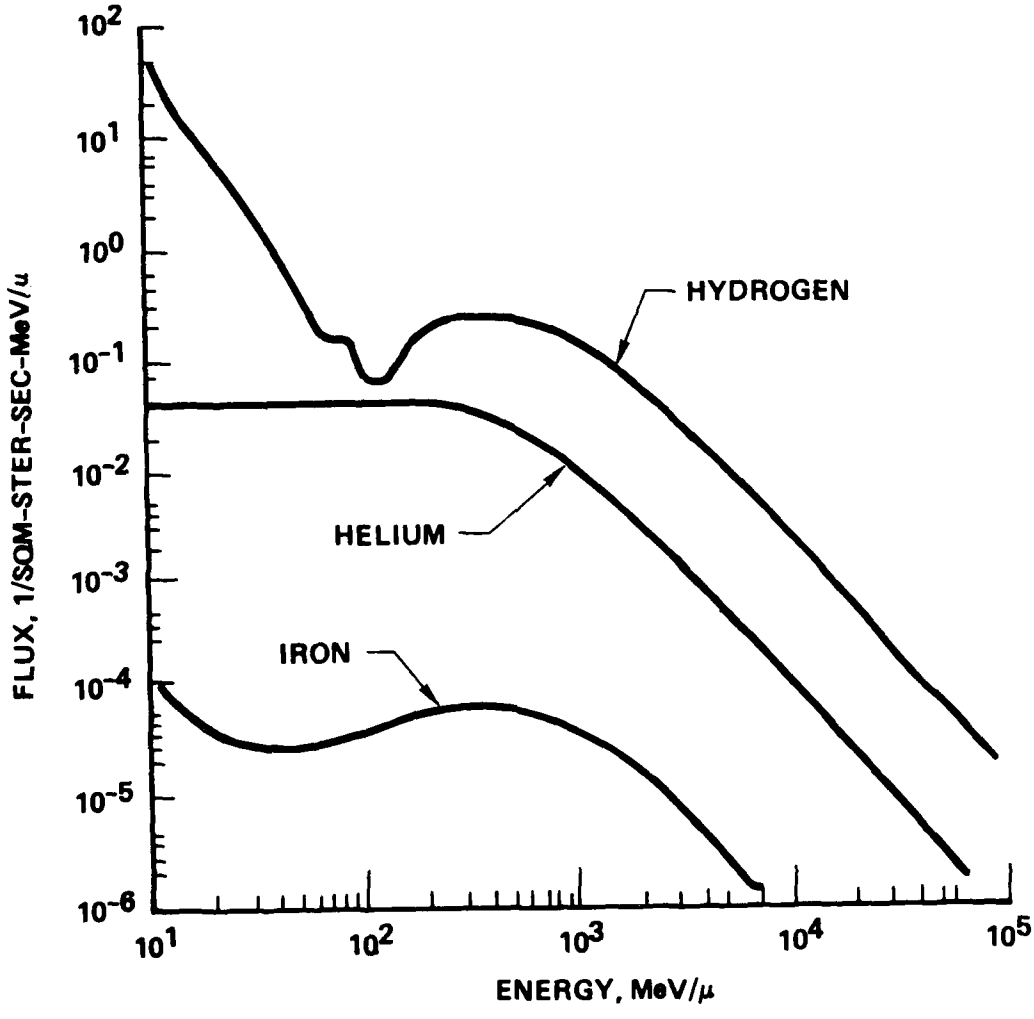

Figure 4.9 Solar Maximum Cosmic Ray Environment:
Free Field during the Disturbed Period

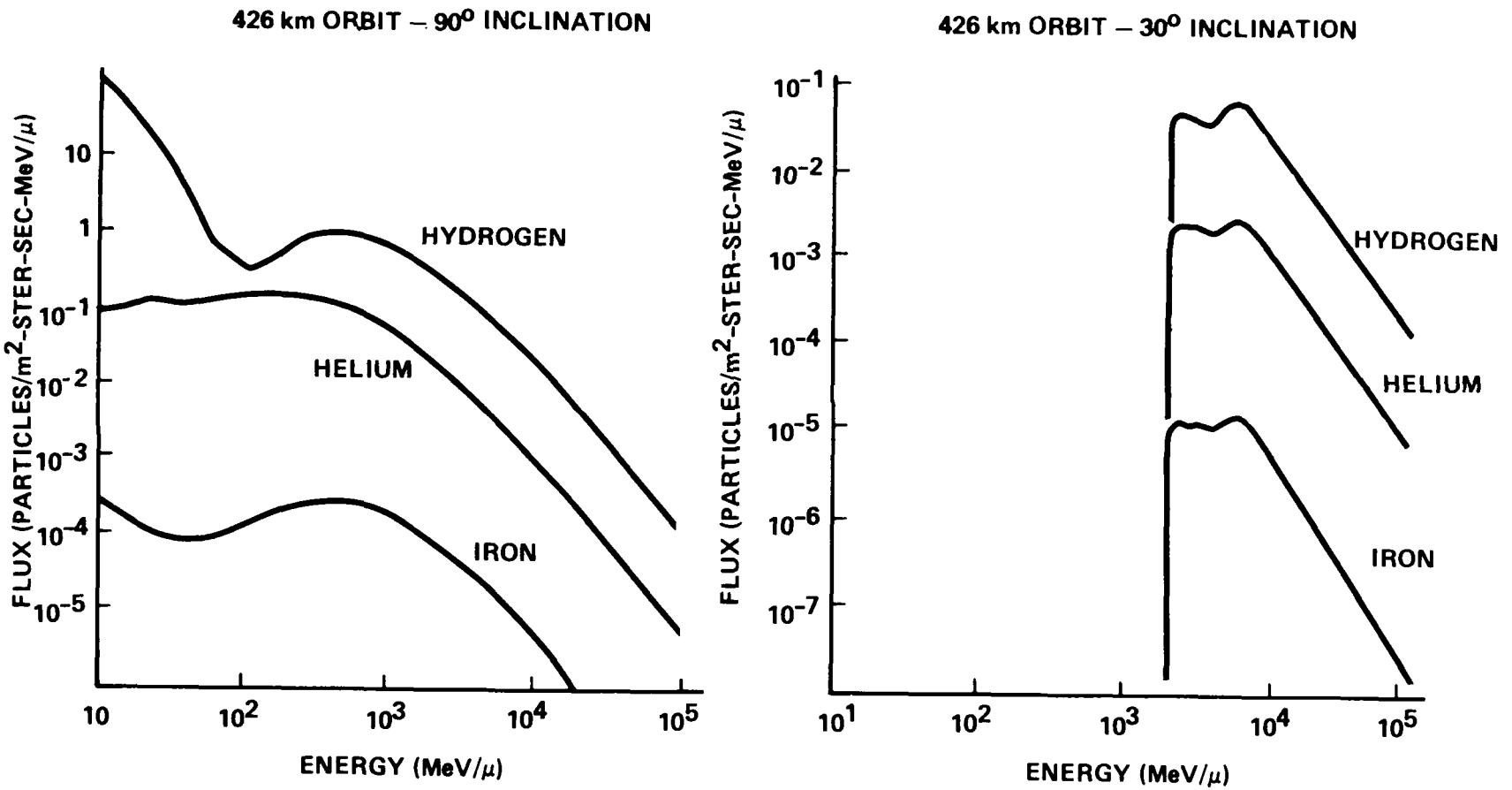

Figure 4.10 Solar Maximum Cosmic Ray Environment: 426 km Orbit during the Disturbed Period

4.2 RADIATION DAMAGE

4.2.1 Interaction Environment

The trapped radiation and solar flare environments discussed in Section 4.1.1 and 4.1.2 are applicable to this discussion. A major concern is the total radiation dose that accumulates over the mission life. The environment is usually obtained from NASA models (currently, AE-5 for electrons and AP-8 for protons). Computer codes such as ORB and ORP [149] or SOLPRO [160] are used to determine the radiation flux seen by a spacecraft in a given orbit. The Earth's magnetic field would shield a spacecraft from solar flare events for a low inclination earth orbit. The solar flare flux is averaged over the mission life and then factored into the computations to determine the radiation levels in polar and geosynchronous orbits.

4.2.2 Discussion of Interaction

The response of electronics, solar arrays, and materials to radiation exposure will be discussed in this section.

4.2.2.1 *Electronics*

Radiation shielding analyses of spacecraft systems have been performed for several years [161]. The objective is to determine the amount of shielding, either spacecraft structure or other surrounding materials, necessary to protect electronic components. If the radiation dose to electronic components exceeds specified levels, then parts can deteriorate, resulting in system performance degradation or even system failure. The attenuated radiation reaching a given component from all directions must be computed to determine the total radiation dose. The attenuation through a given material (e.g. spacecraft wall) can be computed using either sphere or slab models [162].

The example shown in Figure 4.11 indicates that, for a given radiation environment, a total dose of 10^4 rad (Si) would exist within the spacecraft, after attenuation by a 200 mil thick structure. This total dose (outside the box walls), can be tolerated by most electronics [16,17]. If the structure thickness is not adequate to provide the required attenuation, then the analysis must also consider any attenuation due to material between the spacecraft wall and the actual components. Total dose tolerance levels, determined from experimental data, for some typical components are shown in Figure 4.12. As can be seen, the CMOS, NMOS, and PMOS components become questionable at levels of 10^3 rad (Si) and can fail at levels of 10^4 to 10^5 rad. These parts, if required for a spacecraft system, must be protected to function properly for the mission duration. If necessary, spot shielding on the component may be used to provide the required level of protection. A safety factor of two between the predicted radiation level and the component susceptibility is usually desired.

The solar flare environment discussed in Section 4.1.2 has a large impact on spacecraft systems in polar and geosynchronous orbits. Significant component damage arises from effluence effects. Protons in the tens to several hundred MeV range are very

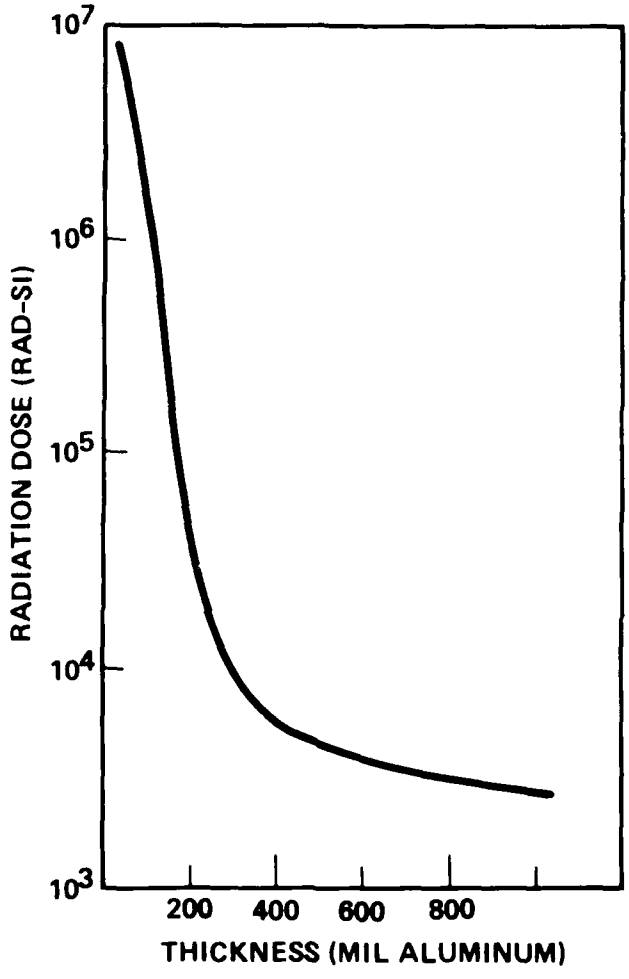

Figure 4.11 Shielding Effectiveness Against Natural Radiation Environment

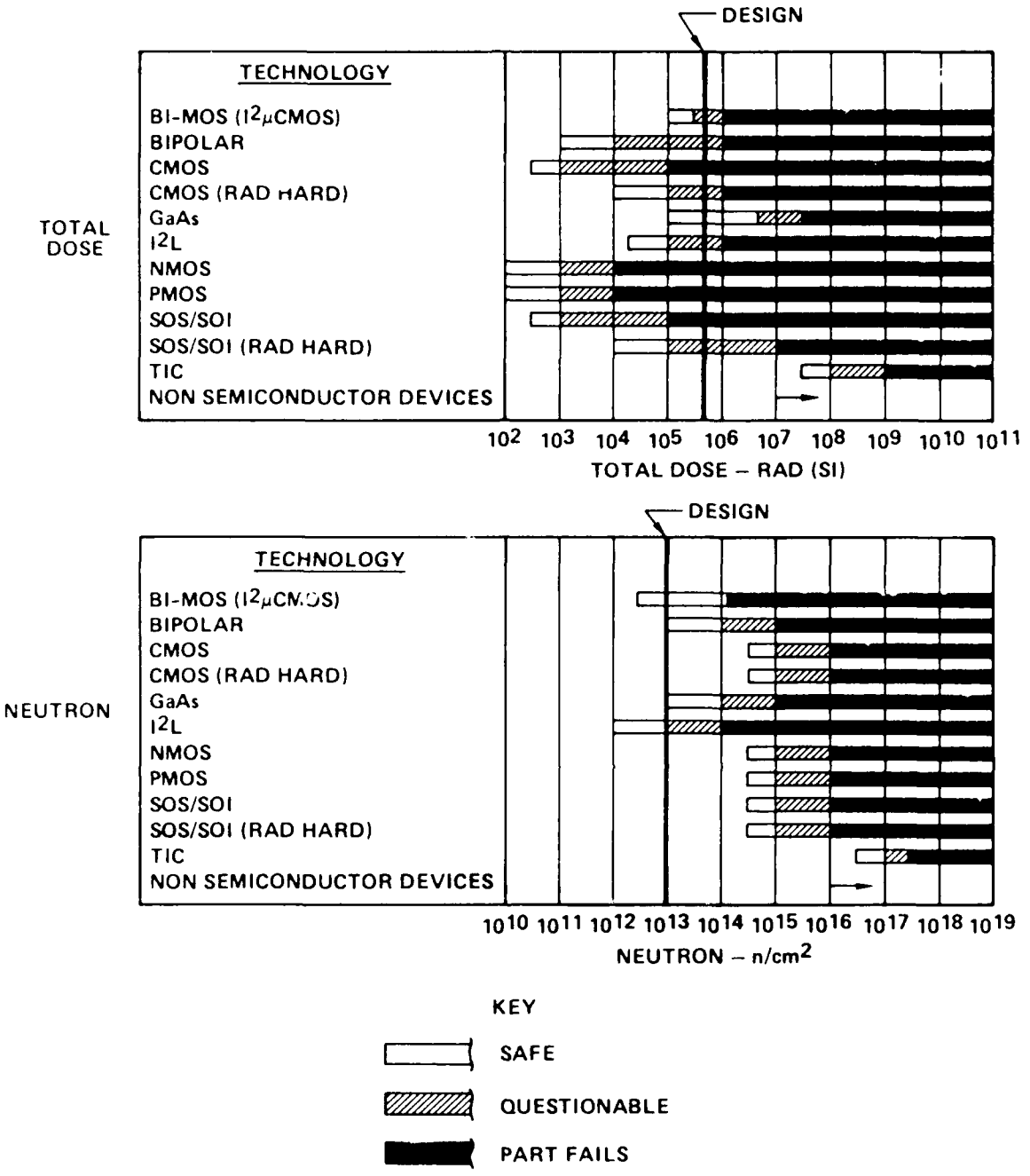

Figure 4.12 Radiation Analysis of Semiconductor Technology

penetrating, and one large flare can be as damaging as years of on-orbit operations in the normal, ambient magnetospheric environment. Intense long-term exposure to high energy proton fluxes produces crystal-lattice structure damage in solid state devices, which could result in component failure. The effects of large doses of heavily ionizing radiation on electronics have been investigated. The damage/flux curves for components are available in many cases. The dose at which individual components fail varies, but most modern electronic space components will suffer some degradation.

4.2.2.2 *Solar Arrays*

It is well known that solar array performance deteriorates in a radiation environment. The study and evaluation of this interaction is a mature technology and will only be briefly summarized here [166,167].

Computer codes have been created to predict the performance of solar arrays in a space environment, as a function of constituent materials and required time on orbit. Array degradation is usually determined experimentally or by use of prior flight data. The end of life power requirement is established by the mission plan. If the predicted power is inadequate, the array size has to be increased or additional protection (usually thicker cover glass) must be added.

4.2.2.3 *Materials*

The effect of radiation on the mechanical properties of composite materials, proposed for use on future spacecraft, has not been fully explored [168-175]. The data available to evaluate this effect is limited. Initial characterization of polyimide, epoxy and polysulfone films, and graphite reinforced composites has shown that significant chemistry changes occur during irradiation. The threshold for these changes is 10^9 rad. Major changes in mechanical properties have not been found. Additional long-term testing is planned to resolve this inconsistency.

4.2.3 Research Maturity Rating

The research maturity of these interactions was evaluated only for polar and geosynchronous orbits since the Earth's magnetic field shields the spacecraft from most of the high energy flux in LEO. The rating is CONSIDERABLE (4) for both the experimental and theoretical maturity for electronics and solar arrays, while MODERATE (3) for materials.

Radiation shielding analysis of spacecraft for space operations has been conducted for many years. These studies verify whether electronics used in spacecraft systems will survive the space radiation environment. Sufficient testing has determined the threshold levels for degradation and part failure. The maturity is NOT rated COMPLETE (5) because new parts are becoming available for space applications, and the reaction of these parts to space is not known. This argument also applies to solar array technology.

The maturity of research on radiation damage to materials is MODERATE (3)

because of the incomplete data available on composite responses to the natural radiation environment. The behavior of metals in spacecraft, however, is well understood. The future trend is to use composites rather than metals, and the effect of this transition on future, large spacecraft is unknown.

4.2.5 System Impact Rating

The system impact of radiation damage interactions for electronics and solar arrays is LARGE (4). Degradation or failure of an electronic component in a system could have a catastrophic impact. The technology is mature, possible failures are recognized, and shielding can be provided. Solar array degradation in the radiation environment must be known to ensure that the array will function throughout the mission. This technology is also mature and capable of accomplishing this task.

The system impact for radiation damage for materials is MODERATE (3). The changes in the material properties of the new composites, while significant, has not yet been determined to be a threat to spacecraft structures.

4.2.6 Mitigation Techniques

The standard mitigation technique to protect electronics from excessive radiation damage is to increase the shielding thickness around the components. This can be accomplished by increasing the spacecraft wall thickness, the box wall thickness, or spot shielding around the delicate component itself. Trade-off studies optimize the shielding for the least impact to weight and volume resources.

Shielding is also the best way to mitigate against the effects of solar proton events. The arrival of these solar particles in the region around Earth can be predicted from observations of the Sun and environmental modeling analysis. Operational spacecraft can expect to experience several solar flare events, in periods of maximum solar activity, during their mission life. Since designers are attempting to extend mission life beyond 10 years, all spacecraft will have to operate in active periods. Thus, shielding must compensate for the additional effluences expected.

Current investigations of structural materials will determine the protection techniques necessary to avoid radiation damage. The use of thin coatings is one possible technique to protect the material from the environment.

4.3 SINGLE EVENT UPSETS (SEUs)

4.3.1 Interaction Environment

Most Single Event Upsets are caused by cosmic rays and high energy protons. The cosmic ray environment was discussed in Section 4.1.3 and the high energy protons of the trapped radiation belt in Section 4.1.1. As was mentioned earlier, the Earth's magnetic field shields low inclination, low altitude spacecraft from cosmic ray and energetic proton effects.

4.3.2 Discussion of Interaction

SEUs occur when a high energy ion (from a cosmic ray or solar flare) or energetic proton (from the trapped radiation belts) penetrates a semiconductor device (Figure 4.13). There are several upset mechanisms [3,176-189]: (1) Direct ionization of the semiconductor; (2) Ionization by recoil nuclei and alpha particles from nuclear reactions; (3) Memory cell discharge; (4) Transients induced in bit lines; and (5) Latchup. A list of satellites that have experienced SEUs is given in Table 4.1.

As an energetic particle penetrates a device, it loses energy by ionizing the silicon along its path. The rate of energy lost along the penetrated path is called dE/dx, stopping power, or Linear Energy Transfer (LET). An electron-hole pair is created in silicon for every 3.6 eV of energy lost. Strong local electric fields (as occur in the sensitive volume of a memory cell) can cause electrons or holes to be collected. If the ionizing particle has a large enough LET, then sufficient charge can be collected within the sensitive volume to cause a state change (bit-flip).

The threshold quantity of charge required for the bit flip is called the critical charge and is a function of the device size and operating characteristics. As shown in Figure 4.14, a 2 micron unhardened device has a critical charge of about 0.1 pC. A single 100 MeV/nucleon iron cosmic ray nucleus can deposit this critical charge in the sensitive volume of a 2 micron scale device. Such particles exist in PEO and GEO.

Table 4.1
Operational Satellites that Experienced Single Event Upsets

TIROS-N
DMSP
Satellite Data System
NAVSTAR/GPS
Solar Maximum Mission
Landsat D
Voyager
Pioneer Venus
LES 8 & LES 9
Intelsat V
TDRSS

The LET of protons is too low to generate the critical charge in the sensitive volume of current generation devices. However, protons can undergo nuclear reactions with the silicon. The reaction products (recoiling silicon atoms or magnesium atoms and alpha particles) have much higher LETs, and can cause the upsets.

The bit flip is a "soft" error, that is, it is easily corrected (though its consequences may not be). Hard errors, such as latchup, can also occur. For example, current paths between adjacent p-channel and n-channel devices in CMOS chips can be created by cosmic ray ionization. The resulting high currents can lead to device burnout if not corrected. The threshold for bit flip is typically higher than the threshold for latchup.

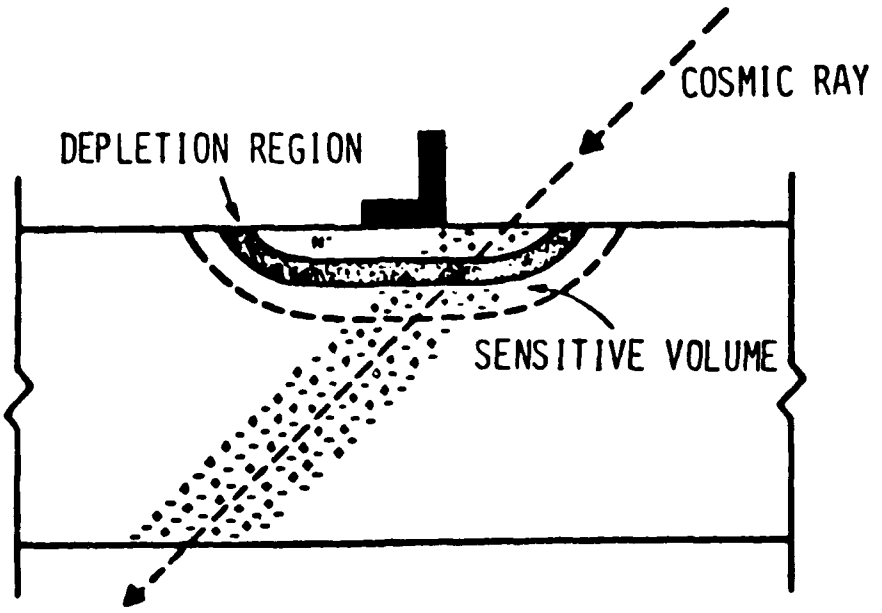

(A) Cosmic Ray Induced Upset

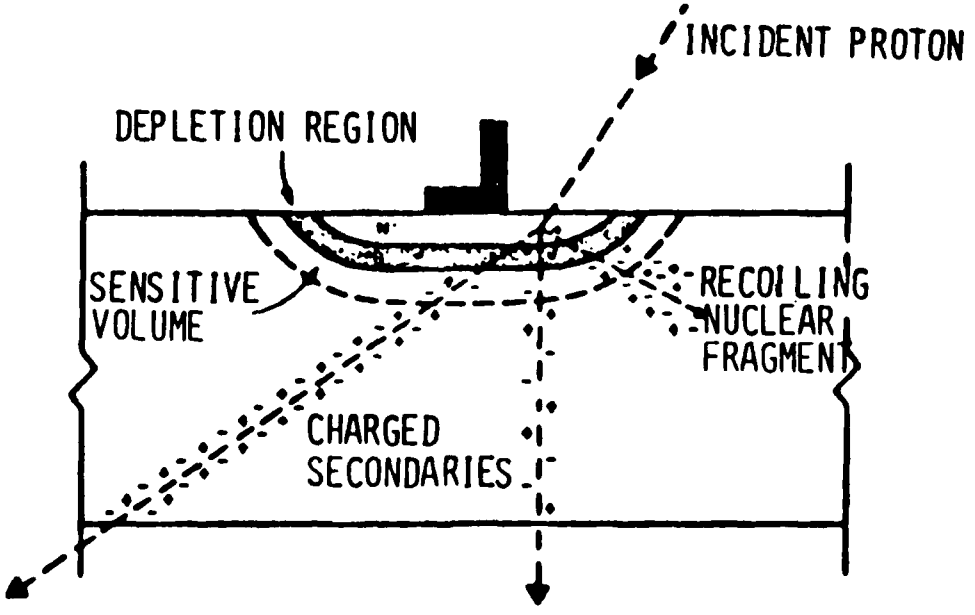

(B) Proton Induced Upset

Figure 4.13 Ionizing Path Through Semiconductors

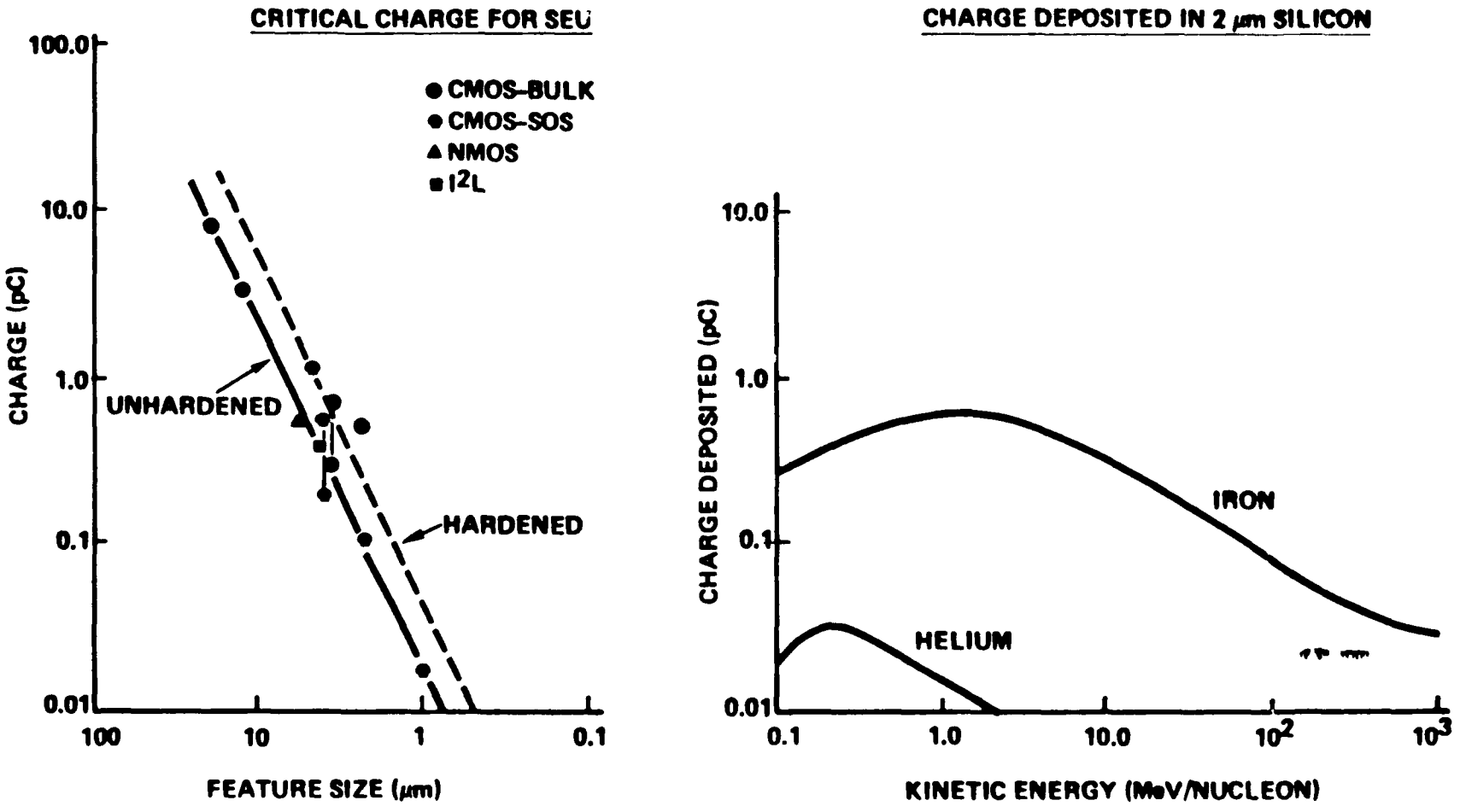

Figure 4.14 Cosmic Ray Effect in Electronic Devices

The susceptibility of various digital components to single event upsets has been studied in ground tests for the past several years. The upset rate (R ≡ flips/bit-day) for a given environmental condition can be estimated from the following equation:

$$R = \frac{KA}{(LET)^2}$$

where: K = proportionality constant
A = upset cross-sectional area
LET = Linear Energy Transfer (measured by ground tests)

Tests can be run on specific devices to determine values for the quantities necessary to estimate upset rates [190-192]. Lists of device susceptibilities are available and a typical set of data is reproduced in Table 4.2 [192]. The components from Table 4.2 that experienced latchup are identified in Table 4.3.

4.3.3 Research Maturity Rating

The maturity level of single event upsets was rated CONSIDERABLE (4) for both analytical and experimental studies. There have been many studies of this phenomenon, both experimental and analytical. The rating would have been COMPLETE (5) if the ground tests agreed better with behavior in space. The ground results indicate a higher susceptibility than space data.

4.3.4 System Impact Rating

The system impact for these interactions was rated LARGE (4) because SEU random events could have serious impact on future, automated systems. Many spacecraft rely upon on-board computers for all operations, especially planetary missions. The memory of these computers could be upset by energetic particles and the mission could be lost due to the long time required for uploading corrective commands. Many existing spacecraft experience SEUs and sometimes entire systems must be reset.

4.3.5 Mitigation Techniques

Procedures have been established to deal with situations where SEUs and latchups cause problems. A systems engineering review of a suspected system is usually conducted. If an event could result in an intolerable system impact, then the component should be replaced with one that is more immune to upsets. In addition, multiple parts could be used or error detection codes and/or multiple circuits could also be installed to circumvent upsets. The latter choices are based on the opinion that not all components, or bits in a word, would be affected simultaneously by cosmic rays. At times, if an event cannot result in a serious operational problem, no changes are made. A simple thing like replacement of an integrated circuit can require extensive, and expensive, requalification of systems and even of the complete spacecraft.

DEVICE I.D.	DEVICE MANU-FACTURER[1]	FUNCTION DESCRIPTION	TECHNOLOGY	TYPE OF TEST[2]	SEU THRESHOLD (MeV/(mg/cm²))	ASYMPTOTIC SEU CROSS-SECTION (cm²/device)	LET INTERVAL (MeV/(mg/cm²))	SIG OF CURVE[3]	DATE TESTED	TEST LOCATION[4]
XTA11246Z	RCA	4K X 1 RAM	CMOS/SOS	UL	50	1.2×10^{-4}	80 120	I	FEB 84	88IN
TA11370	RCA	4K X 1 RAM	CMOS/SOS	UL	≥ 50 (+ 5V)	≥ 1×10^{-4}	≯120	G	DEC 83	88IN
					≥ 80 (+ 10V)	≥ 1×10^{-5}	≯120	G	DEC 83	88IN
TA12702[5]	RCA	16K X 1 RAM	CMOS/SOS	UL	≥ 70	≥ 1×10^{-4}	≯100	G	APR 84	88IN
TCS130S	RCA	4K X 1 RAM	CMOS/SOS	UL	≥ 48	≥ 1×10^{-3}	≯120	G	MAY 82	88IN
TCS146	RCA	4K X 1 RAM	CMOS/SOS	UL	≥ 30	≥ 4×10^{-4}	≯120	G	JAN 80	88IN
1802RH[6]	RCA	MICRO-P	CMOS	UL	> 120	NO UPSET	120		DEC 83	88IN
CDP1821	RCA	1K X 1 RAM	CMOS/SOS	UL	> 120	NO UPSET	120		FEB 79	88IN
HMMP1834	HUG	1K X 8 ROM	CMOS	L	> 120 (L)				MAY 80	88IN
CDP1853	RCA	N-BIT DECODER	CMOS	L	> 120 (L)				MAY 80	88IN
TCS205RH	RCA	1K X 4 RAM	CMOS/SOS	UL	≥ 120	≥ 2×10^{-5}	≯120	G	MAY 82	88IN
TCS210S	RCA	1K X 4 RAM	CMOS/SOS	UL	≥ 37	≥ 3×10^{-4}	≯120	G	MAY 82	88IN
AM25LS07	AMD	HEX D FLIP/FLOP	LS TTL	UL	13	3×10^{-4}	30 80	S	MAY 83	88IN
AM27LS00	AMD	256 X 1 RAM	LS TTL	UL	4	1×10^{-2}	40 80	I-G	MAY 83	88IN[7]
X2816AM	XIC	2K X 8 EEROM	N CH F GATE MOS	UL	< 54	DATA REDUCTION IN PROGRESS			JUN 84	25MV
AM2914	AMD	VP PNT CONT	TTL	UL	5	5×10^{-4}	30 60	I	OCT 82	88IN
AM2914 REV	AMD	VP PNT CONT	TTL	UL	10	5×10^{-4}	30 60	I	FEB 84	88IN
AM29705	AMD	16 X 4 2-PORT RAM	TTL	UL	6	4×10^{-3}	20 40	S	FEB 84	88IN
SA3000[8]	SNL	MICRO-P	CMOS	UL	40 (7.4V)	5×10^{-7}	50 80	S	MAY 83	88IN
SA3001	SNL	256 X 8 RAM[8]	CMOS	UL	≥ 70	≥ 2×10^{-3}	≯120	G	MAY 83	88IN
AM31L01	AMD	16 X 4 RAM	L TTL	UL	< 40	1×10^{-2}	80 128	G	FEB 79	88IN
SA115[8]	SNL	16K X 1 RAM	CMOS	UL	≥ 70	≥ 7×10^{-6} (100 KΩ)	≯100		MAY 83	88IN
SA3240[8]	SNL	16K X 1 RAM	CMOS	UL		DATA REDUCTION IN PROGRESS			JUN 84	25 MV
CD4021B	RCA	8-bit SHIFT REGISTER	CMOS	UL	> 125	NO UPSET	125		FEB 84	88IN
NBRC4042	HUG	4K X 4 RAM	CMOS/SOS	UL	20	2×10^{-3}	80 120	I	MAY 82	88IN
CD4061	RCA	256 X 1 RAM	CMOS	UL	80	> 2×10^{-4}			FEB 79	88IN
CMM5104	RCA	4K X 1 RAM	CMOS/SOS	UL	50	1.2×10^{-4}	80 120	I	FEB 84	88IN
MW5114	RCA	1K X 4 RAM	CMOS	UL	≥ 60	≥ 5×10^{-6}	80		APR 84	88IN
54ALS10	TI	3-INPUT NAND	ALS TTL	L	> 80 (L)				APR 84	88IN
54F109	FSC	DUAL J K FLIP/FLOP	F TTL	UL	11	2×10^{-5}	20 30	S	FEB 84	88IN
54LS109	NSC	DUAL J K FLIP/FLOP	LS TTL	UL	7	2.5×10^{-5}	20 40	I	FEB 84	88IN
54ALS138	TI	3-TO-8 DECODER	ALS TTL	L	> 80 (L)				APR 84	88IN
54HC165	HUG	8-bit SHIFT REGISTER	CMOS	L	> 120 (L)				APR 84	88IN
54LS169	SIG	U/D COUNTER	LS TTL	UL	15	5×10^{-5}	20 40	I	FEB 84	88IN
54LS173	SIG	4-bit REGISTER	LS TTL	UL	12	2×10^{-4}	40 80	I	FEB 84	88IN
54S189	SIG	16 X 4 RAM	S TTL	UL	5	1.5×10^{-3}	20 40	S	FEB 84	88IN
54LS194A	TI	4-bit SHIFT REGISTER	LS TTL	UL	5	8×10^{-5}	20 - 40	I	FEB 84	88IN
54C200	NSC	256 X 1 RAM	CMOS	UL	> 120				FEB 79	88IN
54S201	SIG	256 X 1 RAM	S TTL	UL	5	9×10^{-3}	40 80	I	MAY 84	88IN
54F373	FSC	OCTAL LATCH	F TTL	UL	30	2×10^{-5}	80 120	I	FEB 84	88IN
54LS373	TI	OCTAL LATCH	LS TTL	UL	15	2×10^{-4}	40 80	I	APR 84	88IN
54ALS374	TI	OCTAL FLIP/FLOP	ALS TTL	UL		≥ 2×10^{-4}	> 40		APR 84	88IN
54LS378	SIG	HEX D FLIP/FLOP	LS TTL	UL	13	2×10^{-4}	25 80	S	FEB 84	88IN
54LS670	SIG	4 X 4 REGISTER	LS TTL	UL	5	5.5×10^{-4}	10 40	S	FEB 84	88IN
54ALS74	TI	DUAL D FLIP/FLOP	ALS TTL	UL	4	1.5×10^{-4}	40 - 80	I	APR 84	88IN
54S74	SIG	DUAL D FLIP/FLOP	S TTL	UL	≥ 30	≥ 3×10^{-5}	> 80	G	APR 84	88IN

NOTES: (ALL DEVICES ARE BASED AT 5V UNLESS OTHERWISE STATED)

1. AMD = ADVANCED MICRO DEVICES
   FSC = FAIRCHILD SEMICONDUCTOR
   FUJ = FUJITSU
   HAR = HARRIS
   HUG = HUGHES
   IDT = IDT
   ITS = INTERSIL
   MOT = MOTOROLA
   NSC = NATIONAL SEMICONDUCTOR
   RCA = RCA
   SIG = SIGNETICS
   SNL = SANDIA LABS
   TI = TEXAS INSTRUMENTS
   XIC = XICOR
   ZIL = ZILOG
2. U = SOFT ERROR UPSET. L = LATCH-UP
3. S = SHARP THRESHOLD. I = INTERMEDIATE THRESHOLD
   G = GRADUAL THRESHOLD
4. 88IN = LBL 88 INCH CYCLOTRON; 25 MV = ORNL HHIRF 25MV TANDEM
   BEVALAC = LBL BEVELAC
5. LOT 4437 ONLY
6. REGISTERS ONLY
7. TESTED AT BEVALAC, ALSO
8. EXTENSIVE EXERCISE OF ALL SUBSYSTEMS (SELF TEST)
9. DEVICE CONTAINS CROSS-COUPLED RESISTORS
10. EXTENSIVE EXERCISE OF ALL SUBSYSTEMS

Table 4.2 Devices Tested for Heavy Ion Induced SEU

DEVICE I.D.	DEVICE MANU-FACTURER[1]	FUNCTION DESCRIPTION	TECHNOLOGY	TYPE OF TEST[2]	SEU THRESHOLD [MeV/(mg/cm^2)]	ASYMPTOTIC SEU CROSS-SECTION (cm^2/device)	LET INTERVAL [MeV/(mg/cm^2)]	SIG OF CURVE[3]	DATE TESTED	TEST LOCATION[4]
MM54C929	NSC	1024 X 1 RAM	CMOS	UL	15	1×10^{-2}	30 120	S	FEB 79	88IN
MW55501	RCA	256 X 4 RAM	CMOS/SOS	UL	> 120	NO UPSET			AUG 79	88IN
MCM5901	MOT	256 X 4 RAM	CMOS	L	< 40 (L)				JAN 80	88IN
TA597	SNL	1K X 1 RAM	CMOS	UL	⩾ 70	⩾ 2×10^{-3}	>120	G	MAY 81	88IN
IDT6116	IDT	2K X 8 RAM	NMOS/CMOS	UL	11	6×10^{-2}	40 80	I	DEC 83	88IN
IDT6116RS	IDT	2K X 8 RAM	NMOS/CMOS EPI	UL	11	6×10^{-2}	40 80	I	DEC 83	88IN
IDT6167	IDT	16K X 1 RAM	NMOS/CMOS	UL	< 15	4×10^{-2}				
6434	HAR	OCTAL LATCH	CMOS	L	< 40 (L)				APR 84	88IN
HM6504	HAR	4K X 1 RAM	CMOS	UL	11	3.5×10^{-3}	30 40	I	APR 84	88IN
HM6504	HAR	4K X 1 RAM	CMOS	UL	10	5×10^{-3}		I	FEB 79	88IN
HS6504RH	HAR	4K X 1 RAM	CMOS EPI	UL	36	1.2×10^{-3}	80	S	SEP 81	88IN
HS6504RH[9]	HAR	4K X 1 RAM	CMOS EPI	UL	> 80	NO UPSET (~20 KΩ)	80		FEB 84	88IN
HM6508	HAR	1K X 1 RAM	CMOS	UL	15	1×10^{-2}		I	FEB 79	88IN
HS6508RH	HAR	1K X 1 RAM	CMOS-EPI	UL	56	4×10^{-3}			AUG 79	88IN
HS6508RH[9]	HAR	1K X 1 RAM	CMOS EPI	UL	> 120	NO UPSET (~20 KΩ)	120		DEC 81	88IN
IM65X08	ITS	1K X 1 RAM	CMOS	UL	< 40	3.4×10^{-3}			AUG 79	88IN
HM6514	HAR	1K X 4 RAM	CMOS	UL	10	2×10^{-2}			AUG 82	88IN
HM6514RH[9]	HAR	1K X 4 RAM	CMOS	UL	> 80	NO UPSET (~200 KΩ)	80		FEB 84	88IN
IM65X18	ITS	1K X 1 RAM	CMOS	UL	< 40	3.1×10^{-3}			FEB 79	88IN
HM6561	SNL	256 X 4 RAM	CMOS	UL	60	2.5×10^{-3}			MAY 80	88IN
HM6611	HAR	256 X 4 PROM	CMOS	L	> 120 (L)				AUG 80	88IN
74L78		DUAL J-K FLIP/FLOP	L TTL	UL	> 120				JUN 78	BEVALAC
68010[10]	MOT	MICRO-P	NMOS	UL	3	DATA REDUCTION IN PROGRESS			APR 84	88IN
Z8010	ZIL	MICRO-P	NMOS	UL	1	DATA REDUCTION IN PROGRESS			JUN 84	25MV
NSC800[10]	NSC	MICRO-P	CMOS	UL	5	DATA REDUCTION IN PROGRESS			JUN 84	25MV
NSC810	NSC	128 X 8 RAM-I/O	CMOS	UL	5	DATA REDUCTION IN PROGRESS			APR 84	88IN
82S191	SIG	2K X 8 PROM	S TTL	L	> 120 (L)				AUG 80	88IN
8X300[9]	SIG	MICRO-P	TTL	UL	18	2×10^{-3}	40 80	I	DEC 83	88IN
8x305[9]	SIG	MICRO-P	TTL	UL	2.5	2.5×10^{-3}	60 80	I	DEC 83	88IN
8414	FUJ	1K X 4 RAM	CMOS	UL	12	1.7×10^{-2}	40 80	I	DEC 83	88IN
93422	AMD	256 X 8 RAM	TTL	UL					JUN 84	25MV
93L422	AMD	256 X 8 RAM	L TTL	UL		7×10^{-3}	40 80		JUN 84	25MV
93L425	FSC	1K X 1 RAM	L TTL	UL	< 40	1.5×10^{-2}			FEB 79	88IN
F9445[9]		MICRO-P		UL	25	1.5×10^{-4}	40 80	I	FEB 84	88IN
SBP9989	TI	MICRO-P	IIL	UL				G	DEC 80	88IN

NOTES (ALL DEVICES ARE BASED AT 5V UNLESS OTHERWISE STATED)

1. AMD = ADVANCED MICRO DEVICES
   FSC = FAIRCHILD SEMICONDUCTOR
   FUJ = FUJITSU
   HAR = HARRIS
   HUG = HUGHES
   IDT = IDT
   ITS = INTERSIL
   MOT = MOTOROLA
   NSC = NATIONAL SEMICONDUCTOR
   RCA = RCA
   SIG = SIGNETICS
   SNL = SANDIA LABS
   TI = TEXAS INSTRUMENTS
   XIC = XICOR
   ZIL = ZILOG
2. U = SOFT ERROR UPSET L = LATCH-UP
3. S = SHARP THRESHOLD I = INTERMEDATE THRESHOLD G = GRADUAL THRESHOLD
4. 88IN = LBL 88 INCH CYCLOTRON, 25 MV = ORNL HHIRF 25MV TANDEM BEVALAC = LBL BEVELAC
5. LOT 4437 ONLY
6. REGISTERS ONLY
7. TESTED AT BEVALAC, ALSO
8. EXTENSIVE EXERCISE OF ALL SUBSYSTEMS (SELF TEST)
9. DEVICE CONTAINS CROSS-COUPLED RESISTORS
10. EXTENSIVE EXERCISE OF ALL SUBSYSTEMS

Table 4.2 Devices Tested for Heavy Ion Induced SEU (Continued)

DEVICE I.D.	DEVICE MANUFACTURER	FUNCTION DESCRIPTION	TECHNOLOGY	LATCH-UP THRESHOLD [MeV/(mg/cm^2)]	ASYMPTOTIC LATCH-UP CROSS-SECTION [cm^2/device]	LET INTERVAL [MeV/(mg/cm^2)]	DATE TESTED	TEST LOCATION
MM54C929	NSC	1K x 1 RAM	CMOS	15	1×10^{-4}	: 40 → 120	FEB 79	88 IN
MCM5901	MOT	256 x 4 RAM	CMOS	< 40	4×10^{-5}	: 80 → 120	JAN 80	88 IN
6434	HAR	OCTAL LATCH	CMOS	> 40	5×10^{-5}	: 40 → 80	APR 84	88 IN
IDT6116	IDT	2K x 8 RAM	NMOS/CMOS	< 12	2×10^{-4}	: 30 → 80	DEC 83	88 IN
IDT6167	IDT	16K x 1 RAM	NMOS/CMOS	< 15	4×10^{-4}	: 20 → 80	AUG 82	88 IN
HM6504	HAR	4K x 1 RAM	CMOS	13	$10^{-5} \sim 10^{-4}$	: 20 → 40	APR 84	88 IN
HM6508	HAR	1K x 1 RAM	CMOS	15	1×10^{-4}	: 40 → 120	FEB 79	88 IN
HM6514	HAR	1K x 4 RAM	CMOS	< 15	1.2×10^{-4}	: 20 → 80	AUG 82	88 IN
NSC800	NSC	MICRO-P	CMOS	~ 20	DATA REDUCTION IN PROGRESS		AUG 84	88 IN
NSC810	NSC	128 x 8 RAM-I/O	CMOS	~ 40	DATA REDUCTION IN PROGRESS		APR 84	88 IN

Table 4.3 Summary of Latchup Test Results

4.4 RADIATION HAZARDS TO MAN-IN-SPACE

4.4.1 Interaction Environment

The trapped radiation and solar flare environments discussed in Sections 4.1.1 and 4.1.2 describe this environment.

4.4.2 Discussion of Interaction

The radiation hazards that man operating in a space environment might encounter will be discussed [94,106,107,193,149]. Both biological and equipment interactions are considered. The equipment used for Extra Vehicular Activities (EVAs) is illustrated in Figure 4.15.

The biological effects of energetic particle radiation on man have been studied for years [194]. There is concern for the cumulative effects of this dosage on the various parts of the body, with the eyes being a particularly sensitive area. Eye flashes have been observed in response to certain radiation fluxes. Eye flashes could provide false sensory input as well as involuntary reactions and discomfort. Blindness could result if an astronaut was exposed to the radiation from a major solar flare.

The EVA suit that the astronaut wears is a self-contained spacecraft with its own system electronics. These systems could experience SEUs as do other spacecraft systems responding to high energy fluxes and cosmic rays. While exposure time in the spacesuit is usually short (on the order of hours), the spacesuit provides less shielding. The possible radiation effects on manned operations in space should be carefully reviewed. This is especially true for operations in polar, transfer, and geosynchronous orbits where high energy flux encounters can be expected.

4.4.3 Research Maturity Rating

Biological effects of radiation have been under investigation for years. The goals of these studies included establishing cumulative dose limits for various conditions such as exposure time, parts of the body irradiated, and type of irradiating particle. The maturity for both analytical and experimental areas was rated CONSIDERABLE (4).

4.4.4 System Impact Rating

The potential system impact rating has been established as LARGE (4). This would be applicable to polar and geosynchronous orbits. The probability of encountering high energy particle fluxes in low inclination earth orbits is too low to make this interaction important. The system impacts of both biological and electronic systems have to be considered. Failure could have analogous effects in either case.

4.4.5 Mitigation Techniques

The mitigation techniques suggested for this interaction are to limit time spent

outside the spacecraft in those orbits where high energy particle encounters are possible, particularly following solar flares resulting in energetic solar particles. There should be sufficient warning of the expected arrival of energetic solar particles so that the astronauts could return to their spacecraft where the shielding should be adequate. Such a flare could interrupt or prevent them from completing the operations planned for the EVA. An anomalously large flare, such as occurred in August 1972, could force premature termination of a manned mission.

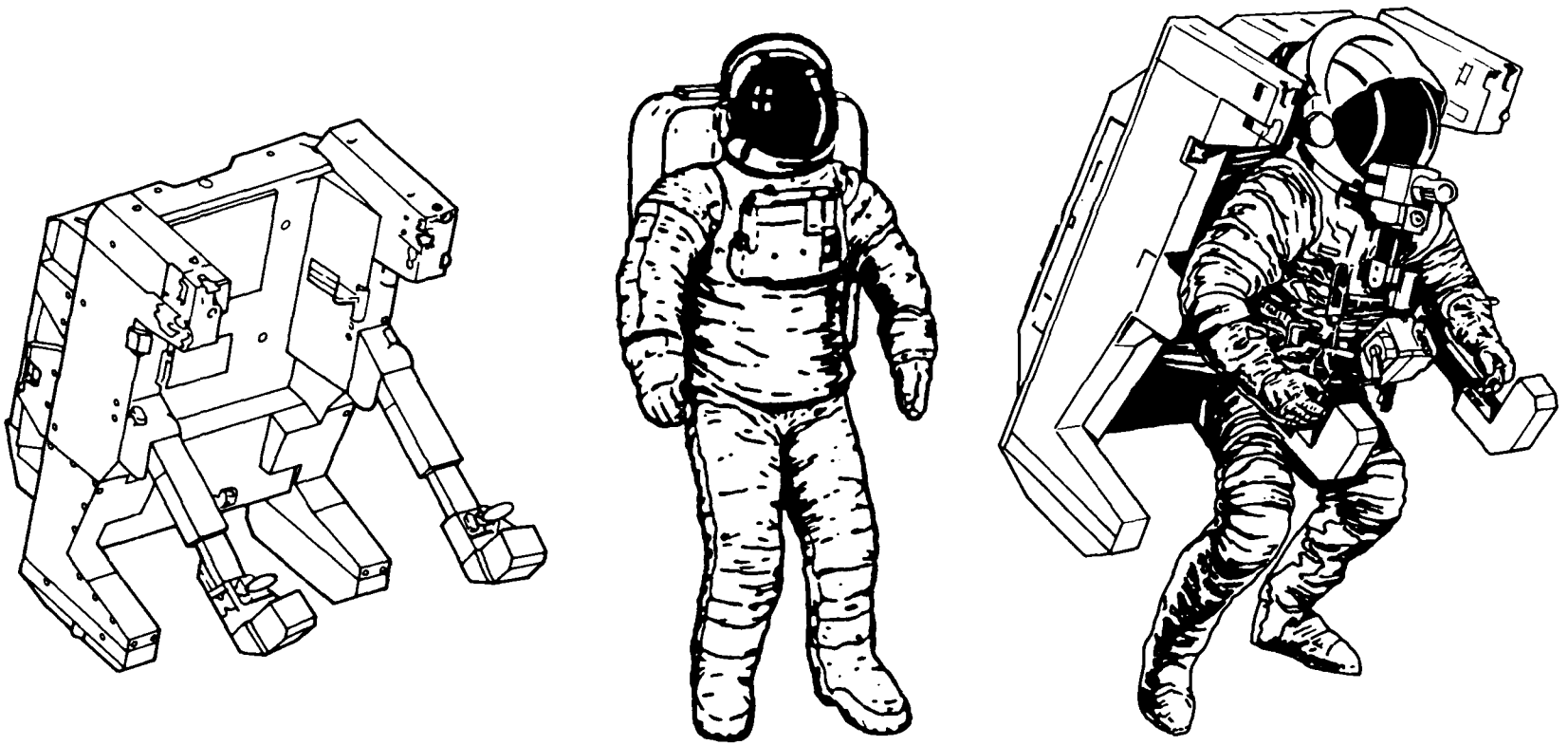

(A) MANNED MANEUVERING UNIT

(B) EMU AND PLSS

(C) MMU MATCHED TO PLSS

Figure 4.15 Astronaut EVA Equipment

5.0 NEUTRAL ENVIRONMENT INTERACTIONS

Interactions between spacecraft systems and the Earth's neutral environment are discussed in this section. The interactions considered are: Atmospheric Drag, Atomic Oxygen Surface Erosion, Surface Glow (Optical Contamination), and Sputtering. The environment common to each of these interactions is described below.

5.1 GENERAL ENVIRONMENT DESCRIPTION

The environment of concern here extends between 60 and 1000 km. Prior to flight of the Shuttle, this environment was expected to influence only drag and orbital heating. Shuttle flights have shown that the interactions with the neutral environment can have additional serious consequences for large spacecraft.

Neutral density varies with altitude and solar activity (Figure 5.1) [6]. The neutral particle density exponentially decreases with altitude so that above 1000 km interactions become negligible. A nominal neutral atmospheric temperature profile is shown in Figure 5.2. In the lower thermosphere (100 to 300 km), solar radiation is absorbed causing temperatures to increase with altitude. Above 300 km, the temperature is isothermal since little or no solar radiation is absorbed. These values, however, can change from about 650° to 2100° K due to solar and geomagnetic activity.

Composition of the neutral environment also changes with altitude (Figure 5.3) [6]. At altitudes below 100 km, atmospheric gases are mixed thoroughly by wind turbulence. Above 100 km, gravity separates the gases so that the composition is a function of altitude. Molecular nitrogen (N_2) is the dominant species in the neutral environment to altitudes of 200 km, where the density of molecular nitrogen and atomic oxygen (O) are equal. Above 90 km, extreme ultraviolet solar radiation causes molecular oxygen to dissociate into atomic oxygen. From 200 to about 650 km, atomic oxygen is the dominant species. Above this altitude, helium (He) is the dominant species.

5.2 ATMOSPHERIC DRAG

5.2.1 Discussion of Interaction

The interaction considered involves resistance to motion through the neutral environment. This is a density dependent interaction and has a more serious impact at lower altitudes. One of the more significant results of this interaction is orbital decay and eventual reentry of the vehicle into the Earth's atmosphere. For LEO spacecraft, the drag force is [195]:

$$F = (1/2)\, C_D A \rho V^2$$

where: C_D = drag coefficient; A = effective cross-section area; ρ = atmospheric density; V = spacecraft velocity

Atmospheric drag is more significant as spacecraft altitude decreases and as the spacecraft ram direction surface area increases. The effect of drag on spacecraft at

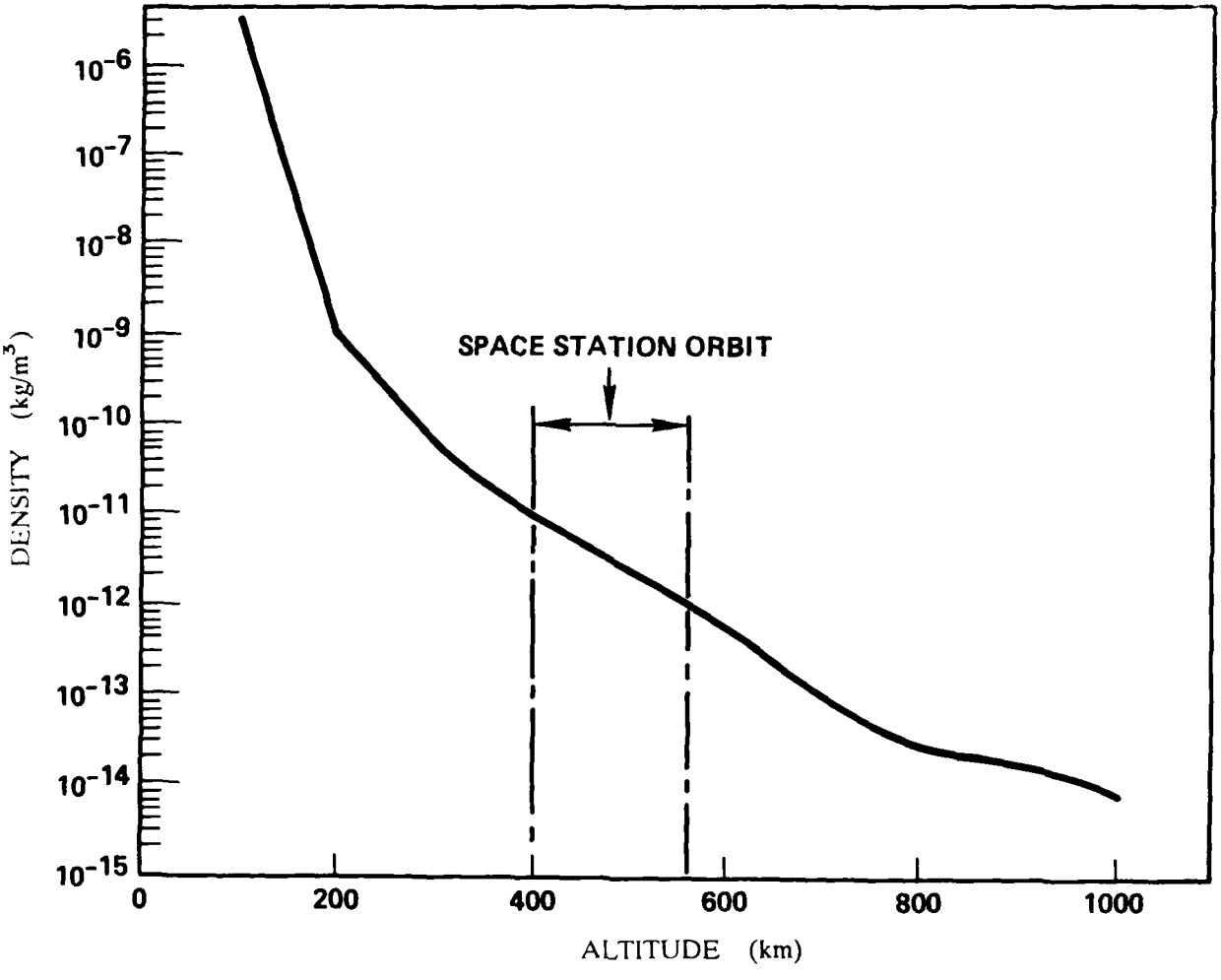

Figure 5.1 Atmospheric Density Profile

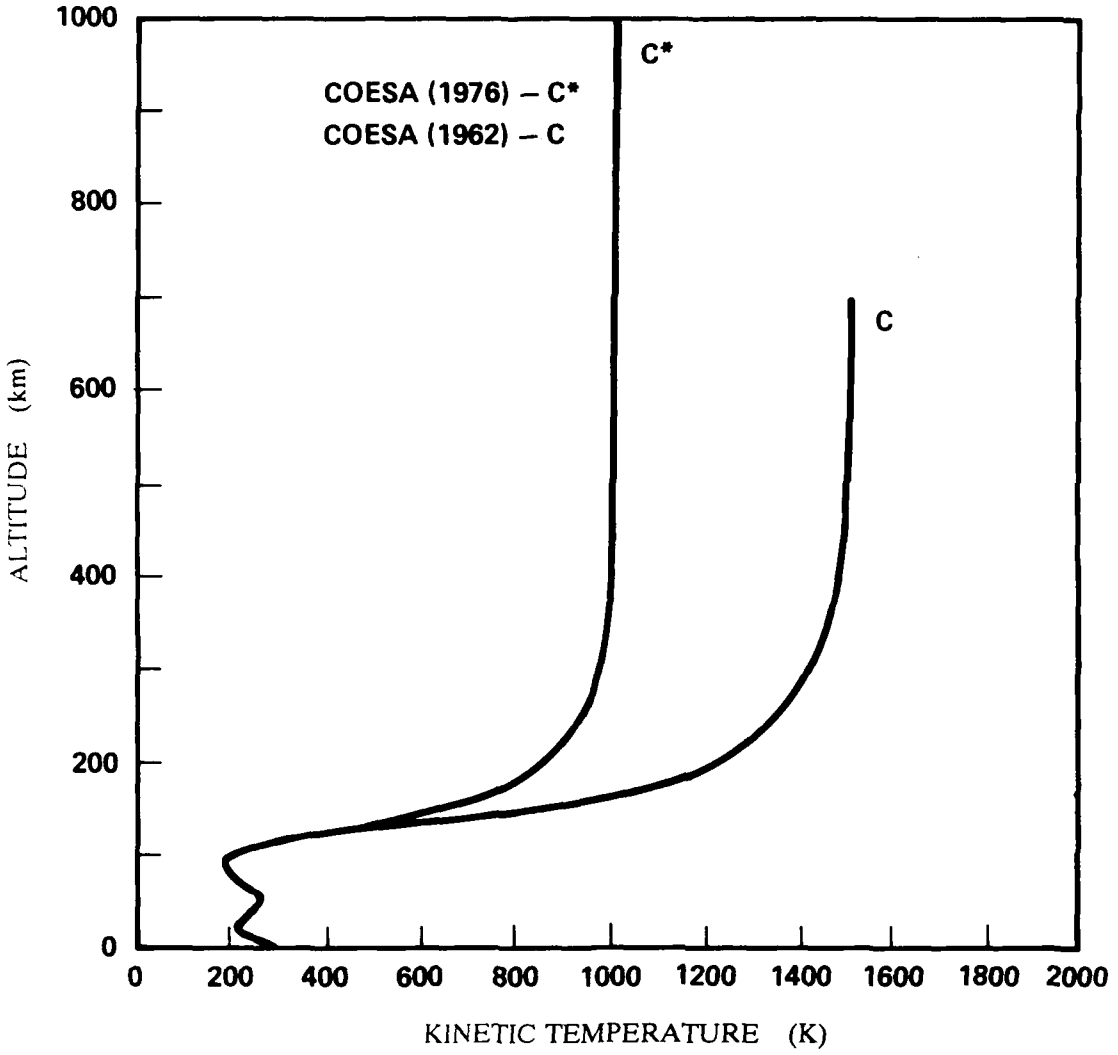

Figure 5.2 Kinetic Temperature vs Altitude

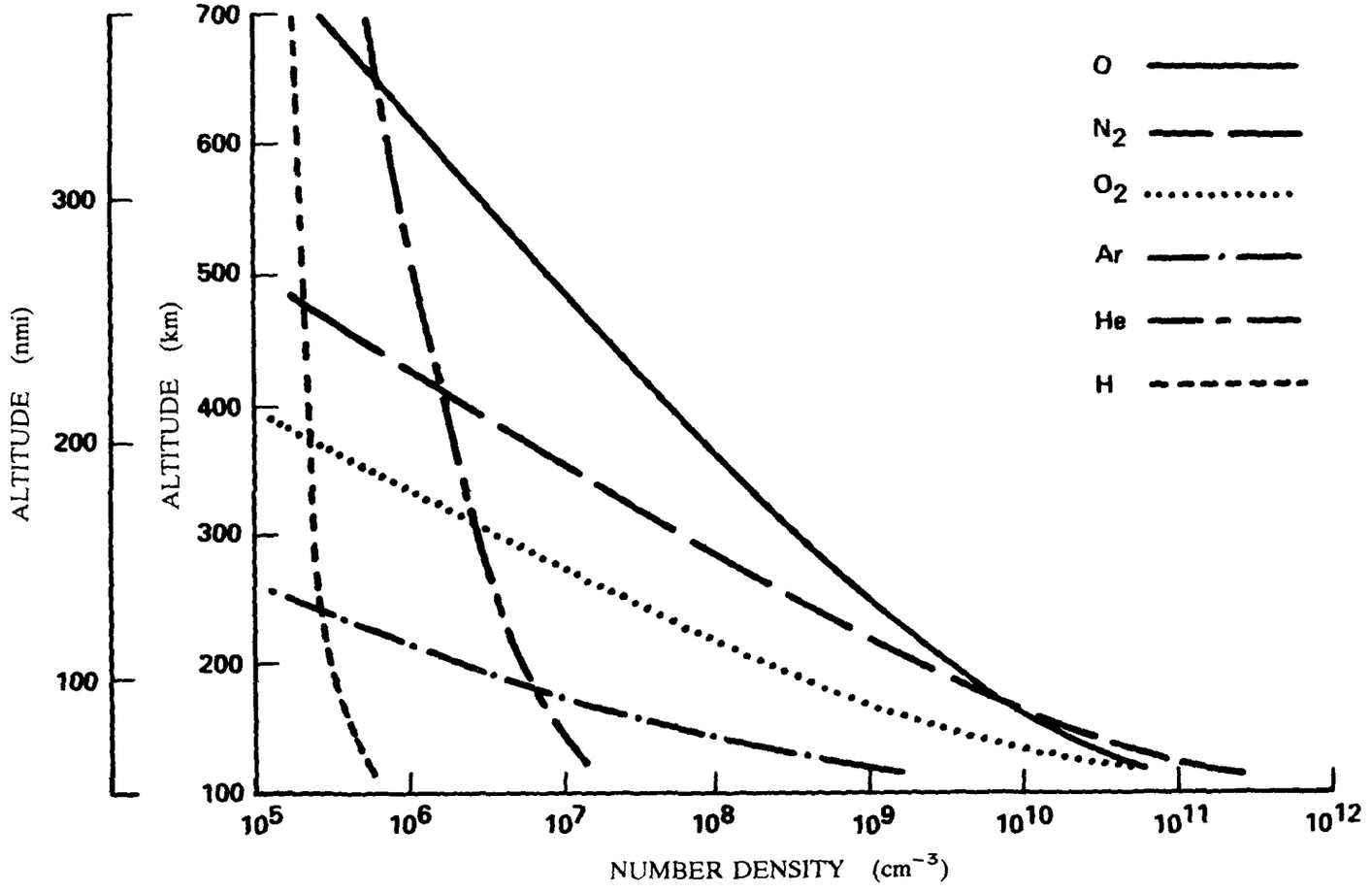

Figure 5.3 Neutral Environment

various altitudes, assuming a constant frontal area (A) and a drag coefficient of two, is illustrated in Figure 5.4. Recall that drag is also a function of spacecraft velocity and atmospheric density. The drag on a spacecraft in a 400 km orbit is comparable to that of a satellite at 600 km with a ten times larger frontal area. Thus, drag will be an important factor affecting future, long mission, low orbiting, large spacecraft. Finally, for future vehicles to safely and efficiently use aerobraking, a partial entry into the upper atmosphere for orbital changes, one must have adequate knowledge of neutral environment conditions at various altitudes.

5.2.2 Research Maturity Rating

Atmospheric drag has been studied for many years. The variation with altitude (above 90 km) is well established and the prediction of drag effects is reasonable. Between 60 and 90 km the environment is not well understood and the capability to predict drag effects is limited. Thus, the maturity was rated MODERATE (3).

5.2.3 System Impact Rating

The system impact for this interaction was rated CATASTROPHIC (5) for LEO and PEO. This rating was given since atmospheric drag will decrease the velocity of a spacecraft. Once the spacecraft station keeping capability is lost, the orbit will decay until the system is destroyed by reentry.

5.2.4 Mitigation Techniques

The mitigation techniques to offset the effects of this interaction are: (1) Reboost the spacecraft to a higher altitude when necessary; (2) Design to minimize drag; and (3) Improve knowledge of the environmental conditions that effect drag at all altitudes. Reboosting has to be accomplished carefully if there will be accelerating forces on fragile spacecraft appendages.

5.3 ATOMIC OXYGEN SURFACE EROSION

5.3.1 Discussion of Interaction

The neutral environment becomes increasingly significant to spacecraft as orbit altitude decreases. Orbital velocities are on the order of 8 km/sec for Shuttle. The effective energy of particles incident on surfaces facing in the direction of motion is determined by this velocity. The most abundant neutral constituent at these altitudes, atomic oxygen, has an incident ram energy of 5 eV. This energy is large enough to cause erosion of surface materials and surface property changes.

Material erosion was seen after the return of the first Shuttle flight and was identified as an erosion problem by the end of the third flight [197]. The erosion phenomenon, presumably due to atomic oxygen, has been the subject of several ground and Shuttle experiments [198-209]. Experiments on flights STS-3 and STS-8 demonstrated that many spacecraft materials experience surface oxidation and adverse

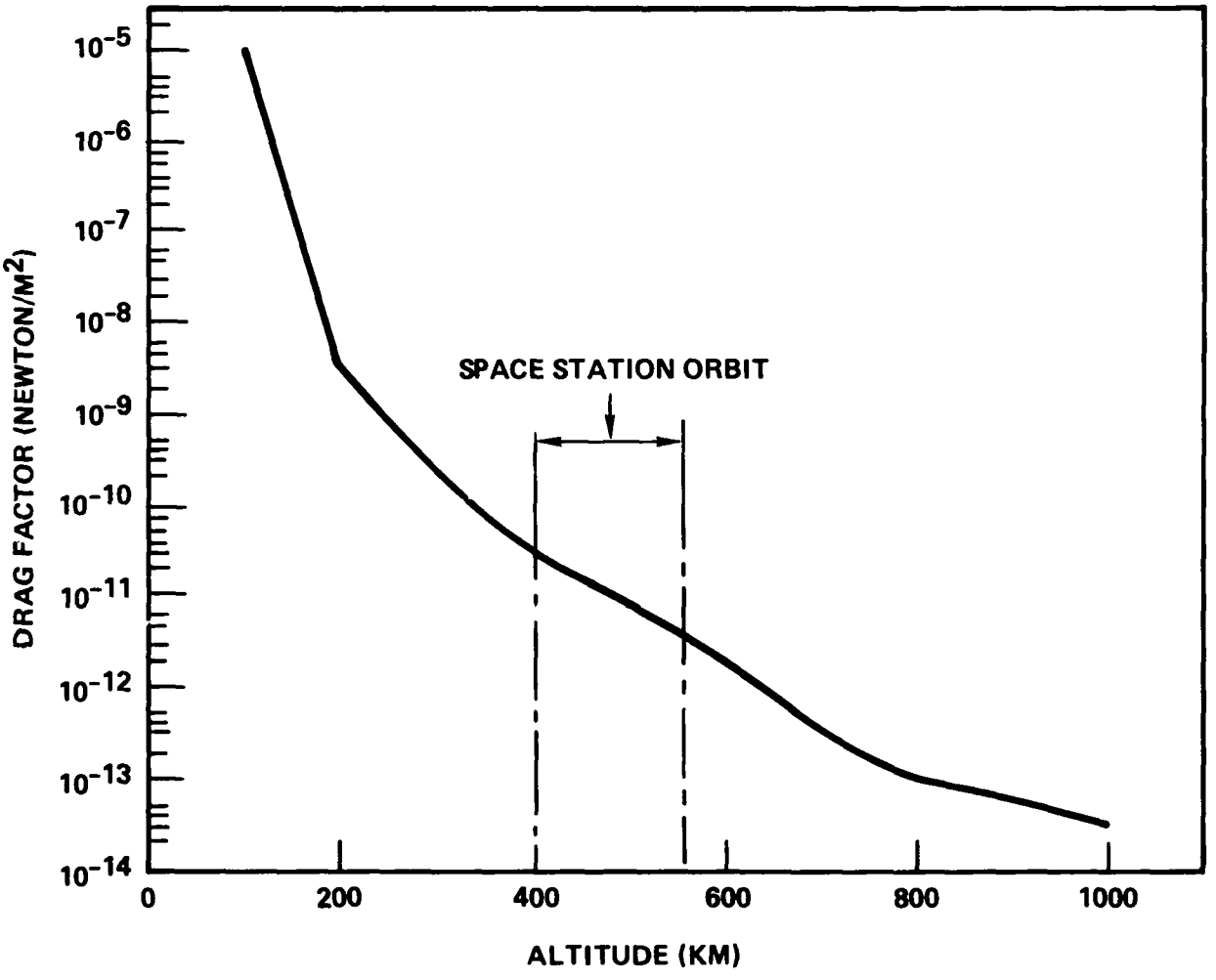

Figure 5.4 Effect of Drag vs Altitude

changes in optical and physical properties after as few as 40 hours of exposure.

The materials that are most reactive to atomic oxygen include Kapton, Mylar, Kevlar, silver, osmium, and carbon. The influence of atomic oxygen on typical spacecraft materials is summarized in Table 5.1 [210]. An illustration of this material loss is shown in Figure 5.5 [211]. A 0.5 mil Mylar sample, returned from the STS-8 mission, completely disappeared (Figure 5.5A) after exposure to a flux of 3.5×10^{20} atoms/cm^2, while the portion covered by the sample holder remained (Figure 5.5B). Analysis after the flight showed some of the Mylar had deposited back onto the sample holder, indicating a possible contamination aspect to the erosion problem.

Research on material erosion, due to atomic oxygen, was not extensive prior to the Shuttle observations. Shuttle flight experiments have been phenomenological in nature. The reaction rates for a large number of materials were determined (Table 5.2). The experiments produced a useful data base and resulted in specific design modifications for several spacecraft under construction. The flight data has been supplemented by ground testing which showed that atomic oxygen caused the erosion and that materials can be tested in the laboratory for their susceptibility.

Data from Shuttle flights was obtained using small material samples with limited space exposure. This data indicates that Kapton and Mylar are particularly susceptible to atomic oxygen erosion. It has been estimated that approximately 2 mils of Kapton would be eroded per year. This implies that polymer films commonly used for thermal blankets and solar array substrates could be completely lost after only a few years in space. This is of particular concern since plans call for newer, larger satellites to use thinner materials. In addition to the concern that materials can be altered or completely eroded away, the remnants from this process could be deposited on other surfaces, causing contamination. While most metals seem to be insensitive to atomic oxygen erosion, silver and osmium, widely used for optical coatings, do oxidize rapidly. This would seriously impact the operation of reflectors and sensors.

The results of system impact studies have been released for only samples returned from the Solar Maximum Spacecraft. Thus, extrapolation of experimental data to larger surface areas must be done carefully. For example, the only large article returned from space, to date, has been a thermal blanket section from the Solar Maximum spacecraft. The impact due to oxygen erosion on its 2 mil Kapton outer layer was reported as negligible (only slight discoloration) after 4.2 years in a 500 km orbit. If the blanket was facing in the ram direction, the Kapton should have completely eroded, based upon experimental data. This discrepancy has not been resolved.

Surface properties of materials can be altered by pitting and erosion from this interaction. The surface changes can affect such properties as reflectivity, solar absorptivity, and secondary emission. These changes would compromise the operation of optical surfaces, sensors, and thermal blankets.

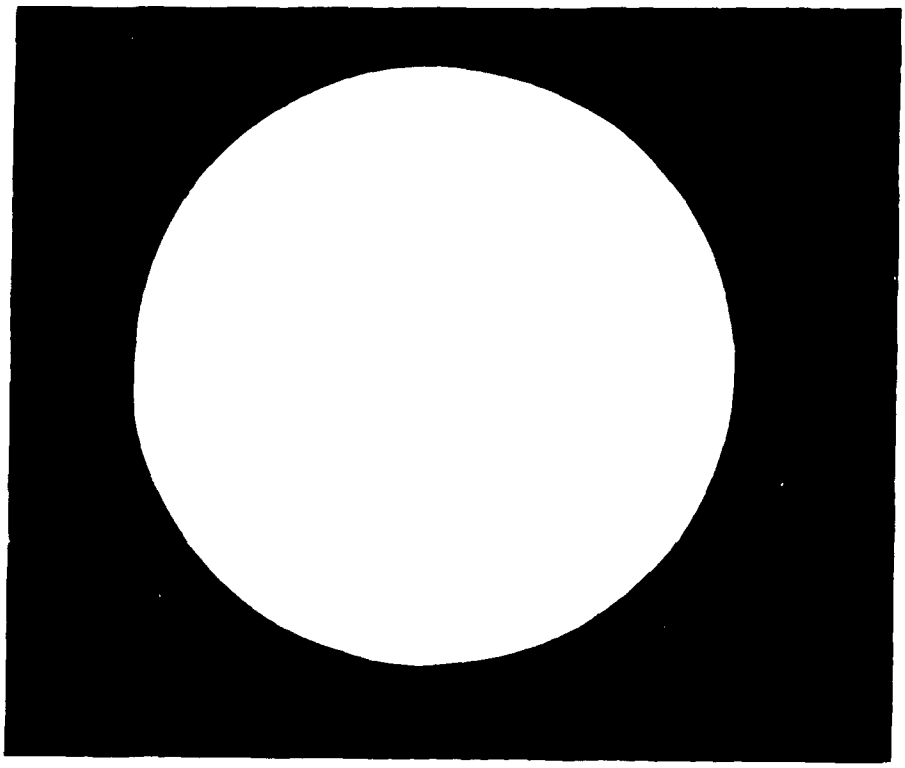

(A) Ram Exposed Mylar Disk

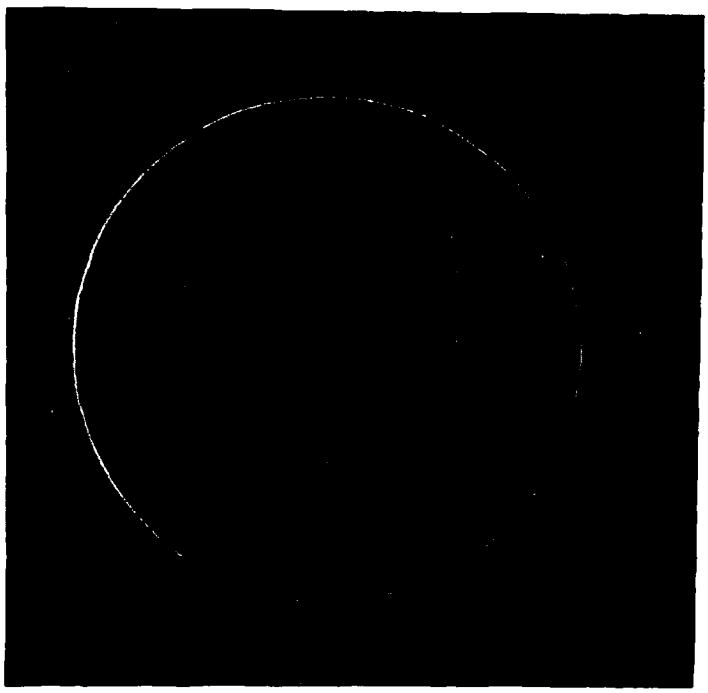

(B) Mylar Disk UV Control Sample

Figure 5.5 Mass Loss on 0.5 mil Mylar Disk

Table 5.1
Atomic Oxygen Surface Erosion: Highly Reactive and Non-Reactive Materials

Highly Reactive	Non-Reactive
Materials Kapton (Clear and Black) Mylar Kevlar Epoxy Polysufone Tedlar (White Clear) Black Conductive Urethane Glassy and Amorphous Carbon Graphite/Epoxy Graphite/Polymide Polyethylene Polymethylmethacrylate RTV-560 Silver and Silver Foil Osmium	Materials Aluminum Germanium Gold HOS-875 Metal Iridium Lead Magnesium Magnesium Fluoride Molybdenum Nickel NiCr Palladium Platinum Solder Tantalum Tophet 30 Metal Tungsten V2000
Paints A276 (White) Z302 (Glossy Black) Z306 (Flat Black) 401-C10 (Flat Black) P1700 Z0853 (Yellow)	Paints S13G-LO YB-71 (ZOT) GSFC (Green) MS74 (White)
Fibers Kevlar Gore-Tex Nomex Viton	Oxides Indium Tin Oxide Aluminum Oxide Silicon Dioxide Titanium Dioxide

Table 5.2
Atomic Oxygen Mass Loss Rates

Material	Surface Erosion (mils/yr)
Kapton	2.4
Mylar	2.8
Teflon	0.025
Silver	8.4
Aluminum	0.0003
Black Conductive Urethane	4.6
Chemglaze Z302	3.1
Carbon	3.1
Indium Tin Oxide	0.0003
Epoxy	1.9

Note: Assumed Flux = 2×10^{21} $cm^{-2}yr^{-1}$ (Solar Cycle Maximum)
Altitude = 500 km

5.3.2 Research Maturity Rating

The practical engineering aspects of atomic oxygen erosion are well understood, leading to a research maturity rating of CONSIDERABLE (4) for experiments. However, it is impossible to make even a qualitative prediction about reaction rates for untested materials. The analytical maturity rating is MODERATE (3) since the theoretical aspects of the interaction are not well known.

5.3.3 System Impact Rating

Atomic oxygen interactions with materials can have CATASTROPHIC (5) impact on spacecraft system performance for satellites in LEO and PEO. Since there is little atomic oxygen in GEO, the interaction was rated NEGLIGIBLE (1) for those orbits.

5.3.4 Mitigation Techniques

Several mitigation techniques have been proposed to minimize the effect of atomic oxygen erosion. The easiest method is to avoid using highly reactive materials. When these materials must be used, controlling vehicle attitude to minimize the amount of exposure to critical surfaces can effectively reduce erosion. Finally, the use protective coatings, such as paint, can further mitigate the effects of atomic oxygen erosion when sensitive materials must be used. Further evaluation of atomic oxygen surface erosion is needed, especially the impact due to spacecraft orientation and orbital altitude parameters, since material losses may not be as severe as Shuttle data would indicate.

5.4 SURFACE GLOW

5.4.1 Discussion of Interaction

Surface glow [213] was first observed on the Shuttle by the STS-3 low light television experiment [214-217]. This glow was observed to be a diffuse, low-visual-intensity layer of enhanced luminosity on, and adjacent to, those surfaces facing in the velocity or ram direction (Figure 5.6). The glow was further measured on subsequent shuttle flights. It was found to extend a maximum of 10 cm from the surface and has been observed predominantly in the 4200 to 8000 angstrom region. The glow intensity is enough (10^5 rayleigh) to seriously interfere with optical sensors on future missions.

Currently, three mechanisms have been proposed as the cause of surface glow [218-223]. The first is an atomic oxygen reaction, since glow seems to correlate with the atomic oxygen environment. However, this seems to be contradicted by experiments on surface glow, since intensity can be greater over non-reactive surfaces. The second mechanism is a complex dissociation-recombination process dependent on the energy associated with the Shuttle velocity. This process can be represented as follows:

$$\text{i)}\ N_2 \Rightarrow 2N$$
$$\text{ii)}\ N + O \Rightarrow NO$$
$$\text{iii)}\ NO + OX \Rightarrow NO_2 + X$$

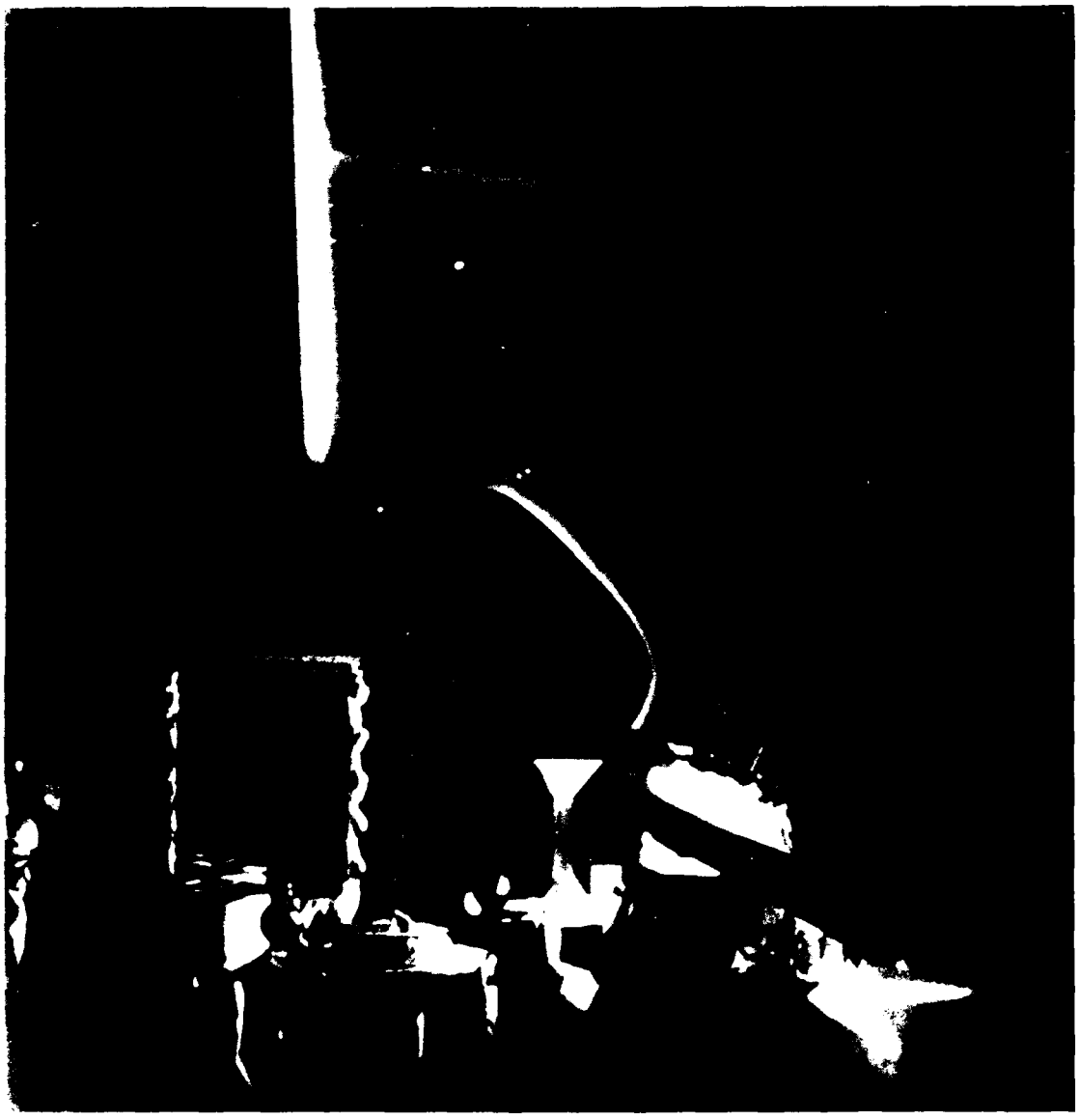

Figure 5.6 Shuttle Glow on STS-3

In step (i), molecular nitrogen (N_2), impacting shuttle surfaces with a relative energy derived from the vehicle velocity, dissociates into atomic nitrogen (N). This, in turn, combines with atomic oxygen (O) to form nitric oxide (NO), part of which adheres to the surface. The NO then reacts with O via a third body (X) to form NO_2 which is liberated. The observed luminosity is postulated as the recombination continuum of NO_2, with the intensity determined by the surface properties of the sample material (X). The observed broad continuum spectrum is consistent with the $2B_1$ state of NO_2. This theory is supported by mass spectrometer data, showing the presence of NO, and laboratory experiments, which have demonstrated the high efficiency of the 3-body formation of NO_2. Recently, it has been pointed out that there is sufficient atomic nitrogen (10^6 to 10^7 cm^{-3}) at shuttle altitudes to produce enough NO to explain the glow measurements by reaction (iii) alone.

A third mechanism which has been proposed to explain surface glow is the Papadopolous-Alfven ionization theory. In this complex plasma process, a two-stream instability develops between incident and reflected ions. The ion instability then generates waves which, in turn, produce suprathermal electrons. These energetic electrons (30 eV) ionize the ambient neutral gas, which emits a characteristic spectrum of radiation. It is not clear whether the observed spectrum is consistent with this theory.

There is no clear consensus on which, if any, theory correctly explains the glow phenomenon. There are many molecular species present, including outgassing products. More data, including expanded spectral measurements in the infrared and ultraviolet, may help to explain surface glow.

5.4.2 Research Maturity Rating

The spectral content, intensity, and spatial extent of the surface glow phenomenon were better understood after the completion of several flight experiments. To date, these experiments have necessarily been simplistic, in order to fly on early Shuttle launch opportunities. Thus, there still remains competing theories to explain the phenomenon. Therefore, the maturity of this interaction was rated MODERATE (3).

5.4.3 System Impact Rating

The principal adverse effect of glow is its potential interference with optical measurements. Impact on systems is not generally catastrophic and sensitive instruments can be compensated. Thus, the impact of this interaction was rated MODERATE (3) for low altitude orbits and NEGLIGIBLE (1) for geosynchronous orbits.

5.4.4 Mitigation Techniques

Optical devices sensitive to the wavelength range of this phenomenon can be shielded or pointed away from surfaces facing into the ram direction. It may be possible to minimize interference by choice of wavelength when more is known about the spectral range of glow. Choice of spacecraft altitude is a potential mitigation technique since glow seems to be dependent upon nitrogen or atomic oxygen concentration.

5.5 CHEMICAL REACTIONS

5.5.1 Discussion of Interaction

Spacecraft orbiting at low altitudes encounter H_2O, NH_3, and C_2H_6 molecules as well as neutral nitrogen and atomic oxygen. Many sequences of chemical reactions are possible at relative kinetic energies of 5 to 10 eV. These reactions create a complex ambient environment near spacecraft surfaces. The possible interactions multiply when plasma effects are added, making interpretation of surface phenomena difficult.

5.5.2 Research Maturity Rating

The identification of atomic and molecular reaction rates that are applicable to spacecraft interactions remains incomplete. The maturity of experimental knowledge was rated MODERATE (3) while analytical was rated CONSIDERABLE (4).

5.5.3 System Impact Rating

The possible chemical reactions near spacecraft surfaces and their consequences have been insufficiently explored. While there is no direct evidence of interactions occurring during Shuttle flights, they are still possible and must be considered, since enhanced contamination could result. In addition, chemical reactions could produce corrosive substances, such as nitric acid.

The impact for this interaction was rated MODERATE (3) for LEO and PEO in view of the lack of definite information in this area. The impact was rated NEGLIGIBLE (1) in geosynchronous orbit.

5.5.4 Mitigation Techniques

Present knowledge is inadequate to identify mitigation techniques.

5.6 SPUTTERING

5.6.1 Discussion of Interaction

Sputtering is the deposition of a thin layer of material onto a surface. In low earth orbits, the principal constituents of the neutral environment are nitrogen molecules and atomic oxygen. The thermal energies for these particle varies from 0.06 to 0.2 eV. The spacecraft velocity (about 8 km/sec) raises the impact energy of the particles for surfaces facing in the velocity or ram direction. Thus, the effective energy is about 10 eV for nitrogen, the measured sputtering threshold for most spacecraft materials. In the ram direction, then, sputtering of the surfaces is possible and should be considered for large space systems. Sputtering could occur even at the effective energy of 5 eV for atomic oxygen.

5.6.2 Research Maturity Rating

Neutral particle sputtering was rated SLIGHT (2) because of the lack of physical models and experimental data in this area.

5.6.2 System Impact Rating

Surface erosion is the principal consequence of neutral particle sputtering. The system impact was rated CONSIDERABLE (4) since the effect of such sputtering over long periods of time on many materials is unknown. The loss of materials from surfaces facing in the velocity direction could be serious if sputtering occurs. The impact on spacecraft systems should be reviewed as the maturity of this interaction improves.

5.6.4 Mitigation Techniques

Mitigation techniques for this interaction are similar to those proposed for atomic oxygen erosion, namely: (1) Orbit selection; (2) Avoid exposure of sensitive materials to the ram orientation; and (3) the use of surface coatings. Mitigation techniques can be expected to expand as more information on this interaction becomes available.

6.0 PARTICLE ENVIRONMENT INTERACTIONS

This section concerns micrometeoroids and man-made debris particle interactions.

6.1 MICROMETEOROID IMPACTS

6.1.1 Interaction Environment

Meteoroids are solid particles, originating from comets and asteroids, and moving through interplanetary space. They are classified either as sporadic, when their orbits about the Sun are random, or as streams (or showers) when they are grouped in large numbers having nearly identical orbits. Streaming meteoroids have definite periods of increased activity throughout the year.

Meteoroid densities have been calculated from photographic and radar observations to be between 0.16 and 4.0 gm/cm^3, with the accepted average value of 0.5 gm/cm^3. Their velocities have been observed to range from 11 to 72 km/sec, with 20.0 km/sec being the accepted average [224]. The average cumulative meteoroid flux mass environment model (available from NASA reports) is presented in Figure 6.1 [224].

Meteoroids can range in size from infinitesimally small to kilometers in diameter. For this interaction discussion, very large and very small meteoroids are not significant, even though impacts from these can cause damage. Large meteoroids, ones which can be detected and tracked from the ground, can be avoided by spacecraft. Very small ones, on the other hand, can be shielded against to minimize damage. The class of meteoroids pertinent to this interaction are those in between these ranges. These meteoroids will be discussed as "micrometeoroids".

6.1.2 Discussion of Interaction

The possibility of damage, as the result of impacts, has led to much concern about interactions between future, large spacecraft and the micrometeoroid/debris environment. A particle with a mass of 10^{-6} grams could have a kinetic energy of 0.2 joule. It could penetrate through most spacecraft surfaces and cause significant damage. The predicted number of impacts per year for a given particle mass is given in Table 6.1. These values indicate this interaction is significant for large area spacecraft with expected lifetimes of 10 to 30 years. Figure 6.2 shows the expected number of impacts of various mass particles per year as a function of spacecraft area.

Micrometeoroid surface impacts, into such objects as thermal blankets or thermal control louvers, can have multiple effects. First, the particle can penetrate through the outer layer producing a hole. This hole can be nearly circular in shape, if the impact occurs normal to the surface, or it can be elliptical, if the impact occurs at an angle. This is illustrated in Figure 6.3A, which is a photograph of a micrometeoroid penetration of a thermal blanket returned from the Solar Maximum repair mission [225]. The particle had a mass of about 10^{-5} grams and produced an elliptical ($\approx$ 0.35mm diameter) hole in the 3 mil Mylar surface.

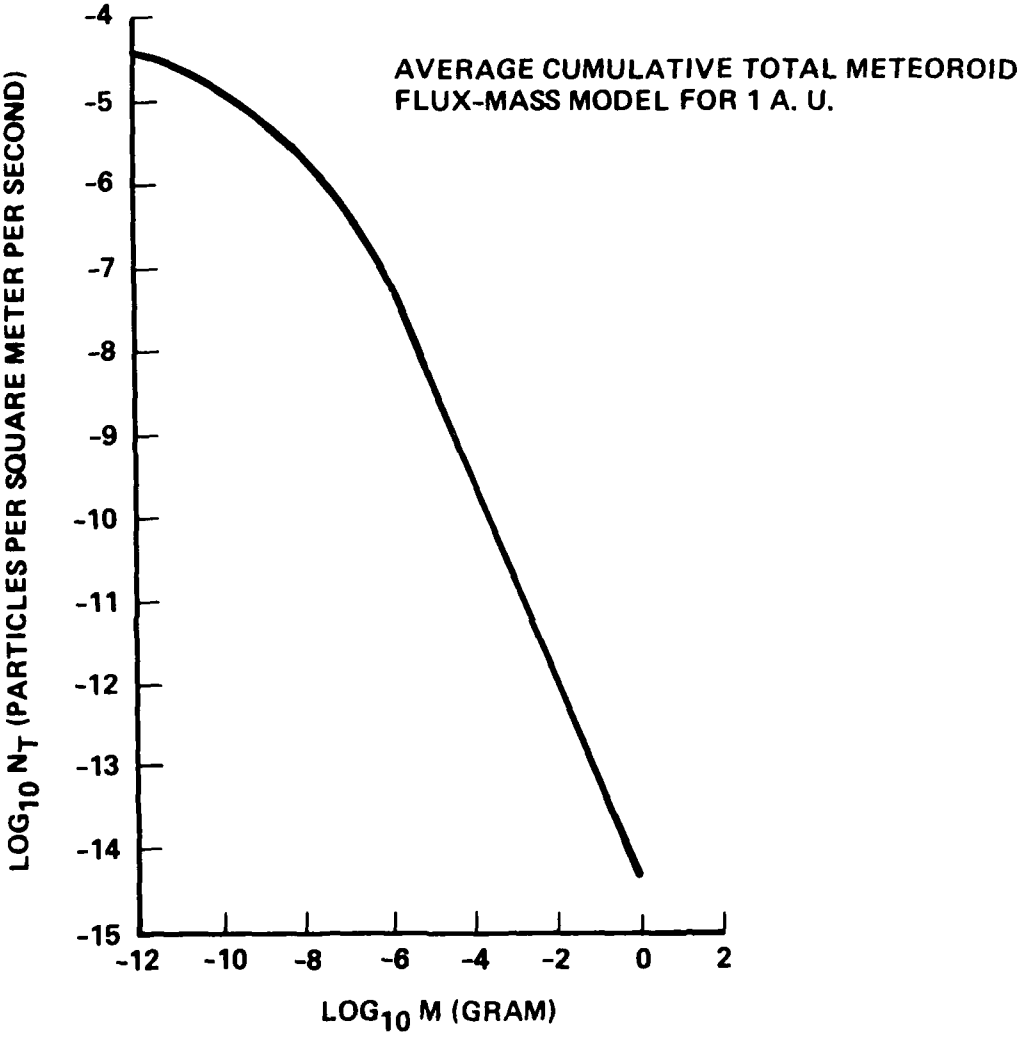

Figure 6.1 Micrometeoroid Environment

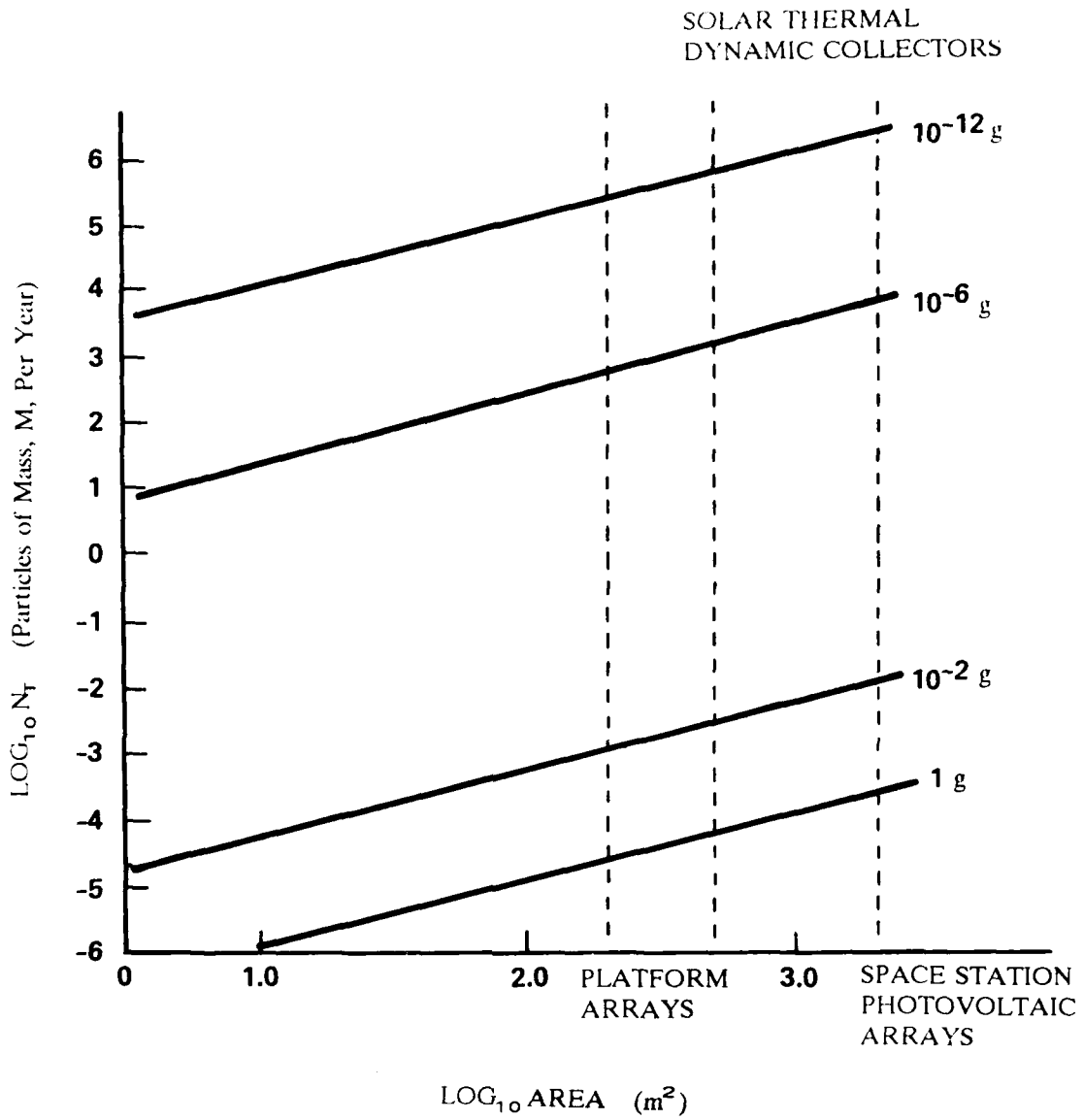

Figure 6.2 Average Cumulative Micrometeoroid Flux vs Spacecraft Area

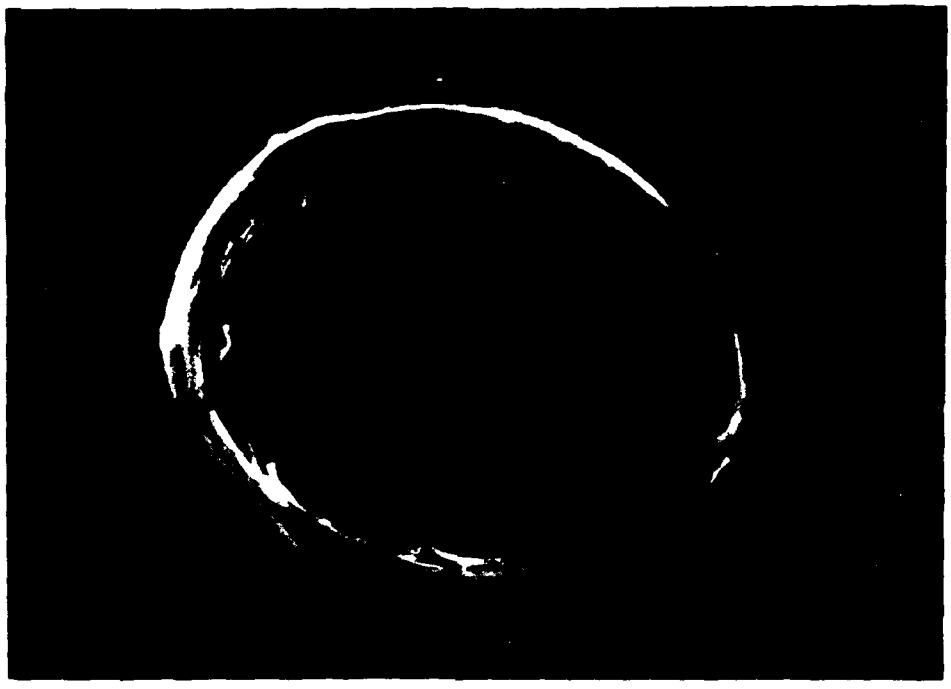

(A) Initial Impact Hole

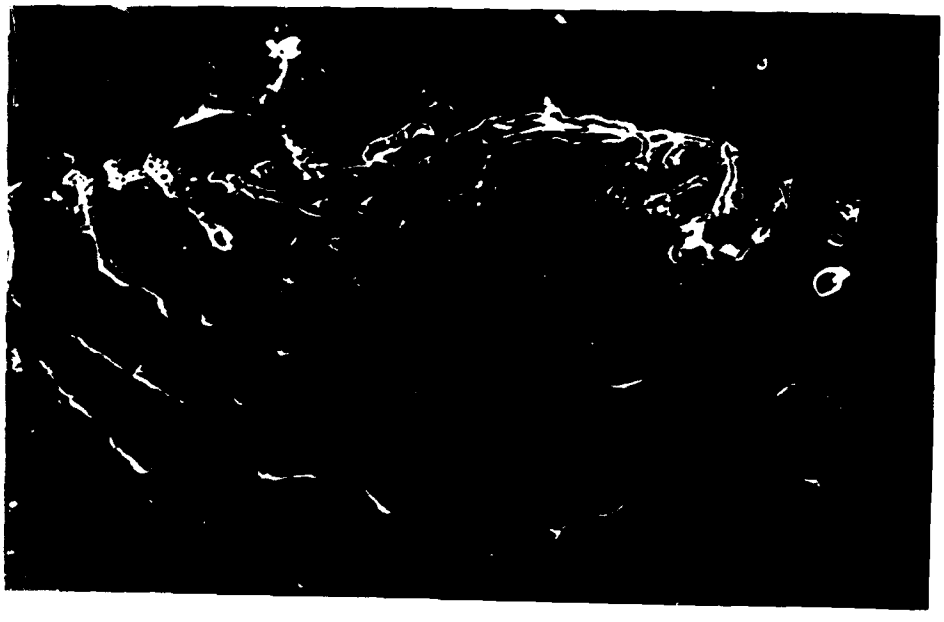

(B) Secondary Layer Spalling Damage

Figure 6.3 Micrometeoroid Impact Damage in a Solar Max Thermal Blanket

Table 6.1
Micrometeoroid Impacts Expected at 1 A.U. from the Sun

Micrometeoroid Mass (gm)	Number of Impacts ($m^{-2} yr^{-1}$)
10^{-12}	773.00
10^{-11}	566.00
10^{-10}	311.00
10^{-9}	127.00
10^{-8}	39.10
10^{-7}	8.90
10^{-6}	1.60
10^{-5}	0.09

Second, a spalling damage pattern is created in the layer beneath. This spalling pattern is the result of the particle, and exterior surface residue, breaking up and spreading out in a conical pattern. This is illustrated in Figure 6.3B. The resulting exterior and/or interior coating damage could effect the thermal balance. The pattern shown here is approximately 1.5 mm across or about 25 times the original impact area.

A final effect, which results from micrometeoroid impacts, is that the underneath layer is now exposed and can react with the environment. This can result in atomic oxygen surface erosion or high voltage system interactions.

Similar effects can be expected to occur in solar arrays [226]. A 6 mil thick cover glass can be penetrated by micrometeoroids with masses greater than 10^{-8} grams, causing entry and spalling damage. The probability of damage to the glass and the blocking diodes on the array increases with increasing array size. The micrometeoroid mass required to penetrate various thickness blankets and cover glasses can be computed, if thin dielectric films are assumed to behave like thin plates. These results are shown in Figure 6.4. The cross on the curve represents a 6 mil thick surface.

Small craters on large, specular surfaces, such as solar thermal dynamic reflectors, could reduce their reflective characteristics, defocus the sunlight, and damage the emissive coating on the rear surface. This would reduce the power output and could raise operating temperatures, due to a reduced heat rejection capability. Micrometeoroid impacts could be serious to mirrors reflecting high power beams, such as a high power laser. Resulting surface defects would absorb energy, cause local thermal distortions, and ultimately destroy the mirror or render it useless. Finally, larger micrometeoroids can penetrate spacecraft surfaces and damage internal structure and pressure vessels. Probability of penetration also increases with spacecraft size. Such impacts could weaken the structure and lead to system failures.

6.1.3 Research Maturity Rating

The model of the micrometeoroid environment, developed and published by NASA in the 1960s, is still valid. The evaluation of the impact of these particles, on

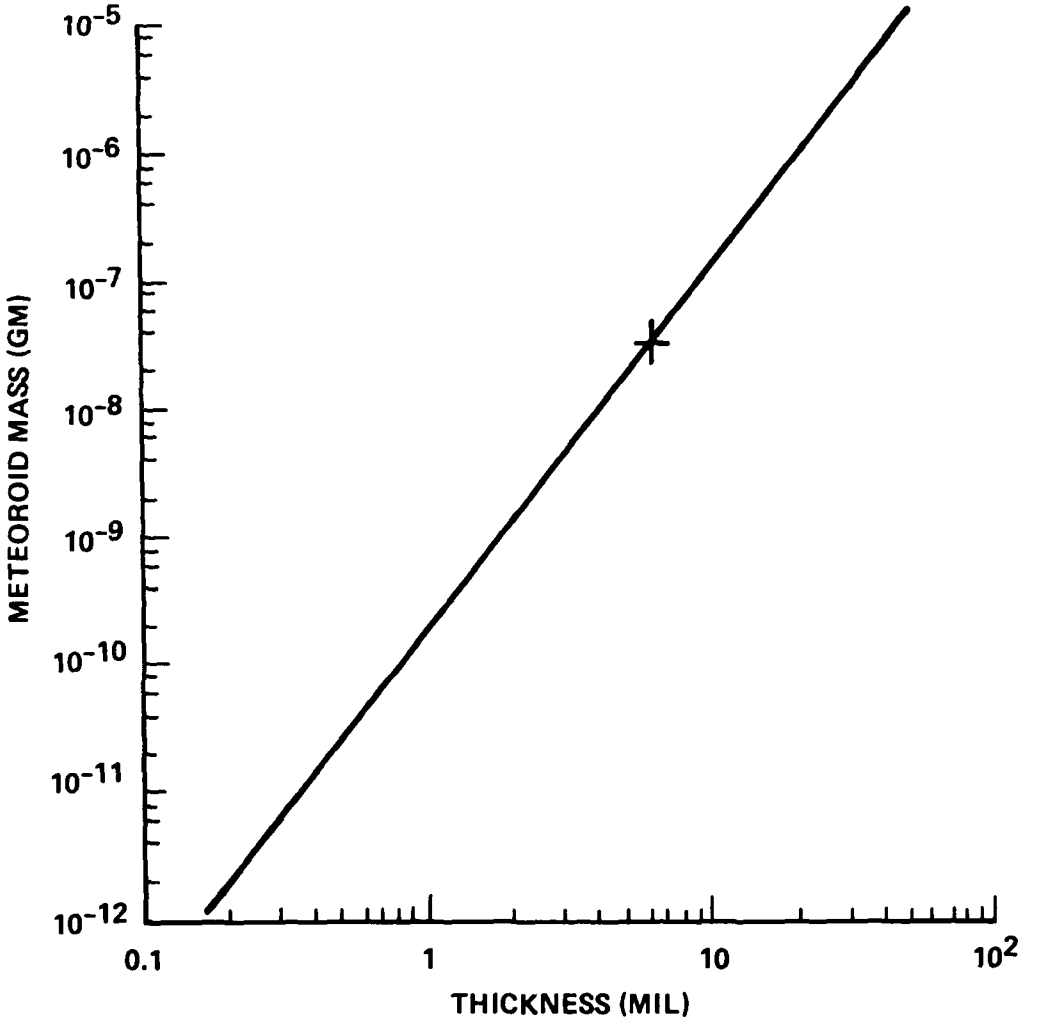

Figure 6.4 Penetration Capability of Micrometeoroid Particles

various materials being considered for future spacecraft, has not yet been completed. The maturity ratings for this interaction were rated CONSIDERABLE (4) for theory and MODERATE (3) for experiment.

6.1.4 System Impact Rating

In the past, the effects of micrometeoroid impingement have been considered to be negligible. Spacecraft were relatively small and the particles that did hit did not interfere with the normal operation of the spacecraft. This will not be true with new, large spacecraft. The number of impacts will increase, since the surface areas will increase. In addition, the probability of damage to sensitive components distributed around the spacecraft will increase, as the number of these components also increase. Thus, the system impact for this interaction was rated LARGE (4).

6.1.5 Mitigation Techniques

The mitigation technique used against this interaction is micrometeoroid "bumpers". These bumpers, or shields, protect sensitive surfaces and instruments. Multi-layer bumpers could provide more protection than single layers of the same thickness. Another possible technique is to reduce the size of sensitive areas, such as using solar thermodynamic power systems instead of solar arrays. Designing an allowance for performance degradation, due to micrometeoroid impacts, is another alternative.

6.2 MAN-MADE DEBRIS IMPACTS

6.2.1 Interaction Environment

The continually increasing man-made space debris environment is potentially of greater concern than the micrometeoroid environment. There are nearly 5,500 Earth orbiting objects currently being tracked by NORAD radars [228], which are greater than 4 cm in diameter. Data has indicated that this number may be 10,000 to 15,000, for objects smaller than 4 cm, and even greater for particles too small to be tracked [229]. A comparison of debris and micrometeoroids is shown in Figure 6.5. Another recent compilation of debris observations now indicates that the debris environment could be eleven times larger than the NORAD catalog [230].

The existing orbital debris flux, as a function of altitude and particle size, is shown in Figure 6.6. This debris is the result of man's space activities, particularly from rocket explosions and thruster effluents. It is expected to worsen with time [231].

A model for small debris particles, developed for the NASA Space Station, is orbit dependent and shows the greatest concentration of debris below 2000 km. The peak density occurs around 800 km (Figure 6.6) [231]. The average velocity for debris particles is 9 km/sec (in orbits with a 30° inclination) with the average particle mass density about 2.8 gm/cm^3 [232]. Debris particles are heavier than micrometeoroids, but move slower. To have the same kinetic energy as the micrometeoroid particle discussed in section 6.1.2 (0.2 joule), the debris mass would have to be five times heavier. The

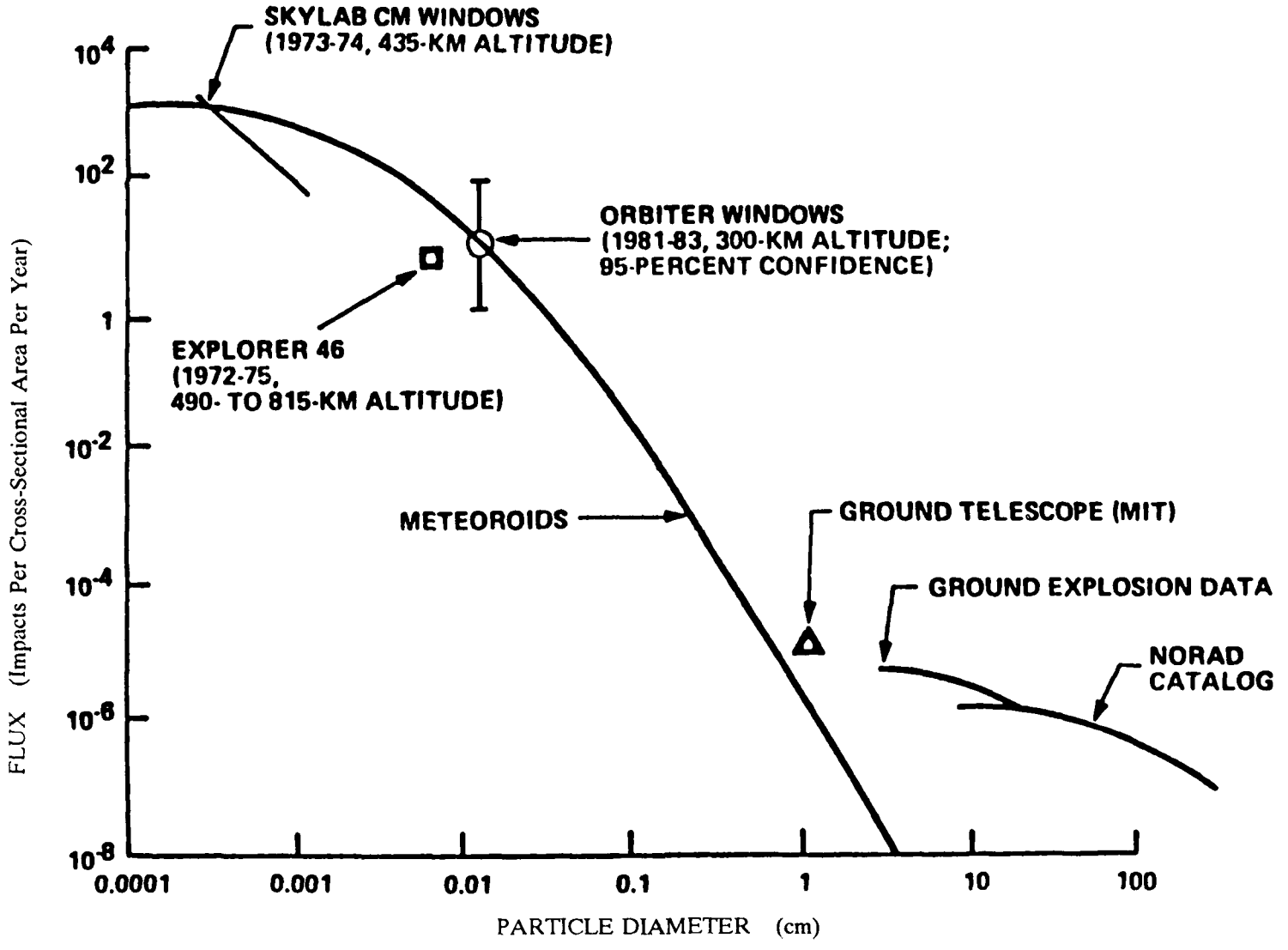

Figure 6.5 Comparison of Orbital Debris Data with Micrometeoroid Model

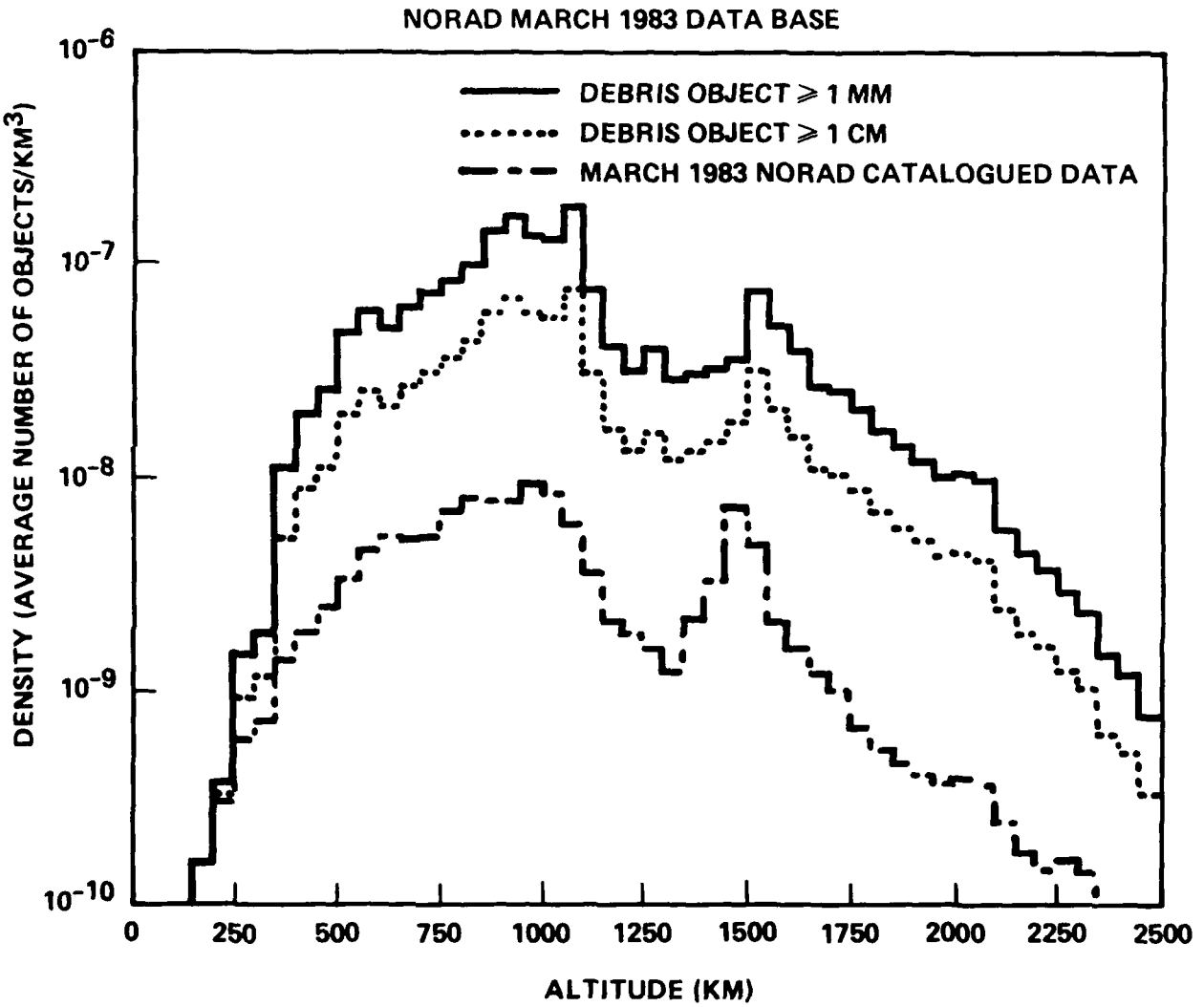

Figure 6.6 Man-Made Debris Environment

distribution of debris at various inclinations was found to be sufficiently uniform so that the collision probability can be assumed to be equal at all latitudes. These models are used to predict the fluxes of objects less than 1 cm in diameter. The uncertainty in the projected flux of 1 cm particles is estimated to be a factor of three. The uncertainty in the flux of 1 mm particles is estimated to be a factor of ten.

6.2.2 Discussion of Interaction

The effects of debris impacts are similar to those expected from micrometeoroids. The particle impact on the surface can penetrate the first layer and damage subsequent layers. This is illustrated in Figure 6.7, which shows a section of a Solar Maximum spacecraft thermal louver returned to Earth after the repair mission. The original damage resulted from the impact of a paint flake. The spalling pattern underneath again exhibited a damaged area larger than the initial impact hole.

The predicted number of impacts per year for a given particle mass is shown in Table 6.2 and is illustrated as a function of surface area in Figure 6.8. The number of very small particles impacting future, large systems can be quite large. Penetration capability of debris particles through thin plates is shown in Figure 6.9. This calculation assumes the relationship used for micrometeoroid penetration is applicable for debris particles. Again, the cross represents a 6 mil thick surface.

Table 6.2
Debris Impacts Expected in a 400 km Orbit

Debris Mass (gm)	Number of Impacts ($m^{-2} yr^{-1}$)
10^{-12}	9863.00
10^{-11}	1539.00
10^{-10}	240.00
10^{-9}	37.50
10^{-8}	5.85
10^{-7}	0.91
10^{-6}	0.14
10^{-5}	0.02

6.2.3 Research Maturity Rating

Uncertainty about the man-made debris environment in space still exists, despite investigation over the past ten years. Orbital debris measurements and analysis, for particles below 10 cm in diameter, have only recently begun. Examination of Shuttle surfaces and parts returned from space, in addition to laboratory analysis, has provided new insights into the small diameter debris environment.

The maturity was rated MODERATE (3) for both experiment and theory. Measurements and analysis to date are insufficient to determine the future environment to the desired degree of certainty. The maturity rating for PEO and GEO orbits is SLIGHT (2) because the debris models are less developed than for LEO models.

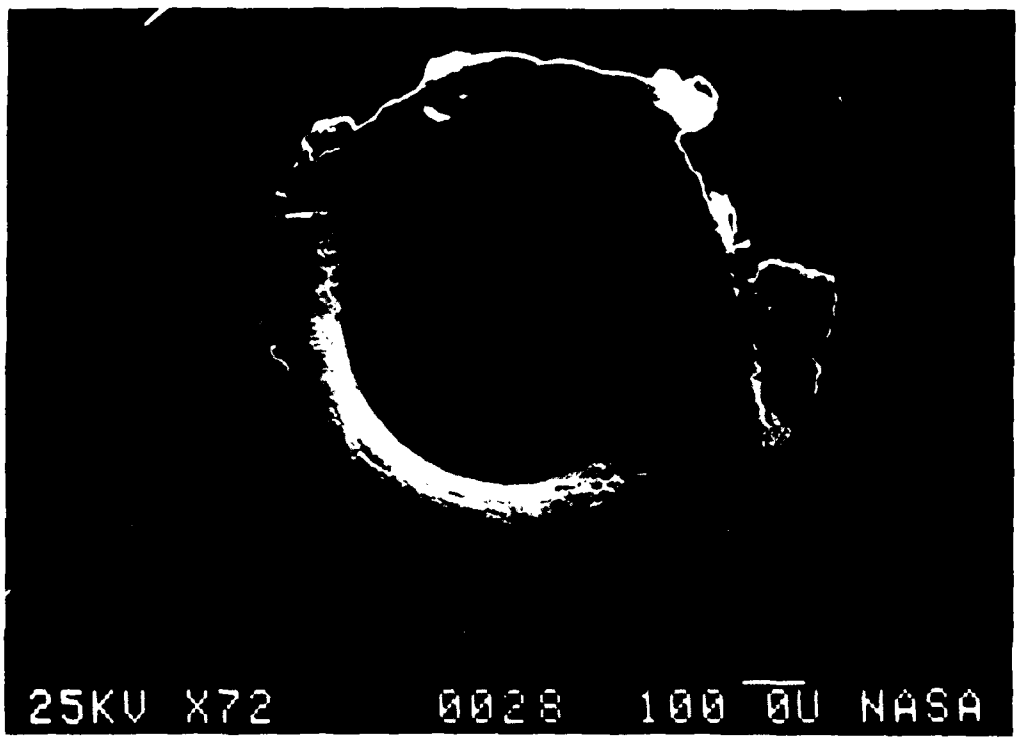

(A) Initial Impact Hole in Aluminum

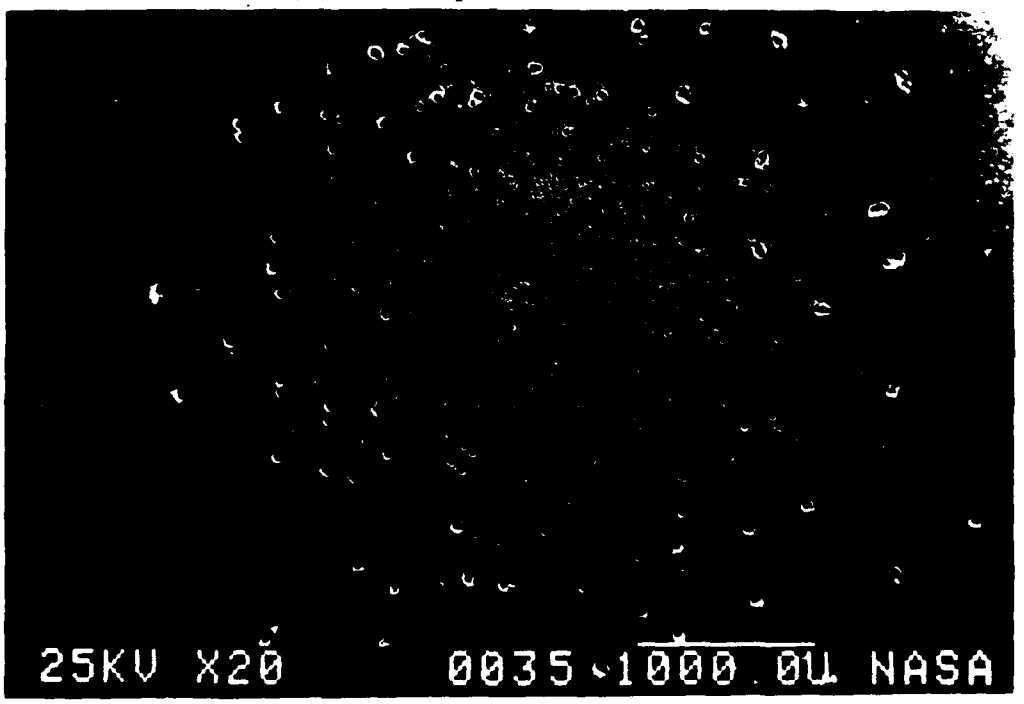

(B) Secondary Layer Spalling Damage

Figure 6.7 Paint Flake Impact Damage in a Solar Max Thermal Louver

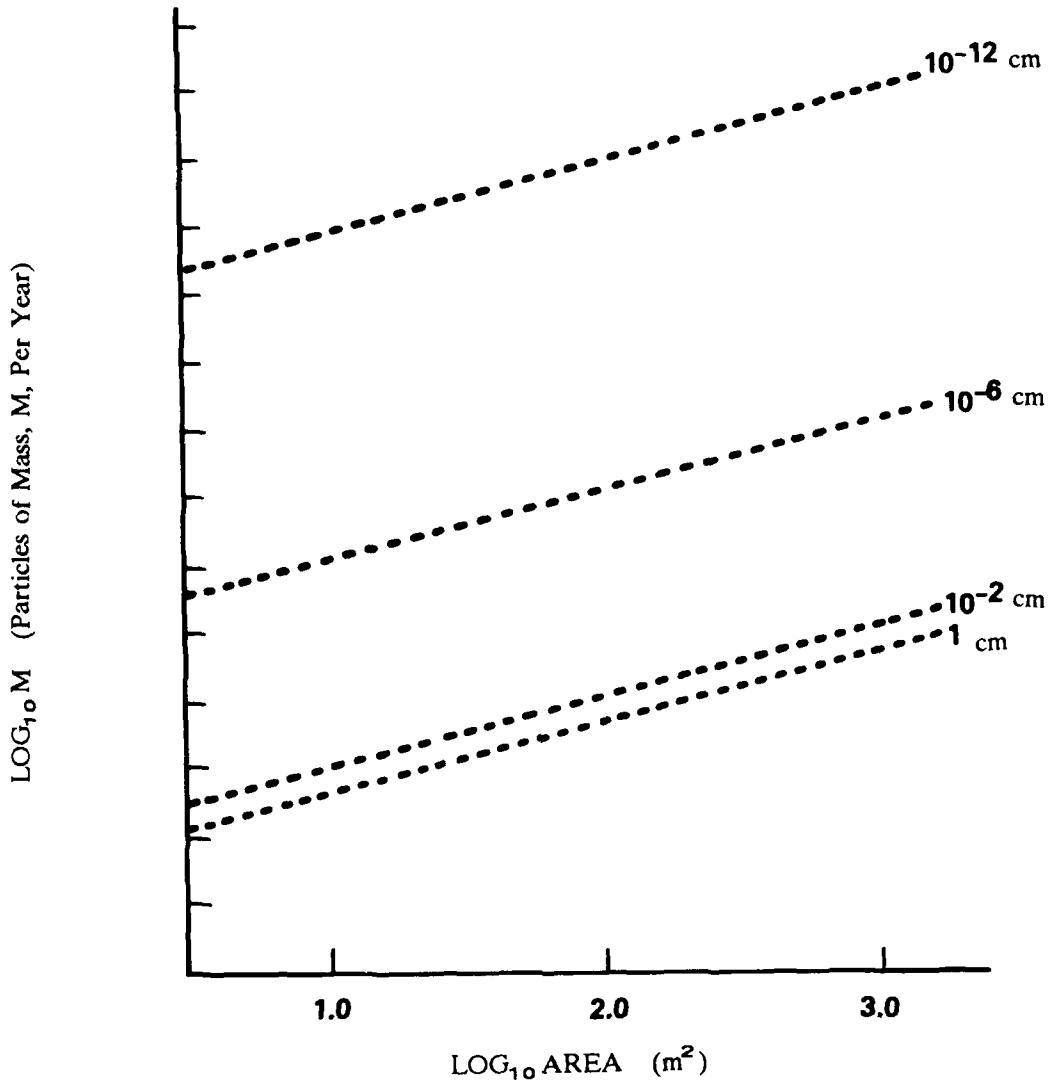

Figure 6.8 Average Cumulative Debris Flux vs Spacecraft Area (400 km Orbit)

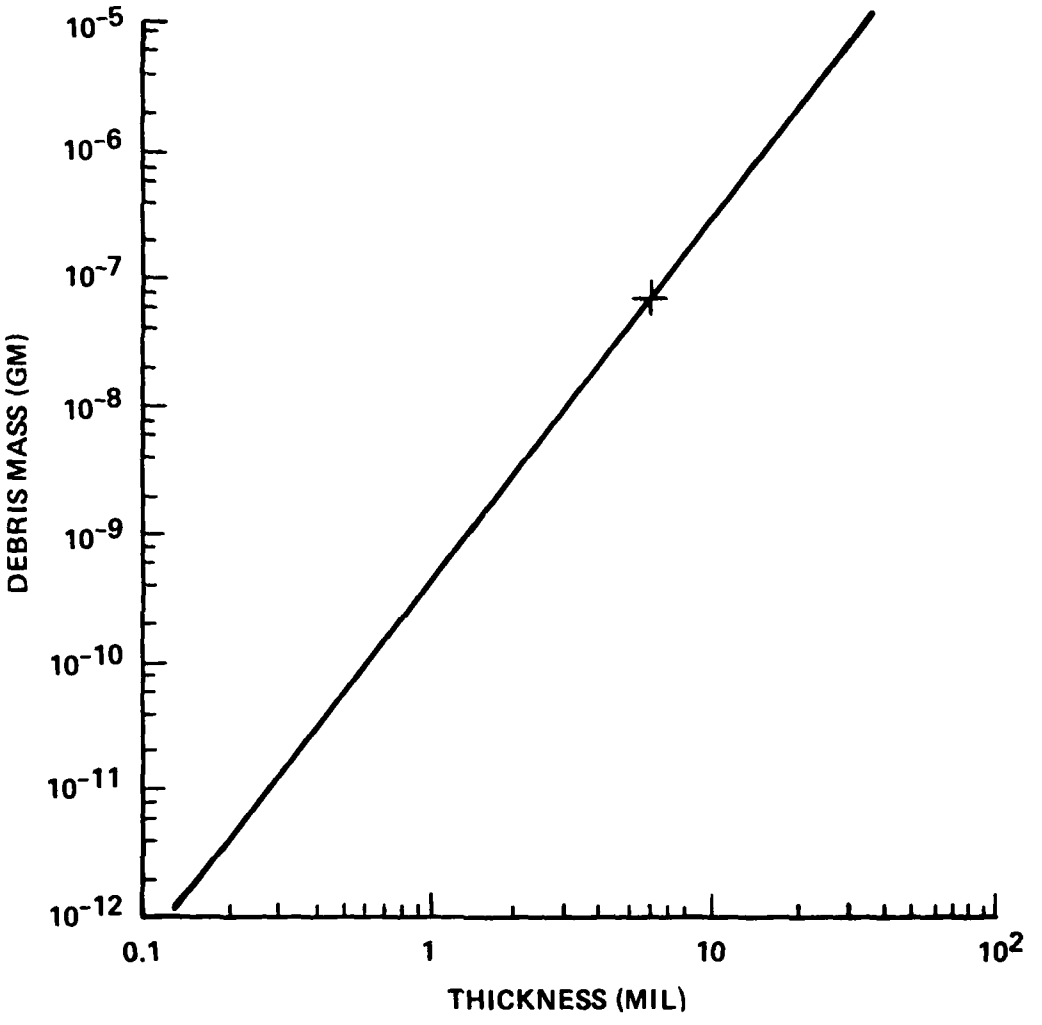

Figure 6.9 Penetration Capability of Debris Particles

6.2.4 System Impact Rating

The system impact for man-made debris interactions was rated LARGE (4) for the same reasons as for micrometeoroid impact interactions.

6.2.5 Mitigation Techniques

The mitigation techniques discussed for micrometeoroid impact interactions are also applicable to man-made debris interactions. In addition to those techniques discussed in section 6.1.5, the amount of man-made debris being placed into space should be minimized and/or reduced. Approaches like those used in the final years of the DELTA missions should be implemented. It was found that the residual fuel and oxidizer in the DELTA's orbiting second stages corroded the tanks and caused an explosion after some time in orbit, creating a large number of small debris particles. In later DELTA rockets, the stage was commanded to burn the remaining fuel after payload separation. This resulted in a single, trackable object rather than thousands of debris items.

7.0 SOLAR OPTICAL RADIATION ENVIRONMENT INTERACTIONS

The interactions associated with the solar optical radiation environment are Degradation of Exterior Coatings, Thermal Forces, and Biological Hazards. The environment common to these interactions will be described below.

7.1 GENERAL ENVIRONMENT DISCUSSION

The Sun continually emits energy and mass into the solar system, and beyond, in the form of electromagnetic radiation, plasma, and energetic particles. The output is not constant but varies with cycles (e.g. 27 day rotation, 11 year sunspot cycle).

The radiated environment from the Sun is the primary concern in this section, since plasma and energetic particles have been covered in previous sections. The spectral energy distribution for the Sun resembles a black body distribution with an effective temperature of 5800° K. This means that the bulk of the solar energy lies in the wavelength range of 150 nm to 10 μm (3×10^{13} Hz to 2×10^{15} Hz) with a maximum near 6.7×10^{14} Hz or 450 nm (Figure 7.1). This portion of the solar spectrum is primarily emitted by the solar photosphere [6,234].

The total amount of radiated energy at Earth orbit (1 Astronomical Unit or A.U.) is known as the Solar Constant. This value has been repeatedly measured over recent years and the current accepted value is 1371 W/m^2 ($\pm$ 5 W/m^2). Spacecraft interactions with solar X-ray and gamma ray fluxes have not been important to date and will not be discussed further.

7.2 SURFACE DEGRADATION

7.2.1 Discussion of Interaction

Solar ultraviolet (UV) radiation, a significant constituent of the space radiation environment, can cause both surface and bulk damage to thin flexible coatings used for thermal control. Typical effects of UV radiation on materials include: outgassing, shrinkage, cracking, pitting, embrittlement, and discoloration. It can also cause degradation of mechanical properties (such as tensile strength, elongation, and modulus of elasticity) as well as optical properties (like transmittance, reflectance, and absorptance), which affect spacecraft thermal balance.

Research on UV radiation effects on spacecraft materials has been documented and will only be summarized here. Thermal control coating research has been supported by the thermophysics community [235-239], and cover glass degradation by solar array engineers [240,241]. Much research has been performed on the thermal control property changes of paints and polymeric films. The stability of these materials is critical, since they are typically used to radiate spacecraft internal heat into space.

The mechanism by which solar UV damages the zinc oxide pigment used in white thermal control paints has been extensively investigated. In space, this material can

NASA-GODDARD SPACE FLIGHT CENTER
GREENBELT, MARYLAND
AUGUST, 1976

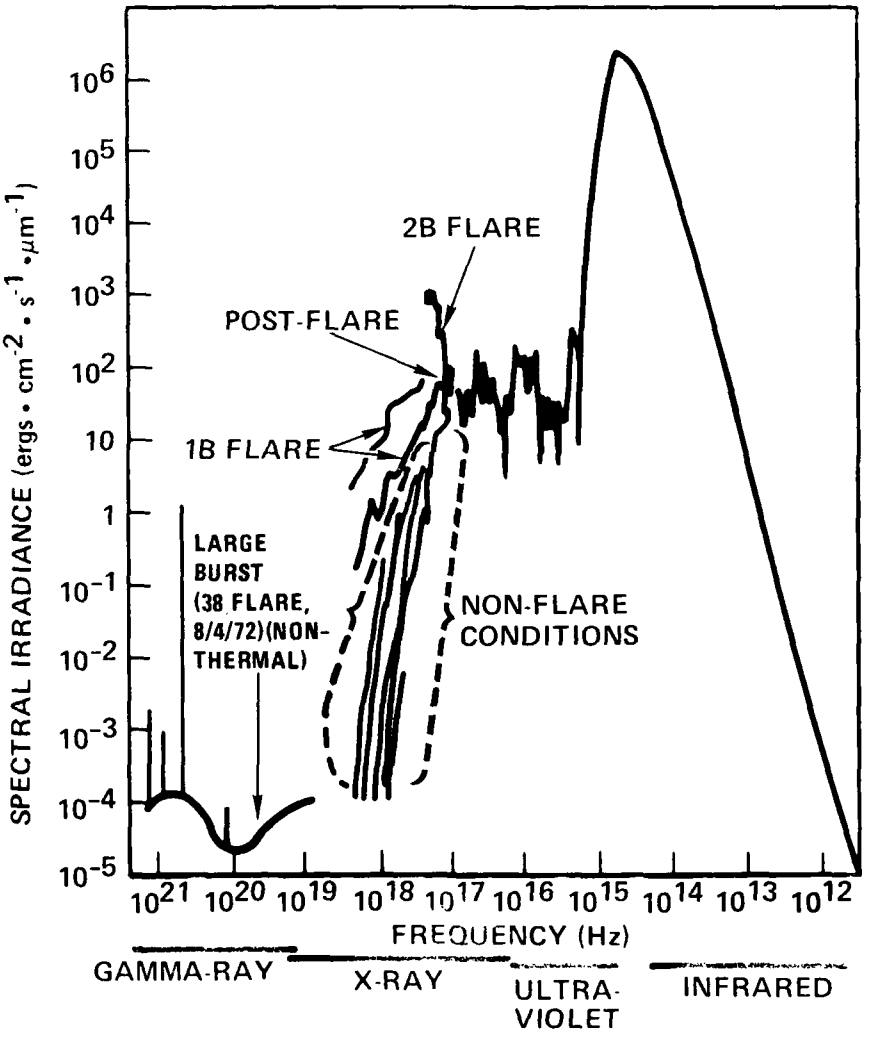

Figure 7.1 The Solar Spectrum

radiate more energy than it can absorb from the solar spectrum. This means that the coating can be used as a radiator, even when it faces the sun. Unfortunately, the oxide's absorptance of solar energy increases with time, resulting in increases in the surface and internal temperatures of the spacecraft, while the emittance of the paint remains essentially constant. The paint is also subject to energetic particle degradation, [235] with a threshold flux of $\approx 10^{14}$ particles/cm^2, as well as degradation due to UV. The degradation of white paint solar absorption capabilities has been improved to levels that can be tolerated in current spacecraft thermal designs. More stable white paint pigments were found and these replaced the zinc oxide. Paint stability should be reviewed to determine if there is a need for further improvement for future longer life, higher powered space systems.

Other types of thermal control coatings use polymeric layers, such as Kapton and Teflon. Laboratory evaluations, using simulated solar UV, have been conducted on a number of these materials. Tables 7.1 and 7.2 show the results on several thermal coatings after the equivalent of 3 years exposure in LEO and 7 years in GEO [239].

Table 7.1
UV Degradation of Thermal control Surfaces at LEO

Material	IR Emissivity	Solar Absorptivity	
		Initial	3 Years
1st Surface Aluminized Kapton	Ø.Ø3	Ø.12	Ø.13
2nd Surface Aluminized Kapton	Ø.8Ø	Ø.45	Ø.55
2nd Surface Aluminized Teflon	Ø.8Ø	Ø.Ø7	Ø.17
1st Surface Goldized Mylar	Ø.Ø25	Ø.2Ø	Ø.21
2nd Surface Silverized Kapton	Ø.8Ø	Ø.Ø7	Ø.17

Table 7.2
UV Degradation of Thermal control Surfaces at GEO

Material	IR Emissivity	Solar Absorptivity	
		Initial	7 Years
Clear Anodized 6Ø61 Aluminum	Ø.79	Ø.38	Ø.55
Cleaned 6Ø61 Aluminum	Ø.Ø4	Ø.24	Ø.26
Cleaned TI-6-4	Ø.1Ø	Ø.5Ø	Ø.5Ø
7306 Black Chemglaze Polyurethane	Ø.87	Ø.38	Ø.55
S13G-LO White Silicone	Ø.88	Ø.22	Ø.55
Bare GR/Epoxy	Ø.78	Ø.92	Ø.85
2nd Surface Aluminized Kapton	Ø.8Ø	Ø.45	Ø.77
2nd Surface Aluminized Teflon	Ø.8Ø	Ø.14	Ø.32

The effects of radiation damage to solar cells has been calculated for most orbits [240]. In LEO, the major performance degradation is due to darkening of the solar cell cover glass by solar UV and trapped particle radiation. In GEO, the degradation of the solar cell output comes from both darkening of the cover glasses (4-10%) and from

deterioration of the silicon (15%). This degradation amounts to a 19-25% reduction in original power output over a nominal seven year mission. The cover glass darkening happens rapidly at first and then decreases. Degradation of the silicon continues throughout the life of the cell at a rate of ≈ 2% per year. Silicon degradation in PEO is about twice the rate in GEO, due to the greater flux of energetic particles encountered.

Conflicting views exist regarding the combined effects of particulate radiation and solar UV on solar cell assemblies. One view, supported by ground testing, is that UV exposure bleaches some of the darkening induced by the particle radiation. The other, supported by comparing ground test data with flight data, holds that the simultaneous combined exposure causes greater darkening than each exposure alone [240].

7.2.2 Research Maturity Rating

The process by which UV radiation interacts with spacecraft coatings is well understood, thus, the theoretical maturity was rated COMPLETE (5). Extensive testing of UV radiation effects on materials has been carried out and is continuing. Testing has included extensive laboratory space simulations of the effects of various orbits on many spacecraft surface materials. A CONSIDERABLE (4) rating for experiment was given, since the behavior of new materials must be verified before future application.

7.2.3 System Impact Rating

The primary impact to systems, due to degradation of thermal control coating properties, is usually warmer than anticipated spacecraft operating temperatures. The main impact of radiation darkening of solar array cover glass is the decline in power output with time. These two effects seriously impact the operation of space systems, however, the degradation is predictable and tolerance is designed into the system during thermal analysis. Thus, the system impact of these interactions was rated SLIGHT (2).

7.2.4 Mitigation Techniques

Designing allowances for solar radiation degradation into the space system, is the primary technique used to mitigate the effects of this interaction.

7.3 THERMAL FORCES

Thermal forces, for this discussion, means the momentum transfer imparted to large spacecraft structures by incident solar photons and the stresses induced by thermal differential expansion.

7.3.1 Discussion of Interaction

7.3.1.1 *Momentum Transfer*

A force is exerted on the surfaces of space systems due to momentum transfer from incident solar photons. This force may cause a torque about the spacecraft's center

of mass [242]. Surface characteristics are a dominant factor in the generation of both radiation and aerodynamic torques on a spacecraft. Radiation torques are generally the more dominant of the two at altitudes above 1000 km. This is true because aerodynamic forces (e.g. drag) diminish rapidly with increasing altitude, while radiation forces remain nearly constant in near-earth orbits. The momentum per unit volume carried by a collimated beam of light is given by H/c^2, where (H) is the power per unit area and (c) is the speed of light [243]. When the light is totally absorbed, the force exerted on the body is the time-rate of momentum deposition. Hence, the pressure exerted in the direction of travel of the light is:

$$F = (\text{momentum/volume}) \times (\text{velocity of light}) = H/c^2 \times c = H/c$$

The net acceleration due to solar radiation pressure is zero for a satellite in a circular orbit which does not enter the Earth's shadow (i.e. a dawn-dusk polar orbit), since the force opposes Earth's rotation for one-half the orbit and enhances it for the other half [244]. The energy of a body in an elliptic orbit that enters the Earth's shadow will change due to radiation pressure unless the accelerating and retarding radiation pressure forces are equal over the complete orbit. This geometry cannot persist for an extended period because of the orbit change in inertial space. Radiation pressure must therefore be considered in the calculation of orbital dynamics [244].

All torques that disturb spacecraft attitude must be considered in the design of attitude control systems. Torque resulting from radiation forces on spacecraft surfaces is one of these. The major factors to be considered in the determination of radiation torques are: (1) The intensity, spectrum, and direction of the incident or emitted radiation; (2) The shape of the surface and the location of the Sun facing side with respect to the spacecraft center of mass; and (3) The absorption, reflection, and emission properties of the surface upon which the radiation is incident or emitted.

A torque will be applied, even in orbits where radiation pressure does not cause a net acceleration of the center of mass, if the area exposed to solar radiation is asymmetric about the body's center of mass. This can be the principal cause of torque, especially in a structure with large, optically opaque surfaces (as opposed to one with an open structure) receiving solar radiation. Photon impact torque can be exploited in spacecraft operations by balancing undesired disturbance torques through careful positioning and trimming open and closed areas of a spacecraft. This use of solar radiation pressure to trim spacecraft attitude was demonstrated on the OTS-2 geosynchronous satellite [245].

7.3.1.2 *Thermal Expansion Stresses*

The expansion rate of various materials as a function of temperature is a well known and understood phenomenon. Differential expansion of materials, constrained by other materials, creates thermal stresses in the materials, which can result in bending and axial forces unless stress relief has been provided. It is important that these stresses be recognized and accommodated into the design of large, flexible systems proposed for future applications.

The 1985 Solar Array Flight Experiment (SAFE) unexpectedly demonstrated the effects of thermal expansion when the solar panel warped [246]. The experiment was designed to evaluated the deployment, stability, and retraction of a 4 × 32 meter solar array blanket from the Shuttle (Figure 7.2). Mass simulators replaced most of the solar cells since SAFE was primarily a mechanical stability test. A 40 cm bow, between the center and free edges, occurred when the panel first moved from eclipse into sunlight (Figure 7.3). The panel straightened after a brief time in sunlight. This bowing was traced to differential thermal expansion of the various materials used.

While this effect may not exist in a real solar array, it should have been anticipated in the experiment design phase. This example is used to emphasize the concern for detail necessary in designing future large, flexible spacecraft, since such design negligence may severely impact these systems.

7.3.2 Research Maturity Rating

Analytical techniques exist which can satisfactorily predict radiation torques in large structures. Current practices for estimating these torques are based upon knowledge accumulated from previous flights and scale model test results. In addition, thermal expansion and differential stresses are also well understood phenomenon. While the data base for this interaction is believed to be adequate, unknowns may emerge due to the size of future systems. Thus, the maturity for both theory and experiment has been rated CONSIDERABLE(4).

7.3.3 System Impact Rating

The system impact was rated MODERATE (3), due to scaling uncertainties. In addition, this interaction is highly configuration dependent since large, flexible spacecraft would be more susceptible than compact, stiff ones.

7.3.4 Mitigation Techniques

Compensating for these stresses and torques during system design is the best mitigation technique.

7.4 BIOLOGICAL HAZARD

The effects of solar radiation on the military man in space must be considered due to the Air Force's decision to plan for astronaut roles in spacecraft assembly, maintenance, and servicing.

7.4.1 Discussion of Interaction

The shielding that is provided by present spacecraft and EVA spacesuits is considered adequate to protect an astronaut from soft X-ray and UV radiation while in space [247]. Future construction of large systems in space could change this. There may be dangers from focused sunlight during the assembly of large, flexible, reflecting sheets

Figure 7.2 Solar Array Flight Experiment (Artist's Conception)

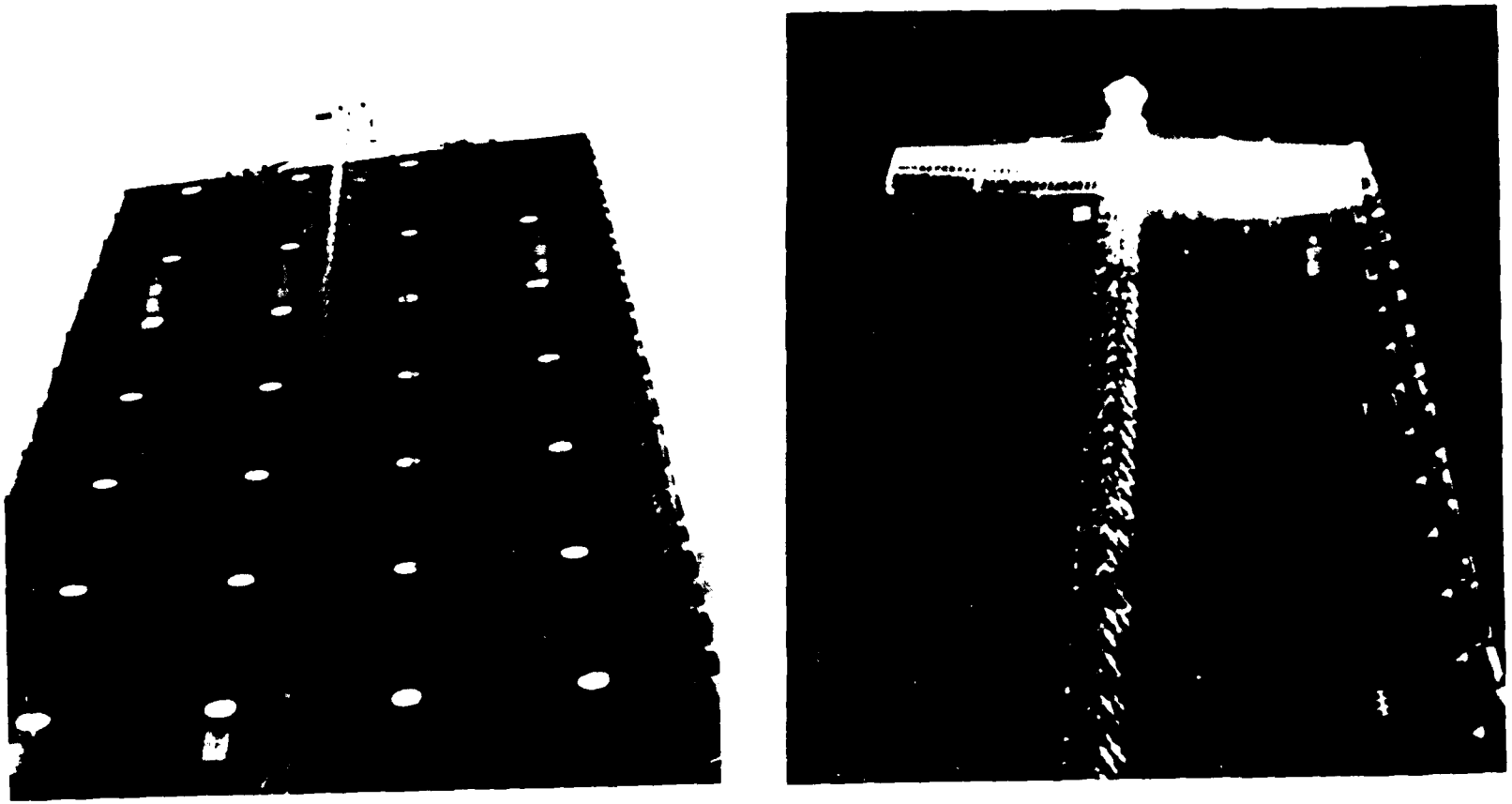

A. Nominal Structure

B. Deformed Structure

Figure 7.3 Thermal Effects on Flexible Structures (SAFE)

that might cause eye damage or burn through a space suit, if an astronaut came near the focal point of such a mirror-like surface.

7.4.2 Research Maturity Rating

The maturity of knowledge about the hazard to man from solar radiation was rated CONSIDERABLE (4) for both theory and experiment.

7.4.3 System Impact Rating

The system impact for this interaction was rated NEGLIGIBLE (1) because it can be prevented through EVA equipment improvements and operational constraints. Future large spacecraft assembly missions must accept operational constraints to avoid creating hazards to man from solar radiation, especially during times of sever solar radiation emissions.

7.4.4 Mitigation Techniques

The techniques for mitigation are shielding man from solar radiation by equipment improvements and constraints on operations.

8.0 SELF-GENERATED ENVIRONMENT INTERACTIONS

In this section, interactions arising from spacecraft operations are discussed. These interactions are: contamination arising from system outgassing, contamination arising from thruster effluent, and operation of nuclear power systems.

8.1 CONTAMINATION DUE TO OUTGASSING MATERIALS

8.1.1 Interaction Environment

This interaction deals with contamination of spacecraft surfaces by vapors or particles originating from the spacecraft [248-252]. Volatile, condensible vapors outgas under space conditions from warm, non-metallic adhesives, paints, and insulators [253-257]. Outgassing can occur from most all spacecraft materials, both interior and exterior. Interior sources include structure and electronic box coatings, as well as components within these boxes. Exterior sources include paints, dielectrics, thermal blankets, adhesives, and lubricants.

Particulate contaminants are essentially pieces of spacecraft materials that flake off due to thermal conditions or in response to natural environment bombardment (i.e. spalling or sputtering). They also include dust particles, which are trapped during ground operations and carried aloft with the launch vehicle [258-261].

8.1.2 Discussion of Interaction

Vapors outgas from the warm surfaces within a spacecraft and flow through the spacecraft towards space [257,262-266]. This flow is illustrated in Figure 8.1. From a material point of view, outgassing does not result in material failure. The concern, however, is that outgassing products can condense on cold surfaces, such as thermal radiators, low temperature sensors, and solar cells. Deposition can change surface properties, resulting in warmer operating temperatures and possible failures.

Cold surfaces act as traps for outgassing products, which tend to localize the areas where contaminants can be a problem. Contamination can also be enhanced by charging of exterior surfaces [267]. The substorm or auroral environment (Section 3.2 and 3.3) can charge exterior surfaces which creates electric fields around the spacecraft [268]. Outgassing products could be ionized by photoionization and, if the fields are strong enough, return along field lines to the spacecraft and redeposit. A SCATHA satellite experiment (Figure 8.2) [269] showed that enhanced contamination exists. Figure 8.2 shows a sample of collected data from a retarding potential mass analyzer. The deposition rate would be independent of the instrument bias voltage, if charge enhanced effects did not occur. The data indicates a small but finite voltage effect. Thus, contamination could become serious on large spacecraft after long periods of time.

Particulate contamination can float around the spacecraft or redeposit onto surfaces, thus disrupting system operations. The particles can be large enough to reflect light to sensors, providing false sensor data (e.g. star trackers) and disrupting the

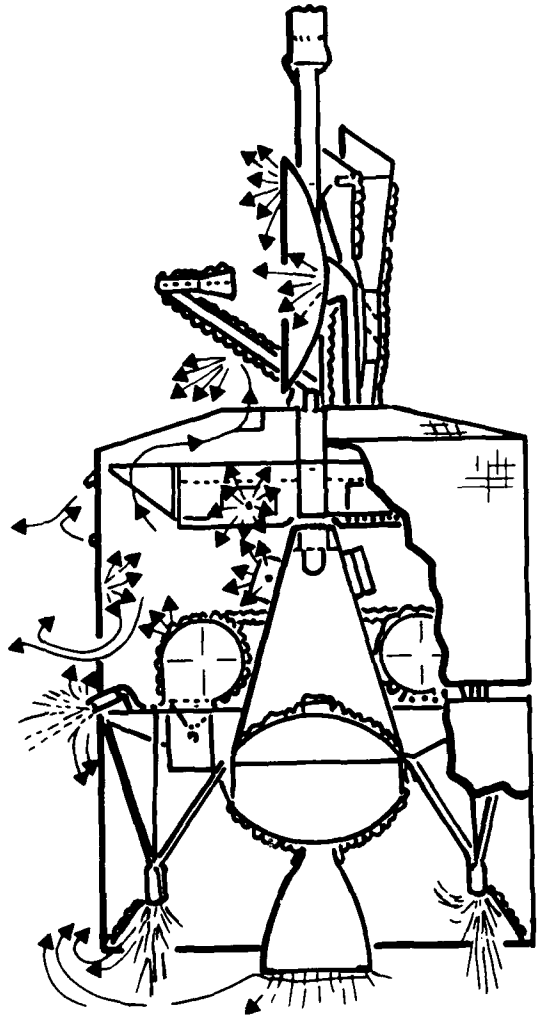

Figure 8.1 Outgassing and Thruster Flow Patterns in a Spacecraft

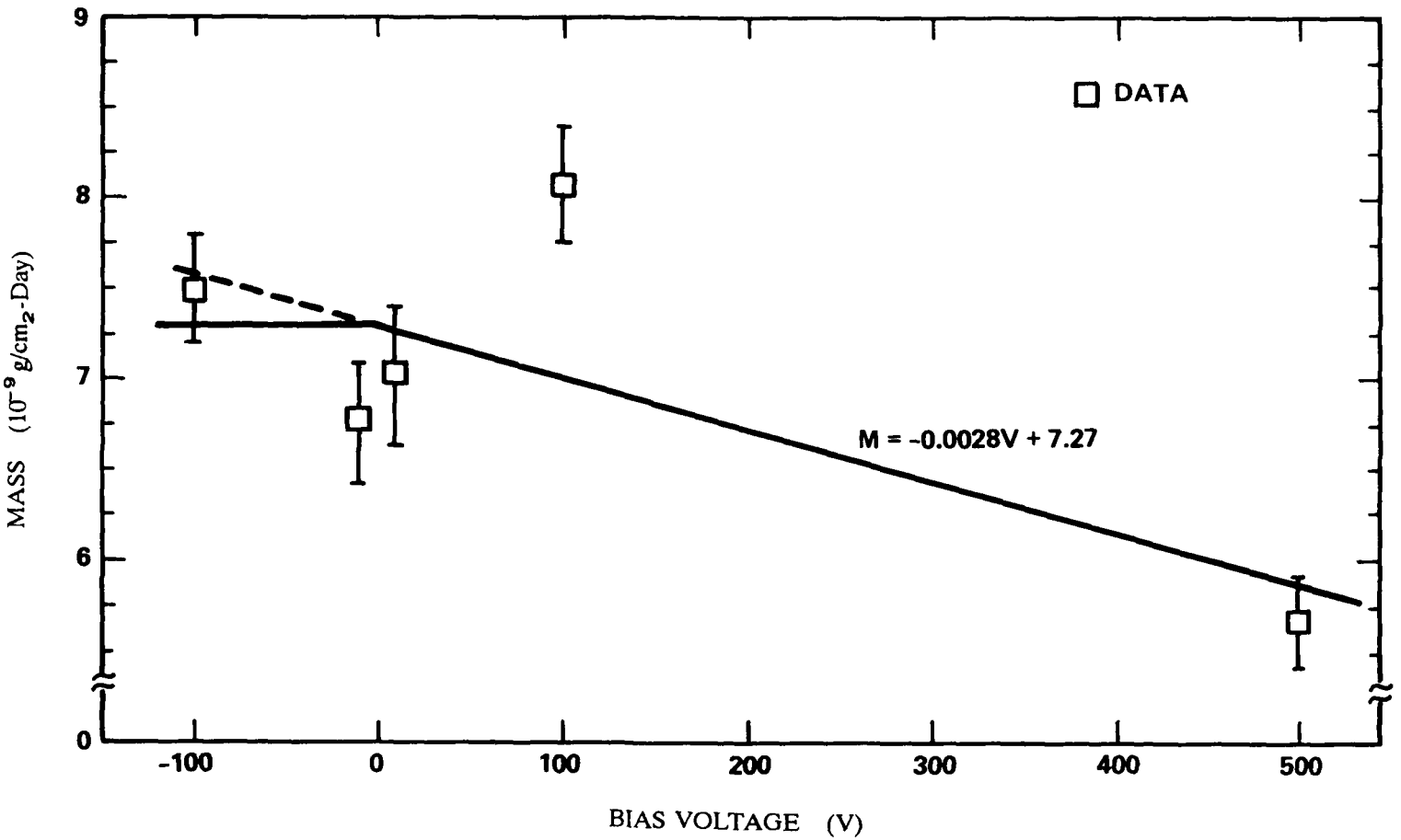

Figure 8.2 Enhanced Contamination Measured on the SCATHA Spacecraft

operation of science instruments. If the particle has sufficient energy, impact with the spacecraft surface could result in surface or sensor damage.

8.1.3 Research Maturity Rating

Contamination is a recognized threat to long-term mission operations and work continues in order to understand the process and alleviate its impact. Theoretical investigation of electrostatically enhanced contamination has only recently started. Finally, the ability to predict outgassing flows and deposition rates is uncertain, even for present day spacecraft designs. On the other hand, experimental techniques to evaluate vapor outgassing rates are well-known and a large data base is available [270-275]. Particle contamination experiments, however, still require more work. Thus, the research maturity for contamination from outgassing materials was rated MODERATE (3) for theory and CONSIDERABLE (4) for experiment.

8.1.4 System Impact Rating

Surface contamination and sensor degradation interactions will be rated. These ratings will apply to all orbits, since the outgassing interaction is independent of orbit.

8.1.4.1 *Surface Contamination*

The impact of surface contamination was rated LARGE (4). "Cold" surfaces, such as Optical Solar Reflectors (OSR's), have a tendency to operate at warmer temperatures as time in orbit increases. This could be due to contamination from outgassing materials. Thus, the present technique, allowing for surface degradation in the thermal design, may be satisfactory for existing spacecraft, however, it may not be sufficient for future, extended life systems. Therefore, the effects of contamination must be understood and anticipated in new system designs.

8.1.4.2 *Sensor Degradation*

Sensors requiring radiator surfaces to operate at cryogenic temperatures could be severely impacted by contamination. Such surfaces would be prime sites for contaminant deposition and possible system malfunctions due to increased radiator temperatures. Thus, the system impact was rated CATASTROPHIC (5).

8.1.5 Mitigation Techniques

There are basically two approaches for controlling the detrimental effects of vapor outgassing. The first approach is to pick materials which have low outgassing rates for the particular application. This requires prior measurement of the outgassing rates of all spacecraft sources as a function of time and temperature [270-275]. This information should be made available to designers in a data base format.

The second approach uses available materials to analyze flow patterns so that the contaminant flow can be directed away from regions where potential problems could

occur [276-278]. In order to conduct this analysis, specific internal and external parameters must be know. Necessary internal parameters include composition, weight, and temperature predictions for all non-metallic materials, as well as the view factors which couple the materials to venting ports. External parameters include the composition and quantity of all non-metallic materials, the area, location, predicted material temperatures, and the view factors coupling all exterior surfaces. Material outgassing rates must be known either from ground tests or prior flight histories. The analysis yields predicted flow patterns and probable deposition sites. If the results show that system performance will be impacted, the outgassing flow pattern can be adjusted with baffles or cold traps.

8.2 THRUSTER EFFLUENT CONTAMINATION

8.2.1 Interaction Environment

This section examines the problem of contamination from chemical rockets, such as propulsion engines and attitude control jets, as well as ion thruster effluents. The principal concern here is how this type of contamination interacts with systems in the space environment, and not during lift-off and ascent to orbit. The elements which significantly contribute to this environment are the combustion products from liquid rockets (i.e. water, nitrogen compounds, etc.), aluminum oxide from solid boosters, and ionized particles from electric devices (probably xenon). The boosters and attitude control systems for each spacecraft system determines the specific substances which contribute to the contamination environment.

8.2.2 Discussion of Interaction

Spacecraft use thrusters to alter orbit and to maintain attitude. Solid or liquid rockets are usually used to change orbit. Attitude control thrusters are smaller and can use cold gas jets. Future missions may use ion thrusters for both orbit changes and attitude control. In all cases, the use of thrusters will generate an enhanced local atmosphere around the spacecraft which can effect the behavior of surfaces and sensors.

8.2.2.1 *Chemical Rockets*

Chemical rockets are used for upper stages, orbit insertion, orbit trimming, and reentry operations. They provide thrust by burning large quantities of fuel. Although a majority of the fuel is ejected, there are still possible interactions that must be considered [277,280-282]. As stated previously, lift-off is not included in this study.

Thruster firing generates heat loads in the combustion chamber and nozzle. In addition, heat generated in the expanding thruster plume can be conducted back to the structure. The exhaust plume may also impinge upon parts of the spacecraft, resulting in local heating and material failure if the impingement was not anticipated. These factors must be considered in the vehicle thermal design.

In addition to localized heating, surfaces and sensors can be contaminated by the

thruster effluents. While most of the thruster products escape, a small fraction can return to the vehicle. The quantity of matter ejected is so large that even a small fraction can have significant consequences. Vapor contaminates returning to the spacecraft could deposit on surfaces. Finally, solid particles returning could impact and damage spacecraft surfaces.

8.2.2.2 *Attitude Control Jets*

Attitude control systems activate automatically when spacecraft attitude exceeds specified limits. These jets eject small volumes of gas sufficient to restore spacecraft orientation. The jet emissions tend to be neutral molecules with a small plasma content. While most of this flow leaves the spacecraft vicinity, a small fraction can either strike spacecraft surfaces or redeposit on them, enhancing contamination [283,284]. This contamination source can be significant, even though small amounts of material are ejected during each operation, since these thrusters function over the mission lifetime.

8.2.2.3 *Ion Thrusters*

Ion thrusters generate thrust by using an electric field to accelerate a plasma. These devices produce low thrust, but satisfy spacecraft velocity change requirements by operating for long periods of time [285-288]. Again, the interaction concern is for contamination effects on surfaces and sensors. The small but finite amount of fuel that is not ionized can drift around the vehicle. These drifting molecules, ionized by residual electric fields or by charge exchange processes, can return to the spacecraft and deposit or impact surfaces.

8.2.3 Research Maturity Rating

The research maturity of thruster effluent interactions was rated MODERATE (3) for both theory and experiment, since the long term effects of cold gas, rocket, and ion thrusters are unclear even though they have been well studied. The increasing physical size of spacecraft is an additional factor considered in this rating. While computer models are used to predict thruster plume expansion, further theoretical and experimental (including space validation) research must be performed.

8.2.4 System Impact Rating

The system impact for thruster interactions was given the same rating as outgassing, namely, LARGE (4) for surface contamination and CATASTROPHIC (5) for sensor degradation.

8.2.5 Mitigation Techniques

An analytical approach is used to mitigate thruster effluent interactions. In addition, experimental data is used to provide parameters needed for the analysis and to calibrate the results.

8.3 NUCLEAR POWER SYSTEM INTERACTIONS

The operation of nuclear power systems in space is discussed in this section. However, the safety of their use in space will not be addressed.

8.3.1 Interaction Environment

The nuclear power system environment is basically concerned with total radiation dose, dose rate, and the neutron flux produced by the source. These parameters are significant to the operation of electronics in the vicinity of the source. The parameters specified in the SP-100 system design for a typical payload located 25 meters from the reactor are: Total Dose = 5×10^5 rad (for a 7 year mission), and Neutron Flux = 10^{13} cm^{-2} [289].

8.3.2 Discussion of Interaction

Nuclear power systems, proposed for future missions requiring large power generators, have been previously operated in space. These nuclear systems cause interactions with both the environment and the host spacecraft.

8.3.2.1 *Effect of the Environment on Reactor Operations*

The natural environment should have no measurable impact on the basic function of the reactor. However, the control circuits should be protected from the energetic particle fluxes since they could be upset just as any other electronic circuit.

Biased conductors in a system which are exposed to the ambient plasma have to be given the same considerations as solar array interconnects. This could result in a parasitic power loss through the plasma or, at worst, there could be arc discharges which generate transients in the system. In addition, interactions with the earth's magnetic field must be considered, if large currents are generated which produce torques in current loops and induce additional system stresses (Section 9.2).

8.3.2.2 *Effect of Reactor Operations on the Environment*

Neutron leakage fluxes from a reactor, resulting in significant alteration of the earth's radiation belts, has been the subject of many studies. Initial results indicated that there would be minimal interactions. However, more recent work has indicated that significant problems could arise, particularly in proposed multi-megawatt systems.

8.3.2.3 *Effects of the Reactor Induced Environment*

Total dose and neutron leakage fluxes from reactors can severely impact spacecraft materials and electronics [165,290]. Thermal control system materials can be damaged and electronic systems could be upset or permanently damaged by reactor fluxes.

8.3.3 Research Maturity Rating

Research maturity for nuclear power system interactions was rated CONSIDERABLE (4) for both experiment and theory. These power systems have been studied for years, and both experimental techniques and analytical approaches are well defined. The long term exposure effects on materials and electronics proposed for future space systems are uncertain and should be further evaluated.

8.3.4 System Impact Rating

The impact of reactor operation on other spacecraft systems was reviewed. The primary hazards are to spacecraft systems and astronauts. The impact was rated CATASTROPHIC (5), since the interactions could cause astronaut death and system degradation, permanent damage, and failure.

8.3.5 Mitigation Techniques

Shielding critical components and placing the reactor in a remote location on the spacecraft, away from sensitive systems and astronaut work areas, are the best techniques for mitigating harmful nuclear power system interactions.

9.0 ELECTROMAGNETIC ENVIRONMENT INTERACTIONS

The interactions discussion within this section are motion generated electric fields, current generated forces, and configuration generated torques.

9.1 GENERAL ENVIRONMENT DESCRIPTION

The interactions considered here depend upon the relationship between spacecraft movement and the Earth's magnetic and electric fields. The effects of the space plasma environment are also relevant. The magnetic field values at the Earth's surface are shown in Figure 9.1 [291,292]. The change in field strength with altitude above the Earth's equator is shown in Figure 9.2. This field is relatively stable and is adequately modeled for both LEO and PEO. The relatively small perturbations due to magnetic storms, substorms, and micropulsations have been studied extensively [293]. The north pole of the field is offset from the Earth's axis by about 10.5°. This offset means that the magnetic field encountered by a spacecraft in most LEO and PEO orbits will vary.

At GEO, the ambient field fluctuates (on a percentage basis) with a greater amplitude and frequency in both magnitude and direction. Occasionally it may change from being magnetospheric to interplanetary in nature [9]. Magnetic fields at GEO are on the order of 10^{-3} gauss, as opposed to 0.3 to 0.6 gauss at LEO. Despite the smaller value, the magnetic interactions can still significantly impact long missions.

The magnitude of electric fields in the ionosphere is limited by the conductivity of the plasma. The maximum values reported range up to a few hundred millivolts per meter. The larger measurements were taken in the auroral zone at times associated with auroral activity. Convection electric fields in GEO are on the order of 100 mV/m. Spacecraft in all orbits experience extreme variability in electric field magnitude. Fields on the order of 1 mV/m are common while 100 mV/m field amplitudes occur during times of geomagnetic disturbances [6,293-295].

9.2 DISCUSSION OF INTERACTIONS

The three interactions considered here are: (1) Electric fields induced by the motion of the spacecraft through the magnetic field (i.e. $\mathbf{V} \times \mathbf{B} \bullet \mathbf{l}$); (2) Forces generated by the interaction between currents circulating in the spacecraft and the magnetic field (i.e. $\mathbf{IL} \times \mathbf{B}$); and (3) Torques generated due to spacecraft configuration and the magnetic field (i.e. $\mathbf{m} \times \mathbf{B}$).

9.2.1 Motion-Generated Electric Fields

Most spacecraft built to date have conductive structures. The electric field generated in a spacecraft, caused by the motion of the spacecraft moving with velocity ($\mathbf{V}$) through the Earth's magnetic field ($\mathbf{B}$) can affect the spacecraft [6,296,297]. This field is given by:

$$\mathbf{E} = \mathbf{V} \times \mathbf{B} \bullet \mathbf{l}$$

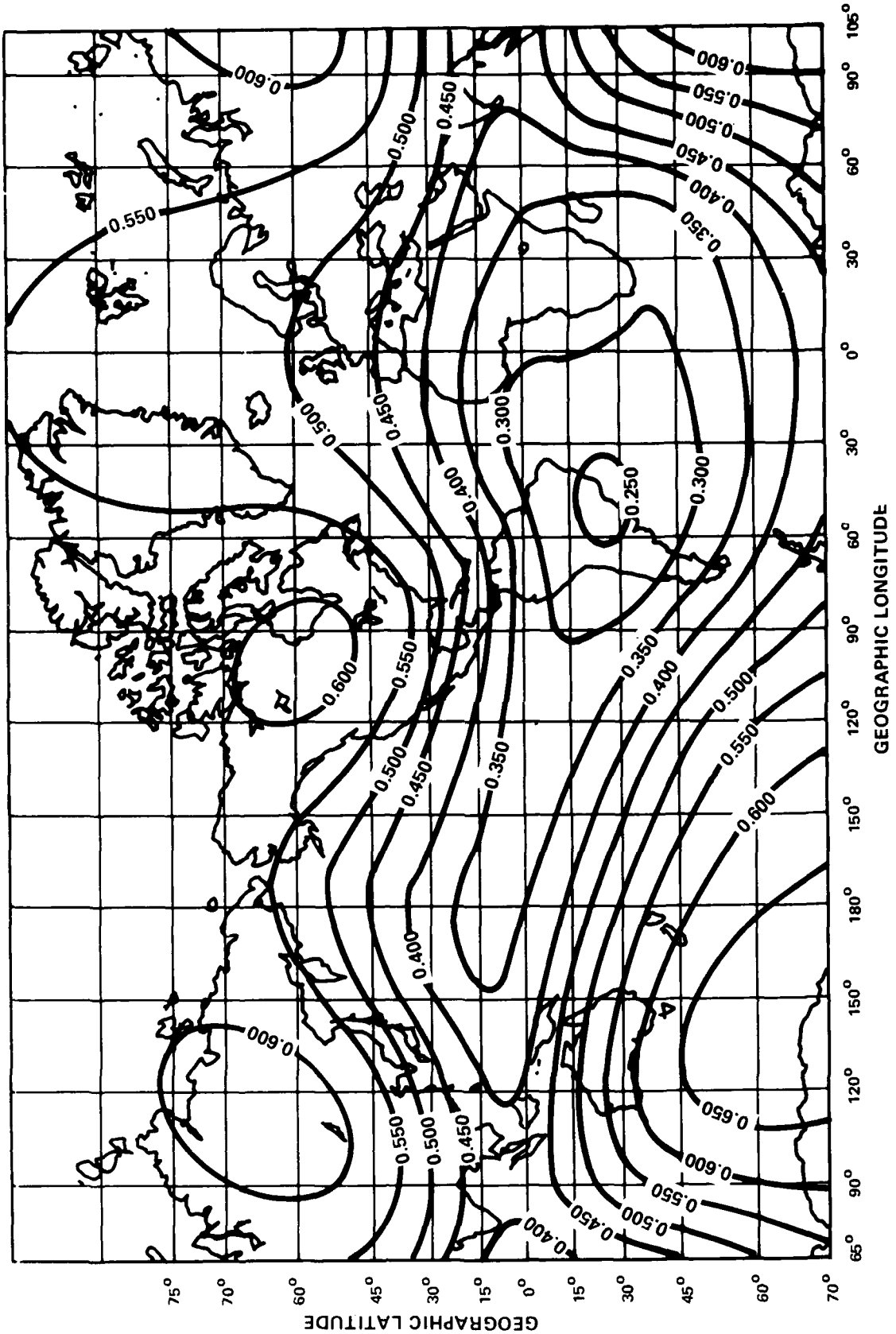

Figure 9.1 Total Magnetic Field Intensity (in Gauss) on the Earth's Surface (Epoch 1965) [7]

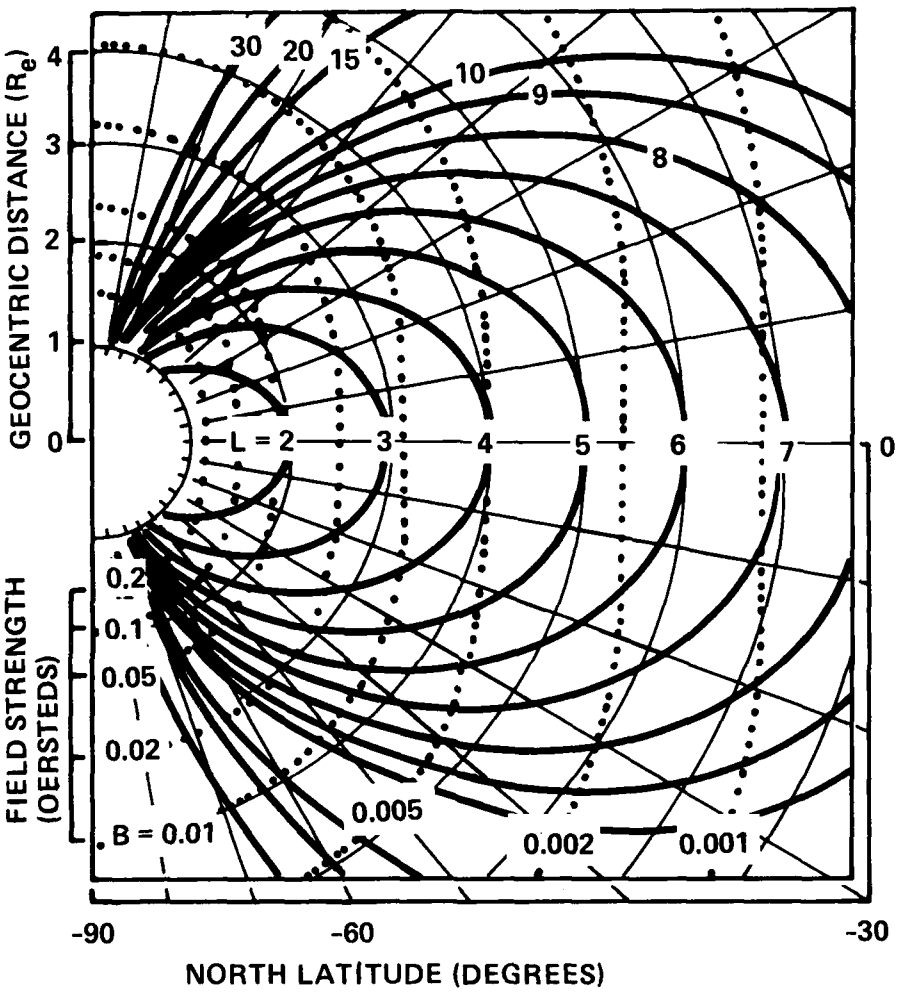

The curves represent the intersection with a magnetic meridian plane of surfaces with constant B and L. The departure of these curves, plotted for a dipole field, from those of the actual field is too small to be apparent in a figure of this scale.

Figure 9.2 The B-L Coordinate System

where **E** is the electric field vector in volts/m, **V** is the spacecraft velocity vector in m/sec and **B** is the magnetic field vector in tesla.

The electric field will vary, since the magnetic field varies with location, altitude, and type of orbit. The induced electric field can vary between ± 0.4 V/m in low earth orbits, where the magnetic field intensity is ≈ 0.5 gauss. While this field is not large, it can permeate into the local plasma environment and disturb conditions around the spacecraft. This could interfere with low energy plasma measurements.

The electric field in a conductive spacecraft structure generates a difference in potential, with the magnitude dependent upon spacecraft dimensions. For a typical present-day spacecraft, with ≈ 2 m typical dimensions, the induced voltage can vary by ± 1 V along the length of the structure. This is not likely to be critical. However, future spacecraft concepts will have dimensions in the hundreds of meters. A spacecraft of this size could experience ± 40 V variations in LEO. These potential values could cause serious complications, especially if the structure is covered with thin dielectric films. The surface of the dielectric would maintain a low voltage (close to the space plasma potential), as a result of the plasma environment, while the conductive structure/ dielectric combination would simulate a capacitor and store a charge [298]. Although the voltage will may not be large, the dielectric area could be sufficiently large to cause a potential problem. For example, for a 2 mil thick Kapton layer, the capacitance would be 5.3×10^{-7} F/m^2. At 40 V, the energy stored would be 0.4 mJ/m^2. The energy released from a few square meters by a discharge could be sufficient to upset electronic systems.

Second, there is a force that results from the field in the dielectric. If this dielectric was a thin, stretched out membrane, the resulting stress in the material could be sufficient to tear the membrane [298]. This force arises when a motion induced voltage is generated in a conductive structure while the space plasma maintains the dielectric surface potential at or near the space plasma potential (Figure 9.3). Preliminary estimates of the stress on a 2 mil thick insulator show it to be on the order of a few tenths of a newton per square meter for a differential voltage of 10 volts and tens of newtons per square meter for 100 volts.

Finally, there exists the possibility that an electric field torque ($\mathbf{p} \times \mathbf{E}$) could be introduced into an elongated structure possessing an electric dipole moment (**p**) in a polar orbit. This effect, while small, could introduce an oscillation related to the orbital frequency. The concern arising here is that the oscillation frequency could match the orbital frequency, producing an unstable oscillation.

9.2.2 Current-Generated Forces

Circulating currents in a spacecraft interact with the Earth's magnetic field resulting in forces between the wires. This force is given by:

$$\mathbf{F} = (I\mathbf{L} \times \mathbf{B})$$

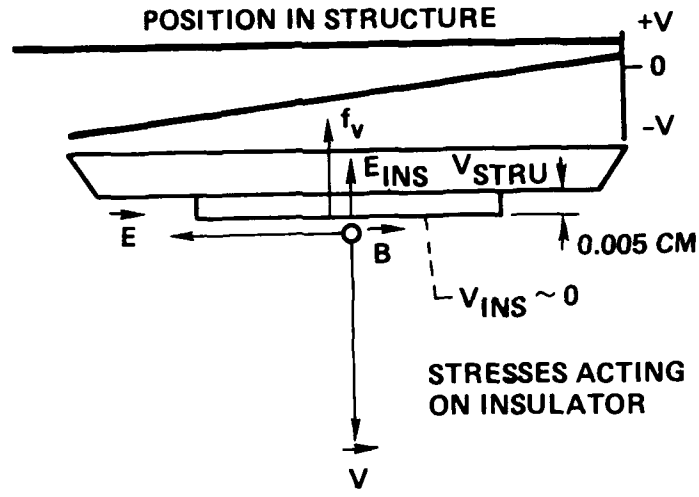

(A) Stresses Acting on a 0.005 cm Insulator

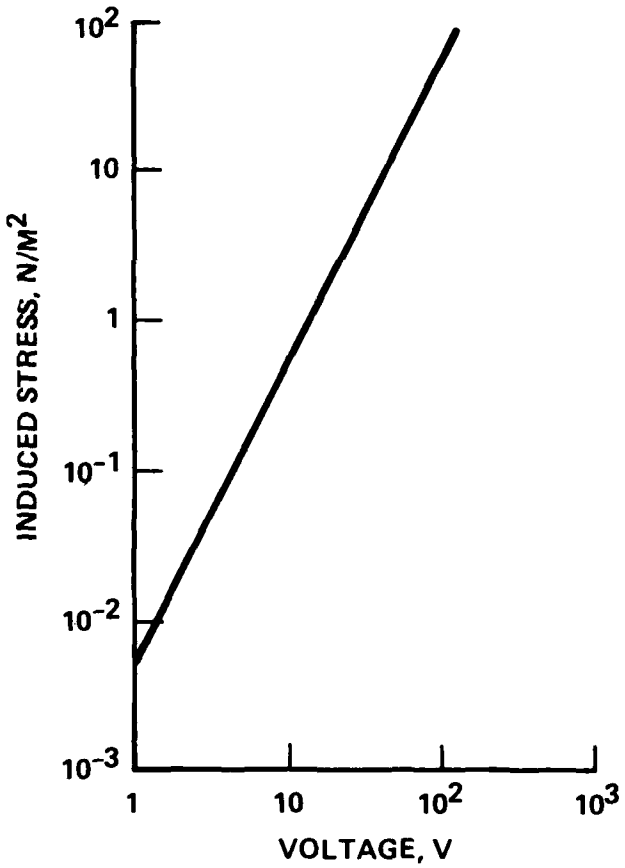

(B) Experimental Results

Figure 9.3 Induced Stress vs Applied Voltage

where **F** is the force vector in newtons, I is the circulating current in amperes, **B** is the magnetic field vector in tesla, and **L** is the wire length vector in meters.

In pairs of wires on spacecraft, the current flows in opposite directions, neutralizing the self-generated magnetic field while attempting to force the wires apart. Present spacecraft power system currents are relatively low (on the order of amps, resulting in forces of about 0.1 mN). Future systems can have currents of hundreds of amperes over lengths of tens of meters. Thus, separation forces (up to 50 mN) must be compensated for during mechanical design.

It is possible for a high current flow to produce a drag force on the spacecraft, under certain current flow and Earth's magnetic field orientations. Normally, wires on spacecraft run in pairs to minimize generation of magnetic fields. However, the use of the structure as a power return in a future, large, high-powered satellites could create significant drag effects. Currents on the order of hundreds of amperes can also make the drag force significant.

9.2.3 Configuration Generated Torques

Currents flowing in loops around large spacecraft can interact with the Earth's magnetic field, producing disturbance torques, and effecting spacecraft attitude [299]. The relationships governing configuration generated torques are:

$$\mathbf{T} = \boldsymbol{m} \times \mathbf{B} \quad \text{and} \quad \boldsymbol{m} = \mathbf{I} \times \mathbf{A}$$

where **T** is the torque (N · m), **m** is the magnetic moment (A-m^2), **B** is the magnetic field vector (tesla or T), **I** is the circulating current vector (amperes or A), and **A** is the loop area vector (m^2). Magnetic materials, such as latching magnets in relays and propellant valves, and motor magnets, also have a dipole moment that can generate torques.

This interaction can be illustrated by considering the solar array shown in Figure 9.4. The array is assumed to be arranged in 26 parallel strings with each string operating at about 2 amperes and 160 volts (this is the nominal NASA Space Station array design). The strings are assumed to be arranged such that self-generated magnetic fields from adjacent strings cancel. However, the overall string current flow can be considered to be a loop which can interact with the Earth's magnetic field producing a torque. The torque is small ($\approx 6 \times 10^{-6}$ N · m) but can affect spacecraft attitude.

9.3 RESEARCH MATURITY RATING

These interactions are well represented by basic electromagnetic field principles and are well understood both analytically and experimentally. Although their maturity was rated COMPLETE (5), evaluation of their effects on future space systems is needed.

9.4 SYSTEM IMPACT RATING

These interactions can be significant in both LEO and PEO. For these orbits, the

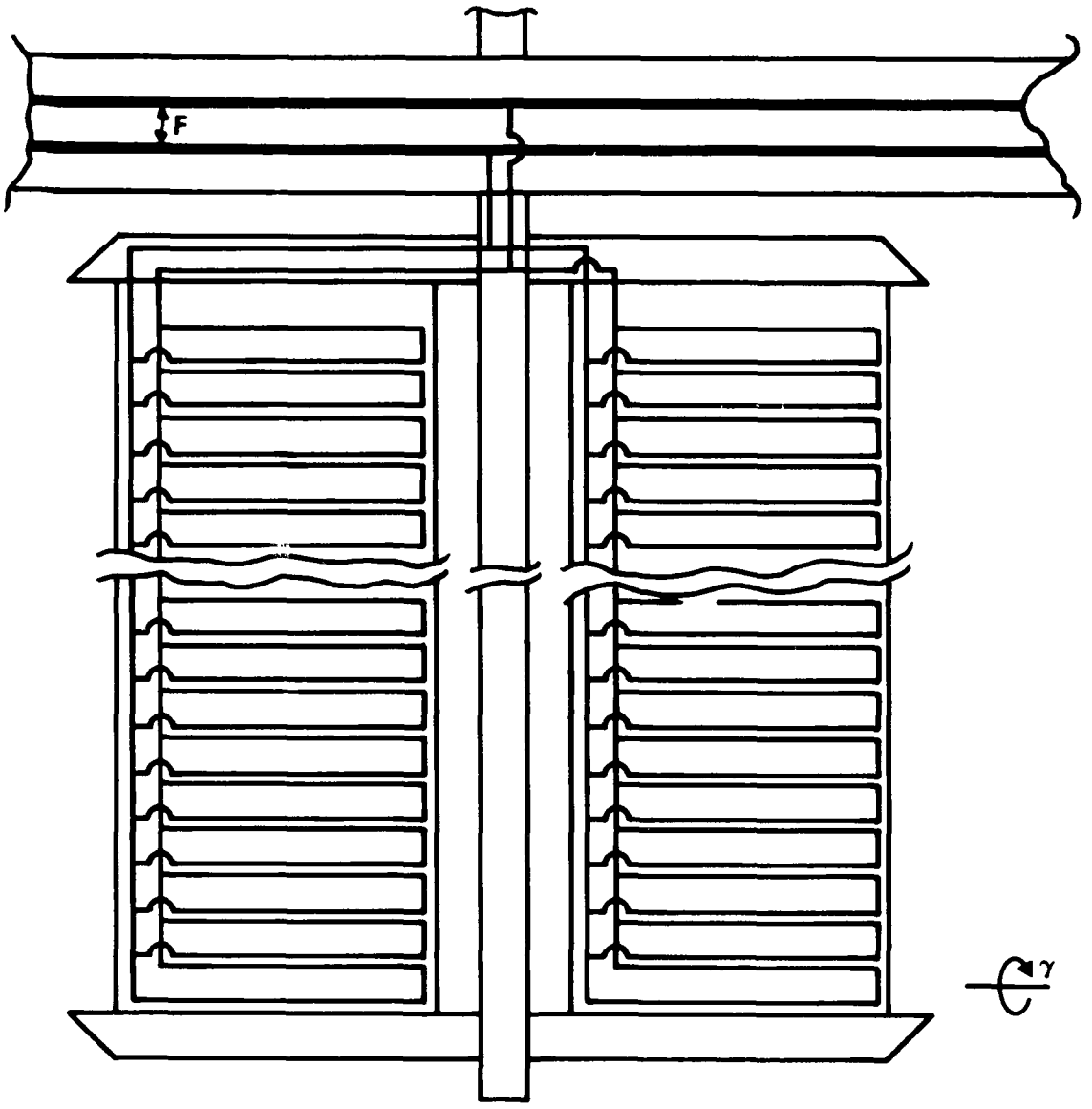

Figure 9.4 Motion and Current Induced Effects in a Solar Array Power Source

system impact was rated LARGE (4), primarily due to the number of small forces and torques that have been identified. These small forces must be recognized, since they could become significant in the design of future, large spacecraft. In GEO, the magnitude of the magnetic field is much less than in PEO or LEO, thus, the impact was rated NEGLIGIBLE (1).

9.5 MITIGATION TECHNIQUES

The effects of these interactions can be avoided by proper consideration during spacecraft design [300]. Structures may have to be strengthened where forces can not be avoided. Since this may involve additional weight, system trade-offs must be conducted to minimize the effect, while simultaneously minimizing the added weight.

10.0 CONCLUDING REMARKS

This Environmental Interactions Technology Status report has attempted to fill the pressing need for a comprehensive survey of the natural hazards which future, large, high-powered Air Force spacecraft will encounter. It is crucial that all potential hazards be recognized early in the design phase to prevent some neglected adverse interaction from compromising spacecraft operations or prematurely ending the mission.

The objective of this report was to assemble and catalog the available information on the environmentally induced interactions that could influence future spacecraft designs. This was accomplished through literature surveys and discussions with people knowledgeable in this field.

The environmentally induced interactions were divided into seven environment categories: (1) Low Energy Plasmas (Particle Energy < 100 KeV), (2) High Energy Radiation (Particle Energy > 100 KeV), (3) Neutral (Non-Charged) Particles, (4) Particle (Meteoroid and Debris) Impacts, (5) Solar Optical Radiation (Degradation and Forces), (6) Self-Generated (Contamination Sources), and (7) Electromagnetic (Magnetic Field Interactions).

The list of seventy-five interactions initially assembled was condensed to 24 topics. These topics, ranging from spacecraft charging to electromagnetically induced stresses, were rated for research maturity and for their potential impact on system performance in typical operational orbits (LEO, PEO, and GEO).

The maturity and impact ratings (on scales of 1 to 5 with 5 representing either the most mature technology or most serious impact) of the interactions were summarized in Table 1.1. These interactions all represent MODERATE to CATASTROPHIC system impacts while having SLIGHT to CONSIDERABLE maturity. The interactions with a SLIGHT to MODERATE maturity rating merit further study. Two interactions in the self-generated environment category have dual system impact ratings. The lower number represents the impact of the interaction on systems in general, while the larger number represents the impact on a specific system (e.g. sensors).

Several interactions were identified that could seriously impact the operation of future, high-power satellite systems. Interactions with an uncertain system impact, due to insufficient information, were also identified. Finally, several interactions, initially thought to have more serious effects, were downgraded to lower impact ratings.

11.0 REFERENCES

11.1 INTRODUCTION (Section 2.0)

1. Elkman, W.R., et al., "Electrostatic Charging and Radiation Shielding Design Philosophy for Hughes Satellites", AIAA No. 82-0116, Aerospace Sciences Conference, Orlando, Florida, January 1982.

2. McPherson, D.A. and W.R. Schober, "Spacecraft Charging at High Altitudes: The SCATHA Satellite Program", Spacecraft Charging by Magnetospheric Plasmas, A. Rosen, ed., Progress in Astronautics and Aeronautics, Vol. 47, AIAA, NY, 1975, pp. 15-30.

3. Binder, D., E.C. Smith, and A. Holman, "Satellite Anomalies from Galactic Cosmic Rays", *IEEE Transactions on Nuclear Science*, Vol NS-22, No. 6, December 1975, pp. 2675-2680.

4. Allen, J.H., "Satellite Anomalies and Solar Terrestrial Activity", *Proceedings Spacecraft Anomalies Conference*, V.G. Patterson and J.S. Schleher, eds., Colorado Springs, Colorado, October 30-31, 1984, U.S. Department of Commerce, pp. 69-93.

11.2 PLASMA ENVIRONMENT INTERACTIONS (Section 3.0)

5. Handbook of Geophysics and the Space Environment, A.S. Jursa, ed., Air Force Geophysics Laboratory, Hanscom AFB, MA, 1985.

6. "Space and Planetary Environment Criteria Guidelines for Use in Space Vehicle Development", 1982 Revision, Vol. 1, R.E. Smith and G.S. West, eds, NASA TM-82478, January 1983.

7. Introduction to Space Science, W.N. Hess, ed, Gordon and Breach, N.Y., 1964.

8. Roederer, J.G., "The Earth's Magnetosphere", *Science*, Vol 183, No. 37, 1974.

9. DeForest, S.E., "The Plasma Environment at Geosynchronous Orbit", *Proceedings of the Spacecraft Charging Technology Conference*, C.P. Pike and R.R. Lovell, eds., AFGL-TR-77-0051/NASA TMX-73537, ADA 045459, 1977, pp. 37-52.

10. Garrett, H.B. and G.C. Spitale, "Magnetospheric Plasma Modeling (0-100 keV)", *Journal of Spacecraft and Rockets*, Vol. 22, No. 3, May-June, 1985, pp. 231-244.

11. Mullen, E.G. and M.S. Gussenhoven, "SCATHA Environmental Atlas", AFGL-TR-83-0002, ADA 131456, 1983.

12. Gussenhoven, M.S. and E.G. Mullen, "A 'Worst Case' Spacecraft Charging Environment as Observed by SCATHA on 24 April 1979", AIAA Paper

82-0271, Aerospace Sciences Conference, Orlando, Florida, January 1982.

13. Johnson, R.G., "Review of Hot Plasma Composition Near Geosynchronous Altitude", *Spacecraft Charging Technology - 1980*, NASA CP-2182/ AFGL-TR-81-0270, ADA 114426, 1981, pp. 412-432.

14. Garrett, H.B., D.C. Schwank, and S.E. DeForest, "A Statistical Analysis of the Low-Energy Geosynchronous Plasma Environment - 1 Electrons", *Planet Space Science*, Vol. 29, October 1981, pp. 1021-1044.

15. Garrett, H.B., "Review of Quantitative Models of the 0 to 100 keV Near-Earth Plasma", *Review of Geophysics and Space Physics*, Vol. 17, No. 3, 1979, pp. 397-417.

16. DeForest, S.E., "Spacecraft Charging at Synchronous Orbit", *Journal of Geophysical Research*, Vol. 77, February 1, 1972, pp. 651-659.

17. DeForest, S.E. and C.E. McIlwain, "Plasma Clouds in the Magnetosphere", *Journal of Geophysical Research*, Vol. 76, June 1, 1971, pp. 3587-3611.

18. Purvis, C.K., et. al., "Design Guidelines for Assessing and Controlling Spacecraft Charging Effects", NASA TP-2361, September 1984.

19. Spacecraft Charging by Magnetospheric Plasma, A. Rosen, ed., Progress in Astronautics and Aeronautics, Vol. 47, AIAA, NY 1975.

20. Space Systems and Their Interactions with Earth's Space Environment, H.B. Garrett and C.P. Pike, eds., Progress in Astronautics and Aeronautics, Vol. 71, AIAA, NY, 1980.

21. Vampola, A.L., et. al., "The Aerospace Spacecraft Charging Document", The Aerospace Corp. Space Sciences Laboratory Report SSL-84(4940-05)-3, May 1984.

22. *Proceedings of the Spacecraft Charging Technology Conference*, C.P. Pike and R.R. Lovell, eds., AFGL-TR-77-0051/NASA TMX-73537, ADA 045459, 1977.

23. *Spacecraft Charging Technology - 1978*, NASA CP-2071/AFGL-TR-79-0082, ADA 084626, 1979.

24. *Spacecraft Charging Technology - 1980*, NASA CP-2182/AFGL-TR-81-0270, ADA 114426, 1981.

25. *Spacecraft Environmental Interactions Technology-1983*, NASA CP-2359/AFGL-TR-85-0018, 1985.

26. Stevens, N.J., R.R Lovell, and J.V. Gore, "Spacecraft-Charging Investigation for

the CTS Project", Spacecraft Charging by Magnetospheric Plasmas, op. cit., pp. 277-288.

27. Stevens, N.J., et. al., "Testing of Typical Spacecraft Materials in a Simulated Substorm Environment", *Proceedings of the Spacecraft Charging Conference*, op. cit., pp. 431-457.

28. Reddy, J. and B.E. Serene, "Effects of Electron Irradiation on Large Insulating Surfaces Used for European Communications Satellites", *Spacecraft Charging Technology - 1978*, op. cit., pp. 570-586.

29. Leung, M.S. and H.K.A. Kan, "Laboratory Study of the Charging of Spacecraft Materials", *Journal of Spacecraft and Rockets*, Vol. 18, No. 6, 1981, p. 510.

30. Staskus, J.V. and J.C. Roche, "Testing of a Spacecraft Model in a Combined Environment Simulator", NASA TM-82723, 1981.

31. DeForest, S.E. and R. Goldstein, "A Study of Electrostatic Charging of ATS-5 During Ion Thruster Operation", NASA CR-145910, (Jet Propulsion Lab., NASA Contract NAS7-100), 1973.

32. Purvis, C.K., R.O. Bartlett, and S.E. DeForest, "Active Control of Spacecraft Charging on ATS-5 and ATS-6", *Proceedings of the Spacecraft Charging Technology Conference*, op. cit., pp. 107-120.

33. Olsen, R.C., "Operation of the ATS-6 Ion Engine and Plasma Bridge Neutralizer at Geosynchronous Altitude", AIAA Paper 78-663, April 1978.

34. Durrett, J.C. and J.R. Stevens, "Description of the Space Test Program P78-2 Spacecraft and Payloads", *Spacecraft Charging Technology - 1978*, op. cit., pp. 4-10.

35. Whipple, E.C., Jr., "The Equilibrium Electric Potential of a Body in the Upper Atmosphere and in Interplanetary Space", NASA TMX-55368, 1965.

36. Purvis, C.K., N.J. Stevens, and J.C. Olgebay, "Charging Characteristics of Materials: Comparison of Experimental Results with Simple Analytical Models", *Proceedings of Spacecraft Charging Technology Conference*, op. cit., pp. 459-486.

37. Garrett, H.B., "Spacecraft Charging: A Review", Space Systems and Their Interactions with Earth's Space Environment, op. cit., pp. 167-226.

38. Garrett, H.B., "The Charging of Spacecraft Surfaces", *Review of Geophysics and Space Physics*, Vol. 19, November 1981, pp. 577-616.

39. Grard, R.J.L., K. Knott, and A. Pedersen, "Influence of Photoelectron and

Secondary Emission on Electric Field Measurements in the Magnetosphere and Solar Wind", Photon and Particle Interactions with Surfaces in Space, R.J.L. Grard ed., D. Reidel Publishing Co., pp. 163-189.

40. Purvis, C.K., "Configuration Effects on Satellite Charging Response", AIAA Paper 80-0040, January 1980.

41. Olsen, R.C., and C.K. Purvis, "Observations of Charging Dynamics of Spacecraft", *Journal of Geophysical Research*, Vol. 86, August 1, 1981, pp. 6809-6819.

42. Katz, I., et. al., "NASCAP, A Three Dimensional Charging Analyzer Program for Complex Spacecraft", *IEEE Transactions on Nuclear Science*, Vol. NS-24, December 1977, pp. 2276-2280.

43. Katz, I., et. al., "A Three Dimensional Dynamic Study of Electrostatic Charging in Materials", NASA CR-135256, (Systems, Science and Software SSS-R-77-3367, NASA Contract NAS3-20119), 1977.

44. Katz, I., et. al., "Extension, Validation and Application of the NASCAP Code", NASA CR-159595, (Systems, Science and Software SSS-R-79-3904, NASA Contract NAS3-21050), 1979.

45. Katz, I., et. al., "The Capabilities of the NASA Charging Analyzer Program", *Spacecraft Charging Technology - 1978*, op. cit., pp. 101-122.

46. Katz, I., et. al., "Application of the NASCAP Code - Volume 1: NASCAP Extension", NASA CR-165349 (Systems, Science and Software SSS-R-81-4847 Vol. 1, NASA Contract NAS3-21762), 1981.

47. Rubin, A.G. et. al., "A Three-Dimensional Spacecraft Charging Computer Code", Space Systems and Their Interactions with Earth's Space Environment, op. cit., pp. 318-336.

48. Katz, I., et. al., "NASCAP Simulations of Spacecraft Charging of the SCATHA Satellite", Spacecraft/Plasma Interactions and Their Influence on Field and Particle Measurements, A. Pedersen, D. Guyenne and J. Junt, eds., European Space Agency, 1983, p. 109-114.

49. Viswanathan, R., G. Barbay, and N.J. Stevens, "Environmentally Induced Discharge Transient Coupling to Spacecraft", NASA CR-174922, (Hughes Aircraft Co., NASA Contract NAS3-23869), May 1985.

50. Olsen, R.C., "A Threshold Effect for Spacecraft Charging", *Journal Geophysical Research*, Vol. 88, January 1, 1983, pp. 493-499.

51. Stevens, N.J., "Analytical Modeling of Satellites in Geosynchronous Environment", *Spacecraft Charging Technology - 1980*, op. cit., pp. 717-729.

52. Feuerbacher, B. and B. Fitton, "Experimental Investigation of Photoemission from Satellite Surface Materials", *Journal of Applied Physics*, Vol. 43, No. 4, April 1972, pp. 1563-1572.

53. Garrett, H.B. and S.E. DeForest, "Time-Varying Photoelectron Flux Effects on Spacecraft Potentials at Geosynchronous Orbit", *Journal Geophysical Research*, Vol. 84, May 1, 1979, pp. 2083-2088.

54. Yang, K., W.L. Gordon, and R.W. Hoffman, "Electron Yields from Spacecraft Materials", *Spacecraft Environmental Interactions Technology - 1983*, op. cit., pp. 537-546.

55. Rubin, A.G., P.L. Rothwell, and G.K. Yates, "Reduction of Spacecraft Charging Using Highly Emissive Surface Materials", Effects of the Ionosphere on Spacecraft and Terrestrial Systems, J.M. Goodman, ed., U.S. Government Printing Office, 1978, pp. 313-316.

56. Balmain, K.G., M. Cuchanski, and P.C. Kremer, "Surface Micro-Discharges on Spacecraft Dielectrics", *Proceedings of the Spacecraft Charging Technology Conference*, op. cit., pp. 519-526.

57. Stevens, N.J. and J.C. Roche, "NASCAP Modeling of Environmental-Induced Discharges in Satellites", NASA TM-79247, 1979.

58. Balmain, K.G., "Surface Discharge Effects", Space Systems and Their Interactions with Earth's Space Environment, op. cit., pp. 276-298.

59. Inouye, G.T. and J.M. Sellen, Jr., "TDRSS Solar Array Arc Discharge Tests", *Spacecraft Charging Technology - 1978*, op. cit., pp. 834-852.

60. Inouye, G.T., et. al., "Thermal Blanket Metallic Film Groundstrap and Second Surface Mirror Vulnerability to Arc Discharges", *Spacecraft Charging Technology - 1978*, op. cit., pp. 657-681.

61. Aron, P.R. and J.V. Staskus, "Area Scaling Investigations of Charging Phenomena", *Spacecraft Charging Technology - 1978*, op. cit., pp. 457-484.

62. Balmain, K.G., "Scaling Laws and Edge Effects for Polymer Surface Discharges", *Spacecraft Charging Technology - 1978*, op. cit., pp. 646-656.

63. Stevens, N.J., H.E. Mills, and L. Orange, "Voltage Gradients in Solar Array Cavities as a Possible Site in Spacecraft-Charging-Induced Discharges", *IEEE Transactions on Nuclear Science*, Vol. NS-28, No. 6, December 1981, pp. 4558-4562.

64. Inouye, G.T. and R.C. Chaky, "Enhanced Electron Emission from Positive Dielectric/Negative Metal Configurations on Spacecraft", *IEEE Transactions on*

Nuclear Science, Vol. NS-29, No. 6, December 1982, pp. 1589-1593.

65. Sanders, N.L. and G.T. Inouye, "Voyager Spacecraft Charging Model Calculations", Effect of the Ionosphere on Space and Terrestrial Systems, op. cit., pp. 285-292.

66. Woods, A.J., et. al., "Model of Coupling of Discharges into Spacecraft Structures", *Spacecraft Charging Technology - 1980*, op. cit., pp. 745-754.

67. Woods, A.J. and E.P. Wenaas, "Spacecraft Discharge Electromagnetic Interference Coupling Models (Survey)", *Journal of Spacecraft and Rockets*, Vol. 22, No. 3, May-June 1985, pp. 265-281.

68. Leung, P., et al., "Environment-Induced Electrostatic Discharges as the Cause of Voyager 1 Power-On Resets", *Journal of Spacecraft and Rockets*, Vol. 23, No. 3, May-June 1986, pp. 323-330.

69. Whittlesey, A.C., "Voyager Electrostatic Discharge Protection Program", *Proceedings of International Symposium on Electromagnetic Compatibility*, IEEE, 1978, pp. 377-383.

70. Whittlesey, A.C. and G.T. Inouye, "Voyager Spacecraft Electrostatic Discharge Testing", *Journal of Environmental Science*, Vol. 23, March-April 1980, pp. 29-33.

71. Cauffman, D.P. and R.R. Shaw, "Transient Currents Generated by Electrical Discharges", Space Science Instrumentation, Vol. 1, 1975, pp. 125-137.

72. Alliot, J.C., "Electromagnetic Coupling Between Environmental Induced Discharges and Internal Cabling", *Proceedings of Space Environment Technology Workshop*, Toulouse, France, April 14-25, 1986. (To be Published)

73. Spearman, K.R., "DSP Experience with Spacecraft Charging", *Proceedings of Spacecraft Anomalies Conference*, op. cit., 1984, pp. 110.

74. Frederickson, A.R., "Discharge Pulse Phenomenology", *Spacecraft Environmental Interactions Technology - 1983*, op. cit., pp. 483-510.

75. Coakley, P., et. al., "Discharge Characteristics of Dielectric Materials Examined in Mono-, Dual-, and Spectral Energy Electron Charging Experiments", ibid, pp. 511-524.

76. Pine, Y.W., B.L. Beers, and S.T. Ives, "Dielectric Charging in Space: Ground Test Data and Model Verification", *IEEE Transactions on Nuclear Science*, Vol. NS-30, No. 6, December 1983, pp. 4290-4295.

77. Frederickson, A.R. and A.L. Chesley, "Charging/Discharging of Space Shuttle Tile

Material Under Irradiation", ibid, pp. 4296-4301.

78. Grossland, M. and K.G. Balmain, "Incident Ion Effects on Polymer Surface Discharges", ibid, pp. 4302-4306.

79. Coakley, P., B. Kitterer, and M. Treadaway, "Charging and Discharging Characteristics of Dielectric Materials Exposed to Low-and Mid-Energy Electrons", *IEEE Transactions on Nuclear Science*, Vol. NS-29, No. 6, December 1982, pp. 1639-1643.

80. Passenheim, B.C., et. al., "Electrical Conductivity and Discharge in Spacecraft Thermal Control Dielectrics", ibid, pp. 1594-1600.

81. Beers, B.L., V.W. Pine, and S.T. Ives, "Internal Breakdown of Charged Spacecraft Dielectrics", *IEEE Transactions on Nuclear Science*, Vol. NS-28, No. 6, December 1981, pp. 4529-4534.

82. Frederickson, A.R., "Radiation Induced Dielectric Charging", Space Systems and Their Interactions with Earth's Space Environment, op. cit., pp. 386-412.

83. Meulenberg, A., Jr., "Evidence for a New Discharge Mechanism for Dielectrics in a Plasma", Spacecraft Charging by Magnetospheric Plasmas, op. cit., pp. 237-246.

84. Beers, B.L., et. al., "First Principles Numerical Model of Avalanche-Induced Arc Discharges in Electron-Irradiated Dielectrics", NASA CR-159560 (SAI-102-79-002, NASA Contract NAS3-21378), March 1979.

85. Beers, B.L., V.W. Pine, and S.T. Ives, "Continued Development of a Detailed Model of Arc Discharge Dynamics", NASA CR-167977 (Beers Associates, 1-82-16-23, NASA Contract NAS3-22530), December, 1982.

86. Cohen, H.A., et. al., "A Comparison of Three Techniques of Discharging Satellites", *Spacecraft Charging Technology - 1980*, op. cit., pp. 888-893.

87. Shuman, B.M. and H.A. Cohen, "Automatic Charge Control System for Satellites", *Spacecraft Environmental Interactions Technology - 1983*, op. cit., pp. 477-482.

88. Birkeland, K., "The Norwegian Aurora Polaris Expedition 1902-1903", Vol. 1, Section 1, H. Aschehoug, Christiania, Norway, 1908.

89. Bostrom, R., "A Model of the Auroral Electrojets", *Journal of Geophysical Research*, Vol. 69, 1964, pp. 4983ff.

90. Whalen, B.A. and I.B. McDiarmid, "Observation of Magnetic-Field-Aligned Auroral-Electron Precipitation", *Journal of Geophysical Research*, Vol. 77, No. 1, 1972, pp. 191ff.

91. Tanskanen, P.J., et. al., "Spectral Characteristics of Precipitating Electrons Associated with Visible Aurora in the Pre-Midnight Oval During Periods of Substorm Activity", *Journal of Geophysical Research*, Vol. 86, No. A3, 1981, pp. 1379ff.

92. Schwann, B.M., et. al., "Field-Aligned Current, Convective Electric Field, and Auroral Particle Measurements During a Major Magnetic Storm", *Journal of Geophysical Research*, Vol. 86, No. A3, 1981, pp. 5561ff.

93. Akasofu, S.L. and J.R. Kan, "Physics of Auroral Arc Formation", Geophysical Monograph 25, AGU, 1981.

94. Hall, W.N., "Astronaut Hazard During Free-Flight Polar EVA", *Spacecraft Environmental Interactions Technology - 1983*, op. cit., pp. 663-674.

95. Hardy, D.A., et. al., "Average and Worst-Case Specifications of Precipitating Auroral Electron Environment", ibid, pp. 131-154.

96. Gussenhoven, M.S., et. al., "High-Level Spacecraft Charging in Low Altitude Polar Auroral Environment", *Journal of Geophysical Research*, Vol. 90, No. A11, 1985., pp. 11,009ff.

97. Hardy, D.A., M.S. Gussenhoven, and Y-C Yeh, "Spacecraft Hazards in the Low Altitude Polar-Space Environment", AIAA Paper 86-0517, Aerospace Sciences Meeting, Reno, NV, January 1986.

98. Burke, W.J., et. al., "Direct Measurements of Severe Spacecraft Charging in Auroral Ionopshere", *Spacecraft Environmental Interactions Technology - 1983*, op. cit., pp. 109-124.

99. Besse, A.L., A.G. Rubin, and D.A. Hardy, "Charging of DMSP/F6 Spacecraft in Aurora on 10 January 1983", ibid., pp. 125-130.

100. Parks, D.E. and I. Katz, "Charging of a Large Object in Low Polar Earth Orbit", *Spacecraft Charging Technology - 1980*, op. cit., pp. 979-989.

101. Cooke, D.L., et. al., "Three-Dimensional Calculation of Shuttle Charging in Polar Orbit", *Spacecraft Environmental Interactions Technology - 1983*, op. cit., pp. 205-228.

102. Katz, I., et. al., "Polar Orbit Electrostatic Charging of O[illegible] .n Shuttle Wake", ibid, pp. 229-234.

103. Parker, L.W., "Wakes and Differential Charging of Large Bodies in Low Earth Orbit", ibid, pp. 235-252.

104. Parks, D.E. and I. Katz, "Electric Field Effects on Ion Currents in Shuttle Wakes",

ibid, pp. 195-204.

105. Katz, I., et. al., "Astronaut Charging in the Wake of a Polar Orbiting Shuttle", AIAA Paper 85-7035-CP, Shuttle Environment and Operations II Conference, Houston, TX, November 13-15, 1985.

106. Hall, W.N., et. al., "Shuttle and Astronaut Charging in Polar Orbit", AIAA Paper 86-0519, Aerospace Sciences Conference, Reno, NV, January 1986.

107. Hall, W.N., et. al., "Polar-Auroral Charging of the Space Shuttle and EVA Astronaut", Paper presented at the AGARD/NATO Conference, The Hague, Holland, June 1986.

108. Cole, R.K., H.S. Ogawa, and J.M. Sellen, Jr., "Operation of Solar Cell Arrays in Dilute Streaming Plasmas", NASA CR-72376, (TRW Systems, TRW 09357-6006-R000), March 1968.

109. Knauer, W., et. al., "High Voltage Solar Array Study", NASA CR-72675, 1970.

110. Herron, B.G., J.R. Bayless, and J.D. Worden, "High Voltage Solar Array Technology", AIAA Paper 72-443, April 1972.

111. Stevens, N.J., "Solar Array Experiments on the SPHINX Satellite", NASA TMX-71458, 1973.

112. Kennerud, K.L., "High Voltage Solar Array Experiments", NASA CR-121280, 1974.

113. Domitz, S. and N.T. Grier, "The Interaction of Spacecraft High Voltage Power Systems with the Space Plasma Environment", Power Electronics Specialists Conference, IEEE, NJ, 1974, pp. 62-69.

114. Stevens, N.J., et al., "Investigation of High Voltage Spacecraft System Interactions with Plasma Environments", AIAA Paper 78-672, April 1978.

115. McCoy, J.E. and A. Konradi, "Sheath Effects Observed On a 10-Meter High Voltage Panel in Simulated Low Earth Orbit Plasmas", *Spacecraft Charging Technology - 1978*, op. cit., pp. 315-340.

116. Stevens, N.J., "Interactions Between Spacecraft and the Charged Particle Environment", *Spacecraft Charging Technology - 1978*, op. cit., pp. 268-294.

117. Bebermeir, H., et. al., "Technology of Elevated Voltage Solar Arrays-Key Items Test and Evaluation", Final Report for ESA under ESTEC Contract 3662/78/NL/HP, AEG-Telefunken, West Germany.

118. Grier, N.T., "Experimental Results on Plasma Interactions with Large Surfaces at

High Voltages", NASA TM-81423, January 1980.

119. McCoy, J.E. and D.T. Martucci, "Experimental Plasma Leakage Currents to Insulated and Uninsulated 10 M^2 High Voltage Panels", *Spacecraft Charging Technology - 1980*, op. cit., p. 931.

120. Stevens, N.J., "Space Environmental Interactions with Biased Surfaces", Space Systems and Their Interaction with Earth's Space Environment, op. cit., pp. 455-476.

121. Stevens, N.J., "Interactions Between Large Space Power Systems and Low Earth-Orbit Plasmas", *Spacecraft Environmental Interactions Technology - 1983*, op. cit., pp. 263-276.

122. Purvis, C.K., N.J. Stevens, and F.D. Berkopec, "Interaction of Large, High Power Systems with Operational Orbit Charged-Particle Environments", NASA TMX-73867, 1977.

123. Stevens, N.J., "Review of Biased Solar Array-Plasma Interaction Studies", NASA TM-82693, April 1981.

124. McKinzie, D.J., Jr. and N.T. Grier, "Dielectric Breakdown in a Dilute Plasma - A 20-Kilovolt Limited Study", NASA TMX-2444, January 1972.

125. Grier, N.T. and D.J. McKinzie, Jr., "Measured Current Drainage Through Holes in Various Dielectrics Up to 2 kV in a Dilute Plasma", NASA TND-6663, February 1972.

126. Grier, N.T. and S. Domitz, "Current From a Dilute Plasma Measured Through Holes in Insulators", NASA TND-8111, December 1975.

127. Grier, N.T. and N.J. Stevens, "Plasma Interaction Experiment (PIX) Satellite Results", *Spacecraft Charging Technology - 1978*, op. cit., pp. 295-314.

128. Purvis, C.K., "The PIX-II Experiment: An Overview", *Spacecraft Environmental Interactions Technology - 1983*, op. cit., 1985, pp. 321-332.

129. Grier, N.T., "Plasma Interaction Experiment II (PIX II): Laboratory and Flight Results", ibid, pp. 333-348.

130. Ferguson, D.C., "Ram/Wake Effects on Plasma Current Collection of the PIX-II Langmuir Probe", ibid, pp. 349-358.

131. Stevens, N.J "Summary of PIX-2 Flight Results Over the First Orbit", AIAA paper 86-0360, Aerospace Sciences Conference, Reno, NV, January 1986.

132. Stevens, N.J., "High Voltage Solar Array Models and Shuttle Tile Charging",

Proceedings of the Air Force Geophysics Laboratory Workshop on Natural Charging of Large Space Structures in Near Earth Polar Orbit: 14-15 September 1982, R.C. Sagalyn, D.E. Donatelli, and I. Michael, eds., AFGL TR-83-0046, January 1983, ADA 134894, pp. 333-336.

133. Mandell, M.J., et. al., "Computer Simulation of Plasma Electron Collection by PIX-II", AIAA paper 85-0386, Aerospace Sciences Conference, Reno, NV, January 1985.

134. Roche, J.C., "NASCAP Simulation of PIX-II Experiments", *Spacecraft Environmental Interactions Technology - 1983*, op. cit., pp. 359-366.

135. Cooke, D., L.W. Parker, and J.E. McCoy, "Three-Dimensional Space Charge Model for Large High-Voltage Satellites", *Spacecraft Charging Technology - 1980*, op. cit., pp. 957-978.

136. Stevens, N.J., et. al., "High Voltage Solar Array Performance in Low Earth Orbit Plasma Environments", Final Report on Contract NAS3-24659. (To Be Published)

137. Stillwell, R.P. and N.J. Stevens, "Plasma Interactions with Biased Concentrator Solar Cells", Paper E-5, IEEE 23rd Annual Conference on Nuclear and Space Radiation Effects, Providence RI, July 21-23, 1986.

138. Snyder, D.B., "Discharges on a Negatively Biased Solar Cell Array in a Charged-Particle Environment", *Spacecraft Environmental Interactions Technology - 1983*, op. cit., pp. 379-388.

139. Miller, W.L., "An Investigation of Arc Discharging on Negatively Biased Dielectric-Conductor Samples in a Plasma", ibid, pp. 367-378.

140. Leung, P., "Characterization of EMI Generated by the Discharge of VOLT Solar Array", JPL Report D-2644, September 1985.

141. Jongeward, G.A., et. al., "The Role of Unneutralized Surface Ions in Negative Potential Arcing", *IEEE Transactions on Nuclear Science*, Vol. 6, December 1985, pp. 4087-4091.

142. Snyder, D.B., "Discharge Mechanisms in Solar Arrays - Experiment", AIAA Paper 86-0363, Aerospace Sciences Meeting, Reno, NV, January 1986.

143. Ferguson, D.C, "The Voltage Threshold for Arcing for Solar Cells in LEO-Flights and Ground Test Results", NASA TM-87259, March 1986.

144. Stevens, N.J., "Environmentally-Induced Voltage Limitations in Large Space Power Systems", *IEEE Transactions on Nuclear Science*, Vol. NS-31, No. 6, December 1984, pp. 381-386.

145. Chaky, R.C. and G.T. Inouye, "Characteristics of EMI Generated by Negative Metal/Positive Dielectric Voltage Stresses Due to Spacecraft Charging", *Spacecraft Environmental Interaction Technology - 1983*, op. cit., pp. 437-452.

146. Underwood, C.S. and S.R. Strader, "Impact of Micro-Discharges on Solar Array Power Generating Systems", AIAA Paper 86-0365, Aerospace Sciences Meeting, Reno, NV, January 1986.

147. Finke, R.C., et. al., "Power Management and Control for Space Systems", Future Orbital Power Systems Technology Requirements, NASA CP-2058, 1978, pp. 195-208.

148. Renz, D., et. al., "Design Considerations for Large Space Electric Power Systems", NASA TM-83064, April 1983.

Also see references: 1-4

11.3 HIGH ENERGY RADIATION ENVIRONMENT (Section 4.0)

149. Teague, M.J. and J.I. Vette, "The Use of Inner Zone Electron Model AE-5 and Associated Computer Programs", NSSDC 72-11, November 1982.

150. Teague, M.J. and J.I. Vette, "A Model of the Trapped Electron Population for Solar Minimum", NSSDC 74-03, April 1974.

151. Sawyer, D., and J.I. Vette, "AP-8 Trapped Proton Environment for Solar Maximum and Minimum", NSSDC/WDC-A-R and S 76-06, December 1976.

152. Stassinopoulos, E.G., "World Maps of Constant B, L, and Flux Contours", NASA-SP-3050, August 1969.

153. Cladis, J.B., G.T. Davidson, and L.L. Newkirk, "Trapped Radiation Handbook", Defense Nuclear Agency Report DNA-2524H, January 1977.

154. King, J.H. and E.G. Stassinopoulos, "Energetic Solar Proton Versus Terrestrially Trapped Proton Fluxes for the Active years 1977-83", NASA TMX-601-74-221, July 1974.

155. King, J.H., "Solar Proton Fluences for 1977-1983 Space Missions", *Journal of Spacecraft and Rockets*, Vol. 11, No. 6, June 1984, pp. 401-408.

156. Reagan, J.B., W.L. Imhof, and V.F. Moughan, "Characteristics of the August 1972 Solar Particle Events as Observed Over the Earth's Polar Caps", Collected Data Reports on August 1972 Solar-Terrestrial Events, Report UAG-Z8, Part III, July 1973, p. 676.

157. Meyer, P., R. Romaty, and W.R. Webber, "Cosmic Rays-Astronomy with

Energetic Particles", *Physics Today*, October 1974, pp. 23-32.

158. Adams, J.H., Jr., R. Silberberg, and C.H. Tsao, "Cosmic Ray Effects on Microelectronics-Part 1: The Near Earth Particle Environment", NRL Memorandum Report 4506, August 25, 1981.

159. Adams, J.H., Jr., J.R. Letaw, and D.F. Smart, "Cosmic Ray Effects on Microelectronics - Part II: The Geomagnetic Cutoff Effects", NRL Memorandum Report 5099, May 26, 1983.

160. Stassinopoulos, E.G., "SOLPRO: A Computer Code to Calculate Probabilistic Energetic Solar Proton Fluences", NSSDC 75-11, April 1975.

161. Seltzer, S., "SHIELDOSE: A Computer Code for Space-Shielding Radiation Dose Calculations", NBS Technical Note 1116, National Bureau of Standards, Washington DC, May 1980.

162. Vampola, A., "Radiation Effects on Space Systems and Their Modeling", Space Systems and Their Interactions with Earth's Space Environment, op. cit., pp. 339-348.

163. Price, W.E., et. al., "Total-Dose Radiation Effects Data for Semiconductor Devices", Vol. 1, NASA CR-164707, August 1981, Vol. 2, NASA CR-168428, December 1981.

164. Hill, C.W., "A Survey of Space Radiation Effects", NASA CR-161687, March 1980.

165. Gauthier, M.K. and D.K. Nichols, "SP-100 Power System: Semiconductor Radiation Review", Jet Propulsion Laboratory, JPL-D-836, July 1983.

166. Tada, H.Y. and J.R. Carter, "Solar Cell Radiation Handbook", Jet Propulsion Laboratory, JPL 77-56, November 1977.

167. Rahilly, W.P., "Radiation Effects on Solar Cells", Space Systems and Their Interactions with Earth's Space Environment, op. cit., pp. 365-385.

168. Fornes, R.E., J.D. Memory, and N. Naranong, "Effect of 1.33 MeV Gamma Radiation and 0.5 MeV Electrons on the Mechanical Properties of Graphite Fiber Composites", NASA CR-169117, 1982.

169. Tenney, D.R., G.F. Sykes, and D.E. Bowles, "Space Environmental Effects on Materials", NATO AGARD Specialists Meeting on Environmental Effects on Materials, Toronto, Canada, ADA 129847, March 1983.

170. Tennyson, R.C., B.A.W. Smith, and L.P. Hebert, "The Effect of Combined UV Radiation and High Energy Electrons on the Behavior of Polymer Matrix Composites in Hard Vacuum", ibid.

171. Mauri, R.E and F.W. Crossman, "Space Radiation Effects on Structural Composites", AIAA Paper 83-0591, Aerospace Sciences Conference, Reno, NV, January 1983.

172. Bowles, D.E., S.S. Tompkin, and G.F. Sykes, "Electron Radiation Effects on the Thermal Expansion of Graphite/Resin Composites", AIAA Paper 84-1704, 19th Thermophysics Conference, Snowmass, CO, June 1984.

173. Sykes, G.F. and W.S. Slemp, "Space Radiation Effects on an Elastomer-Toughened Epoxy-Graphite Composite", Presented at 30th National Symposium/Exhibition, Society for the Advancement of Materials and Process Engineering, Anaheim, CA, March 19-21, 1985.

174. Sykes, G.F., S.M. Milkovich, and C.T. Herakovich, "Simulated Space Radiation Effects on a Graphite Epoxy Composite", Presented at American Chemical Society Spring National Meeting, Miami Beach, FL, April 28-May 3, 1985.

175. Tompkins, S.S., G.T. Sykes, and D.T. Bowles, "The Thermal and Mechanical Stability of Composite Materials for Space Structures", Presented at IEEE/ASM/ASME/SME Space Technology Conference, Anaheim, CA, September 23-25, 1985.

176. Shapiro, P., et al., "Proton-Induced Single Event Upsets in NMOS Microprocessors", *IEEE Transactions on Nuclear Science*, Vol. NS-29, No. 6, December 1982, pp. 2072-2075.

177. Peterson, E.L., "Radiation Induced Soft Failures in Space Electronics", *IEEE Transactions on Nuclear Science*, Vol. NS-30, April 1983.

178. Soliman, K. and D.K. Nichols, "Latchup in CMOS Devices from Heavy Ions", *IEEE Transactions on Nuclear Science*, Vol. NS-30, No. 6, December 1983, pp. 4514-4519.

179. Bendel, W.L. and E.L. Peterson, "Proton Upsets in Orbit", ibid, pp. 4481-4485.

180. Adams, J.H., Jr., "The Variability of Single Event Upsets in the Natural Environment", ibid, pp. 4475-4480.

181. Peterson, E.L., "Single Event Upsets in Space", AIAA paper 83-0164, Aerospace Sciences Conference, Reno, NV, January 1984.

182. Chenette, D.L. and W.F. Dietrich, "The Solar Flare Heavy Ion Environment for Single-Event Upsets: A Summary of Observations Over the Last Solar Cycle, 1973-1983", *IEEE Transactions on Nuclear Science*, Vol. NS-31, December 1984, pp. 1217-1222.

183. Adams, J.H., Jr., and A. Gelman, "The Effect of Solar Flares on Single Event

Upset Rates", ibid, pp. 1212-1216.

184. Zoutendyk, J.A., C.J. Malone, and L.S. Smith, "Experimental Determination of Single Event Upsets (SEU) As A Function of Collected Charge in Bipolar Integrated Circuits", ibid, pp. 1167-1174.

185. Diehl-Nagle, S.E., "A New Class of Single Event Soft Errors", ibid, pp. 1145-1148.

186. Kreskovsky, J.P. and H.L. Grubin, "Simulation of Charge Collection in a Multilayer Device", *IEEE Transactions on Nuclear Science*, Vol. NS-32, No. 6, December 1985, pp. 4140-4144.

187. Hsueh, F.L. and L.S. Napoli, "CMOS/SOS High Soft-Error Threshold Memory Cell", ibid, pp. 4155-4158.

188. Giddings, A.E., et al., "Single Event Upset Immune Integrated Circuits for Project Galileo", ibid, pp. 4159-4163.

189. Letaw, J.R., et. al., "Geometric Considerations in Single Event Upset Estimation", ibid, pp. 4212-4215.

190. Nichols, D.K., W.E. Price, and C.J. Malone, "Single Event Upset (SEU) of Semiconductor Devices - A Summary of JPL Test Data", *IEEE Transactions on Nuclear Science*, Vol. NS-30, No. 6, December 1983, pp. 4520-4526.

191. Nichols, D.K., et. al., "A Summary of JPL Single Event Upset Test Data From May 1982 through January 1984", *IEEE Transactions on Nuclear Science*, Vol. NS-31, No. 6, December 1984, pp. 1186-1189.

192. Koga, R. and W.A. Kolasinski, "Heavy Ion-Induced Single Event Upsets of Modern Microcircuits: A Summary of Aerospace Test Data", ibid, pp. 1190-1195.

193. Hall, W.N. and N.J. Stevens, "Ionospheric Effects on Astronaut Extravehicular Activity Equipment", Proceedings of IES 84, A Symposium on the Effect of the Ionosphere on C^3I Systems, May 1984.

194. Todd, P., "Unique Biological Aspects of Radiation Hazards - An Overview", COSPAR Workshop and Topical Meeting on Life Sciences and Space Research, *Advances in Space Research*, Vol. 3, No. 8, 1983.

Also see references: 3, 6, 94, 106, 107

11.4 NEUTRAL ENVIRONMENT (Section 5.0)

195. Lyle, R. and P. Stahbekis, "Spacecraft Aerodynamic Torques", NASA SP-8058, January 1971.

196. Hansen, R., et. al., "Effect of Atomic Oxygen on Polymers", *Journal of Polymer Science*, Vol. 3A, 1965, pp. 2205ff.

197. Leger, L.J., "Oxygen Atom Reaction with Shuttle Materials at Orbital Altitudes" NASA TM-58246, May 1982.

198. Leger, L.J., "Oxygen Atom Reaction with Shuttle Materials at Orbital Altitudes - Data and Experiment Status", AIAA Paper 83-0073. Aerospace Sciences Conference, Reno, NV, January 1983.

199. Peters, P.N., R.C. Linton, and E.R. Miller, "Results of Apparent Atomic Oxygen Reactions on AG, C, and OS Exposed During the Shuttle STS-4 Orbits", *Geophysics Research Letters*, Vol. 10, 1983, pp. 569ff.

200. Ferguson, D.C. "Laboratory Studies of Kapton Degradation in an Oxygen Ion Beam", *Spacecraft Environmental Interactions Technology - 1983*, op. cit., pp. 81-90.

201. Leger, L.J., J.T. Visentine, and J.F. Kuminecz, "Low Earth Orbit Atomic Oxygen Effect on Surfaces", AIAA Paper 84-0548, Aerospace Sciences Conference, Reno, NV, January 1984.

202. Leger, L.J., J.T. Visentine, and J.A. Schliesing, "A Consideration of Atomic Oxygen Interactions with Space Station", AIAA Paper 85-0476, Aerospace Sciences Conference, Reno, NV, January 1985.

203. Whitaker, A.F., et. al., "Orbital Atomic Oxygen Effects on Thermal Control and Optical Materials - STS-8 Results", AIAA Paper 85-0416, ibid.

204. Arnold, G.S. and D.R. Peplinski, "Kinetics of Oxygen Interactions with Materials", AIAA Paper 85-0472, ibid.

205. Visentine, J.T, et. al., "STS-8 Atomic Oxygen Effects Experiment", AIAA Paper 85-0415, ibid.

206. Ferguson, D.C., "The Energy Dependence and Surface Morphology of Kapton Degradation Under Atomic Oxygen Bombardment", *Proceedings of 13th Space Simulation Conference*, NASA Goddard Space Flight Center, October 1984, pp. 205-221.

207. Arnold, G.S., "Translational Energy Dependence of the O^+ Polymide Reaction", AIAA Paper 85-7016-CP, AIAA Shuttle Environment and Operations II Conference, Houston, TX, November 1985.

208. Whitaker, A.F., et. al., "Protective Coatings for Atomic Oxygen Susceptible Spacecraft Materials", AIAA Paper 85-7017, ibid.

209. Smith, K.A., "Evaluation of Oxygen Interaction with Materials (EIOM) - STS-8 Atomic Oxygen Effects", AIAA Paper 85-7021, ibid.

210. Ferguson, D.C., Private Communication.

211. Leger, L.J., Private Communication.

212. Fristrom, R.M., et al., "Studies of Erosion of Solar Max Samples of Kapton and Teflon", *Proceedings of SMRM Degradation Study Workshop*, NASA Goddard Space Flight Center, May 1985.

213. Torr, M.R., et. al., "Intercalibration of Airglow Observations with the Atmospheric Explorer Satellites", *Planet Space Science*, Vol. 25, 1977, pp. 173ff.

214. Banks, P.M., P.R. Williamson, and W.J. Raitt, "Observations of Optical Emissions from STS-3", *Geophysics Research Letters*, Vol. 10, 1983, pp. 118-121.

215. Mende, S.B., O.K. Garriott, and P.M. Banks, "Observations of Optical Emissions on STS-4", ibid, pp. 1221ff.

216. Mende, S.B., et. al., "Observation of Orbiting Vehicle Induced Luminosities on the STS-8 Mission", *Geophysics Research Letters*, Vol. 11, 1984, pp. 527-530.

217. Mende, S.B., et. al., "Measurements of Vehicle Glow Characteristics During STS-41-D", AIAA Paper 85-0475, Aerospace Sciences Conference, Reno, NV, January 1985.

218. Green, B.D., "Review of the Vehicle Glow", AIAA paper 85-6095-CP, AIAA Shuttle Environment and Operations II Conference, Houston TX, November 13-15, 1985.

219. Green, B.D., "Atomic Recombination Into Excited Molecular States - A Possible Mechanism for Shuttle Glow", *Geophysics Research Letters*, Vol. 11, 1984, p. 576-579.

220. Shimazaki, T. and M. Mizushima, "Shuttle Glow Emissions Due to Radiative Relaxation of Highly Vibrationally Excited NO Molecules Produced by Surface Reflections", AIAA Paper 85-6098, Shuttle Environment and Operations II Conference, Houston TX, November 1985, pp. 79-87.

221. Swenson, G.R., S.B. Mende, and K.S. Clifton, "Ram Vehicle Glow Spectrum; Implications of NO^2 Recombination Continuum", *Geophysics Research Letters*, Vol. 12, 1985, pp. 97ff.

222. Papadopolous, K., "On the Shuttle Glow (The Plasma Alternative)", *Radio Science*, Vol. 19, 1984, pp. 571ff.

223. Kofsky, I.L., "Spectroscopic Consequences of Papadopolous Discharge Model of Spacecraft Ram Glows", *Radio Science*, Vol. 19, 1984, pp. 578ff.

Also see reference: 6

11.5 PARTICLE ENVIRONMENT (Section 6.0)

224. Cour-Palais, B.G., "Meteoroid Environment Model-1969: Near Earth to Lunar Surface", NASA SP-8013, March 1969.

225. McKay, D., NASA Johnson Space Center, Houston, TX, Private Communication.

226. Vedder, J.F. and J.C. Mandeville, "Microcraters Formed in Glass by Projectiles of Various Densities", *Journal of Geophysical Research*, Vol. 79, No. 23, August 10, 1974, pp. 3247-3256.

227. Frost, V.C., "Meteoroid Damage Assessment", NASA SP-8042, May 1970.

228. Chobotov, V.A., "Space Object Density Nears 5,500", *Aerospace America*, Vol. 22, No. 9, September 1984.

229. Kessler, D.J., "Orbital Debris Issues", *Advances in Space Research*, Vol. 5, No. 2, 1985.

230. Taff, L.G., "Satellite Debris: Recent Measurements", *Journal of Spacecraft and Rockets*, Vol. 23, No. 3, May-June 1986.

231. Kessler, D.J., "Sources of Orbital Debris and the Projected Environment for Future Spacecraft", *Journal of Spacecraft and Rockets*, Vol. 18, No. 4, July-August 1981.

232. Kessler, D.J., "Orbital Debris Environment for Space Station", JSC-20001.

233. Kessler, D.J., "Summary of Orbital Debris Workshop", Space Safety and Rescue 1982-1983, Vol. 58, IAA 82-254, pp. 3-10.

11.6 SOLAR OPTICAL RADIATION ENVIRONMENT (Section 7.0)

234. "Solar Electromagnetic Radiation", NASA Space Vehicle Design Criteria: Environment, May 1971.

235. Brown, R.R., L.B. Fogdall, and S.S. Cannadav, "Electron-Ultraviolet Irradiation Effects on Candidate Space Lab Thermal Control Coatings", AIAA/IES/ASTM 10th Space Simulation Conference, AIAA Paper 78-1621, October 1978, pp. 104-113.

236. Crossman, F.W., "Spacecraft Material Applications-Long-Term Stability

Questions", Large Space Antenna Systems Technology, NASA-Langley Research Center, 1982, pp. 241-256.

237. Kroes, R.L., et al., "Studies of Ultraviolet Irradiation Effects in ZnO-Type Thermal Control Pigments", AIAA 4th Thermophysics Conference, AIAA Paper 69-639, June, 1969.

238. Kroes, R.L, et al., "Effects of Ultraviolet Irradiation on Zinc Oxide", Heat Transfer and Spacecraft Thermal Control, Progress in Astronautics and Aeronautics, Vol. 24, AIAA, 1970, pp. 29-60.

239. Kurland, R.M., et. al., "Properties of Metallized Flexible Materials in Space Environments", Final Technical Report, SAMSO TR-78-31, January 1978.

240. Rauschenbach, H.S., "Solar Cell Array Design Handbook", JPL SP 43-38, Vol. 1, October 1976.

241. Statler, R.L. and D.J. Cartin, "Silicon Solar Cell Degradation in the Space Environment", Solar Cells, C.E. Backus, ed., IEEE Press, NY, 1976.

242. "Spacecraft Radiation Torques", NASA Space Vehicle Design Criteria: Guidance and Control, SP-8027, October 1969.

243. Ayer, F. and K. Soosaar, "Structural Distortions of Space Systems Due to Environmental Disturbances", Space Systems and Their Interactions with Earth's Space Environment, op. cit., pp. 601-632.

244. Wildman, P.J.L., "Dynamics of a Rigid Body in the Space Plasma", ibid, pp. 633-661.

245. Renner, U., "Attitude Control by Solar Sailing - A Promising Experiment with OTS-2", *European Space Agency Journal*, Vol. 3, No. 1, 1979, pp. 35-40.

246. Young, L.E., "SAFE/DAE: Solar Array Flight Experiment/Dynamic Augmentation Experiment Preliminary Report", NASA Marshall Space Flight Center, 1985.

247. Rugge, H.R., "Space Radiation and its Possible Effects on Man in Space", Space Systems and Technology Workshop II, September 23, 1982, pp. 23-1 to 23-15.

Also see reference: 6

11.7 SELF-GENERATED ENVIRONMENT (Section 8.0)

248. Jemiola, J.M., "Spacecraft Contamination-A Review", Space Systems and Their Interactions with Earth's Space Environment, op. cit., pp. 680-706.

249. Jemiola, J.M., "Contamination Control Program for Spacecraft", *Proceedings of the*

24th National Symposium and Exhibition, SAMPE, Vol. 24, 1979, pp. 699-706.

250. Borson, E.N., "The Control of Spacecraft Contamination - Where Are We Going", *Proceedings of USAF/NASA International Spacecraft Contamination Conference*, NASA CP-2039/AFGL-TR-78-190, Colorado Springs, CO, March 1978, pp. 1129-1135.

251. Hale, R.R., "An Improved Analytical Technique to Predict Space System Contamination", ibid, pp. 230-249.

252. Phillips, R.W., L.V. Tolentino, and S. Feuerstein, "Spacecraft Contamination Under Simulated Orbital Environments", *Journal of Spacecraft and Rockets*, Vol. 14, August 1977, pp. 501-508.

253. Miller, E.R., "Induced Environment Contamination Monitor Ascent/Entry, Optical and Deposition Measurements", The Shuttle Environment Workshop, J. Lehmann, S.G. Tanner, and T. Wilkerson, eds., NASA Office of Space Science and Applications, Calverton, MD, October 5-7, 1982, pp. A-123 to A-137.

254. Walters, W.P. and S.M. Yen, "Mean Free Path of Emitted Gas from Spacecraft", *Journal of Vacuum Science and Technology*, Vol. 20, February 1982.

255. Bird, G.A., "Spacecraft Outgas Ambient Flow Interaction", *Journal of Spacecraft and Rockets*, Vol. 18, January-February, 1981.

256. Harvey, R.L., "Spacecraft Neutral Self-Contamination by Molecular Outgassing", *Journal of Spacecraft and Rockets*, Vol. 13, May 1976, pp. 301-305.

257. Scialdone, J.J., "Molecular Fluxes from a Spacecraft Measured with a Quartz Microbalance", *Journal of Vacuum Science and Technology*, Vol. 12, January-February, 1975.

258. Kelley, J.G., "Measurement of Particle Contamination", AIAA Paper 85-7003, AIAA Shuttle Environment and Operations II Conference, Houston TX, November 13-15, 1985, pp. 99-103.

259. Borson, E.N., "Evaluation of the Ground Contamination Environment for STS Payloads", The Shuttle Environment Workshop, op. cit., pp. A-69 to A-99.

260. Berengoltz, J., C. Maag, and F. Kuykendall, "STS-3 'Snowflake' Study", ibid, pp. A-289 to A-294.

261. Davis, R.W., "Evaluation and Comparison of Airborne and Settled Particulate for Controlled Equipment Work Stations", 24th National SAMPE Meeting, May 1979, Society for the Advancement of Materials and Process Engineering, Vol. 24, pp. 707-716.

262. Ahern, J.E., R.L. Belcher, and R.D. Ruff, "Analysis of Contamination Degradation of Thermal Control Surfaces on Operational Satellites", AIAA Paper 83-1449, June 1983.

263. Glassford, A.P.M., et. al., "Improved Methods for Characterizing Material-Induced Contamination of Spacecraft", AIAA Paper 83-1496, June 1983.

264. Triolo, J., et. al., "Results from a 'Small Box' Real-Time Molecular Contamination Monitor on STS-3", AIAA Paper, January 1983.

265. Narcisi, R.S. "Quantitative Determination of the Outgassing Water Vapor Concentrations Surrounding Space Vehicles from Ion Mass Spectrometer Measurements", AFGL TR-82-0123, ADA 119963, June 1982.

266. Scialdone, J.J., "An Equivalent Energy for the Outgassing of Space Materials", NASA TND-8294, August 1976.

267. Hall, D.F., et. al., "Experiment to Measure Enhancement of Spacecraft Contamination by Spacecraft Charging", 8th Conference on Space Simulation, NASA SP-379, 1975, pp. 85-107.

268. Stevens, N.J., J.C. Roche, and M.J. Mandell, "NASA Charging Analyzer Program - A Computer Tool That Can Evaluate Electrostatic Contamination", *Proceedings of the USAF/NASA International Spacecraft Contamination Conference*, op. cit., pp. 274-289.

269. Clark, D.M. and D.F. Hall, "Flight Evidence of Spacecraft Surface Contamination Rate Enhancement by Spacecraft Charging Obtained with a Quartz Crystal Microbalance", Spacecraft Charging Technology - 1980, op. cit., pp. 493-508.

270. Scialdone, J.J., "Characterization of the Outgassing of Spacecraft Materials", *Proceedings of Shuttle Optical Environment Meeting*, Washington D.C., 1981.

271. Glassford, A.P.M. and C-K Liu, "Outgassing Rates of Multilayer Insulation Materials at Ambient Temperatures", *Journal of Vacuum Science and Technology*, Vol. 17, May-June 1980.

272. Hughes, T.A., "Outgassing of Materials in the Space Environment", *Proceedings of the USAF/NASA International Spacecraft Contamination Conference*, op. cit., pp. 14-33.

273. "Listing of Materials Meeting JSC Vacuum Stability Requirements", NASA Johnson Space Center, JSC 07572, April 1978.

274. Campbell, W.A., Jr., R.S. Marriott, and J.J. Park, "An Outgassing Data Compilation of Spacecraft Materials", NASA RP-1014, 1978.

275. McNutt, R.C., "Chemical Analysis of Outgassing Contaminants", NASA CR-123794, May 1972.

276. Zeiner, E.A., "A Multinodal Model for Surface Contamination Based Upon the Boltzmann Equation of Transport", *Proceedings of the USAF/NASA International Spacecraft Contamination Conference*, op. cit., pp. 34-82.

277. Millard, J.M. and C.R. Maag, "Spacecraft Contamination Model Development", ibid, pp. 208-229.

278. Rantanen, R.O., "Spacecraft Contamination Modeling", AIAA Paper 77-739, June 1977.

279. Zeiner, E.A., "AESC Multinodal Free Molecular Contamination Transport Model", 8th Conference on Space Simulation, op. cit., pp. 1-32.

280. Furstenau, R.P., T.D. McCay, and D.M. Mann, "U.S. Air Force Approach to Plume Contamination", Optics in Adverse Environments, The Society of Photo-Optical Instrumentation Engineers, February 1980.

281. Barsh, M.K., et. al., "Contamination Mechanisms of Solid Rocket Motor Plumes", *Proceedings of the USAF/NASA International Spacecraft Contamination Conference*, op. cit., pp. 347-384.

282. Maag, C.R., "Backflow Contamination from Solid Rocket Motors", ibid, pp. 342-384.

283. Maag, C.R., J.A. Jeffrey, and J.M. Millard, "Effect of Bipropellant Plume Exhaust Effluents on Spaceborne Optical Instruments", Optics in Adverse Environments, op. cit.

284. McKay, T.D., et. al., "Exhaust Plume Contamination from an Aged Hydrazine Monopropellant Thruster", *Proceedings of the USAF/NASA International Spacecraft Contamination Conference*, op. cit., pp. 456-517.

285. Carruth, M.R., Jr. and Y.S. Kuo, "[illegible] Thruster Plume Effects on Spacecraft Surfaces", AIAA 16th Joint Propul[illegible] Conference, July 1980.

286. Olsen, R.C. and E.C. Whipple, "Operations of the ATS-6 Ion Engine", Spacecraft Charging Technology - 1978, op. cit., pp. 59-68.

287. Randolph, L.K. and R.M. Jones, "Pulsed Plasma Thruster Contamination Studies", AIAA Paper 79-2106, November 1979.

288. Liemohn, H.B., R.L. Copeland, and W.M. Leavens, "Plasma Particle Trajectories Around Spacecraft Propelled by Ion Thrusters", Spacecraft Charging Technology - 1978, op. cit., pp. 419-436.

289. Ambrus, J.H., "SP-100 Space Power Program", NASA-CP-2352, 1984.

290. Johnson, R.T., Jr., F.V. Thome, and C.M. Craft, "A Survey of Aging of Electronics with Applications to Nuclear Power Plant Instrumentation", *IEEE Transactions on Nuclear Science*, Vol. NS-30, No. 6, December 1983, pp. 4358-4362.

Also see reference: 165

11.8 ELECTROMAGNETIC ENVIRONMENT (Section 9.0)

291. Harris, M. and R. Lyle, "Magnetic Fields-Earth and Extraterrestrial", NASA Space Vehicle Design Criteria: Environment, NASA SP-8017, March 1969.

292. Knecht, D.J., "The Geomagnetic Field", Air Force Geophysics Laboratory, AFCRL 72-0570, September 1972.

293. Kane, R.P., "Geomagnetic Field Variations", *Space Science Review*, Vol. 18, 1976, pp. 413ff.

294. Aggson, T.L. and J.P. Heppner, "Observations of Large Transient Magnetospheric Electric Fields", *Journal of Geophysical Research*, Vol. 82, 1977, pp. 5155ff.

295. Stern, D.P., "Large Scale Electric Fields in the Earth's Magnetosphere", *Review of Geophysics and Space Physics*, Vol. 15, 1977.

296. Whipple, E.C., Jr., "An Overview of Charging of Large Space Structures in Polar Orbit", *Proceedings of the AFGL Workshop on Natural Charging of Large Space Structures in Near Earth Polar Orbit*, AFGL TR-83-0046, January 1983, ADA 134894, pp. 11-28.

297. Shawhan, S.D. and G.B. Murphy, "STS-3/OSS-1 Plasma Diagnostics Package (PDP) Measurements of Orbit-Generated $\mathbf{V} \times \mathbf{B}$ Potentials and Electrostatic Noise", ibid, pp. 119-124.

298. Stevens, N.J., "Review of Interactions of Large Space Structures with the Environment", Space Systems and Their Interactions with Earth's Space Environment, op. cit., pp. 437-454.

299. "Spacecraft Magnetic Torques", NASA Space Vehicle Design Criteria: Environment, NASA SP-8018, March 1969.

300. "Assessment and Control of Spacecraft Magnetic Fields", NASA SP-8037, September 1970.

*U.S. GOVERNMENT PRINTING OFFICE: 1994- [illegible]